8-2017

Water-Tree Modelling and Detection for Underground Cables

Qi Chen
Clemson University, qichen85@gmail.com

WATER-TREE MODELLING AND DETECTION FOR UNDERGROUND CABLES

A Dissertation
Presented to
the Graduate School of
Clemson University

In Partial Fulfillment
of the Requirements for the Degree
Doctor of Philosophy
Electrical Engineering

---

by
Qi Chen
August 2017

Accepted by:
Chair: Dr. Daniel L. Noneaker
Advisor: Dr. Elham B. Makram
Committee Member: Dr. Richard E. Groff
Committee Member: Dr. Carl W. Baum
Committee Member: Dr. John R. Wagner

ABSTRACT

In recent years, aging infrastructure has become a major concern for the power industry. Since its inception in early 20th century, the electrical system has been the cornerstone of an industrial society. Stable and uninterrupted delivery of electrical power is now a base necessity for the modern world. As the times march-on, however, the electrical infrastructure ages and there is the inevitable need to renew and replace the existing system. Unfortunately, due to time and financial constraints, many electrical systems today are forced to operate beyond their original design and power utilities must find ways to prolong the lifespan of older equipment. Thus, the concept of preventative maintenance arises. Preventative maintenance allows old equipment to operate longer and at better efficiency, but in order to implement preventative maintenance, the operators must know minute details of the electrical system, especially some of the harder to assess issues such water-tree. Water-tree induced insulation degradation is a problem typically associated with older cable systems. It is a very high impedance phenomenon and it is difficult to detect using traditional methods such as Tan-Delta or Partial Discharge.

The proposed dissertation studies water-tree development in underground cables, potential methods to detect water-tree location and water-tree severity estimation. The dissertation begins by developing mathematical models of water-tree using finite element analysis. The method focuses on surface-originated vented tree, the most prominent type of water-tree fault in the field. Using the standard operation parameters of North American electrical systems, the water-tree boundary conditions are defined. By applying finite element analysis technique, the complex water-tree structure is broken down to homogeneous components. The result is a generalized representation of water-tree

capacitance at different stages of development. The result from the finite element analysis is used to model water-tree in large system.

Both empirical measurements and the mathematical model show that the impedance of early-stage water-tree is extremely large. As the result, traditional detection methods such Tan-Delta or Partial Discharge are not effective due to the excessively high accuracy requirement. A high-frequency pulse detection method is developed instead. The water-tree impedance is capacitive in nature and it can be reduced to manageable level by high-frequency inputs. The method is able to determine the location of early-stage water-tree in long-distance cables using economically feasible equipment. A pattern recognition method is developed to estimate the severity of water-tree using its pulse response from the high-frequency test method.

The early-warning system for water-tree appearance is a tool developed to assist the practical implementation of the high-frequency pulse detection method. Although the equipment used by the detection method is economically feasible, it is still a specialized test and not designed for constant monitoring of the system. The test also place heavy stress on the cable and it is most effective when the cable is taken offline. As the result, utilities need a method to estimate the likelihood of water-tree presence before subjecting the cable to the specialized test. The early-warning system takes advantage of naturally occurring high-frequency events in the system and uses a deviation-comparison method to estimate the probability of water-tree presence on the cable. If the likelihood is high, then the utility can use the high-frequency pulse detection method to obtain accurate results.

Specific pulse response patterns can be used to calculate the capacitance of water-tree. The calculated result, however, is subjected to error margins due to limitations from the real system. There are both long-term and short-term methods to improve the accuracy. Computation algorithm improvement allows immediate improvement on accuracy of the capacitance estimation. The probability distribution of the calculation solution showed that improvements in waveform time-step measurement allow fundamental improves to the overall result.

DEDICATION

To my parents, Yicheng Chen and Huibin Qi, your love and support made my work possible.

ACKNOWLEDGEMENTS

I would like to thank my advisor, Dr. Elham Makram, for her continued guidance and support during my studies. She introduced me into the wonderful world of power systems. Her knowledge and experience allow me to pursue complex subjects like water-tree.

I would like to thank my committee members: Dr. Daniel Noneaker, Dr. Richard Groff, Dr. Carl Baum and Dr. John Wagner. They provided valuable knowledge and advice for my studies.

I would like to thank Dr. Xufeng Xu for valuable support to my work.

I would like to thank Dr. Ramtin Hadidi for providing insight to my research.

I would like to thank my friends in the power system group for their help and companionship. It is a wonderful time at Clemson University.

TABLE OF CONTENTS

Title Page....i
Abstract....ii
Dedication....v
Acknowledgements....vi
CHAPTER 1 INTRODUCTION....1
1.1 Research Objectives: Water-Tree in Insulated Cables....1
1.1.1 Water-Tree in Aged Infrastructure....2
1.1.2 Water-tree Modeling....4
1.1.3 Water-tree Detection....4
1.1.4 Early-Warning of Water-tree Appearance....5
1.1.5 Water-Tree Capacitance Estimation....6
1.2 Literature Review....6
1.2.1 Underground Cable Operation....6
1.2.2 Aging Infrastructure....10
1.2.2.1 State of the Overall Power Infrastructure....10
1.2.2.2 Underground Cable in Aging Infrastructure....13
1.2.3 Water-Tree Characteristics....15
1.2.4 Effect of Water-Tree in Power System....17
1.2.5 Detection of Water-Tree....19
1.2.5.1 Tan-Delta....20
1.2.5.2 Partial-Discharge....23
1.3 Research Contribution....28
1.3.1 Mathematical Modeling of Water-Tree in Underground Cable Insulation....29
1.3.2 High Frequency Pulse Detection of Water-Tree....30
1.3.3 Early-warning of Water-Tree Presence using Deviation Comparison Method 31
1.3.4 Computational Margin Accumulation in Water-Tree Analysis....33
1.4 Chapter Summary....34
CHAPTER 2 MATHEMATICAL MODELING OF WATER-TREE IN UNDERGROUND CABLE INSULATION....35
2.1 Water-tree Formation and Structure Analysis....36
2.1.1 Water-tree Formation....37
2.1.2 Bow-Tie Tree....46
2.1.3 Vented Tree....48
2.2 Building the Model....50
2.2.1 Model Building Background....51
2.2.2 Modeling Building Concept....53
2.2.3 Model Building Assumptions....56
2.2.3.1 Assumption #1: Tree Type Selection: Surface-Originated Vented Tree....56
2.2.3.2 Assumption #2: Tree Cause Selection: Type-Two Origination Cause....58
2.2.3.3 Assumption #3: Tree Shape Selection: Ellipsoidal Distribution Area with Fixed Axial Ratio....59

2.2.3.4 Assumption #4: Tree Electrical Permittivity Distribution: Linear ····· 59
2.2.4 Finite Element Analysis of Water-tree ····· 61
2.2.4.1 Conception Design Based on Cylindrical Capacitor Model ····· 61
2.2.4.2 Finite Element Breakdown on Location Region ····· 65
2.3 MODEL RESULT ····· 69
2.4 CHAPTER CONCLUSION ····· 75

CHAPTER 3 HIGH FREQUENCY PULSE DETECTION METHOD FOR WATER-TREE ····· 76

3.1 GENERAL BACKGROUND ON HIGH-FREQUENCY PULSE DETECTION ····· 76
3.2 HIGH-FREQUENCY PULSE DETECTION OF WATER-TREE ····· 79
3.2.1 Motivation for High-Frequency Pulse Detection Method ····· 79
3.2.2 Methodology for High Frequency Pulse Detection ····· 83
3.2.3 Method Testing Preparation ····· 84
3.2.2.1 Water-Tree Model ····· 84
3.2.2.2 Pulse Generation ····· 87
3.2.2.3 Testing System Conditions ····· 88
3.2.2.4 Test Procedure ····· 90
3.2.3 Test Case Results ····· 93
3.2.3.1 Water-Tree Pulse Response Cases ····· 93
3.2.3.2 Pulse Response Pattern Identification ····· 98
3.2.3.3 Benchmark Frequency Trends ····· 101
3.3 CHAPTER CONCLUSION ····· 104

CHAPTER 4 EARLY-WARNING OF WATER-TREE PRESENCE USING DEVIATION COMPARISON ····· 106

4.1 MOTIVATION FOR THE EARLY-WARNING SYSTEM ····· 106
4.2 METHODOLOGY ····· 107
4.2.1 Method Requirements ····· 107
4.2.2 Naturally Occurring High-Frequency Phenomena in the System ····· 109
4.2.3 Extrapolation-Comparison Method ····· 110
4.2.3.1 Extrapolation ····· 113
4.2.3.2 Comparison ····· 117
4.3 IMPLEMENTATION ····· 118
4.4 OBSERVATIONAL RESULTS ····· 120
4.4.1 System Response for Naturally Occurring High-Frequency Event ····· 120
4.4.2 Effect of Filtering on the Result ····· 125
4.4.3 Deviation Comparison Results ····· 126
4.4.4 Impact of Harmonics on Deviation-Comparison Chart ····· 135
4.4.5 Impact of Noise on Deviation-Comparison Chart ····· 140
4.5 CHAPTER CONCLUSION ····· 143

CHAPTER 5 COMPUTATIONAL MARGIN ACCUMULATION IN WATER-TREE ANALYSIS ····· 145

5.1 ACCURATE WATER-TREE ESTIMATION USING TERMINAL VOLTAGE DATA ····· 145
5.1.1 Motivation ····· 145
5.1.2 Capacitance Estimation Process ····· 147
5.1.3 Test Case Result ····· 152
5.2 ERROR ACCUMULATION IN WATER-TREE DETECTION ····· 154
5.2.1 Water Detection Limitations ····· 155
5.2.1.1 Material Limitation on Water-Tree Detection ····· 155
5.2.1.2 Computational Limitation on Water-Tree Detection ····· 156
5.2.1.3 Fundamental Limitation on Water-Tree Detection ····· 157
5.2.2 Errors Margins in Water-Tree Capacitance Estimation ····· 157
5.2.2.1 Error Accumulation ····· 157
5.2.2.2 Material Limitation Induced Error Margins ····· 158
5.2.2.3 Computational Limitation Induced Error Margins ····· 159
5.2.3 Potential Method for Improvement on Fundamental Limitation ····· 162
5.3 CHAPTER CONCLUSION ····· 166

CHAPTER 6 CONCLUSION ····· 167

APPENDICES ····· 172

APPENDIX A SAMPLE FINITE ELEMENT ANALYSIS CODE FOR WATER-TREE MODEL ····· 173

APPENDIX B CABLE PARAMETERS FOR BENCHMARK FREQUENCY IDENTIFICATION ····· 177

APPENDIX C DEVIATION COMPARISON CHART CODE FOR TWO POINT EXTRAPOLATION SCHEME WITH GAUSSIAN NOISE ····· 179

REFERENCE ····· 184

LIST OF FIGURES

FIGURE 1: WATER-TREE FAULT IN OLD CABLES 2
FIGURE 2: HYBRID-TREE FAULTS 18
FIGURE 3: PURE-TREE FAULTS 18
FIGURE 4: VOLTAGE AND CURRENT PHASE SHIFT IN TAN-DELTA METHOD 20
FIGURE 5: INSULATION MATERIAL: FRONT VIEW (LEFT) VS SIDE VIEW (RIGHT) 36
FIGURE 6: MICRO-FRACTURE CHAMBER IN CABLE INSULATION 37
FIGURE 7: INTERCONNECTIONS BETWEEN MICRO-FRACTURE CHAMBERS 40
FIGURE 8: ROOT MICRO-FRACTURE CHAMBER OF WATER-TREE 41
FIGURE 9: CROWN OF THE WATER-TREE 42
FIGURE 10: BRANCH DIAMETER COMPARISON 43
FIGURE 11: WATER-TREE BRANCHING POINT 44
FIGURE 12: BALL-SHAPED TREE (LEFT) VS HAND SHAPED TREE (RIGHT) 45
FIGURE 13: SAMPLE CABLE SLICE OF CONTAINING A WATER-TREE 45
FIGURE 14: SAMPLE REPRESENTATION OF A BOW-TIE SHAPED WATER-TREE 46
FIGURE 15: VENTED TREES: SURFACED ORIGINATED (LEFT) AND CONDUCTOR ORIGINATED (RIGHT) 48
FIGURE 16: CATEGORIZED WATER-TREE CHARACTERISTICS 50
FIGURE 17: WATER-TREE BRANCHES IN INSULATION LAYER 54
FIGURE 18: LOCALIZED VIEW OF WATER-TREE BRANCH AND THE INSULATION LAYER 54
FIGURE 19: CAPACITOR WITH MULTIPLE-DIELECTRIC MATERIAL 55
FIGURE 20: SAMPLE CABLE Π-MODEL 55
FIGURE 21: SAMPLE CABLE MODEL WITH WATER-TREE PRESENT 56
FIGURE 22: TREE-BRANCH DIAMETER CHANGE ALONG CENTRAL DEVELOPMENT AXIS 60
FIGURE 23: CYLINDRICAL CAPACITOR MODEL 61
FIGURE 24: CYLINDRICAL CAPACITOR WITH TWO DIELECTRICS 62
FIGURE 25: A CAPACITOR WITH J ADDITIONAL DIELECTRICS AND IN I LAYERS 65
FIGURE 26: RESOLUTION OF RELATIVE PERMITTIVITY AT A SPECIFIC REGION 66
FIGURE 27: RESOLVING THE DIELECTRIC MATERIAL ANGLE WITH CONDUCTOR AS ORIGIN 68
FIGURE 28: EQUIVALENT CIRCUIT OF SIMULATED CAPACITANCE 69
FIGURE 29: CAPACITANCE OF WATER-TREE AFFLICTED AREA 71
FIGURE 30: CAPACITANCE OF WATER-TREE AFFLICTED AREA (ZOOMED-IN) 72
FIGURE 31: GRAPHICAL REPRESENTATION OF C_COMPROMISED VALUE 73
FIGURE 32: OVERALL CAPACITANCE OF WATER-TREE AT DIFFERENT DEVELOPMENTAL STAGES 74
FIGURE 33: LUMP MODEL FOR WATER-TREE: LATE STAGE (LEFT) VS EARLY-STAGE (RIGHT) 84
FIGURE 34: WATER-TREE AFFLICTED CABLE SEGMENT 85
FIGURE 35: WATER-TREE UNDER FINITE ELEMENT ANALYSIS 86
FIGURE 36: LIGHTNING PULSE MODEL 87
FIGURE 37: LIGHTNING PULSE MODEL WITH FUNDAMENTAL COMPONENT 87
FIGURE 38: SAMPLE HVDC SYSTEM 88
FIGURE 39: SAMPLE HVAC SYSTEM 88
FIGURE 40: DC SIDE LIGHTNING PULSE GENERATOR IN HVDC SYSTEM 89

FIGURE 41: HIGH-VOLTAGE SIDE LIGHTNING PULSE GENERATOR IN HVAC SYSTEM····· 89
FIGURE 42: OFFLINE TEST SYSTEM: WITHOUT WATER-TREE (TOP) VS WITH WATER-TREE (BOTTOM)····· 90
FIGURE 43: PULSE GENERATOR IN OFFLINE TEST SYSTEM····· 90
FIGURE 44: PSCAD CABLE TEST PARAMETERS····· 92
FIGURE 45: HIGH FREQUENCY INPUT PULSE: INITIAL MOMENT (LEFT) AND OVERALL (RIGHT)····· 93
FIGURE 46: THREE-SYSTEM COMPARISON CASE····· 93
FIGURE 47: OVERALL PULSE RESPONSE FROM HFPD METHOD····· 94
FIGURE 48: PULSE RESPONSE FROM WATER-TREE····· 94
FIGURE 49: PATTERN IDENTIFICATION POSSIBILITIES····· 95
FIGURE 50: BENCHMARK FREQUENCY PATTERN····· 96
FIGURE 51: OVER FREQUENCY WATER-TREE PULSE RESPONSE FROM 6MHZ PULSE····· 97
FIGURE 52: ESTABLISHMENT OF THE BENCHMARK FREQUENCY····· 98
FIGURE 53: WATER-TREE RESPONSE TREND TEST CASE FOR 1 METER CABLE UNDER 1085KHZ PULSE····· 99
FIGURE 54: WATER-TREE DISTANCE VS BENCHMARK FREQUENCY····· 101
FIGURE 55: WATER-TREE CAPACITANCE VS BENCHMARK FREQUENCY····· 102
FIGURE 56: WATER-TREE DISTANCE VS WATER-TREE CAPACITANCE VS BENCHMARK FREQUENCY····· 103
FIGURE 57: BENCHMARK FREQUENCY TREND····· 104
FIGURE 58: WATER-TREE RESPONSE TO HIGH-FREQUENCY EVENTS····· 111
FIGURE 59: OVERALL VIEW OF WATER-TREE RESPONSE FROM A HIGH-FREQUENCY PULSE····· 111
FIGURE 60: SPECIFIC VIEW OF WATER-TREE RESPONSE FROM A HIGH-FREQUENCY PULSE····· 112
FIGURE 61: NORMAL OPERATION WAVEFORM····· 113
FIGURE 62: NORMAL SYSTEM OPERATION IN THE TIME SCALE OF WATER-TREE DETECTION····· 113
FIGURE 63: STRAIGHT LINE EXTRAPOLATION USING TWO DATA POINTS····· 114
FIGURE 64: WATER-TREE JUNCTION····· 116
FIGURE 65: FLOW CHART FOR EARLY-WARNING SYSTEM····· 119
FIGURE 66: TESTING SYSTEM FOR EARLY-WARNING SYSTEM DETECTION····· 121
FIGURE 67: SYSTEM RESPONSE TO 3 KHZ LIGHTNING PULSE····· 122
FIGURE 68: LOW-IMPEDANCE FAULT RESPONSE TO 3KHZ PULSE····· 123
FIGURE 69: FILTERED RESULTS FROM THE TEST CASE····· 125
FIGURE 70: TIME-STEP DIFFERENCE VS STANDARD DEVIATION····· 128
FIGURE 71: TIME-STEP DIFFERENCE VS STANDARD DEVIATION FOR HEALTHY SYSTEM· 129
FIGURE 72: TIME-STEP DIFFERENCE VS STANDARD DEVIATION WITH WATER-TREE IN THE MIDDLE····· 130
FIGURE 73: HEALTHY SYSTEM OVER FOUR CYCLES····· 131
FIGURE 74: WATER-TREE AFFLICTED SYSTEM OVER FOUR CYCLES····· 131
FIGURE 75: WATER-TREE AT 5KM FROM THE INPUT TERMINAL (15KM FROM THE OTHER TERMINAL)····· 132
FIGURE 76: STANDARD DEVIATION GRAPHS OF MULTIPLE WATER-TREES····· 133

FIGURE 77: STANDARD DEVIATION GRAPHS FOR MULTIPLE WATER-TREES (ZOOMED IN) 133
FIGURE 78: COMPARISON BETWEEN OFFLINE (LEFT) AND ONLINE (RIGHT) TEST 134
FIGURE 79: DEVIATION-COMPARISON IN THE PRESENCE OF 5^{TH}, 7^{TH}, 11^{TH} AND 13^{TH} ORDER HARMONICS 135
FIGURE 80: HEALTHY SYSTEM DEVIATION-COMPARISON OUTPUT WITH LARGE HARMONIC INJECTION 136
FIGURE 81: SYSTEM COMPARISON WITH LARGE HARMONICS 137
FIGURE 82: ZOOMED-IN VIEW OF WATER-TREE AFFLICTED SYSTEM OUTPUT 137
FIGURE 83: SYSTEM COMPARISON WITH ONLY 5^{TH} AND 7^{TH} HARMONICS 138
FIGURE 84: SYSTEM COMPARISON WITH ONLY 11^{TH} AND 13^{TH} HARMONICS 138
FIGURE 85: SYSTEM RESPONSE WITH 43^{RD} ORDER HARMONIC 139
FIGURE 86: WATER-TREE AFFLICTED SYSTEM WITH SNR OF 30 141
FIGURE 87: WATER-TREE AFFLICTED SYSTEM WITH SNR OF 150 141
FIGURE 88: WATER-TREE AFFLICTED SYSTEM WITH SNR OF 300 142
FIGURE 89: WATER-TREE AFFLICTED SYSTEM WITH SNR OF 1000 142
FIGURE 90: HIGH CORROSION PROGRESSION (LEFT) VS LOW CORROSION PROGRESSION (RIGHT) 146
FIGURE 91: PULSE REFLECTION EXPERIMENT SETUP 147
FIGURE 92: NON-PLATEAU PATTERN 149
FIGURE 93: PLATEAU PATTERN (N=1) 149
FIGURE 94: PLATEAU PATTERN #2 (N>2) 150
FIGURE 95: THRESHOLD BENCHMARK FREQUENCY 153
FIGURE 96: PULSE FREQUENCY MEASUREMENT 154
FIGURE 97: FINITE ELEMENT ANALYSIS ALGORITHM FLOW CHART 173
FIGURE 98: CABLE DIMENSIONS 177
FIGURE 99: LIGHTNING PULSE GENERATION 178
FIGURE 100: OVERALL SYSTEM WITH HARMONICS INJECTED 178
FIGURE 101: DEVIATION-COMPARISON CHART OUTPUT ALGORITHM FLOW CHART 179

LIST OF TABLES

TABLE 1: WATER-TREE PULSE RESPONSES FROM HFPD METHOD ····· 97
TABLE 2: BENCHMARK FREQUENCY UNDER DIFFERENT TEST CASE PARAMETERS ····· 100
TABLE 3: DEVIATION COMPARISON TABLE ····· 118
TABLE 4: SAMPLE DEVIATION-COMPARISON TABLE ····· 127
TABLE 5: ERROR ACCUMULATION: PERCENTAGE ERROR VS NUMBER OF VARIABLES ···· 158
TABLE 6: SOURCE OF ERROR IN WATER-TREE CAPACITANCE ESTIMATION ····· 161

Chapter 1

Introduction

1.1 Research Objectives: Water-Tree in Insulated Cables

Power system is one of the oldest research fields in electrical engineering. The ability to implement and maintain a stable electric grid remains the cornerstone of industrial society. The research-focus of power system study shifts according to the demands of power industry and society as a whole. In the recent decade, there has been an increasing concern on infrastructure aging and its effect on the electric systems.

A number of factors contribute to these concerns. The root of the issue is simply the age. For example, the US electrical infrastructure has begun its development more than a century ago. While many system components have been replaced and redesigned over the years, a surprisingly large number of the old equipment continues to operate today. This is especially true for electro-mechanical components and stationary infrastructures. These components naturally have long lifespan and their service is further lengthened by factors such as financial constraint and opportunity cost. In many situations, decisions such as funding, labor availability and service interruption may force utilities to refurbish old systems instead of replacing them.

The transmission and distribution (T&D) systems are particularly affected by these decisions. The T&D systems are the backbone of the electric grid. Thus, the utilities are highly motivated to keep the system operating at optimal capacity. In theory, aged equipment would be closely monitored and replaced as soon as possible. In practice,

however, it is often difficult or impossible to do so. For example, monitoring individual segments of long-distance under-sea cable will require large numbers of waterproof, pressure resistant devices to be installed across a long distance. Replacing the entire cable will incur cost such as labor and service interruption. Due to these factors, the associated operation cost quickly escalates and becomes impractical. As the result, aged equipment must remain in service beyond their original design.

1.1.1 Water-Tree in Aged Infrastructure

One particular problem associated with aging cables infrastructure is the appearance of water-tree induced fault. Water-tree fault is a type of line-to-ground (LG) fault typically observed in older insulated-cables, such as Cross-Link Polyethylene (XLPE) cables. It occurs in cables that have been exposed to a high level of moisture. Typically, the phenomenon affects infrastructures that have been in service for more than a decade. Figure 1 shows the result of a water-tree fault.

Figure 1: Water-Tree Fault in Old Cables

In recent years, water-tree has received increasing amount of attention from the research community. This is mainly due to two reasons. The first reason is the gradual aging of US power transmission and distribution infrastructure. Older infrastructures tend to be more vulnerable to water-tree development and there is an increasing chance for water-tree induced faults to occur.

The second reason is the overall increasing presence of insulated cables. Traditional electrical grids have been dominated by overhead lines, but insulated cables have become more popular in recent years. This is partly due to the increasing wind-power penetration around the world. Wind-power has gained such prominence that land-based wind-power is no longer sufficient to satisfy many countries around the world. To supplement the existing capacity, the industry has begun to exploit ocean-based wind resources. In these offshore windfarms, wind-power is often delivered to the grid through high-voltage long-distance transmission cables. Since water-tree is a problem uniquely associated with insulated cables, the increasing presence of these cables in the grid resulted in a higher priority for water-tree research.

Monitoring and maintaining long-distance cables have proven to be difficult comparing to their in-land counterparts. Among the myriad of problems, water-tree induced fault is a particular nuisance. Water-tree fault is a category of very-high impedance faults. It is difficult to monitor and detect using standard techniques. The issue is particularly problematic for long-distance cables. For these cables, the innate impedance of the cable masks the presence of the water-tree fault. The high cost of replacing these cables also means maintenance and repair must be done at the precise location of the water-tree instead of the whole cable segment. Thus, there is the need for

understanding their behavior in long-distance cables, detecting their presence and estimating their severity.

1.1.2 Water-tree Modeling

One important challenge is creating a functional mathematical model for the water-tree. By nature, water-tree formation is a highly random process. The tree growth process depends on a number of factors, such as environment condition, physical stress from the installation process, operational electric field intensity and frequency, load switching, manufacturing defects in the cable, molecular structure of the insulation material and many more. As the result, each water-tree is unique even under near identical developmental conditions.

Despite its random nature, however, the water-tree development process follows certain trends. Its characteristics can be extrapolated and estimated based on parameters such as cable specification and service data. By taking advantage of advancements in computer-assisted modeling techniques, it becomes possible to estimate certain electrical properties of the water-tree, such as capacitance and resistance. These parameters can be used to determine water-tree behavior in large systems.

1.1.3 Water-tree Detection

The second challenge associated with water-tree study is its high impedance. In theory, water-tree faults can be detected and observed like other types of electrical faults. In practice, equipment limitations severely restrict possible methods for the water-tree detection process, especially in long distance transmission cables. For example, the typical low-impedance fault on low-voltage cable can be detected and analyzed with

minimal difficulty and equipment. As the fault impedance increases, the accuracy requirement of the instrument increases accordingly. Beyond a certain threshold, the cost for higher instrument accuracy begins to increase exponentially. Unfortunately, fault impedance from water-tree can be eight orders of magnitude greater than most LG fault. Thus, instrument limitation and cost becomes an important factor in designed water-tree detection process.

A potential method for water-tree detection is taking advantage of the capacitive nature of the water-tree structure. In low-impedance faults, the resistive element is the main-focus of the detection process. In water-tree faults, however, the resistive element is simply too high; therefore, the capacitive element becomes the only choice. Comparing to the unchanging resistive impedance, the impedance associated with the capacitance element can be altered. By utilizing very-high frequency (VHF) methods, the required instrument accuracy can be reduced to a manageable level.

1.1.4 Early-Warning of Water-tree Appearance

The next issue associated with the water-tree detection process is the actual implementation of the method. Although VHF method is effective on locating and estimating the characteristic of the water-tree, it still requires specialized instruments. In addition, the test itself also place heavy stress on the cable. Thus, a supplementary method is developed to serve as an early-warning system for water-tree appearance.

The goal of the early-warning system is to estimate the probability of water-tree presence without the need of specialized instruments. Many high-frequency events naturally exist in a system. Although their magnitude and frequency are lower than a dedicated high-frequency pulse generator, they still cause small disturbances and

deviations in the system. Over a long period, certain trends can be observed from these deviations. They can be used to estimate the probability of water-tree presence and if additional tests are justified.

1.1.5 Water-Tree Capacitance Estimation

Remote estimation of water-tree capacitance provides many important advantages. With accurate information on the corrosion progress and development rate, the maintenance plans become much more efficient. There exist, however, many limitations on the estimation process. For example, measurements are subjected to error. Mathematical model may deviate from actual behavior. Calculated results may contain error. As the result, it is necessary to understand the factors that influence the accuracy of the estimation process. These factors also present future improvement direction for water-tree detection.

1.2 Literature Review

1.2.1 Underground Cable Operation

Insulated cables have many advantages over exposed wire. Chief among them is the ability to prevent electricity from discharging into the earth due to direct contact. In addition, armored/shielded insulation layer can also be designed to resist a number of environmental hazards, such as corrosion, physical impact and radiation, but since insulated cable is more expensive than exposed-wire, exposed-wire connections dominate over insulated cable in applications such as overhead transmission. On the other hand, for many underground and surface-level applications, insulated cable is a necessity. In these

situations, contact with earth, flowing water and other types of hazards are inevitable; therefore, insulated cables must be used despite their higher expense.

The development of insulated cable has a long history. The idea of an electricity carrying wire proofed against contact leakage is older than any large-scale implementation of power system. There had been records of insulated cable utilization as early as 1812. According to the records, an individual from Russia name Schilling has used insulated cables to detonate ores remotely [1].

Utilization of insulated cable in an actual power grid came much later. In United Kingdom, insulated cable was first deployed for public grids in 1890. Dr. Ferranti designed a connection for London Electric Supply Corporation. A section of the connection used insulated cables. The design utilized multi-layer laminated dielectric insulation in 20 feet segments. The overall line length was 30 miles and there were more than 7000 slices along the connection [1]. The project was fully commissioned on February 15, 1891. It would continue to operate until 1933, more than four decades later.

In United States, Thomas Edison built the first central power station in 1882. Before the station itself was operational, however, Edison already registered a patent on his version of insulated cable. In his US Patent No. 251,552 dated December 27, 1881, Edison described a form of insulated cable under the title “Street Pipes”. By September 4, 1882, the Pearl Street Station was deliver 110V DC current to local customers using the patented insulated cable. Specifically, the patent described a form of insulated cable using copper bars as conductors. The conductors were wrapped by jute and placing in an iron tube. The space in the iron tube was filled with a bituminous or wax compound [2].

Across the ocean, other types of insulated cables saw their early use as well. In 1923, Dr. Emanueli of Pirelli invented the first oil-insulated cable. Comparing to paper, wax or rubber insulated cables, oil-filled (OF) cables are more suitable for high voltage applications, especially when higher operational temperature is expected. Seven years after its invention, the first commercial OF cable circuit went into operation at Tokyo, Japan [3]. The connection delivered 66kV currents in OF cables.

Along with rubber and oil, other types of insulation material were also explored in the early years of cable development. For example, as early as 1870, both United Kingdom and France utilized porcelain and glass insulated cable in sewers. Unfortunately, although porcelain and glass are resistant to high temperature and chemical corrosion, they are susceptible to both thermal shock and physical impact [1]. It is also problematic to perform maintenance on ceramic insulations, especially for long apparatus such as cables.

The early history of cable development is dominated by oil, rubber, wax and paper insulated cables. Each type of material has its strength and weakness. For example, oil is suitable for applications with high operational temperature. Its dielectric breakdown strength, however, is lower than rubber. At the same time, long OF cables segments are also much more difficult to maintain. Another example is plant-fiber based insulations such as paper or Edison's jute insulation. Plant-fiber insulations have good thermal expansion properties and they are relatively easy to produce. In addition, the later wax paper insulations also have good dielectric breakdown strength, but they are much more susceptible to organic decay and chemical corrosion.

Eventually, polymer insulation became the mainstream choice. This is due to both technological progressions in the chemical industry and increasing demands in the power industry. The earliest polymer insulations are represented by rubber. The dielectric breakdown strength of rubber insulation such as neoprene rubber is between 15.7MV/m to 26.7MV/m. In comparison, silicone and mineral-based oil's dielectric breakdown strength is between 10MV/m to 15MV/m and much more difficult to maintain. Wax-paper insulation does offer stronger dielectric breakdown strength. Its breakdown strength is generally between 40MV/m to 60 MV/m. Newer polymer materials such as polyethylene, however, can reach dielectric breakdown strength up to 160MV/m. Polymer material is also more resistant to corrosion and decay, which significantly reduce the maintenance need.

Many types of polymers have been developed over the years to replace rubber. The most common type today is polyethylene and its derivatives. Polyethylene had been synthesized in laboratory conditions as early as 1898 by Hans Von Pechmann. The first industrial viable synthesis, however, was not done until 30 years later by Eric Fawcett and Reginald Gibson. Their process is later refined to a mass-production version by Michael Perrin in his high-pressure synthesis method. The method produces low-density resin of polyethylene. It is used in the later cross-link polyethylene (XLPE) development [4].

Polyethylene is a thermoplastic material. As the result, it can be easily molded at high temperature and retain its shape after cooling. The polymer possesses high ductility and impact strength. Thus, it is resistant to long-term physical wear. Chemically, polyethylene consists of non-polar, saturated and high molecular weight hydrocarbons

and has a tendency to crystalize. Overall, it is resistant to both acid and base corrosion. It also has low gas and water permeability. This makes it an ideal material for underground cable insulation applications. Later improvement such as XLPE changes the material type from thermoplastic to thermoset. This allows the cable to retain its shape during high temperature operations. In general, XLPE retain its strength in environment up to 150° Celsius. The first commercial XLPE insulated cable is developed by General Electric Company in 1963 [4]. Since then, XLPE has gained wide acceptance as cable insulation material. For example, by 1991, more than 90% of the installed cables in Japan utilize XLPE as insulation material [5].

1.2.2 Aging Infrastructure

1.2.2.1 State of the Overall Power Infrastructure

In recent times, aging infrastructure has become one of the central research topics. The phenomenon is observed in many fields of studies, including power system and the power utility industry. Due to the nature of power industry, aging infrastructure can have a significant ripple effect. It has far-reaching consequences for other parts of the society that depend on the continued and stable delivery of electricity.

In the past, many studies and assessments have been carried out on the problems faced by power utilities. A sample case study focuses on Minnkota Power Cooperative, Inc. It is a conglomerate power-utility, which focuses on generation and transmission. It is located in upper Midwest, USA. The company has eleven sub-members and twenty-five regionally associated electrical suppliers. Together, they serve more than 112,000 customers in North Dakota and northwestern Minnesota. In 2006, a study is carried out by the company in order to assess the condition of their existing infrastructures,

specifically, the condition of the power poles. In their study, it is discovered that their pole rejection rate is increasing at about 1% every decade since 1980. Rot has also been observed in the cross arms and it is increasing at a rate of 5% every decade. Equipment previously believed to be safe, such as pole anchors, is also showing signs of degradation and in need of maintenance. In summary, out of the 2,000 miles of 69kV lines maintained by the company, 33% are over 50-years old [6].

The situation experienced by Minnkota is not an isolated case. After the 2003 Northeast blackout, the US-Canada Power System Outage Task Force reported that the North American electrical grid included more than 200,000 miles of transmission lines operating at 230kV and higher, 950,000MW of power generation capacity and nearly 3,500 power utilities, which serve more than 100 million customers. A 2001 assessment from American Society of Civil Engineers (ASCE) gave the US energy infrastructure a rating of D+. The rating degraded to D in 2003 and continued to 2005. Assessment in 2013 gave the energy industry infrastructure a rating of D+ and it estimated that by 2020, there will exist an investment gap of 56 billion USD in distribution and 37 billon USD in transmission [7].

There are several reasons for the harsh assessment of US energy infrastructure. These reasons include natural cycles in infrastructure development, financial constraint and cultural shift. The electrical industry itself is more than 110 years old. During this time, it has become more and more important to the society. Thus, it continues to expand and grow. The overall expansion rate, however, is not linear. There were historical periods of rapid development where the infrastructure expanded at accelerated rates. The most relevant period to the current infrastructure-aging problem is the rapid expansion

between 1950 and 1960. It is estimated that in many power utilities, as much as 50% of the equipment is installed in the time-period between 1950 and 1960. This means by 2016, a large portion of the grid is operating equipment more than 50-years old [8].

The very nature of development cycle leads to the next cause of infrastructure aging---financial constraints. Rapid infrastructure expansion over a short period means a large portion of the existing infrastructure also reaches replacement age over a short period. Although this is a common phenomenon in many industries, the effect on power industry is somewhat different. For power infrastructures, the end of a cycle is marked by investments in very large amount of fixed sets. Understandably, this also means high capital requirement. As the result, the replacement process has been slow and in some cases, they are halted completely.

The culture shift is a complex issue. On the surface, culture shift can be observed in form of the aging work force in the power industry. In the Minnkota case mentioned above, one of the main difficulties faced by the maintenance team is reduction in available work force. The total number of employee in Minnkota has steadily declined since 1979. In 2006, Minnkota employs 320 employees at both headquarter and generation plants. The company asset includes 2,143 miles of 69kV lines, 226 miles of 11kV lines, 577 miles of 230kV lines and 465 miles of DC lines. The construction and maintenance of these lines are coordinated by merely four employees. On the operations sides, company has 28 linemen at both headquarter and in the field. They are expected to serve a 34,500 square miles region [6]. The decrease in available work force means there is insufficient number of personnel to service and operate the equipment, even if the equipment itself is physically intact.

A deeper part of the culture shift lies with fundamental understanding of power infrastructure. Research on the effect of aging on infrastructure performance had begun almost as soon as power system itself becomes reality. Due to the development cycle issue, however, until 1990s, maintaining aging infrastructure was not deemed a critical issue. Before 1990s, vast majority of the grid is less than 30 years old. Since the industry operates in a priority system, the need to mitigate the effect of aging equipment is overridden by other tasks. Although the need for replacement does continue to occur, the relative young-age of the infrastructure means the industry devoted little effort on research new technologies and techniques on prolonging the operational lifespan of the equipment. During this period, infrastructure aging is generally viewed as an issue that will eventually occur, but it will be far enough in the future and not an immediate concern. As the result, many engineers and managers in the industry did not gain any experience or skill in preventing infrastructure aging. In fact, some of the traditional measures on aging equipment management actually atrophied during this time-period [8]. The combined effect of development cycle, financial constraint and culture shift means the new generation of power engineers must face an issue that is long overlooked and overdue.

1.2.2.2 Underground Cable in Aging Infrastructure

Among various aspects of the power system, underground cable system is one of the worst affected. According to US Department of Energy, there are about 5000 circuit-miles of underground transmission cables in US. These cables generally have a designed service life of 40 years. By the current decade, almost half of the underground cables in

US are approaching the limit or already exceeded it. In comparison, it is estimated that about 40% of the transformers are approaching the limit of their service life [9].

When assessing the condition of underground cable system, an important piece of information to remember is the cyclical nature of infrastructure development also implies periods of slow expansion. WWII is one example of slow expansion in power infrastructure. Another example is discovered after researching into overall US power pole replacement. The research indicated that immediately following the rapid expansion in the 1950s, there is a period of limited expansion. Specifically, in late 1960s, the oil embargo from Arabic states triggered a period of slow expansion in US power industry [10].

From financial perspective, this means there are periods of "calm". In these periods, less number of equipment needs to be replaced and capital availability is less constrained. These periods represent opportunities for the industry to catch up on its infrastructure investment gap. In order to take advantage of these periods, it becomes important to prolong the lifespan of the existing equipment.

Over the past decade, the industry has discovered a number of procedures that allow power utilities to extend the lifespan of their equipment. In general, these procedures focus on proper maintenance of the equipment [11~12]. They can be summarized in the following steps:

1. Understanding Aging Effect on the Equipment
2. Monitoring Status of the Equipment
3. Performing Preventative Maintenance Procedures on Any Observed/Predicted Issues

In this dissertation, the effort will concentrate on understanding the effect of water-tree in long-distance cables, methodology on monitoring the system for water-tree appearance and assessing the condition of water-tree affected system.

1.2.3 Water-Tree Characteristics

Water-tree is a material degradation process typically associated with non-metallic materials such as cable insulation. The process occurs in the presences of liquid (primarily water) and changing electric field. If aged electrical infrastructures are exposed to high level of humidity for prolonged period, there will be high possibilities of water-tree formation.

Water-tree formation is characterized by strings of ellipsoidal micro-fracture chambers forming within the insulation material. These strings are referred as branches. The micro-fractures are the main sites of cable insulation breakdown. Typically, the fracture chambers will be a few microns to a few hundred microns in diameter. Adjacent chambers will be interconnected by additional, smaller fractures in the shape of thin tubes. These tubes are a few microns in diameter [13].

The mechanic behind water-tree growth is still a subject of ongoing research. One hypothesis is that the micro-fractures are created by Maxwell-Wagner interaction induced by the shifting electric field across the water/XLPE interface. Specifically, when there is sufficient amount of moisture present, water and XLPE insulation will form a material interface within the fracture sites. According to Maxwell-Wagner polarization theory, a shifting electric field will cause a charge-separation at the material interface, even if the individual material is not responsive to the electric field by itself. The process is

accelerated by the presence of impurities. This charge-separation may create fracture chambers through two difference mechanisms:

First, it is observed that under Maxwell-Wagner polarization, the charge separation generates a shifting mechanic stress across the material interface [14]. This stress causes physical breakdown of the insulation layer through mechanical wear.

Secondly, the charge separation itself leaves ionic residue at the material interface, thus increasing the possibility of oxidation of the material [15].

` Currently, certain cables are manufactured with tree retardant property. For these cables, the insulation layer is doped with additional chemicals to inhibit charge separation at the material interface. Long-term exposed to strong, shifting electric field, however, will force many of these chemicals to migrate. Consequently, these cables may lose its tree retardant property after a few decades in service [16].

Unlike the more commonly recognized electrical-trees, water-tree formation is a significantly slower process. For electrical-trees, strong overload can create intense corona discharges. The resultant heat will burn through the cable insulation in the matter of minutes. In comparison, water-tree growth is not accompanied by secondary phenomenon such as corona discharge [17]. As a result, water-tree formation often requires years or even decades. On the down side, it is a mechanical/chemical process and it will continue to occur as long as moisture and electric field are present. The process occurs regardless of temperature; therefore, electrical-tree prevention methods, such as insulation, do not completely inhibit water-tree growth. Currently, the main treatment for water-tree is sealing the breach at the affected section of cable using adhesive fillings.

The presence of a fracture chamber nearby tends to weaken insulation integrity. As the result, strings of the fracture chambers tend to show tree like growth pattern. It starts from a certain origin and grows into branch like structure. The origin of a specific water-tree can appear due to a number of reasons. For example, it can be irregularity in chemical composition in form of impurities. Alternatively, it may be physical in nature such as small damage to the cable insulation surface or manufacturing defects such as micro-crack in the insulation material. One of the laboratory methods to stimulate water-tree growth is using sand paper to create physical wounds on cable insulation.

The growth pattern for a specific water-tree can be random. In particular, water-tree growth experiments in the past have demonstrated that even under identical laboratory conditions, water-tree can grow into different shapes [18]. This random nature makes difficult to build a mathematically model for water-tree. Fortunately, water-tree growth does have a number of common trends. For example, stronger electric field strength tends to produce long tree branches. Overall shape of the water-tree is tied directly with the frequency composition of the applied electric field [19]. As a result, it is possible build a general model for water-tree using parameters from typical operating conditions of the cable.

1.2.4 Effect of Water-Tree in Power System

The presence of water-tree can lead to a number of problems. Depending on terminal-stage development, water-tree can be classified into two categories:

Category-1 water-tree faults, hereby referred as hybrid-tree faults, are characterized by the appearance of severe electrical-treeing in the final stage of insulation breakdown. They can be seen below in Figure 2:

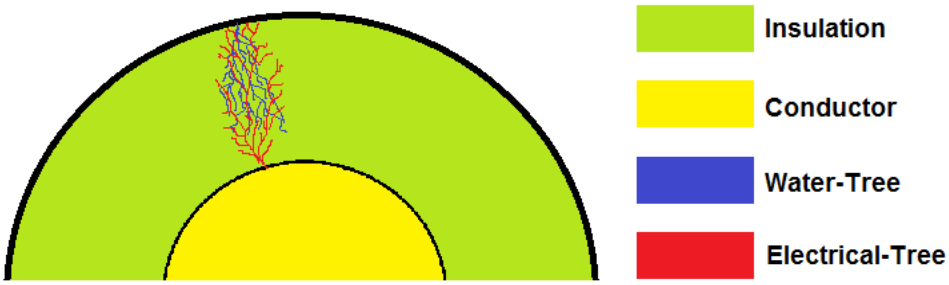

Figure 2: Hybrid-Tree Faults

In hybrid-tree faults, after water-tree corrodes through a large portion of the insulation (but not completely), the service voltage of the cable becomes sufficiently high, which the remainder of the insulation can no longer withstand the electrical stress. The insulation rapidly burns out in catastrophic electrical discharges. Depending on the severity of the discharge, the insulation material above the discharge point can be damage as well.

Unlike water-trees, the terminal-stage electrical-trees can be created in seconds instead of years. Hybrid-tree faults have short creation time and high voltage/current requirement; therefore, they are mainly influenced by system transients instead of steady state conditions.

Category-2 water-tree faults, hereby referred as pure-tree faults, are caused by water-tree branches fully breaching the insulation layer. They are can be seen below in Figure 3:

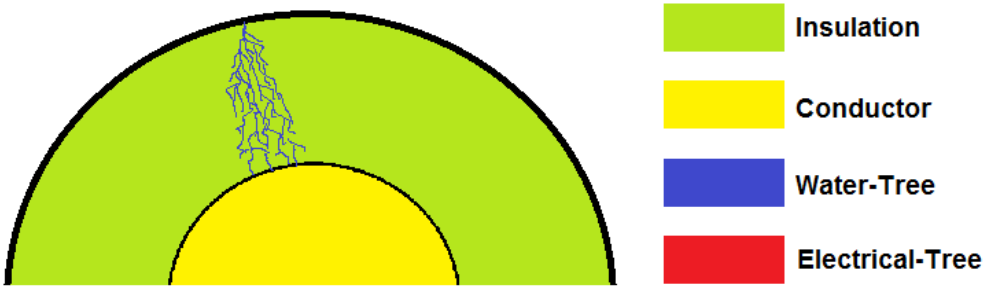

Figure 3: Pure-Tree Faults

In pure-tree faults, the sole conducting channel is formed by water-tree branches. Although these final-stage tree branches are larger comparing to their developing counterparts, they are still only a few hundreds of microns in diameter. As the result, pure-tree faults have significantly higher fault impedance due to smaller insulation-breakdown passageways.

The creation of pure-tree faults is mainly influenced by the steady state operating condition of the system. A unique characteristic of purely-tree faults is that the conductivity of the fault region fluctuates with environmental moisture. Specifically, when the environmental moisture is low, purely-tree faults impedance increases and sometimes become unidentifiable by conventional observation and detection techniques. When the moisture content is high, pure-tree fault impedance decrease and may produce noticeable voltage drop in the system.

Although purely-tree faults appear to be the lesser issue to the grid stability, especially if the moisture content is low, the very presence of a breach in the insulation layer means possibility for future corona discharge. A sufficiently large transient will break through the weakened insulation layer and the resultant discharge will rapidly breaks down the insulation material; therefore, pure-tree faults should be treated with the same level of caution as its hybrid-tree fault counterparts.

1.2.5 Detection of Water-Tree

Due to its random nature, water-tree modeling is a relatively new topic only made possible by computer-assisted analysis. The detection processes, however, have existed much longer. The industry has long been aware of the existence of water-tree. Over the years, a number of attempts have been made to detect the presence of water-tree in cable

insulations. In general, two classes of methods have been used to assess the condition of cable insulation: Tan-Delta and Partial-discharge.

1.2.5.1 Tan-Delta

Tan-Delta measurement is one of the most common testing methods used in the industry. The principle behind Tan-Delta assumes ideal cable insulation behaving as a capacitive element in the system; therefore, electrical current passing through the cable will exhibit similar behaviors to current in a perfect parallel-plate capacitor. The voltage and current will be phase-shifted 90 degrees apart. If the insulation is not perfect, however, then the phase shift will no longer be 90 degrees. The irregularity in the insulation will appear as resistive current. These elements will cause the voltage-current shift to become less than 90 degrees apart. The Delta part of the method refers to the angular difference between the ideal phase shift and the actual phase shift angle as show below in Figure 4

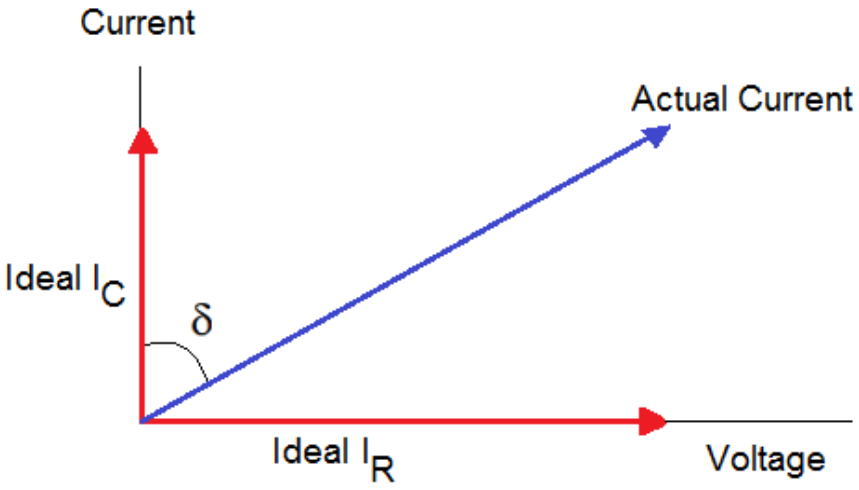

Figure 4: Voltage and Current Phase Shift in Tan-Delta Method

The x-axis and y-axis are voltage and current for ideal insulation. The phase difference between the ideal current and actual current is referred as the loss angle. Greater loss angle indicates more degradation in the cable insulation.

There are several ways to apply Tan-Delta testing method and they can be broadly classified into three categories: very low frequency (VLF), operational power frequency (OPF), and very high frequency tests (VHF).

The VLF test takes advantage of the fact that the impedance of the capacitive element increases drastically at near-DC frequency. Under VLF, the cable degradations functions as resistive elements and become more visible in the output readings. As the result, VLF reduces the power requirement for the test and it is the more practical method in the field. In general, VLF tests are conducted at the frequencies between 0.1Hz and 1Hz.

In theory, OPF test (50Hz or 60Hz depending on the area) should reveal the exactly behavior of the cable under standard operating conditions. Unfortunately, Medium and high voltage cables often have very large innate capacitance; therefore, to perform the Tan-Delta test, a large charging current is required. The equipment requirement may make OPF tests impractical in the field [20].

Although VLF method proves to be effective in many situations, its low frequency can be a hindrance in other situations. For example, when dealing with very-low capacitance and very-high resistance phenomenon such as water-tree growth, low frequency can be a hindrance. Field-testing indicates that for low capacitance situations, the dielectric current from VLF testing method is simply too small to be identified [21].

For these situations, VHF methods are used. Similar to VLF methods, VHF methods take advantage of the behavior of capacitive elements in different frequencies. Under high frequency, the impedance of the capacitive elements is greatly reduced and the result becomes more visible to the observer. There are several methods for analyzing the result from VHF tests. Some of the methods observe the terminal voltage/current phase shift. Other method such as capacitor tests are developed to observe material behavior. The testing frequency for VHF tests can range from 300kHz to several GHz [22].

In the past, all three categories of the Tan-Delta methods have been applied to water-tree detection. The tests yielded various results depending on the specific conditions of the test. In one OPF test, the source voltage was injected to medium-voltage underground XLPE cables. The testing voltage started at 2kV and increased in 2kV increments all the way to 10kV. The test indicated that for cables with sufficient amount of moisture, OPF method delivers tan-delta reading at scale satisfactory to IEEE standards. Unfortunately, it is also indicated that for dry scenarios, the resultant Tan-Delta is much smaller [23].

VLF water-tree detection also had success in certain situations. In one case, 22 kV-rated cables were submerged under water for 45 days due to flash flooding. Afterwards, VLF tests were performed in 6kV increments all the way up to 23kV. The test determines that the IR values of the cables were in the range of 3GΩ to 4GΩ. Subsequent DC test at 50kV also revealed leakage current from 73μA to 76μA. Similar to the OPF test, the VLF test indicated that the primary reason for the large leakage current

reading is significant water ingress into the cable, including reasons such as cracked insulation layer due to poor workmanship [24].

There exists other example of water detection using VLF tan-delta methods. For example, Hong Kong authorities discovered that the Tan-Delta loss factor is also highly influenced by water ingress into cable joins [25].

In general, successful examples of VLF and OPF water-tree tests have a common theme. In all the successful examples, water-tree has already made significant advancement into the cable insulation and the insulation layer has been fully breached, by water-tree itself or other environmental damage. Unfortunately, this condition is not necessarily true for every water-tree related situation. For example, in preventative maintenance, water-trees are general small and still in development. These water-trees may not breach the insulation layer for decades. In these situations, VHF testing methods are significantly more effective. Many of the VHF methods, however, such as the aforementioned capacitor method, have very limited range. Other methods such as traveling-wave methods are only useful to determine the presence of degradation, but not its severity.

1.2.5.2 Partial-Discharge

Partial-Discharge (PD) refers to both a physical phenomenon and a method for detecting weakness in cable insulation. The physical phenomenon refers to an event in which the electrical current flows into unintended destination via break in insulation. In this sense, partial-discharge and line faults are similar. In practice, partial-discharge typically refers to the specific phenomenon where the insulation material is broken down

by events such as high electrical stress or physical wear and electrical currents are leaking through.

At the same service voltage level, partial-discharge current is generally lower than line-to-ground fault current; therefore, partial-discharge's immediate threat to system stability is smaller than line faults. Unfortunately, partial-discharge is an evolving phenomenon. Prolonged presence of partial-discharge may weaken insulation material and allows other disruptions to occur. For example, if electric field strength is high, partial-discharge may evolve into corona discharge. In this case, the ionization of the surrounding air will produce large amount of heat and permanently damage the insulation material. Furthermore, partial-discharge may be create large scale, permanent break in the insulation material and allows line-to-ground faults to occur.

The Partial-Discharge detection method is used to detect potential weaknesses in the insulation material by searching for signs of partial-discharge. Comparing to the capacitive-element focused Tan-Delta, PD test focuses on leakage current and conductive pathways. As the result, PD methods emphasize on resistive aspect of the system. In some situations, both Tan-Delta and PD tests can be carried out simultaneously [20].

PD test may be carried out both online and offline. Currently, offline test is the preferred method for two reasons: First, since the magnitude partial-discharge measurement is typically much smaller than the operational voltage/current level, the measurement is best taken without interference from other sources. Second, PD tests place heavy stress on the cable. In some situations, the test itself may shorten the lifespan of the cable; therefore, it is preferable to use the less stressful offline test.

Similar to Tan-Delta tests, PD tests can be conducted at various frequency ranges. Although Tan-Delta method prefers the low power requirement of the VLF tests, the effect of PD test is better at OPF since larger voltage source directly increases the clarity of the test result [26].

The International Electrotechnical Commission (IEC) has established key guidelines for offline cable test. The standards are available at IEC60270 and IEC60885-3. Offline PD test can be conducted using these standards [27].

In off-line tests, one of the most commonly used methods is time-domain reflectometry (TDR). TDR shares the same principle as other detection methods such as travelling-wave. In both cases, the target location (fault or partial-discharge site) will function as a discontinuity in the line and creates reflected waveform that can be analyzed.

In case of the PD test using TDR, the current source is typically capacitive-coupled to the cable terminal. A pulse is generated by the current source and travels along the cable. The current profile at the cable terminal is recorded and interpreted to determine if partial-discharge is present.

In practice, TDR has a few limitations. For example, if the partial-discharge site is too close to the other end of the cable segment, the TDR test may encounter difficulty in differentiating the reflected waveform of the partial-discharge site and the reflection from cable terminal.

In general, proper interpretation techniques are critical for successfully performing PD tests. In the past, data interpretation from PD test can be classified into three categories: time-domain, frequency-domain and impulse response.

In time-domain analysis, the data interpretation focuses on pattern recognition. Since the partial-discharge sites represent a fixed set of weakness in the insulation layer, the reflected pattern should be relatively stable and predictable. By identifying the waveform patterns, it is possible to determine if a partial-discharge site has appeared on the cable.

In frequency-domain analysis, the emphasis is on proper separation of the frequency bands produced by potential partial-discharge sites from other sources. By applying Fourier-Transformation on the TDR data, the time-domain representation is converted to a range of frequency responses from the cable. Similar to the time-domain analysis, since the potential partial-discharge sites are relatively stable features, it will generate a predictable set of frequency responses.

The principle of impulse response approach is similar to the other methods. In this approach, band pass filters are applied to the terminal reading at predicted range. The resultant impulse response of the filter is proportional to the actual partial-discharge event and can be used to determine if a potential site has appeared [28].

One of the main issues associated TDR interpretation is the presence of noise. Unlike faults analysis, the scale associated with PD test parameters is significantly smaller. Thus, the test result is much more susceptible to interference from noise. In all three approaches, noise elimination is a critical part of the actual implementation process.

Noise is an even more significant issue for online PD tests. Both the fundamental and harmonic components of the operational voltage/current may generate noise. In addition, the operational waveform itself may negatively affect data clarity. In recent years, however, improved frequency filtering methods and more accurate measurement

instruments have brought renewed interest in online PD tests. Although the cable stress of online test remains high, it does not require the line to be disconnected. In this case, the benefit of maintaining critical grid connection may out weight the risk for cable damage.

Another significant issue associated with TDR is the range of the detection process. Due to the small scale of PD test parameters, distance attenuation sets a limit on the length of cable segment. Experiment results indicated the maximum range of TDR in PD test is determined by the following parameters: insulation material characteristic, high-frequency cable characteristic, types of shielding and cable dimensions. Combined with the filtering methodology and the instrument accuracy, these parameters determine the maximum range of the TDR in PD test [29].

The presence of noise also affects the range of the test. Distance attenuated signal is further degraded by the presence of noise. In certain situation, if the noise is too great, the effective range of TDR may be greatly reduced.

The relationship between PD test and water-tree detection is complex. Depending on the stage of water-tree development, the effectiveness of PD test varies drastically. If a water-tree has fully breached the insulation layer, its structure is more resistive than capacitive. In this case, PD test is often more effective than VLF or OPF Tan-Delta tests. On the other and, early-stage water-tree is capacitance-dominant in nature and it exhibits very limited amount of partial-discharge.

Empirical experiment showed that under the current technology, PD measure is observable for insulation voids greater than 3mm [30]. Since early-stage water-tree micro-fracture chambers are often measure in microns, the accompanied partial-discharge

is insignificant. Overall, PD tests are more effective on later-stage water-tree detection instead of preventative maintenance.

1.3 Research Contribution

Currently, water-tree is still a less researched phenomenon. In particular, there is a notable deficiency of mathematical evaluation of water-tree characteristics. For example, empirical measurement of water-tree impedance has been available for decades. There is however, limited research on the specific mechanic of water-tree impedance.

As the result of this deficiency, the currently available water-tree detection methods are general reactionary. Their methodology and implementation are both under the assumption that water-tree has developed into a certain stage and its behavior is relatively stable. For example, although Tan-Delta methods exists for water-tree detection, the method emphasize on water-trees that have already developed enough to cause a phase shift in the output waveform. Similarly, PD methods suffer range limitation on very long distance cables and they can only be used for late-stage water-trees.

Due to the rapidly aging power infrastructure, reactionary detection is no longer sufficient. For example, if water-tree develops to the point that it is visible to the conventional PD method, then its leakage current is already strong enough to reduce the remaining service life of the cable. If the situation worsens and the partial-discharge develops into a full-fledge line to ground fault, then the customers may suffer prolonged power outage. As the result, utilities prefer potential issues to be resolved by preventative maintenance instead of reacting to a power failure. In order to perform preventative maintenance, however, the utilities must be able detect and locate water-trees when they are still in early development stage.

To meet this demand, mathematical models must be constructed to understand water-tree behavior in all development stages. Next, a method must be developed to detect and locate water-tree in early development stage. Finally, the implementation of the method must be reasonable.

1.3.1 Mathematical Modeling of Water-Tree in Underground Cable Insulation

The first step of understanding water-tree behavior is developing a mathematical model. In past, the main challenge on constructing the mathematical model has been the randomness of the water-tree structure. Water-tree growth is motivated by a very large number of parameters and many of these parameters are highly random as well. As the result, model construction and analysis have not been practical. Recent advancements in computation and modeling technology, however, have reduced the difficulty of the task; therefore, it is now possible to construct generalized water-tree models in order to observe the effect of early stage water-trees on the system.

Empirical observations from Tan-Delta tests indicate that early-stage water-tree is primarily a capacitive structure. Physically, the capacitance of water-tree afflicted cable insulation is determined by the local material composition. Specifically, it is decided by the arrangement of dielectric insulation material and water passageways. Thus, at fundamental level, the physical structure of water-tree afflicted insulation shares similarity with multi-dielectric capacitors and the model can be built using similar principles.

The structure of water-tree afflicted insulation is more much complex than the average cylindrical capacitor with multi-dielectric; therefore, the mathematical representation must be adjusted accordingly. Fortunately, under finite element analysis

scales, the complex structure of water-tree can be simplified and mathematical resolution becomes feasible.

Determining the mathematical model of the water-tree offers several advantages: First, mathematical model allows understanding and prediction of cable parameters associated with water-tree growth. Second, the model can be integrated in larger system studies and determine its effect on overall system. Third, the model can be used to test potential detection and estimation methods.

1.3.2 High Frequency Pulse Detection of Water-Tree

Results from the mathematical model shows that an early stage water-tree is primarily capacitive and its magnitude is in pico-Faraday range. Since the impedance is extremely high and no conductive path is available, PD methods cannot be directly applied. Due to the low capacitance, VLF and OPF Tan-Delta methods also cannot be applied to early stage water-tree detection.

In the past, VHF Tan-Delta methods have proven to be useful in detecting low-capacitance cable insulation weakness. After testing the VHF Tan-Delta method using synchronous PMU measurement, however, Tan-Delta method proved to be ineffective due to the extremely low amount of phase shift; therefore, new method must be developed.

The main issue associated with Tan-Delta test in early-stage water-tree test is the small phase shift. Fortunately, TDR based PD tests in the past have proven to be effective on dealing with the particular issue; therefore, the new method will consist of elements from both Tan-Delta and Partial-discharge test.

By applying TDR to the cable under VHF conditions, a visible response can be obtained from the early-stage water-tree. The new method is named High-Frequency Pulse Detection Method (HFPD).

TDR data is not useful without corresponding data interpretation method. Experiments show that for early-stage water-tree of a specific capacitance, a corresponding frequency range can determined using the HFPD Method. The frequency range will produce a distinct response pattern on the TDR waveform and it is named the benchmark frequency range. A method is then developed to determine the water-tree capacitance using cable parameters and the benchmark frequency range.

The HFPD method and the mathematical interpretation method will allow utilities to determine the location and severity of an early-stage water-tree. Using the information, utilities can estimate the remaining lifespan of the cable and site of the eventually breakdown. Thus, preventative maintenance can be performed to prolong the lifespan of the cable. In addition, determination of water severity and development rate also allow utilities to estimate the urgency of the maintenance process and allocates resources accordingly.

1.3.3 Early-warning of Water-Tree Presence using Deviation Comparison Method

Although the HFPD and its interpretation method can determine water-tree location and severity, its practical implementation has a few issues. Like all high-frequency methods, HFPD requires a large magnitude input pulse. The required instrument is commercially available, but it places high stress on the cable; therefore, it must be a selective test. The implication is that before HFPD Method can be applied, the utilities must already be certain of water-tree presence in the cable segment. To this end,

a method is developed for estimating the probability of water-tree presence in the cable and serves as the early-warning system for water-tree appearance.

Since the method is meant to be omnipresent, it cannot use specialized instruments such as high-frequency pulse generator of any kind. VLF and OPF methods remain ineffective, thus the only alternative is utilizing naturally existing high-frequency events in the system, such as very high frequency switching transients and greater than 3kHz harmonics.

From HFPD results, it is known that the naturally occurring high-frequency events in the system meet the minimum requirement for identification purpose. Their frequencies, however, are sufficiently low, in which data clarity is an issue. The high-frequency events also vary greatly in both magnitude and frequency. In addition, their magnitudes in general are small comparing to the requirement for HFPD. These factors greatly reduce the accuracy of the data interpretation process. It is determined that the original data interpretation process for HFPD Method is not sufficient.

A new data interpretation method is developed for the early-warning system. The deviation-comparison method determines the difference between predicted data and actual data. The difference is then compared across multiple time intervals. Finally, the resultant standard deviation is compiled. Experiment results show that potential sites of water-tree appear as large spikes in the complied standard deviation comparison graph. The method is highly sensitive and does not requirement specialized instruments and it estimates the probability of water appearance on the cable segment.

The early-warning system is a critical part of implementing the early-stage water-tree detection process. Without the early-warning system, water-tree detection process is

simply too resource intensive and potentially damaging to the grid infrastructure. In addition, the principle behind the early-warning process can be modified and adapted for other types of cable monitoring process.

1.3.4 Computational Margin Accumulation in Water-Tree Analysis

Even after the implementation of the HFPD method and early-warning system, it is important to improve their accuracy and reliability continuously. Error and margins exist for many engineering methods and techniques, particular for high sensitivity processes such as early-stage water-tree detection; therefore, it is necessary to explore potential directions that will further refine these methods.

The first task is developing a mathematical solution to the capacitance of water-tree. The solution will allow the utilities to estimate the progression of water-tree corrosion. The next task is to determine potential sources of error margins associated with the solution. Since the water-tree detection process is subjected to many limitations, such as accuracy of the measuring instrument and modeling accuracy, error margins inevitably appear in the computation process. More importantly, these margins will accumulate and adversely affect the accuracy of the final capacitance estimation.

The detection methods can be improved in many ways. Short-term solution such as numerical averaging can eliminate certain amount of error. Improvement at fundamental level, however, can only be made by increasing the quality of the raw data measurement. The standard deviation distribution of the final solution demonstrated that error margins in water-tree detection process are fundamentally dominated by system time-measurement; therefore, it is possibly to greatly advance and improve the water-tree

detection process by developing better technologies and techniques for operational time-measurement.

1.4 Chapter Summary

For utilities, information has become more precious by the day. The aging power infrastructure created the need for preventative maintenance and the process is entirely dependent on the obtaining proper operational information from the system. Early-stage water-tree detection is part of this need and solution is only possible due to continued advancement in computation and measurement tools.

By constructing a mathematical model for water-tree using computer assisted analysis techniques, water-tree behavior in power system can be studied in detail. HFPD and its data interpretation method are developed based on this mathematical model and they demonstrate potential abilities to locate and assess the condition of cable insulation using only terminal data. The early-warning system ensures proper implementation of the method. Finally, the error margin analysis shows potential direction to refine the accuracy and reliability of these methods.

Chapter 2

Mathematical Modeling of Water-Tree in Underground Cable Insulation

Establishing a mathematical model for water-tree is advantageous for many reasons. First, the mathematical model can be used to determine the behavior of water-tree in large systems. Throughout its development stage, changes in water-tree characteristic are represented by gradual expansion of tree branches into adjacent cable insulation. The shift in physical structure produces corresponding electrical changes. For water-tree, these changes can be observed as long-term change in cable parameters. By studying these changes, it becomes possible to develop appropriate detection techniques for water-tree.

Second, mathematical models allow better understanding on the effect of tree-branch distribution. One of the fundamental issues associated with water-tree detection is that many water-tree characteristics are only made into mathematically viable and computable data through estimations and generalizations. One such example is the relative permittivity for different regions of water-tree afflicted cable insulation material. Technically, the specific location and dimension of each individual tree-branch can be observed using microscope and they can be recreated in 3D simulation. The computation power and time investment required for such an approach, however, is simply too large to be practical; therefore, viable method of water-tree modeling needs to analyze the distribution of tree-branches at a higher and more generalized level. For example, assuming the water-tree case is an average representation of the phenomenon, the

relatively permittivity of the insulation material changes linearly and gradually from one material boundary to another.

Third, mathematical models provide theoretical support and validation for empirical measurements of water-tree characteristics. Currently, vast majority of the available water-tree related studies are limited to empirical observations. These studies were carried out by separate groups and often yielded vastly different results. A mathematical model will provide better understanding on the significance of these empirical measurements. It will also explain the cause of discrepancies in the previous studies.

For these reasons, building a mathematical model is the first step towards developing accurate detection methods for early-stage water-tree in long-distance underground cable insulations.

2.1 Water-tree Formation and Structure Analysis

Physically, water-tree is the collective representation of a series of insulation cracks and fractures. A sample insulation material is shown below in Figure 5:

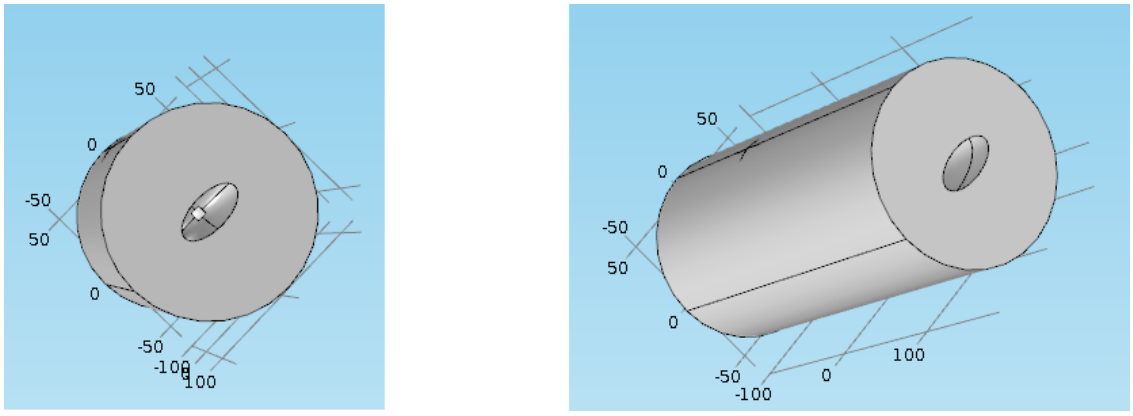

Figure 5: Insulation Material: Front View (Left) vs Side View (Right)

The micro-fracture chambers are small, ellipsoidal voids in the insulation layer. They are ellipsoidal structures and represent the smallest unit in the water-tree structure. Depending on the corrosion progression of water-tree, their sizes may vary from a few microns to hundreds of microns. A sample fracture-chamber is shown below in Figure 6:

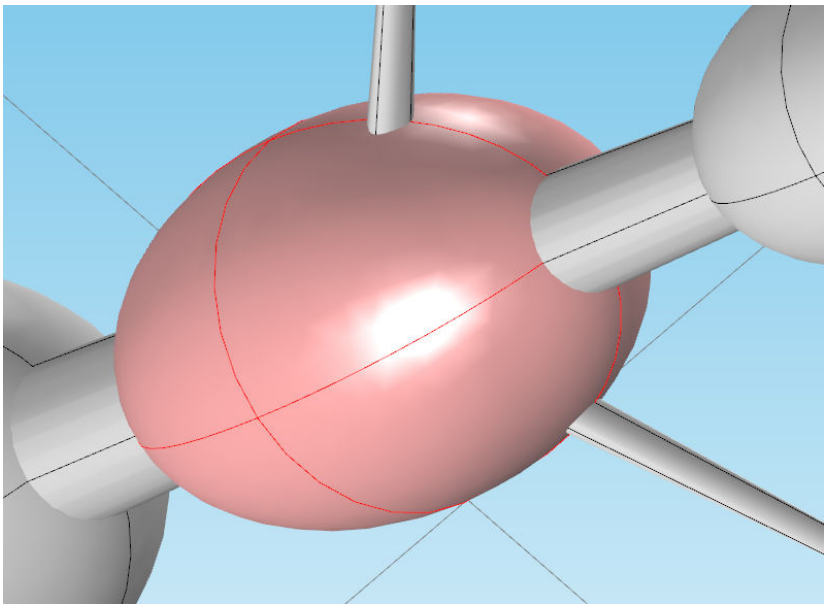

Figure 6: Micro-Fracture Chamber in Cable Insulation

2.1.1 Water-tree Formation

The micro-fracture chambers can be created by a number of processes. These processes can be either mechanical or chemical in nature. For example, manufacturing defects may leave cationic impurities in the material such as sodium, potassium, and iron deposits [31~36].

Alternatively, the impurities may also be ionic in nature, such as chloride. These impurities may create fracture chambers in two processes: heating and impurity diffusion. Both processes are characterized by a disruption in the established polymer chain. The disruptions weaken the crystallinity of the polymer insulation material. When these weak

points are exposed to both strong shifting electric field (but not strong enough to cause outright dielectric breakdown) and moisture, fractures can occur due to chemical corrosion and mechanical breakdown through Maxwell-Wagner force.

Chemical breakdown of the insulation material can be the result of oxidation. The oxidation process may be driven by the free alkyl radical to alkoxy radical process [37].

As of 2016, most of the commercial underground-cable insulation utilizes cross-linked polyethylene. Comparing to the traditional high-density polyethylene, XLPE tends to have better thermal characteristics, but it does not possess direct resistance to the alkyl radical oxidation process. It is observed that higher operational temperature may accelerate the process.

Another cause of micro-fracture chamber formation is localized oxidation due to ionic impurity migration. In this process, electrical field drives the existing ionic impurities within the cable insulation layer into new locations. If the new location is exposed to oxygen, such as surface of the insulation layer or pre-existing micro-fracture chamber, then localized oxidation may occur. The ionic impurity migration is especially significant in DC cables lines [38~45].

In both processes, the immediate result is a break in the polymer chain; therefore, the crystallinity of the material is weakened and micro-fracture formation becomes more likely. Although the oxidation processes are accelerated by the presence of water and the alkyl radical process itself does produce water as a byproduct, both processes can also occur without the presence of water. This is in contradiction with the empirically observed water-tree formation conditions. Namely, water-tree formation is only observed when there is significant amount of moisture present (greater than 65% humidity) [46].

Additionally, the oxidation process typically occurs in localized regions. Although pre-existing micro-fracture chambers weakens the material, the oxidation process alone is insufficient to create the long chains of micro-fracture chambers in the typical water-treeing process. For example, in ionic-migration oxidation, although it is certainly possible for the process to create a single or clusters of localized micro-fractures, creating a long chain of micro-fracture chambers like the water-tree branch will require ionic impurities to be present at the entire length of the chain. Furthermore, a single water-tree may include dozens to hundreds of branches. The likelihood is very low for ionic impurities to be available along the all the branch locations. Thus, additional mechanics must exist for the water-tree formation process.

One likely cause of the continued chamber-formation process is the Maxwell-Wagner force generated by liquid/material interfaces [47]. In Maxwell-Wagner model, the interface of two materials, especially when one is a dielectric material, will react to a frequency shifting electrical field. In particular, a directional mechanical force will be generated and it will be repeated applied to the interface. In the case of the micro-fracture chambers, when sufficient amount of moisture is present, the accumulated water in the chamber will form an interface with the insulation material at the fracture-chamber wall. When sufficient electric field is applied, the generated Maxwell-Wagner force will apply repeated mechanical stress to the chamber wall. Although the force is relatively small comparing to the structural integrity of the insulation material, prolonged application of the stress may eventually wear down the material. This is consistent with the empirically observed water-tree growth rates in the field.

There are other hypotheses on the factors that influence water-tree formation. For example, previous laboratory testing indicates that water-tree development in polyethylene with the presence of aqueous salt solutions is influenced by the diffusion constant of the salt in the polymer. Salt molecules will accumulate in locations with increased electric fields and serve as condensation nuclei for liquid water. Aqueous solution of the salt will be formed as result. Reduction of saturation pressure for the salt solution will attract additional water through the diffusion. Specific chemical property of the salt does not seem to have a major effect [48].

Water-tree growth is still a less understood subject. For example, under with the Maxwell-Wagner force hypothesis, the formation of inter-fracture chamber connection is not explained. An inter-micro-fracture chamber connection is show below in Figure 7:

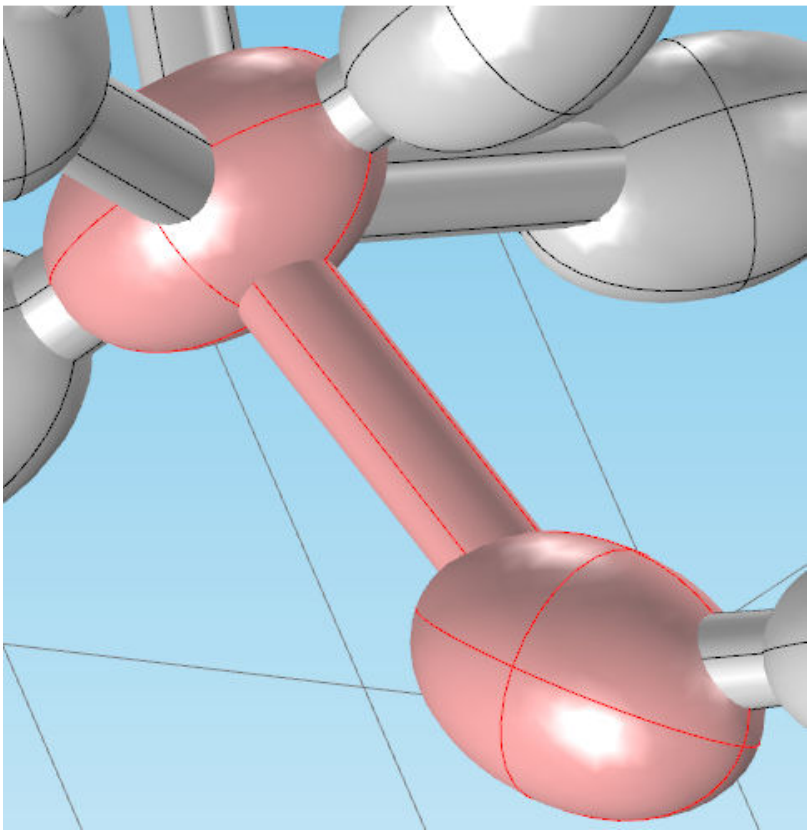

Figure 7: Interconnections between Micro-Fracture Chambers

A “branch” of the water-tree is formed by dozens of interconnecting ellipsoidal micro-fracture chambers. The chambers are connected by very thin tubular structures, which are less than five microns in diameter [49]. From electrical perspective, these tubular structures represent high impedance choke points during the formation of water-tree. Once the final breakdown occurs, however, the tubular structures will rapidly widen due to dielectric heating.

The initial breakdown point of the insulation material is referred as the root of the water-tree. It is shown below in Figure 8:

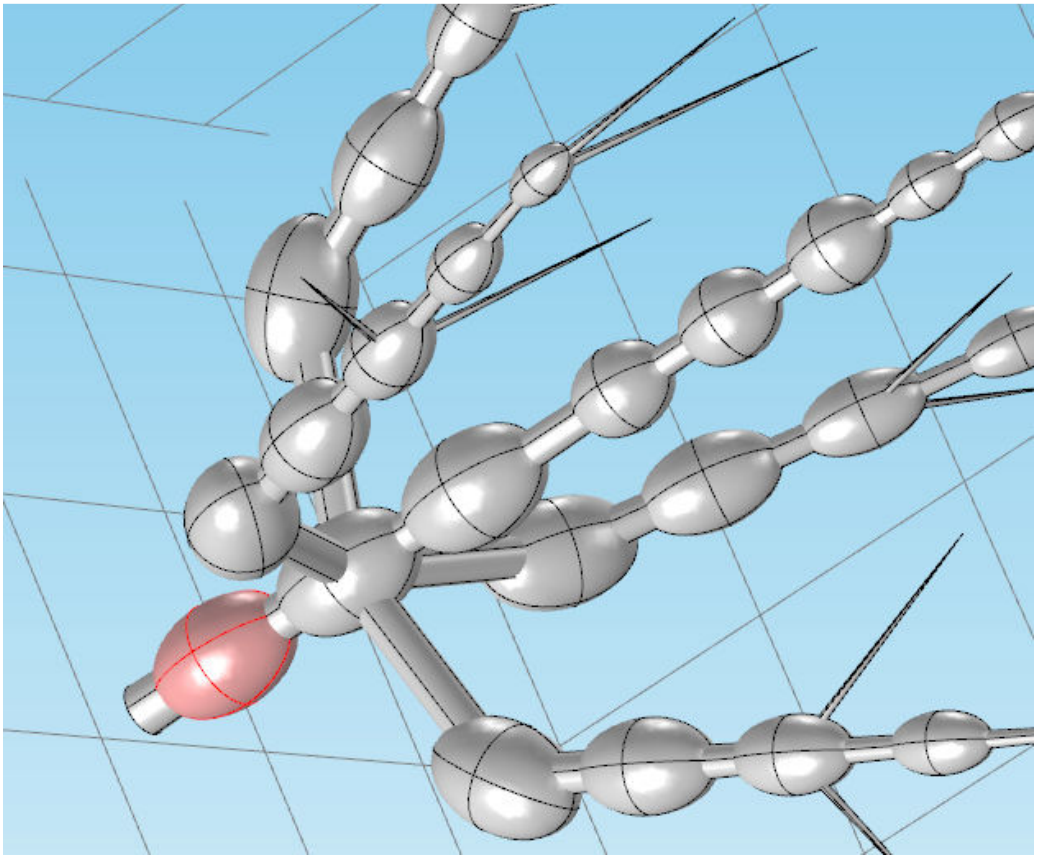

Figure 8: Root Micro-Fracture Chamber of Water-Tree

The latest sites of insulation breakdown are referred as the crown of the water-tree as shown below in Figure 9:

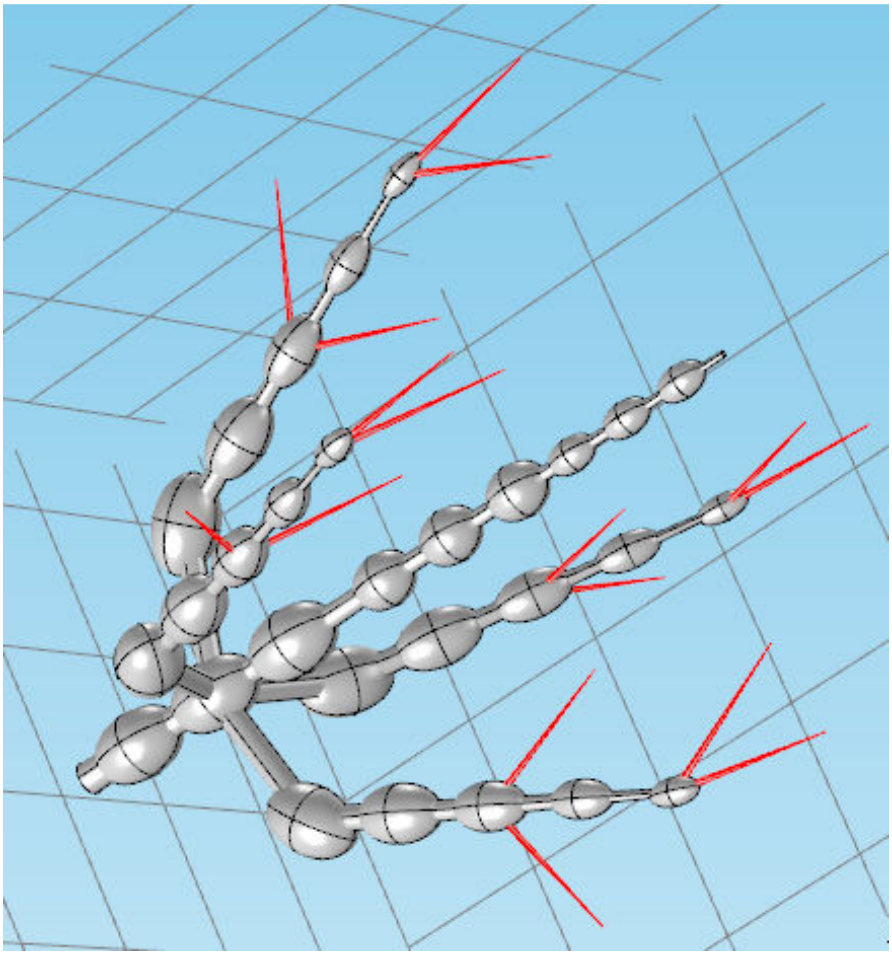

Figure 9: Crown of the Water-Tree

The diameter of micro-fracture chamber will gradually decrease from the root of the water-tree to the crown.

For large water-trees, the diameter of a micro-fracture chamber at the root may be dozens of times larger than the diameter of a chamber at the crown. A sample representation is shown below in Figure 10:

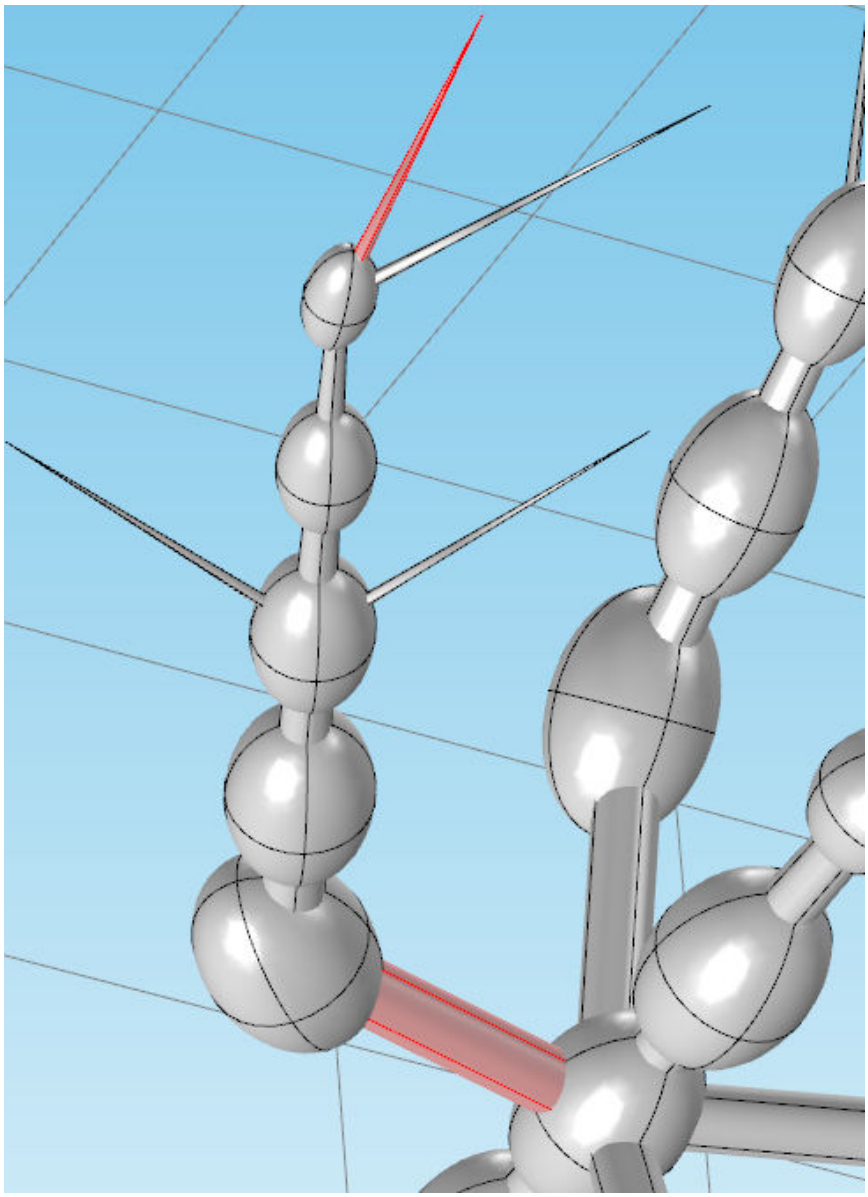

Figure 10: Branch Diameter Comparison

A single large micro-fracture chamber can be connected to multiple small chambers. When a large chamber is connected to two or more smaller chambers, this is referred as a branching point. Multiple water-tree branches may split off from the same root as shown below in Figure 11:

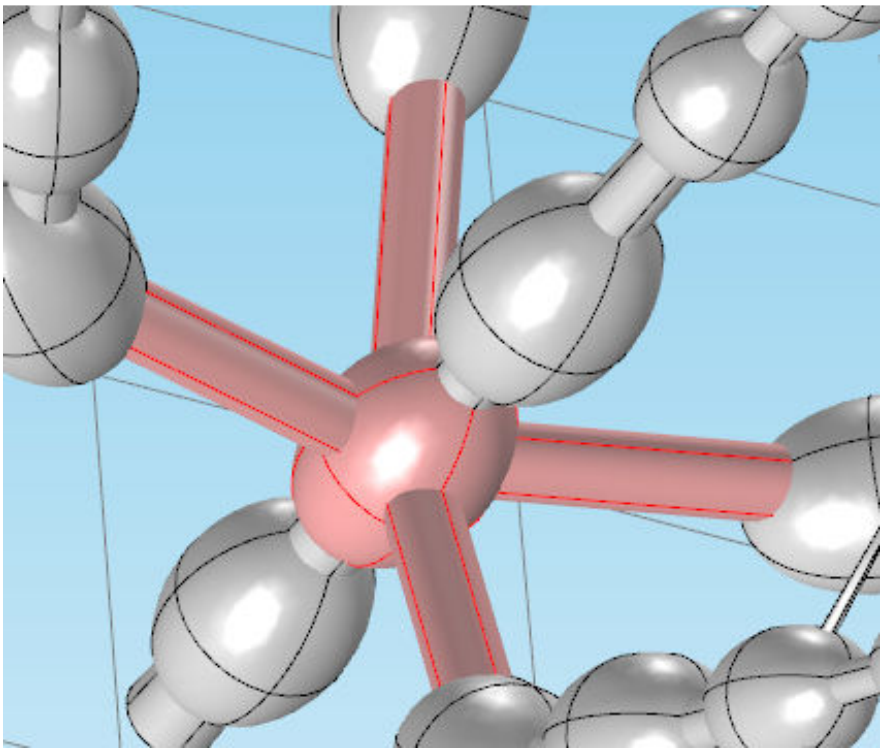

Figure 11: Water-Tree Branching Point

The physical cause of a branching point is poorly understood. One hypothesis is that sites of polymer molecule chain breaks are somewhat randomly distributed in the insulation material and branching may occur at these sites.

Additionally, laboratory aging experiments have demonstrated that the "spread" of water-tree is heavily influences by frequency characteristic of the service conditions. Specifically, the number of zero-crossings is directly related to the spread and direction of water-tree branch development [50~55]. In field conditions, the service voltage and current generally compose of various frequency components. Experimental results show

that when the overall service waveform has less zero-crossings, the water-tree tends to cluster together in a closely packed ball shape. In comparison, if the overall waveform has more zero-crossings, the water branch will be spread out like a hand. The comparison is shown below in Figure 12:

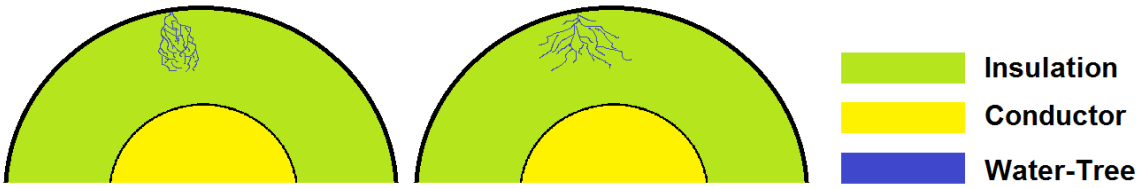

Figure 12: Ball-Shaped Tree (Left) vs Hand Shaped Tree (Right)

The overall picture of an actual water-tree is shown below in Figure 13. The picture is a cable insulation sample-slice containing water-tree. The central metallic conductor has been removed for the ease of slicing.

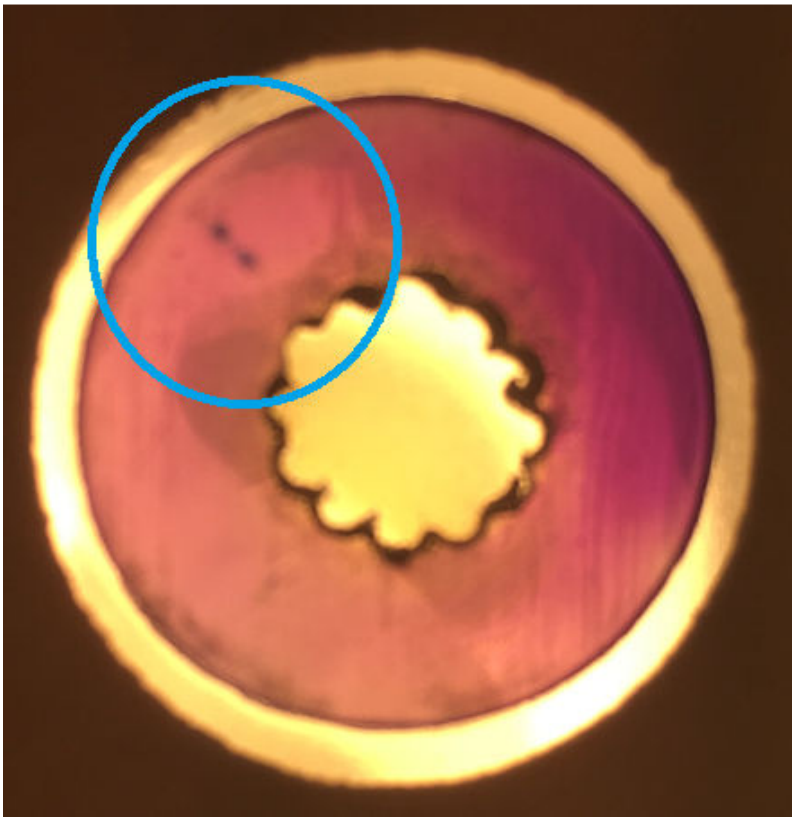

Figure 13: Sample Cable Slice of Containing a Water-tree

Large numbers of micro-fracture chambers are interconnected together and they form the water-tree branches. These tree branches are originated from a single starting point referred as the origin of the water-tree.

2.1.2 Bow-Tie Tree

Depending on the specific location of the origin, water-tree can be broadly classified into two categories: bow-tie tree and vented tree. Figure 14 shows a representation of the bow-tie tree:

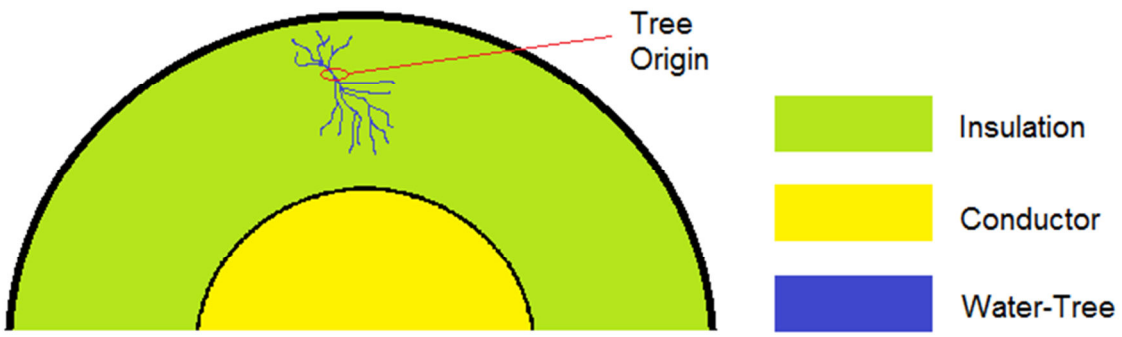

Figure 14: Sample Representation of a Bow-Tie Shaped Water-Tree

The Bow-Tie trees are named as such because the shape of the tree-branch development tends to resemble a bowtie. The origin of the bow-tie trees is located in the middle of the insulation layer. Due to the effect of Maxwell-Wagner force, the micro-fracture chambers will develop along a path that is approximately perpendicular to the central conductor. The path will be referred as the central development axis. Since the origin is located within the insulation layer, the tree branches will develop towards both the center conductor and the outer surface. Along the central development axis, micro-fracture chambers will also branch off into slightly different directions and form a fan shaped area (cone shaped when viewed from three-dimensional perspective).

It is observed that the specific amount of spread is determined by the frequency composition of the service voltage [56]. In comparison, the development along the central axis is primarily driven by the strength of the electric field. Thus, the two bows of the bow-tie tree may not be developing at the same rate (without factoring in other issues that may affect the water-tree development rate, such as distribution of chemical impurities). In general, the bow towards the inner conductor will develop quicker due to increasing electric field strength.

Although the origin of water-tree may appear due to a number of reasons, the main cause of bow-tie tree is generally manufacturing defect. Air bubbles or localized impurity cluster due to manufacturing detect can create the initial micro-fracture chamber that serves as the origin of water-tree. Micro-fracture chamber alone, however, is not sufficient for the appearance of water-tree. Another key factor in the appearance of water-tree is the presence of sufficient amount of moisture. There are several potential source of water in this situation. For example, some of the ethylene propylene rubber (EPR) insulation may absorb environmental water after prolong exposure [57]. The absorbed water may collects in the micro-fracture and serves as the source of water-tree.

Comparing to EPR, XLPE is more resistant to water absorption, but aging test indicates that XLPE is not immune to bow-tie tree [58]. In fact, as the service temperature increase, XLPE tends to have an increase number of bow-tie trees and the trees tend to have greater length. Submergence test indicates XLPE is still vulnerable to environment water seepage despite its greater resistance than EPR. The water-absorption remains the main factor aiding the development of bow-tie trees.

The specific location of the origin has significant impact on the potential risk of water-tree breakdown. For example, if the origin is located near the outer surface of the insulation, the bow-tie tree may quickly breach the remaining insulation between the surface and origin. From that point, the tree will then develop as a vented tree. A similar case will occur if the origin is very close to the inner conductor. Technically, when origin is closer to the inner conductor, the water-tree will initially develop at faster rate. From the long-term risk perspective, however, a bow-tie tree located near the outer-surface of the insulation will present a greater risk. The specific reason will be covered in the model assumption section along with surface-originated vented trees.

2.1.3 Vented Tree

A vented water-tree refers to a water-tree with its origin at the insulation surface. Depending on the location of the origin, vented tree can be classified into two categories: surfaced-originated vented tree and conductor-originated vented tree. Figure 15 shows the appearance of both types of vented trees:

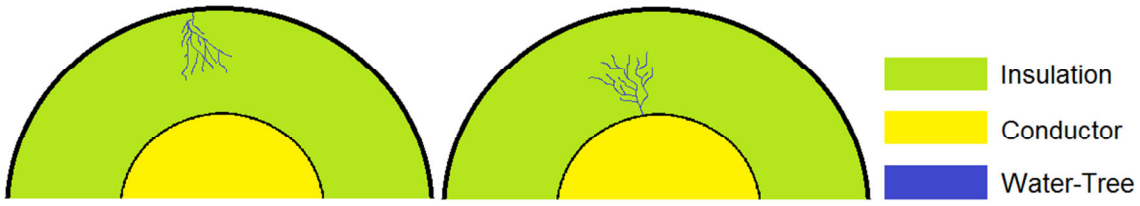

Figure 15: Vented Trees: Surfaced Originated (Left) and Conductor Originated (Right)

As the name described, the origin of surface-originated vented trees is located at the outer surface of the cable insulation. Similar to bow-tie trees, vented trees will grow

along the central development axis. In the case of surface-originated trees, the water-tree will grow towards the center conductor (or the shield for tape-shielded cables).

In comparison, the conductor-originated tree refers to vented trees that grow from current conducting components to the outer surface. In the case of concentric neutral cables, it is generally from the central conductor to the outer surface. In the case of taped shielded cables, it can be a vented tree that grows either from the shield to the outer insulation or from the central conductor to the shield.

There are two key differences between surface-originated and conductor-originated trees. The first difference is the initial formation condition. Second, the potential risks posed by the two categories of vented trees are also significantly different

Similar to bow-tie trees, conductor-originated water-tree may be the result of manufacturing defects. One of the potential causes is protrusions on the metallic surface of the conductor. For a normal, smooth conductor surface, the electric field distribution is uniform. A protrusion, on the other hand, will cause a localized spike in the electric field intensity. Similarly, the protrusion may generate high heat due to the combination of higher resistance and skin effect. If the protrusion is sufficiently sharp, the heat and electrical stress may cause micro-chambers to appear and form conductor-originated vented trees.

The surface-originated vented trees, on the other hand, have a large variety of causes. These causes can be categorized in a number of ways. For water-tree modeling, the causes can be divided into two types, type-one causes produce non-uniform clusters of tree origins and type-two causes produce uniform clusters as part of the tree origination process.

In general, type-one causes are events with short time intervals. Certain events will rapidly damage the outer insulation surface of the cable. For example, construction work may accidentally damage the buried cable. In comparison, type-two causes often occur over long time. For example, chemical corrosion from ground water seepage may damage the cable surface and in this case, the event occurs over a long time interval.

The key difference between type-one and type-two causes is the structure of the water-tree origin. In type one surface-originated vented trees, the initial fracture chamber at the tree origin is often larger and deeper into the insulation layer. More importantly, from the modeling perspective, the two types of the surface-originated vented trees have different distribution patterns for the electric permittivity at the base of the tree.

The categorized water-tree characteristic can be seen below in Figure 16:

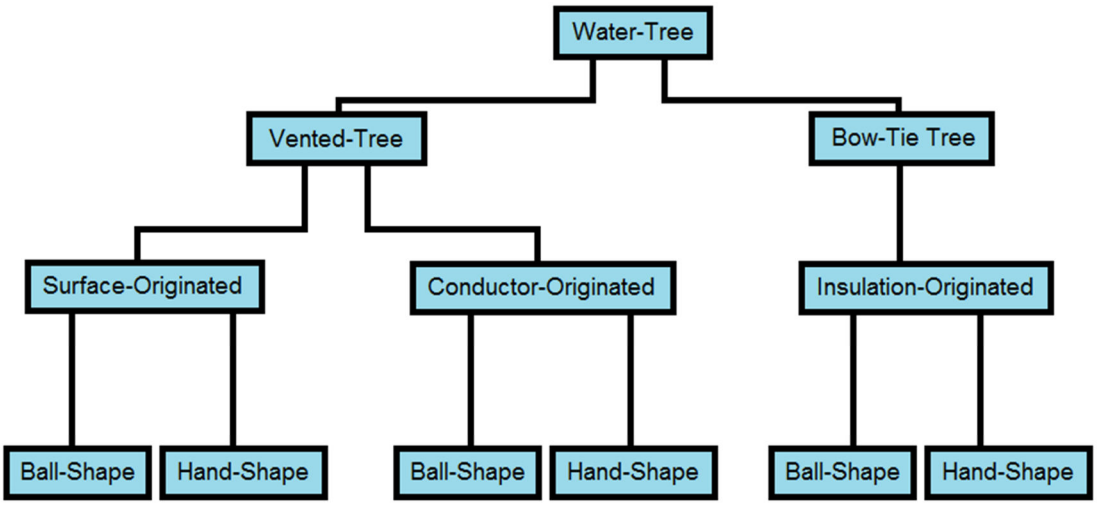

Figure 16: Categorized Water-tree Characteristics

2.2 Building the Model

By understanding the formation process and general structure of water-tree, it becomes possible to build mathematical models for specific types of water-trees. The

goal of this section is to develop a mathematical representation of water-tree. The model will be used to study the effect of water-tree in large systems such as long distance cables.

2.2.1 Model Building Background

In chapter one, the historical background of underground cable development is discussed. The academia and industry have been aware of water-tree since 1940s. After World War 2, the rebuild process saw rapid expansions of power infrastructure around the world. Underground cable deployment and its corresponding research have progressed accordingly.

For water-tree related studies, progress in the decades following World War 2 was generally in form of empirical observation and measurement on water-tree characteristics, such as physical dimension, structure, chemical composition, dielectric strength and equivalent impedance. Despite the achievements, however, there was precious little progress on developing a fully fledge mathematical model for water-trees, especially the ones that are still in early development stage. This is due to a number of reasons:

The first reason is relatively low industry awareness. In chapter one, the concept of infrastructure development cycle has been introduced. Much of the modern day power infrastructure is developed in the 1960s. Since water-tree growth rate is measured in decades, water-tree simply did not cause any significant impact on power-system performance until the recent decades. As the result, the overall industry aware of the issue is quite low and there is simply insufficient amount of effort invested into the issue.

The second reason is the difficulty on modeling a complex structure like water-tree. The previous sections in this chapter illustrated the randomness in water-tree branch development. Each individual branch will cause its own dielectric interaction with the

rest. Although it is possible to simplify some of the details, water-tree remains a very complex structure. As the result, it is difficult to create an accurate representation.

The third reason is the limitation on computation technology. Hand calculation on complex electromagnetic phenomenon is both time consuming and prone to error. Computation tools such as personal computers did not become widely available until 1990s. The processing power of these early PCs was also limited. Back then, the available computation and simulation algorithms simply could not adequately represent complex structures such as water-tree. For example, finite element analysis is an excellent tool on managing complex physical phenomena, but its accuracy and resolution speed is directly dependent on the available process power. As the result, mathematical modelling of water-tree did not become possible until recent years. Even with the computation power available in 2016, it is still ill advised to insertion full water-tree models into large system simulations.

The fourth reason is the auxiliary equipment limitation. Technically speaking, both computation limitation and model complexity fall under equipment limitation. The auxiliary equipment limitation specifically refers to the limitation of necessary equipment used in water-tree model verification process. For example, many verification processes require high accuracy voltage and current sensors. Without appropriate advancement in these auxiliary technologies, mathematical model of water-tree remains a theoretical process and it cannot be reliably verified.

Nowadays, water-tree received much more attention. The task of building and testing a mathematical model for water-tree also become feasible. This is primarily due to advancement in technology and shifting demand. In chapter one, the demand for

prolonging the lifespan of the equipment is discussed. As of 2016, the power infrastructure built immediately after World War 2 has been in service for more than sixty years. Since underground cables generally have a service life of forty years, many of these cables are past the original design limit and in dire need of preventative maintenance. As the result, industry has devoted more attention and resource to study the behavior of water-tree and explore potential methods for water-tree prevention.

It is difficult to pin down the exact date for invention of the finite element analysis technique, but as early as 1950s, engineering projects have been resolved using similar principles. The development in this field allowed complex structures to be broken down into smaller and easier to analyze pieces. In combination with the rapidly advancing computer-assisted analysis tools, mathematically resolution of water-tree becomes possible.

Finally, advancement in voltage and current measuring device resulted in higher data accuracy. Estimation techniques also help to further refine and improve the accuracy of the measurement result. Due to these advancements, it is now possible to build a mathematical model for water-tree.

2.2.2 Modeling Building Concept

From system perspective, early stage water-tree mainly exists as a capacitive anomaly. Figure 17 shows the appearance of water-tree branch in a cable insulation layer:

Figure 17: Water-Tree Branches in Insulation Layer

Figure 18 shows a localized view of the insulation layer and the water-tree branch:

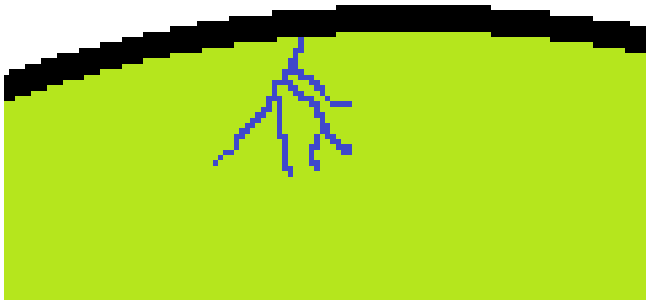

Figure 18: Localized View of Water-tree Branch and the Insulation Layer

The scales and water-tree branch distribution in Figure 17 and 18 are not to scale. They are intended for the easy of viewing. One key observation can be made from the Figures: early stage water-tree is a capacitive phenomenon because the interaction between water filled tree branches and the insulation material. Specifically, water-filled tree branches acts as material of certain dielectric strength and the original insulation acts as another material with different dielectric strength.

This configuration is remarkably similar to a capacitor with multiple dielectric materials. In fact, Figure 19 shows a cylindrical capacitor with multiple dielectrics:

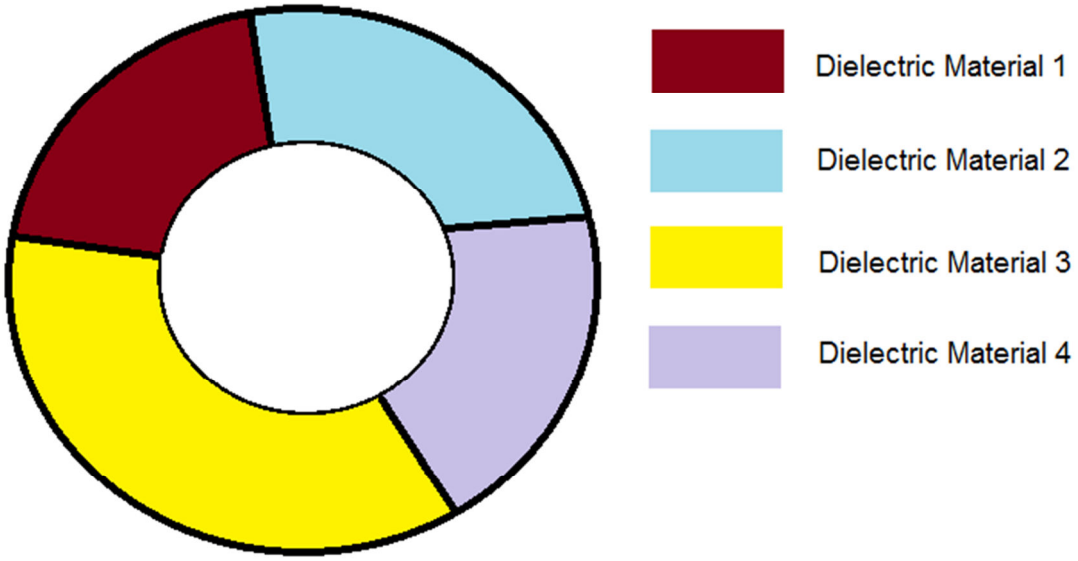

Figure 19: Capacitor with Multiple-Dielectric Material

Structure wise, water-tree branch distribution is equivalent to interlacing materials of difference dielectric strength. The materials are mixed together much more finely than any multiple-dielectric capacitor. The principle, however, remains the same and the mathematical model can be developed using this concept.

From the cable impedance perspective, water-tree behaves as an additional shunt capacitor added to the existing cable system. Although there are many models for underground cable, a simple, generalized cable π-section model is shown below in Figure 20:

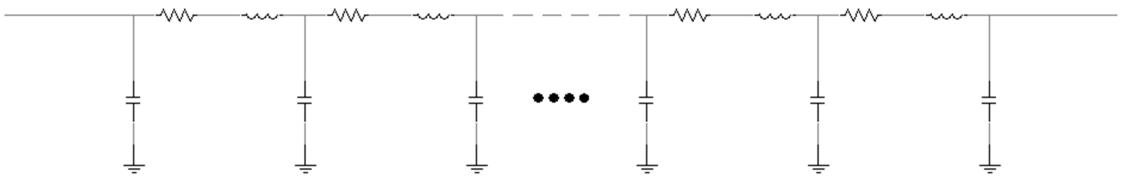

Figure 20: Sample Cable π-Model

The shunt capacitance of an underground cable includes both the conductor-conductor capacitance and the conductor-ground capacitance. The components of the

shunt capacitance have different distances between conducting surface and material media have potentially different electrical permittivity. Their values, however, are ultimately determined with respect to the main conducting path. Thus, they can be represented by a shunt element connected to the conductor. Similarly, the water-tree capacitance is determined with respect to the central conductor. As the result, it behaves like an additional shunt element as shown in Figure 21:

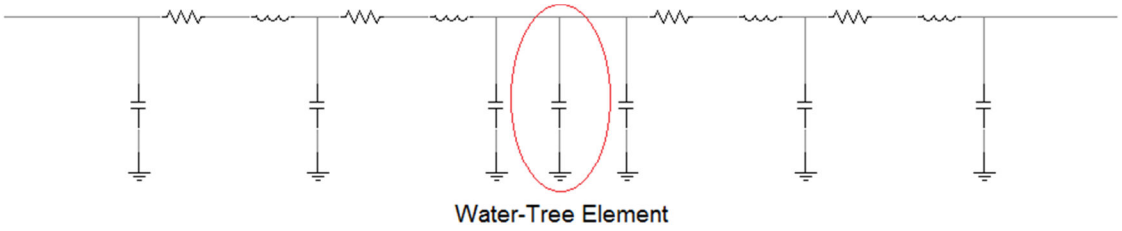

Figure 21: Sample Cable Model with Water-Tree Present

2.2.3 Model Building Assumptions

Although the advancements in computation tool and methodology allow the water-tree to be modeled, it is still necessary to make adequate assumptions. The assumptions reduce computation complex and assist the analysis process.

2.2.3.1 Assumption #1: Tree Type Selection: Surface-Originated Vented Tree

The three possible choices of water-tree types are surface-originated vented tree, conductor-originated vented tree and bow-tie tree. Out of the three types of water-trees, the surface-originated water-tree is responsible for majority of the incidents in the field. (As mentioned earlier in the chapter, a bow-tie tree with origin near the surface will behave like a surface-originated vented tree.) This is due to the interaction between water-tree and the cable electrical field.

The growth of water-tree is a process driven by the electrical field. Stronger field will cause the growth to speed up and weaker field will reduce the growth rate. For both bow-tie trees and conductor-originated vented trees, they must grow away from the central conductor before it can fully breach the insulation layer. The electrical field weakens as it moves away from the central conductor.

The electric field strength around the cable is similar to the relationship between the electric field strength at a certain space point and an infinite line charge. As the result, the electric field strength experienced by the water-tree is inversely proportional to its distance away from the conductor. For bow-tie and conductor-originated water-trees, two scenarios may occur:

Scenario #1: The field weakens to the point that micro-fracture chamber formation no longer occurs. In this case, the water-tree growth will stop and cable will not suffer water-tree related breakdown.

Scenario #2: The field is sufficiently strong that micro-fracture chamber continues to occur even close to the insulation surface. This is, however, a rarer scenario comparing to surface-originated trees. If bow-tie trees and conductor-originated vented trees can grow, then high amount of moisture must be present in the environment. If the field from the normal service voltage level is sufficiently strong to cause micro-fracture formation near the surface, then the condition allows surface-originated tree to occur as well. Essentially, if the condition allows bow-tie trees and conductor-originated trees to cause insulation breach, then the same condition also allows surface-originated trees to induce insulation breach. On the other hand, the reverse is not true.

Surface-originated vented tree will experience increasing electric field strength as it develops. The root of the tree is also on the surface; therefore, if the environment has sufficient amount of moisture to initiate water-tree formation, then the same environment condition will continue to supply water to the tree formation process. As the result, surface-originated trees are more likely to fully breach the insulation layer and create water-tree faults than other types of water-trees. Thus, they will be the primary focus in the modelling work.

2.2.3.2 Assumption #2: Tree Cause Selection: Type-Two Origination Cause

Technically, water-tree develops faster in non-uniform cluster situations. Non-uniform clusters are typically created by strong impact and these impacts leaves rougher impact sites. The sites are hosts to more material/water interface and they cause faster water-tree development than uniform cluster origins. In addition, slashing impacts may also cut deep into the insulation material. In this case, water-tree effectively bypasses the initial insulation layers and the time required to breach the insulation is greatly reduced.

On the other hand, non-uniform cluster trees are also easier to locate than uniform cluster trees. The impact events for non-uniform cluster tree creation, such as construction work or landslide, can be tracked through alternative methods like construction record or weather report.

Uniform cluster trees, on the other hand, occur under more subtle conditions. Small impact, chemical corrosion all tends to create uniform cluster trees and they can only be tracked using water-tree detection techniques; therefore, uniformed origin water-tree will be the focus of the study.

2.2.3.3 Assumption #3: Tree Shape Selection: Ellipsoidal Distribution Area with Fixed Axial Ratio

Aging experiments have shown that the tree branch distribution of water-tree is determined by the frequency of the service voltage.

In US, the normal service frequency is 60Hz. For European grid, the service frequency is 50Hz. The other parts of the world also use either 50Hz or 60Hz as the base frequency for their power grid. Aging experiment shows that for 50Hz~60Hz range, the water-tree distribution tends to resemble an ellipsoid. The axial ratio of such an ellipsoidal area is also within a certain range; therefore, the modeling will be made using these parameters.

2.2.3.4 Assumption #4: Tree Electrical Permittivity Distribution: Linear

The final assumption is the distribution of the material permittivity in water-tree afflicted region. Under uniformed tree cluster condition, the tree branch diameter changes linearly from the base to the tip of the water as shown below in Figure 22:

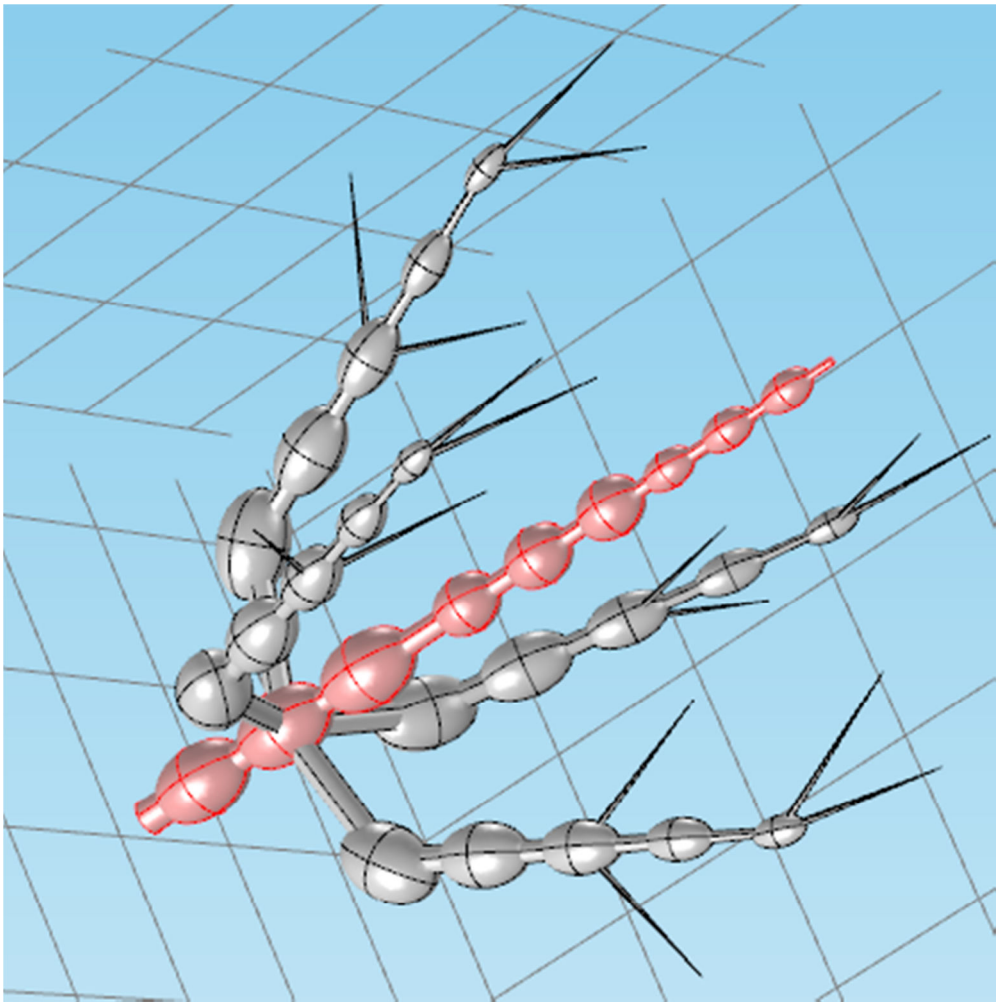

Figure 22: Tree-Branch Diameter Change along Central Development Axis

The density of the tree branch cluster also decreases proportionally to the distance away from the root of the water. The electrical permittivity of the water-tree affected region is complex. Fortunately, localized the tree branch-insulation mixture is relatively even. Thus, a simplified representation is simply a multiple direction linearly shifting electric permittivity. Higher tree branch concentration and larger branch diameter results in electrical permittivity closer to water than XLPE. The reverse is also true.

2.2.4 Finite Element Analysis of Water-tree

Under the assumptions in section 2.2.3, it is possible to build a mode for the water-tree. For a localized region, water-tree affected insulation material will be treated as a homogeneous dielectric material. The overall capacitance can be calculated using the same principle of cylindrical capacitor with multiple dielectric materials.

2.2.4.1 Conception Design Based on Cylindrical Capacitor Model

The standard, single material cylindrical capacitor is shown below in Figure 23:

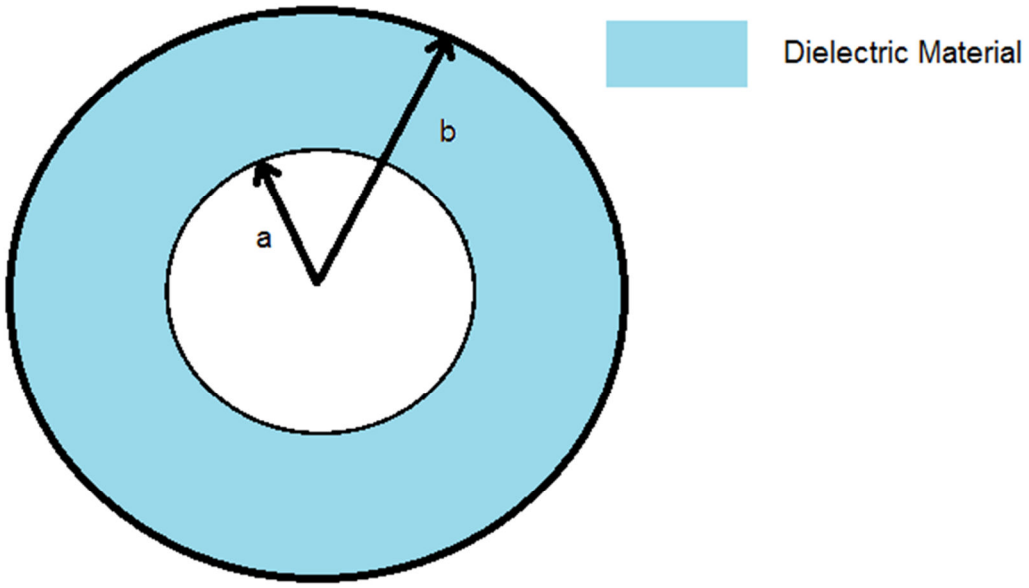

Figure 23: Cylindrical Capacitor Model

Deriving from Gauss' Law, the electric field is for cylindrical capacitor is:

$$\vec{E}(r) = \frac{\lambda}{2\pi\varepsilon\varepsilon_0\vec{r}} \quad \text{.....(1)}$$

The Potential Difference is:

$$V(r) = -\oint_a^r \vec{E}(r)dr = -\frac{\lambda}{2\pi\varepsilon\varepsilon_0}\oint_a^r \frac{1}{\vec{r}}dr =$$

$$-\frac{\lambda}{2\pi\varepsilon\varepsilon_0} ln\frac{r}{a} \quad \text{.....(2)}$$

Evaluate between the outer and inner conductor:

$$V(capacitor) = V(a) - V(b) = 0 + \frac{\lambda}{2\pi\varepsilon\varepsilon_0} ln\frac{b}{a} = \frac{\lambda}{2\pi\varepsilon\varepsilon_0} ln\frac{b}{a} \quad \text{.....(3)}$$

Therefore, the resultant capacitance is:

$$C = \frac{Q(capacitor)}{V(capacitor)} = \frac{\lambda L}{\frac{\lambda}{2\pi\varepsilon\varepsilon_0} ln\frac{b}{a}} = \frac{2\pi\varepsilon\varepsilon_0 L}{\ln\frac{b}{a}} \quad \text{.....(4)}$$

Where:

a is the radius of the inner conductor

b is the radius of the outer conductor

r is the radius of the current material layer

L is the length of the capacitor

λ is the charge per unit length

Q is the overall charge of the cylinder

ε is the relative permittivity of the dielectric

ε_0 is the permittivity of air

Next, expanding to the capacitance of cylindrical capacitor with two dielectrics, the Diagram is shown below in Figure 24:

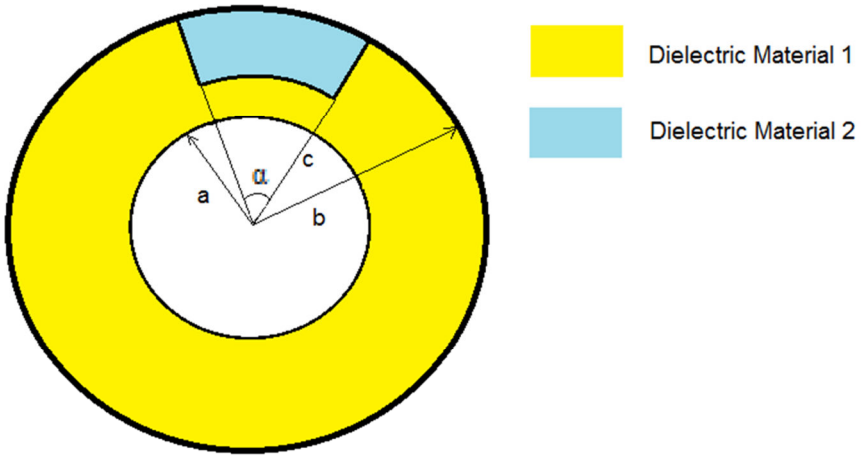

Figure 24: Cylindrical Capacitor with Two Dielectrics

Since the later finite element analysis will break down the water-tree affected insulation region in arc shaped pieces, the sample two-dielectric capacitor will also have the different dielectric materials arranged in arcs, therefore:

For the inner capacitor,

$$V_1 = \oint_a^c \vec{E}_1 \, ds \quad \text{.....(5)}$$

$$Since\ q = \varepsilon_1\varepsilon_0 E_1 A_1 = \varepsilon_1\varepsilon_0 E_1 2\pi rL \rightarrow E_1 = \frac{q}{2\pi rL\varepsilon_1\varepsilon_0} \quad \text{.....(6)}$$

$$\therefore V_1 = \oint_a^c \frac{q}{2\pi rL\varepsilon_1\varepsilon_0} dr = \frac{q}{2\pi rL\varepsilon_1\varepsilon_0} ln\frac{c}{a} \quad \text{.....(7)}$$

For the outer capacitor,

$$q = \varepsilon_1\varepsilon_0 E_2 A_2 \left(1 - \frac{\alpha}{2\pi}\right) + \varepsilon_2\varepsilon_0 E_2 A_2 \frac{\alpha}{2\pi} = [\varepsilon_1\varepsilon_0 \left(1 - \frac{\alpha}{2\pi}\right) + \varepsilon_2\varepsilon_0 \frac{\alpha}{2\pi}] E_2 A_2 \quad \text{.....(8)}$$

$$\therefore\ E_2 = \frac{q}{[\varepsilon_1\varepsilon_0\left(1-\frac{\alpha}{2\pi}\right)+\varepsilon_2\varepsilon_0\frac{\alpha}{2\pi}]A_2} = \frac{q}{[\varepsilon_1\varepsilon_0\left(1-\frac{\alpha}{2\pi}\right)+\varepsilon_2\varepsilon_0\frac{\alpha}{2\pi}]2\pi rL} \quad \text{.....(9)}$$

$$V_2 = \int_c^b E_2 \, ds = \int_c^b \frac{q}{[\varepsilon_1\varepsilon_0\left(1-\frac{\alpha}{2\pi}\right)+\varepsilon_2\varepsilon_0\frac{\alpha}{2\pi}]2\pi rL} dr = \frac{q}{[\varepsilon_1\varepsilon_0\left(1-\frac{\alpha}{2\pi}\right)+\varepsilon_2\varepsilon_0\frac{\alpha}{2\pi}]2\pi L} ln\frac{b}{c} \quad \text{.....(10)}$$

$$V_{total} = V_1 + V_2 = \frac{q}{2\pi L}\left(\frac{\ln\left(\frac{c}{a}\right)}{\varepsilon_1\varepsilon_0} + \frac{\ln\left(\frac{b}{c}\right)}{\varepsilon_1\varepsilon_0\left(1-\frac{\alpha}{2\pi}\right)+\varepsilon_2\varepsilon_0\frac{\alpha}{2\pi}}\right) \quad \text{.....(11)}$$

$$C_{total} = \frac{2\pi L}{\frac{\ln\left(\frac{c}{a}\right)}{\varepsilon_1\varepsilon_0} + \frac{\ln\left(\frac{b}{c}\right)}{\varepsilon_1\varepsilon_0\left(1-\frac{\alpha}{2\pi}\right)+\varepsilon_2\varepsilon_0\frac{\alpha}{2\pi}}} \quad \text{.....(12)}$$

Where:

a is the radius of the inner conductor

b is the radius of the outer conductor

c is the radius of the layer, which the different material begins

L is the length of the capacitor

Q is the overall charge of the cylinder

ε_1 is the relative permittivity of the first material

ε_2 is the relative permittivity of the second material

ε_0 is the permittivity of air

α is the angle of the range of 2nd dielectric material, in radians

The result from the two-dielectric material capacitor can be generalized to create an equation for a capacitor with n additional dielectric materials and in m layers, the equation is:

$$C_{total} = (2\pi L) \Bigg/ \left(\frac{\ln\left(\frac{c}{a}\right)}{\varepsilon_{original}\varepsilon_0} + \frac{\ln\left(\frac{b_1}{c}\right)}{\varepsilon_{original}\varepsilon_0\left(1-\frac{\alpha_{11}}{2\pi}-\frac{\alpha_{21}}{2\pi}\ldots-\frac{\alpha_{n1}}{2\pi}\right)+\varepsilon_1\varepsilon_0\frac{\alpha_{11}}{2\pi}+\varepsilon_2\varepsilon_0\frac{\alpha_{21}}{2\pi}+\cdots+\varepsilon_n\varepsilon_0\frac{\alpha_{n1}}{2\pi}} + \frac{\ln\left(\frac{b_2}{b_1}\right)}{\varepsilon_{original}\varepsilon_0\left(1-\frac{\alpha_{12}}{2\pi}-\frac{\alpha_{22}}{2\pi}\ldots-\frac{\alpha_{n2}}{2\pi}\right)+\varepsilon_1\varepsilon_0\frac{\alpha_{12}}{2\pi}+\varepsilon_2\varepsilon_0\frac{\alpha_{22}}{2\pi}+\cdots+\varepsilon_n\varepsilon_0\frac{\alpha_{n2}}{2\pi}} + \frac{\ln\left(\frac{b_3}{b_2}\right)}{\varepsilon_{original}\varepsilon_0\left(1-\frac{\alpha_{13}}{2\pi}-\frac{\alpha_{23}}{2\pi}\ldots-\frac{\alpha_{n3}}{2\pi}\right)+\varepsilon_1\varepsilon_0\frac{\alpha_{13}}{2\pi}+\varepsilon_2\varepsilon_0\frac{\alpha_{23}}{2\pi}+\cdots+\varepsilon_n\varepsilon_0\frac{\alpha_{n3}}{2\pi}} + \cdots + \frac{\ln\left(\frac{b_m}{b_{m-1}}\right)}{\varepsilon_{original}\varepsilon_0\left(1-\frac{\alpha_{1m}}{2\pi}-\frac{\alpha_{2m}}{2\pi}\ldots-\frac{\alpha_{nm}}{2\pi}\right)+\varepsilon_1\varepsilon_0\frac{\alpha_{1m}}{2\pi}+\varepsilon_2\varepsilon_0\frac{\alpha_{2m}}{2\pi}+\cdots+\varepsilon_n\varepsilon_0\frac{\alpha_{nm}}{2\pi}} \right) \quad \ldots$$

……...(13)

Where:

a is the radius of the inner conductor

b_m is the radius of different layers of difference dielectric material

c is the radius of the layer, which the different material begins

L is the length of the capacitor

Q is the overall charge of the cylinder

ε_1 is the relative permittivity of the first material

ε_2 is the relative permittivity of the second material

ε_0 is the permittivity of air

α_{ij} is represents the angle of ith material angle with different permittivity in the jth layer as demonstrated below in Figure 25:

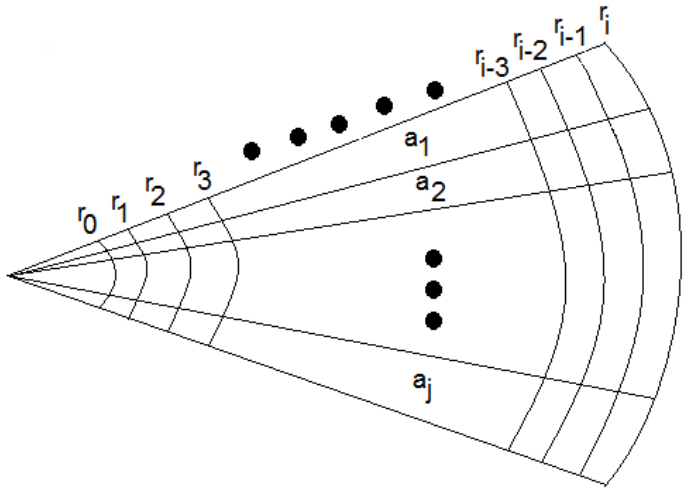

Figure 25: A Capacitor with j Additional Dielectrics and in i Layers

This generalized equation is the main principle behind the finite element analysis of water-tree.

2.2.4.2 Finite Element Breakdown on Location Region

In Figure 25 above, it is shown that capacitor with n additional dielectric materials and arrange in m layers can be resolved by the generalized equation. The same principle is applied to water-tree analysis. By increasing the n and m value, the dielectric materials of the water-tree can be divided into smaller and smaller components. At very n and m high value, each localized region, is effective a homogenous piece of material and its permittivity is determined by its distance from the water root.

The specific permittivity of each localized region is determined by its position in the ellipsoidal bounded area. The very root of the tree, the permittivity value will be approach the relative permittivity of water at 2.3. As the position moves away from the water root (either in x-axis or y-axis), the permittivity will gradually increase. At the very edge of the ellipsoidal bounded area, the relative permittivity of the localized region will be approach the relative permittivity of the XLPE at 6.9. The resolution of the relative permittivity at a specific region follows Figure 26 below:

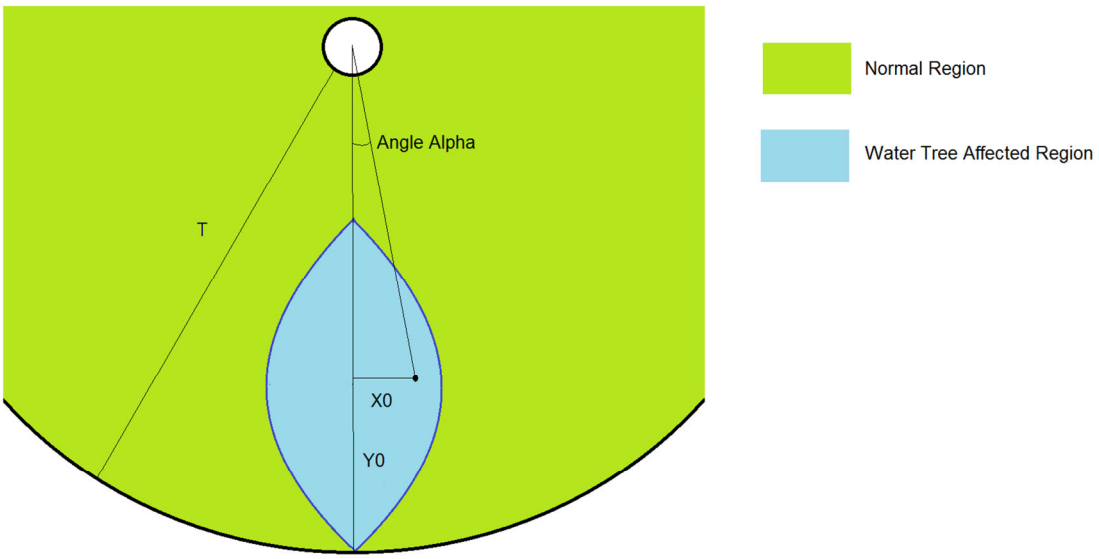

Figure 26: Resolution of Relative Permittivity at a Specific Region

x_0, y_0, x_m, Z and T are known parameters

$$y_m = T * Z \quad \text{.....(14)}$$

The line segment equation is:

$$y_r = \frac{y_0}{x_0} * x_r \quad \text{.....(15)}$$

The ellipse equation is:

$$\frac{{x_r}^2}{{x_m}^2} + \frac{\left(y_r - \frac{y_m}{2}\right)^2}{{y_m}^2} = 1 \quad \text{.....(16)}$$

Resolving the previous two equations yield:

$$x_r = \frac{x_m y_m x_0}{2x_0{}^2 y_m{}^2 + 2y_0{}^2 x_m{}^2} * (x_m y_0 + \sqrt{3x_0{}^2 y_m{}^2 + 4y_0{}^2 x_m{}^2}) \quad \text{.....(17)}$$

$$y_r = \frac{x_m y_m y_0}{2x_0{}^2 y_m{}^2 + 2y_0{}^2 x_m{}^2} * (x_m y_0 + \sqrt{3x_0{}^2 y_m{}^2 + 4y_0{}^2 x_m{}^2}) \quad \text{.....(18)}$$

Length of the line segment is given by:

$$r_{max} = \sqrt{(x_r - 0)^2 + (y_r - 0)^2} = \sqrt{x_r{}^2 + y_r{}^2} \quad \text{.....(19)}$$

The distance of the specified point to the tree root is:

$$r_0 = \sqrt{(x_0 - 0)^2 + (y_0 - 0)^2} = \sqrt{x_0{}^2 + y_0{}^2} \quad \text{.....(20)}$$

The relative permittivity of the specified point is:

$$\varepsilon_{point} = (\varepsilon_{insulation} - \varepsilon_{water}) * \frac{r_0}{r_{max}} + \varepsilon_{water} \quad \text{.....(21)}$$

Where

x_0 is the x-axis coordinate of the specific point (set parameter)

y_0 is the y-axis coordinate of the specific point (set parameter)

x_r is the x-axis coordinate of the ellipsoid intercept of the line segment through origin and specified point

$y_r$is the y-axis coordinate of the ellipsoid intercept of the line segment through origin and specified point

x_m is the horizontal ellipsoid axis bound (set parameter)

y_m is the vertical ellipsoid bounded area (determined using Z)

Z is the water-tree progression indicator (set parameter.)

T is the thickness of the total thickness cable insulation (set parameter)

r is the length from the specific point to the root of the water-tree

r_{max} is the total length of the line, which the resolution point is on.

ε_{water} is the relative permittivity of water

$\varepsilon_{insulation}$is the relative permittivity of the insulation layer

ε_0 is the air electric permittivity

The water-tree root is taken as the origin of the measurement.

Z is the indicator for the water-tree corrosion process. For example, Z=0.8 indicate water-tree has corroded through 80% of the insulation layer.

r_{max} represents the line segment that starts at the tree root. It passes through the resolution point and ends at the boundary of the ellipsoidal bounded area.

The angle α_{ij} in the generalized multiple-dielectric material equation can be resolved using x_0 and y_0. For example, if the finite element analysis algorithm placed origin at the center of the conductor as shown in Figure 27:

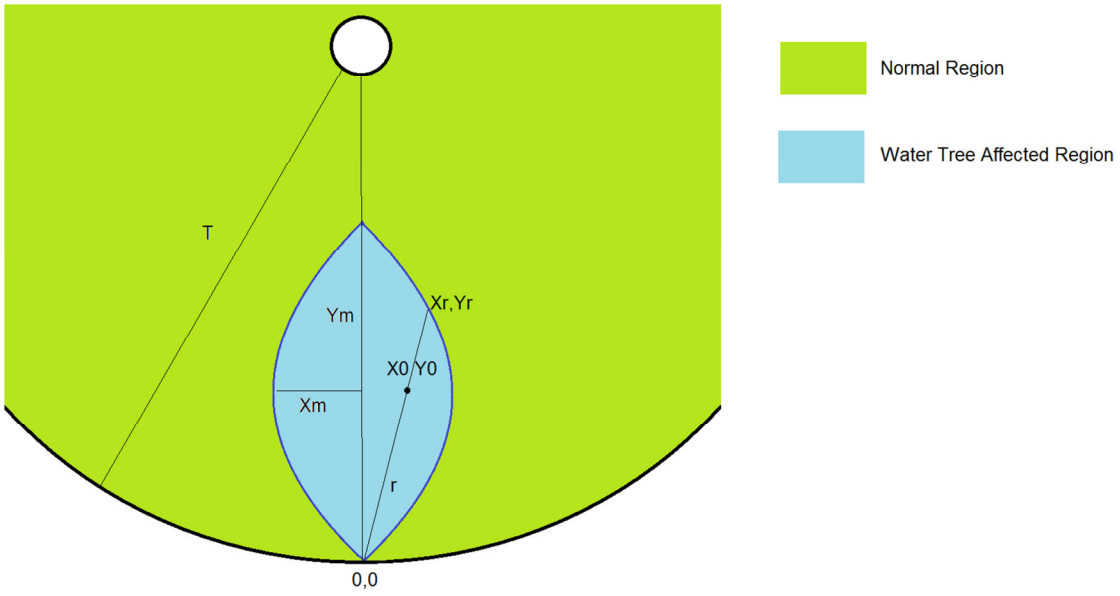

Figure 27: Resolving the Dielectric Material Angle with Conductor as Origin

Then angle α for a specific point can be solved as:

$$\alpha = \tan^{-1}\frac{x_0}{T+r_{conductor}-y_0} \quad \text{.....(22)}$$

$r_{conductor}$ represents the radius of the conductor.

The equation set can also be expended to include z-axis for three-dimensional evaluation.

2.3 Model Result

It is necessary to remember that water-tree is a very complex structure. The main objective of the current mathematical model is provide understand and insight into the overall characteristic of the water-tree behavior.

The result from this section is calculated from a 2-dimensional cross section model. The capacitance has two distinct large layers: the inner layer without water-tree and the outer layer with water-tree as shown below in Figure 28:

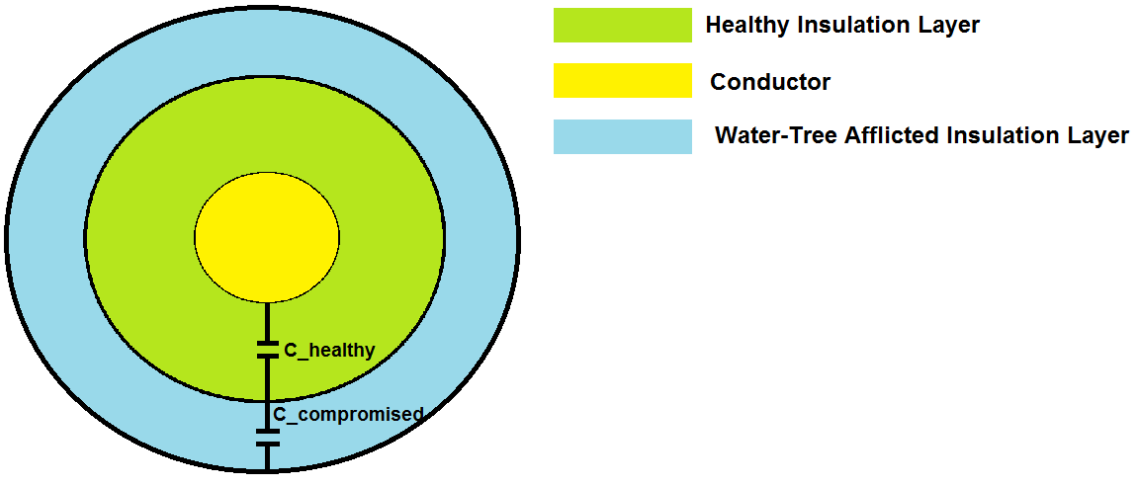

Figure 28: Equivalent Circuit of Simulated Capacitance

The healthy insulation layer is represented by $C_{healthy}$. The water-tree afflicted insulation layer is represented by $C_{compromised}$.

In the finite element analysis algorithm, the cable insulation will be broken down into individual, thin rings shapes referred as layers. Each layer consists of two parts:

healthy insulation and regions affected by water-tree. The permittivity of the water-tree afflicted region will depend on its specific coordinate within the boundary region. The permittivity values will be integrated to obtain the corresponding value used in the generalized water-tree capacitance formula derived in the previous section.

In the simulation algorithm, a number of parameters are needed:

Relative Permittivity of the Insulation: The value will be 2.3 in the following simulation. It is the relative permittivity of XLPE.

Relative Permittivity of Water-Tree Root: Close to the Permittivity of Water (88 in the following simulation)

Cable Radius: Depending on the Scenario (2.27cm in the following simulation, arbitrarily chosen)

Conductor Radius: Depending on the Scenario (1.24cm in the following simulation, arbitrarily chosen)

Ellipsoidal Ratio of the Water-Tree Afflicted Area: Depending on the Scenario (narrow axis = 0.2*long axis in the following simulation, arbitrarily chosen)

The arbitrarily chosen values in the following simulations are chosen to resemble a real world cable.

Figure 29 shows the simulation result from the finite element analysis algorithm. The vertical axis is capacitance in Farads/m. The horizontal axis shows the water-tree corrosion process from 0% to 100%. Zero percent represents a completely healthy cable and one hundred percent represents a cable segment with fully breached insulation layer.

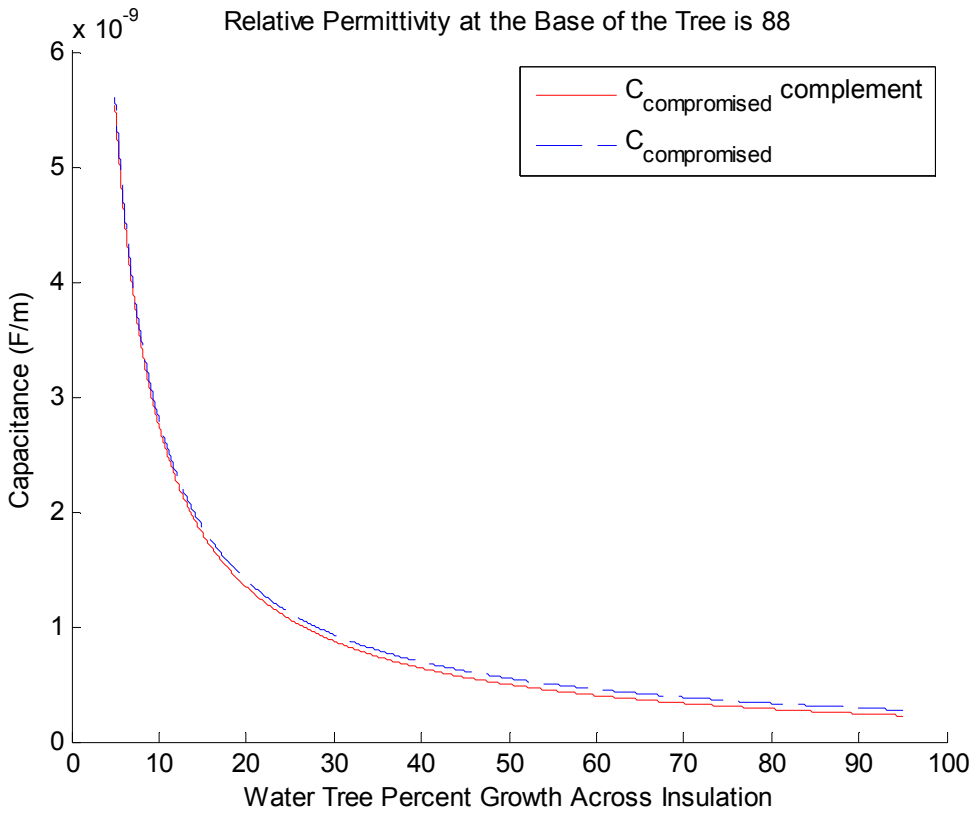

Figure 29: Capacitance of Water-Tree Afflicted Area

The capacitance/length information in the figure refers the overall capacitance of the ring-shaped layer containing the water-tree. The simulation is represents the capacitance/length obtained from a two-dimension slice.

$C_{compromised}$ is the capacitance of the ring shaped slice if it contains water-tree.

$C_{compromised}Complement$ is a comparison plot. It represents the capacitance of a complete healthy insulation layer resolved using the same algorithm. A zoomed-in version of the figure is shown below in Figure 30:

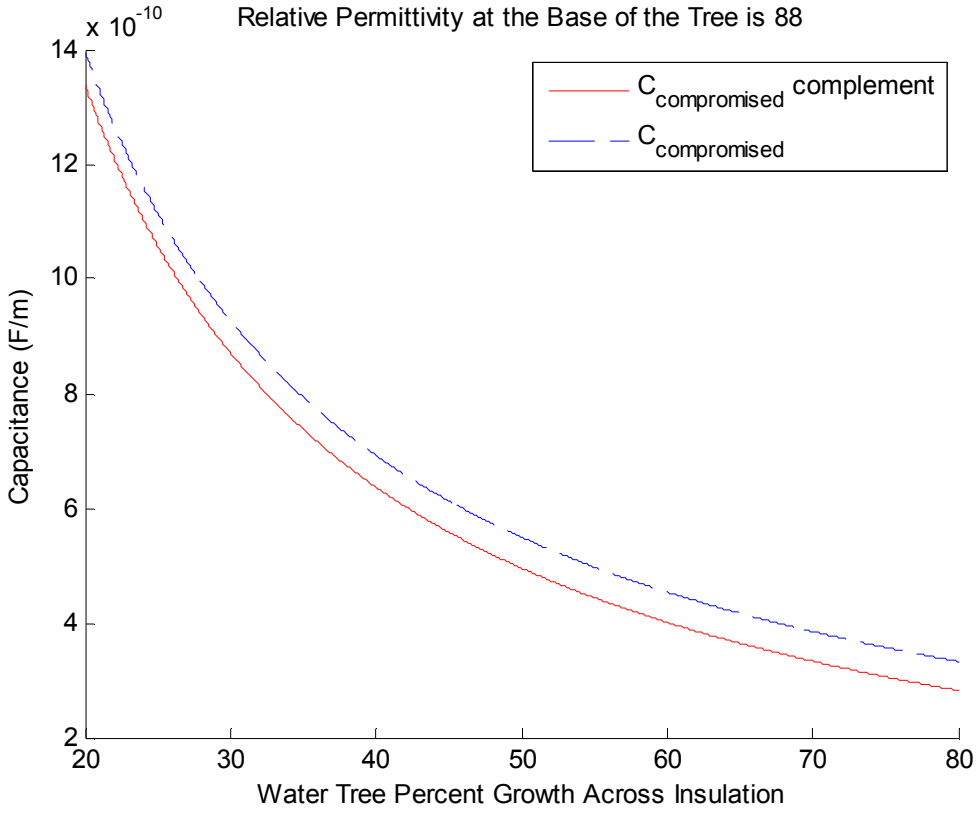

Figure 30: Capacitance of Water-Tree Afflicted Area (Zoomed-in)

According to the model, the capacitance difference between a healthy system and water-tree afflicted system is in the range of nF/m. This result illustrates the main challenge associated with water-tree detection. The innate capacitance of underground cable generally ranges from 0.2μF/km to 0.7μF/km. The capacitance of water-tree afflicted section is only slightly different from a healthy section of the same dimension. By extension, the water-tree is only differentiated from the characteristic capacitance of healthy cable segment by nF range capacitance increases.

A graphical representation of these values is shown below in Figure 31:

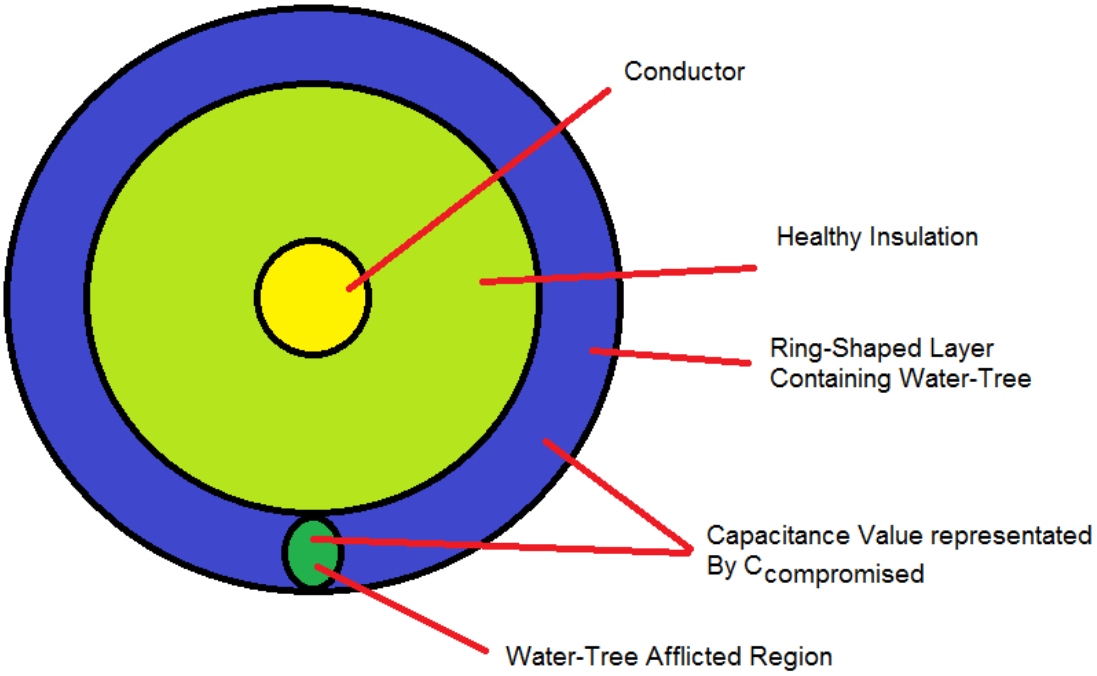

Figure 31: Graphical Representation of C_compromised Value

The values in the previous graphs represent the capacitance of the ringed shaped layer, including both healthy insulation and the water-tree bounded region. The comparison plot represents a ring-shaped layer, which is completely healthy.

As the water-tree corrosion depth increases, the thickness of the ring-shaped layer increases as well. As the result, the capacitance value natural decreases due to increased distance between charged surfaces.

The overall capacitance of water-tree under various stage of corrosion is shown below in Figure 32:

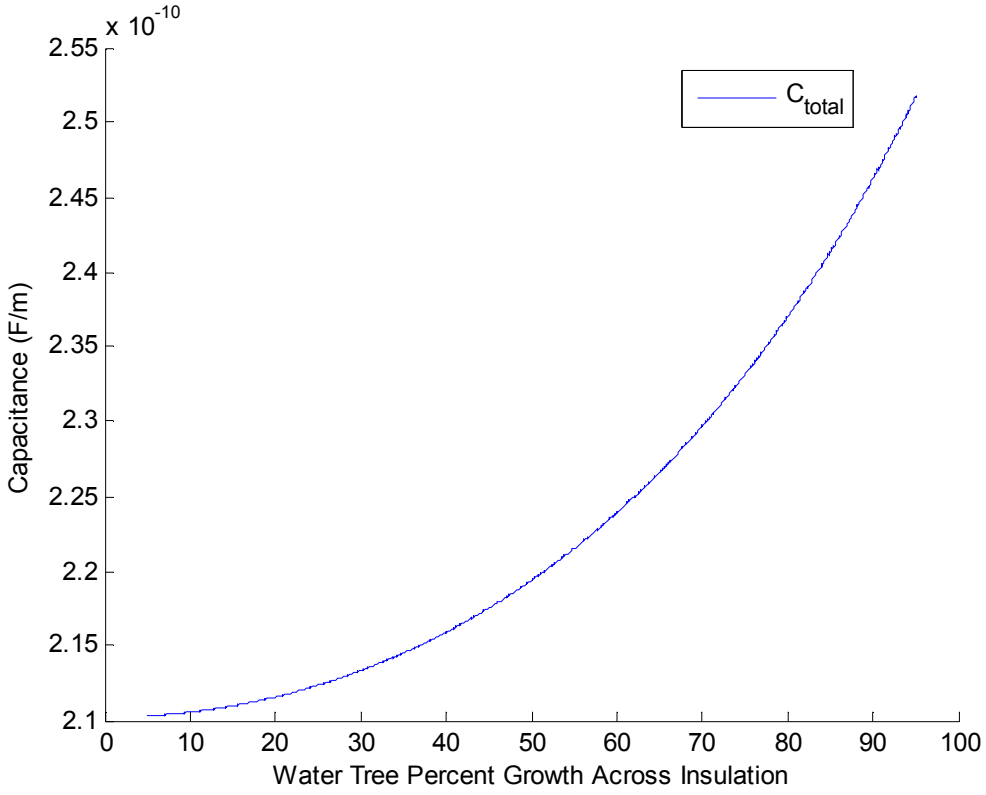

Figure 32: Overall Capacitance of Water-Tree at Different Developmental Stages

The capacitance of water-tree will gradually increase as it breaches the insulation layer. Prior to the critical breakdown, however, the overall magnitude change of water-tree capacitance is relatively small.

The finite element analysis method provides two-dimension values of the water-tree afflicted cable slices. Due to the very complex electromagnetic interactions from the three-dimensional water-tree structures, it is necessary to use a simplified model for the three-dimensional water-tree capacitance estimation. An approximation is obtained by multiplying the two-dimension capacitance/length value with the narrow axis length from the water-tree boundary condition. Since water-tree is approximately cone-shaped in 3D, the narrow axis length is roughly enough to three-dimensional width of the water-tree afflicted area.

2.4 Chapter Conclusion

By learning its underlying mathematical principle, water-tree behavior in large systems can be studied and predicted; therefore, modeling is the first step in developing a reliable method for water-tree location and estimation.

Due to the complexity of water-tree structure, appropriate assumptions and approximations must be made for the modelling process. Since surfaced–originated, uniform cluster vented trees are the most common and significant type of water-tree, it becomes the focus of the study. The final capacitance calculation for a three-dimension water-tree is estimated using the values obtained from the two-dimension cable slices.

The principle and approach developed in this chapter is not limited to the given assumptions. Finite element analysis is a valuable tool in water-tree modeling because the method can be modified and expanded to fit many situations. For example, by changing the permittivity distribution pattern, the method can be altered to study bow-tie tree or conductor-originated vented tree. By adding weight ratios to the generalized multiple dielectric-material equation, non-uniform cluster water-tree can be modeled. By changing the boundary conditions for the water-tree afflicted region, water-tree developed from other voltage and current sources can be modeled. It is a flexible method with potential to fit many complex scenarios.

Chapter 3

High Frequency Pulse Detection Method for Water-tree

3.1 General Background on High-Frequency Pulse Detection

Currently, the fault detection techniques in the power industry tend to focus on VLF and OPF methods. High-frequency methods, however, do exist for some applications. Although they may not be directly applicable to early-stage water-trees detection, their results have yielded useful information and provided potential solutions for water-tree detection using VHF methods.

Previously, Texas A&M University has done research on high-impedance fault detection using VHF method. The specific method focused on high-impedance arcing faults. During the research, 86 separate faults stages were studied across six different feeders. Their system responses were collected and analyzed. The results showed that high-impedance arcing faults produce drastically increased amount of high frequency components. Using this observation, a detection method was developed to track the "signature" of the fault through identification of high frequency component composition [59~64].

The arcing fault detection technique provides valuable insight on potential methods for water-tree detection. Similar to arcing faults, water-tree is a complex structure and produces a number of high-frequency components. Thus, it is theoretically possible to build signature profiles for different water-tree corrosions progress.

Adaptation of the technique to early-stage water-tree detection, however, is much more challenging due to a few key differences. These differences are illustrated by the high frequency characteristics of water-tree.

Swedish Royal Institute of Technology has carried out research on high-frequency characteristics of water-tree afflicted cable. In their experiments, both laboratory-aged and ex-service XLPE cables were tested for their insulation leakage conductivity and water content. The experiment was done using a two-port setup. The result showed that for cables with a water content of 13% and 7%, the corresponding conductivities are approximately 0.005S/m and 0.22S/m [65~70].

The implication is that the conductivity of water-tree is entirely dependent on the water content of the cable. By extension, it also depends on the continuous water pathways in the insulation layer. In the field, the real-time water content of the cable may vary with the environment. For normal operating conditions, the cables will not be submerged in high concentration of moisture/water over prolonged period. Although it is possible for events such as large-scale flooding or collapse of cable housing structure to place the cable in watery environment, such events are highly visible from outside and the affected cable segment can be tracked using methods much simpler than water-tree detection. For the scenarios where remote location of water-tree is the only viable option, the water content of the cable tends to be significantly less comparing to its counterpart under the laboratory condition. This results in very low conductivity; therefore, the expected water-tree structure will be almost purely capacitive as discussed in chapter two.

Experiments also showed that the high-frequency characteristic of water-tree is different from the characteristic of an arcing fault. Specifically, TDR reading were taken

for a water-tree afflicted cable segment utilizing 300kHz to 300MHZ generated waves. The readings showed significant high-frequency attenuation. The attenuation was not attributed to water-tree, but it still served to hinder the detection process [71~77].

In chapter two, it is shown that early-stage water-tree capacitance ranges from 1nF to 12pF. The basic concept of the VHF model is reducing the equivalent impedance of the water-tree into a more manageable level.

Since it is impractical to insert full physical models of the water-tree into a large system, simplified representations must be used. Fortunately, water-tree develops at a very slow rate; therefore, its physical characteristics remain constant over a short period. Thus, a lump model is sufficient for observing the water-tree frequency response.

The required frequency for water-tree detection is inversely proportional to the equivalent impedance of water-tree. Due to the small capacitance of a developing water-tree, the required frequency is very large. At this frequency, measurements will be subjected to high-frequency attenuation. The presence of high-frequency attenuation unrelated to water-tree also means that the attenuation itself cannot be used as an indicator of water-tree presence and it exists purely as a hindrance to the detection process.

The various attenuation effect experienced by VHF method is not limited to the high-frequency range. The innate high impedance of a developing water-tree renders standard Tan-Delta or Partial Discharge methods ineffective, especially in long cables. For example, dielectric spectroscopy measurement showed that an early-stage water-tree had limited frequency dependent response. The Tan-Delta deviation was very small at less than 0.5°. The overall result was a significantly weaker travelling wave [78~82].

There are several issues associated with a weak travelling wave. For example, equipment sensitive is a significant problem. At the same technology level, more precise instrument means higher cost.

Other problems include mathematical singularities in the detection algorithm. Traditionally, traveling wave is analyzed through various transformation algorithms. Unfortunately, low-amplitude and heavily attenuated travelling waves tend to create many singularity points. Thus, frequency domain observations of weak travelling waves are often unreliable [83~92].

3.2 High-Frequency Pulse Detection of Water-Tree

From economical perspective, VHF methods are not the first choice for cable testing. They are complex testing methods that require specialized instruments and can potentially place heavy stress on the cable. They are, however, uniquely suited in this situation detection due to the high-frequency characteristic of water-tree.

3.2.1 Motivation for High-Frequency Pulse Detection Method

In recent years, there has been an increasing demand for renewable energy. Due to the rising cost of fossil fuel and greater awareness on the environment, nations around the world have focused their effort on creating clean and renewable supplies of electrical power. For this purpose, wind power has received large amount of attention.

By 2014, the installed wind-power capacity in United States has exceeded 60GW and it is increasing each year [93~96]. Researchers have dubbed the recent years the “era of wind”. Wind power expansion is characterized not only by the increasing capacity, but also by the greater integration with the grid [97~98]. The expansion process, however, is

not without challenges. One significant issue is encountered by southeastern power utilities. In eastern United States, owing to its high population density, new wind farms have gradually become cost ineffective due to limited wind availability and land acquisition expense. Thus, utilities must now secure new sources of wind. Amongst the potential choices, oceanic locations have emerged as a potent solution to the problem.

Oceanic wind facilities as such offshore windfarms offer many advantages. For example, lacking geographical barriers, oceanic wind is generally stronger comparing to its inland counterpart. In addition, the different heat capacities of rock and water also serve to create stronger wind current during day/night cycle. Finally, the land acquisition cost of oceanic locations is greatly reduced, especially for high population density regions.

There are, however, some significant issues associated with offshore windfarms. For example, one aspect of the issue is technological limitation, such as platform construction in deep water or equipment operation in high moisture environment. Legal limitation is also a potent issue for offshore facility placement. In South Carolina, state law prevents offshore windfarms to be placed near shore; therefore, the turbines have to be constructed in federal water instead. In United States, federal water generally refers to regions more than 30 miles (50 kilometers) from the shore. Other reasons may influence windfarm placement. For example, they may be placed far away from the shore to take advantage of locations with particularly strong wind.

In either case, power delivery to the grid is an unavoidable issue. Although power transmission to a distance target has always been a basic function of the electric grid, delivering power across the ocean is much more challenging. On land, long-distance

transmission is typically handled by high-voltage overhead lines. In ocean, however, building transmission towers for overhead lines is much more expensive. In addition, locations ideal for wind facilities are guaranteed to experience strong wind and by extension, strong waves as well. In this case, overhead transmission lines are also vulnerable to environmental hazards. As the result, cross-ocean connections tend to favor submarine transmission cables instead of overhead lines.

Submarine cable is a sub-category of underground cables. Like inland underground cables, submarine cables are conducting wires protected by insulation. Since construction on ocean floor is both technologically challenging and economically prohibitive, the cables are generally placed directly on ocean floor instead of cable ducts. Due the oceanic hazards, the submarine cable is also protected by armor or other type of protective wrapping.

A very important characteristic of submarine cable is the individual segment length, especially for transmission level voltage. Since these cables are typically point-to-point power cables by design, there is reduced need for underwater splices. In addition, splices also tend to increase the risks of failure (for both electrical and mechanical reasons). As the result, submarine cable segments are generally significantly longer comparing to their inland counterparts.

In chapter one, the effect of aging power infrastructure and the role of underground cable in the situation is discussed. The aftermath of a submarine cable failure also compounds the problem. Due to the high service voltage for transmission cables, a critical stage water-tree has a high probability of developing into a hybrid-tree. The hybrid-tree is characterized by creation of electrical-trees in the final insulation

breakdown stage. Thus, hybrid-tree induced faults have significantly lower fault impedance and larger fault current. The large fault current may also create secondary effects that amplify the problem.

Point-to-point transmission cables also serve to deliver large amount of power across the grid connection. Consequently, a fault on submarine cable may also drop large amount of generation from the grid and creates further imbalance in the system.

Repairing a submarine cable fault is also problematic. After disconnecting the service and identifying the fault location, specialized vessels must be dispatched to the region. Optimistically, the process can still take up several days.

Due to the resource cost of the repair work and the service interruption, it is highly desirable to locate the water-tree before it reaches the critical stage. Researches have indicated that preventative maintenance is the key for ensuring long, healthy cable operational lifespan. Unfortunately, extracting operational information from submarine cables is not an easy task. The oceanic environment prohibits most forms of direct observational techniques and the long cable segment creates problems for remote detection techniques. The situation is especially problematic for water-tree detection, due to the extremely high impedance of early-stage water-tree.

Thus, it is necessary to develop a detection method, which can identify an early-stage water-tree despite its high impedance. The method needs to be a remote-location technique and does not require the utilities to dive under the ocean. The method must also be able to determine the severity of the water-tree for preventative maintenance. Finally, the method must be none destructive so the cable may resume normal operation afterwards.

3.2.2 Methodology for High Frequency Pulse Detection

Early-stage Water-tree detection in long distance cables can be separated into two objectives: locating the water-tree and estimating its severity.

For locating the water-tree, the main challenge is overcoming the innate high impedance of the water-tree structure. In chapter one, the advantages and disadvantages of various detection methods are discussed. Most of these methods are ineffective against an early-stage water-tree. An early-stage water-tree is simply not visible under OPF or VLF. More specifically, under OPF and VLF, the accuracy requirement for the instrument is simply too high for economical implementation. Fortunately, VHF methods have shown more promise. In VHF method, the high frequency lowers the impedance associated with the capacitance portion of the tree. For sufficiently high frequency, the water-tree impedance is reduced to a level that commercially available instruments are sufficient to differentiate healthy and water-tree afflicted insulation. By locating the pulse reflection from the cable discontinuity created by water-tree, the specific location of the water-tree can be determined.

For estimating water-tree severity, it has been observed that for water-tree of a given capacitance, there exist certain pulse frequencies that generate specific and computer-recognizable reflect patterns. Thus, it is possible to estimate the water-tree capacitance, by extension its corrosion progress, using pattern recognition techniques.

A VHF pulse detection method is developed using these principles. The method generates a high-frequency pulse at one of the cable segment terminals and observes the pulse response pattern at the same terminal. The location of the water-tree is determined by the pulse reflection time and the severity of the water-tree is determined by the pulse

reflection pattern under various frequencies. The method will be referred as High-Frequency Pulse Detection (HFPD) method.

3.2.3 Method Testing Preparation

3.2.2.1 Water-Tree Model

Before HFPD method can be tested, it is necessary to setup an appropriate simulation system. A mathematical model for water-tree is provided in chapter two. Since the finite element analysis method for water-tree is very computation intensive, it is impractical to insert the full water-tree model into the system simulation; therefore, for the HFPD tests, simplified lump models will be used to represent the water-tree. The lump models are shown below in Figure 33:

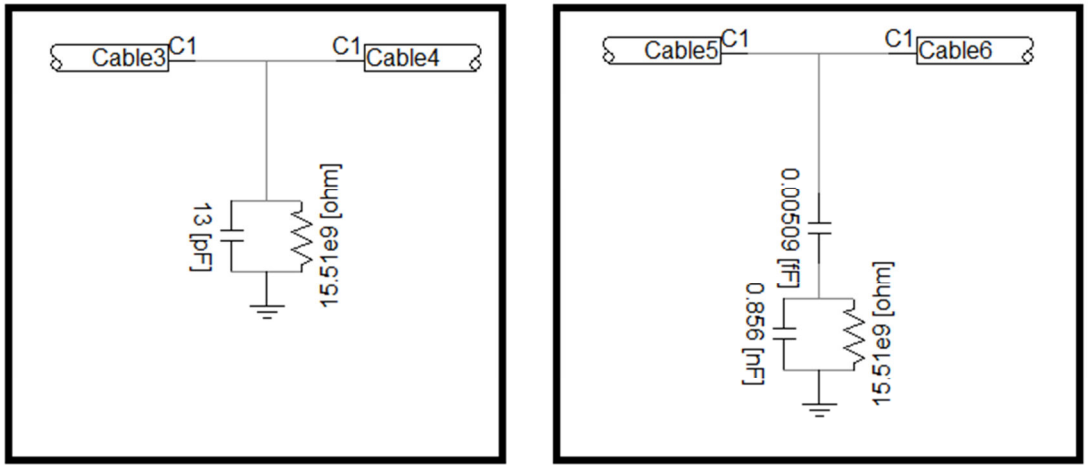

Figure 33: Lump Model for Water-Tree: Late Stage (Left) vs Early-stage (Right)

There are two choices for the lump model. The lump model on the left represents a late-stage water-tree where the water-tree branches have penetrated more than 80% of the cable insulation. The lump model on the right represents the early-stage water-tree where less than 30% of the insulation layer has been breached. Between 30% and 80% corrosion, either model can be used for HFPD purpose.

It is necessary to note that the capacitance value for lump models used in this chapter will be arbitrarily chosen within a reasonable range. According to the mathematical model obtained in chapter two, the developing water-tree is primarily a capacitance structure. More specifically, the resistance value is simply too high. Since the resistance value cannot be altered by changing input frequency, it will remain too high for detection purpose. Thus, the HFPD method only concerns the capacitance of water-tree. For this purpose, the lump models will consist of a capacitive element of variable magnitude and a parallel resistive element greater than 1GΩ.

From chapter two, water-tree is modelled for cable shown in Figure 34:

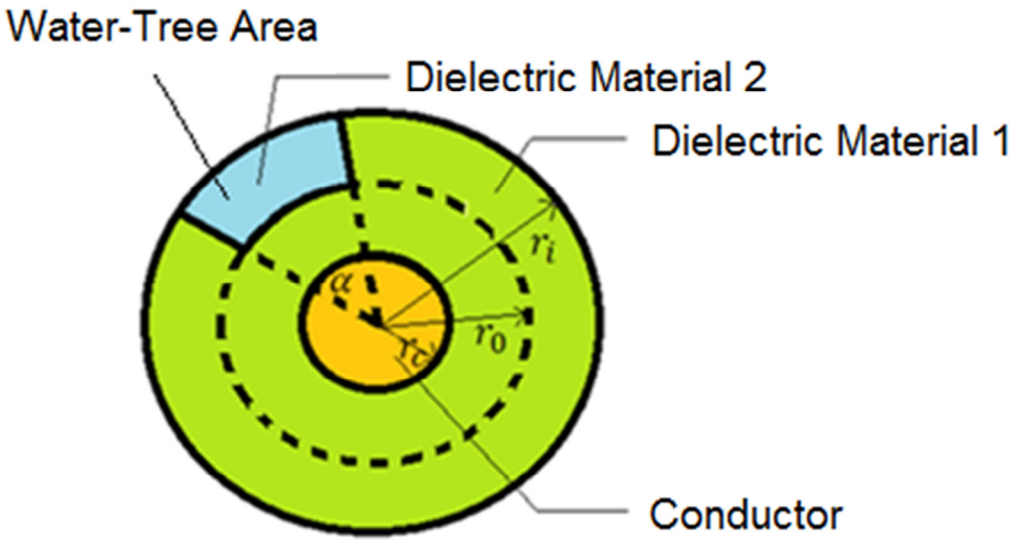

Figure 34: Water-Tree Afflicted Cable Segment

The water-tree is placed under finite element analysis as shown below in Figure 35:

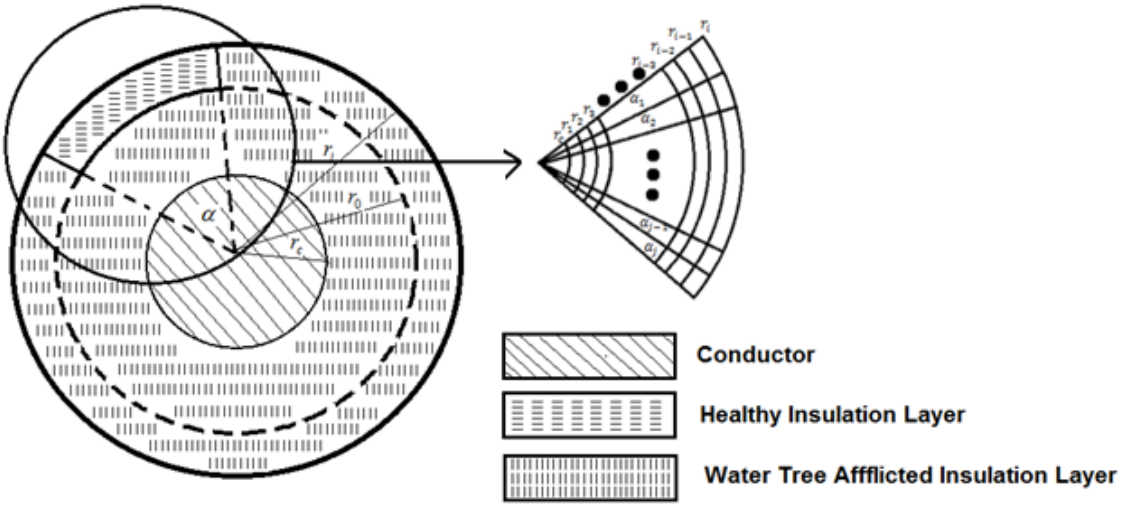

Figure 35: Water-Tree under Finite Element Analysis

The water-tree capacitance parameter is obtained using the following formula based on finite element analysis:

$$C_{total} = \frac{2\pi L}{\frac{\ln\left(r_0/r_c\right)}{\varepsilon_2} + \frac{\ln\left(r_i/r_0\right)}{\varepsilon_1 * \frac{\alpha}{2\pi} + \varepsilon_2 * \left(1 - \frac{\alpha}{2\pi}\right)}} \quad \text{.....(23)}$$

Where:

L is the length of the segment

r_i is the radius of the cable

r_0 is the radius of the inner ring of insulation

r_c is the radius of the conductor

α is the angle of the area with permittivity of ε_1

The capacitance value in the lump model will be determined using the equation above. The resistance value is determined empirically.

3.2.2.2 Pulse Generation

The simplest pulse generation strategy for the test system is the lightning pulse shown below in Figure 36:

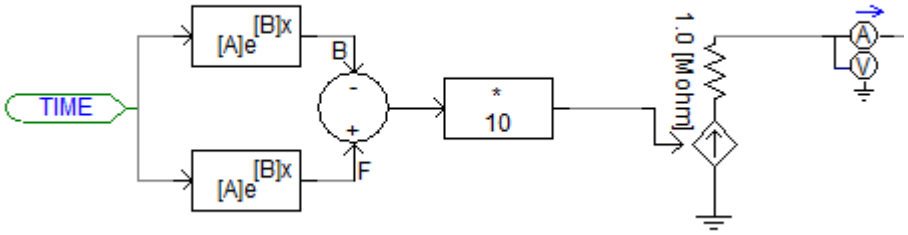

Figure 36: Lightning Pulse Model

The lightning pulse generator provides a simple mathematical model for the capacitance estimation process. The model can also be modified to include the fundamental component as shown below in Figure 37:

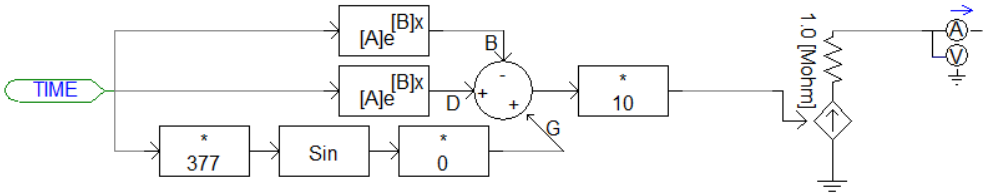

Figure 37: Lightning Pulse Model with Fundamental Component

Experimental results show that the difference between the two models is minimal in regards to the HFPD test.

Mathematically, the lightning pulse is modelled by the equation below:

$$y(t) = A * (e^{-Bt} - e^{-Ct}) \quad \text{.....(24)}$$

Where:

A: Controls the magnitude of the pulse. Commercially available pulse generator can generate a pulse up to 10kA

B and C: (C > B): Controls the frequency of the pulse. For fixed C values, larger B value results in higher pulse frequency

3.2.2.3 Testing System Conditions

There are several variations of the testing system: DC, AC, online and offline. Many of the European submarine transmission systems are HVDC based. In contrast, United States systems tend to favor HVAC instead.

A sample HVDC system is shown below in Figure 38:

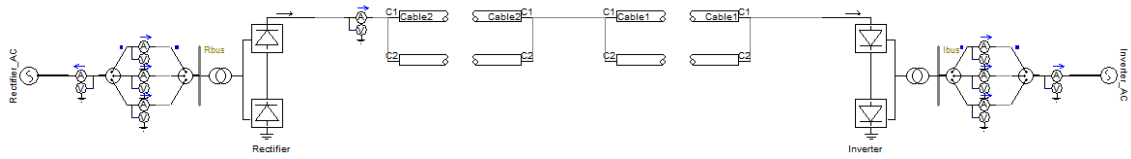

Figure 38: Sample HVDC System

A sample HVAC system is shown below in Figure 39:

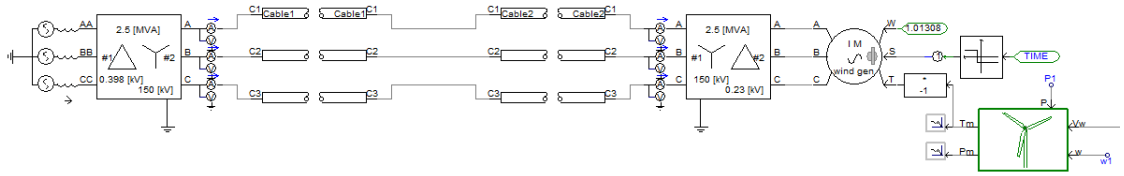

Figure 39: Sample HVAC System

It is necessary to note that for offline test, DC and AC systems have no significant difference.

For HVDC simulations, the pulse generator can either be placed on the AC side or the DC side of the converter. Due to the frequency elimination effect from the converter, the pulse generator should be placed on the DC side as shown below in Figure 40:

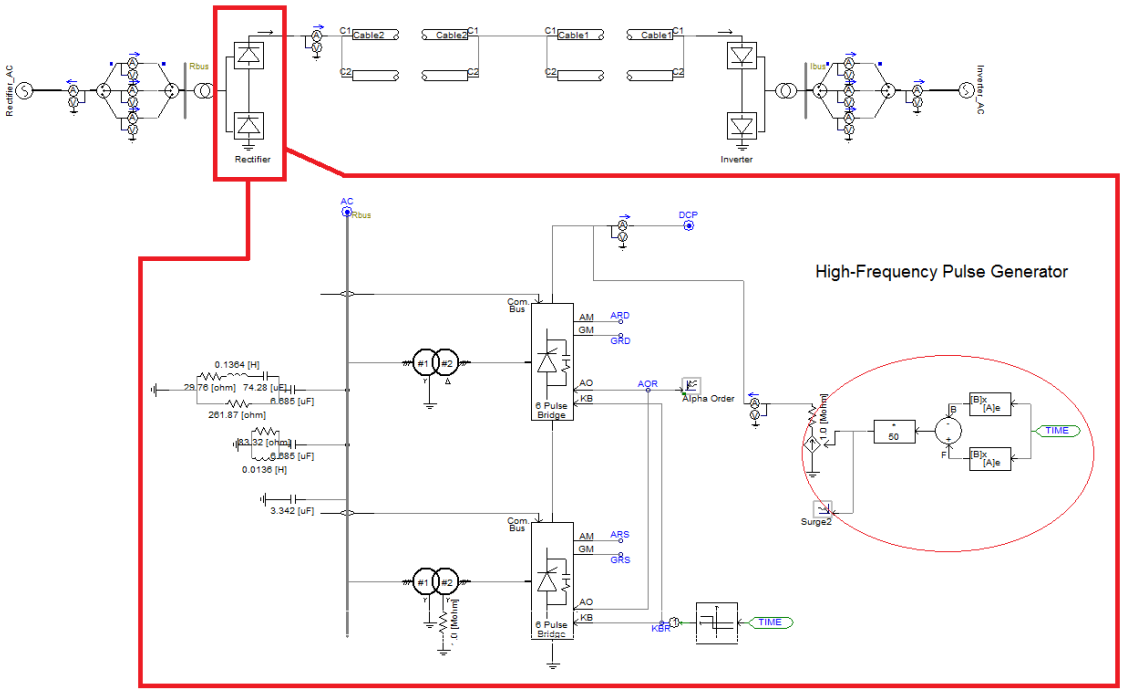

Figure 40: DC Side Lightning Pulse Generator in HVDC System

Similar, HVAC simulation also has two potential pulse-generator placement locations: low-voltage side and high-voltage side of the transformer. Like the converter, the transformer may also eliminate certain pulse responses. Thus, the pulse generator is placed on the high-voltage side as shown below in Figure 41:

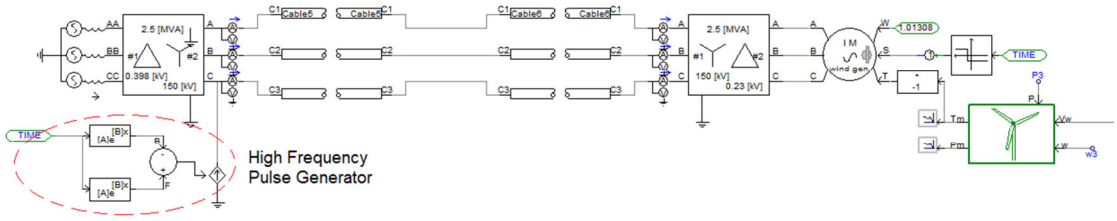

Figure 41: High-Voltage Side Lightning Pulse Generator in HVAC System

In regards to the online and offline test comparison, the pulse response is proportional to the magnitude of the input pulse. Since the magnitude of the water-tree response is small, it is preferable to use an input pulse of large magnitude. It should be

noted that like many PD tests, exceedingly large input pulse may cause permanent damage to the cable insulation; therefore, it is preferable to perform the offline test.

For offline tests, DC side of HVDC system and high-voltage side of HVAC system has no practical difference. Both cases can be represented by a single cable system as shown below in Figure 42:

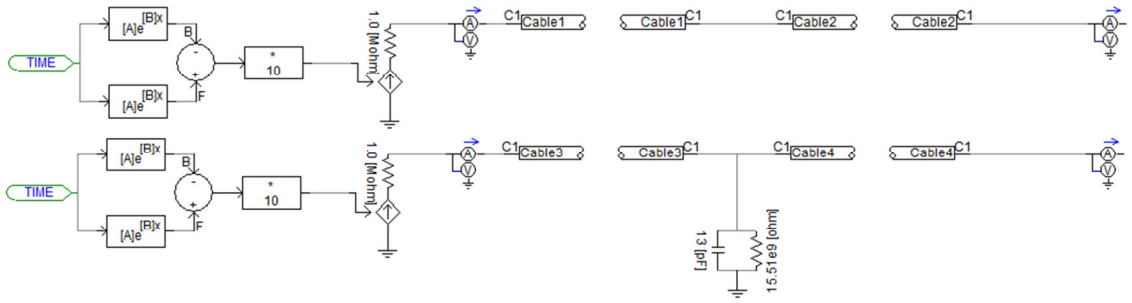

Figure 42: Offline Test System: Without Water-Tree (Top) vs With Water-Tree (Bottom)

For offline tests, the pulse generator is the sole source of voltage and current in the system as shown below in Figure 43:

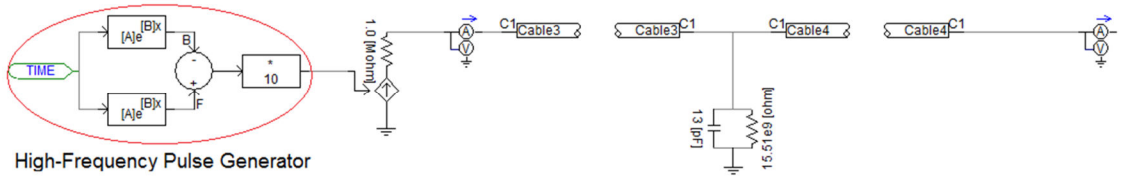

Figure 43: Pulse Generator in Offline Test System

3.2.2.4 Test Procedure

1) The high frequency pulse is triggered at time = zero, the voltage at the input terminal is recorded until pulse reflection from the other cable terminal appears. This is referred as a single cycle of the test procedure.

2) The water-tree pulse response waveform is recorded for comparison purpose.

3) The lightning pulse parameters are altered to obtain responses for different frequencies.

4) The water-tree parameters are altered to obtain responses for different water-tree capacitances.

5) The water-tree locations are altered to obtain responses for different water-tree distances.

The HFPD test is done in PSCAD and the following parameters are utilized:

1) For the high-frequency pulse generator blocks in Figure 43, the subtraction block is based e; coefficient of base is one and the coefficient of exponent is fixed at -3e9.
2) For the addition block of the high-frequency pulse generator, the block is based e; coefficient of base is one and the coefficient of exponent will be varied between -1e4 and -2e9 to adjust the input pulse frequency.
3) The cable model uses the PSCAD frequency dependent underground cable model. The parameters are shown below in Figure 44. Depending on the specific need of the user, the cable parameters should be adjusted to match the condition of the actual cable.

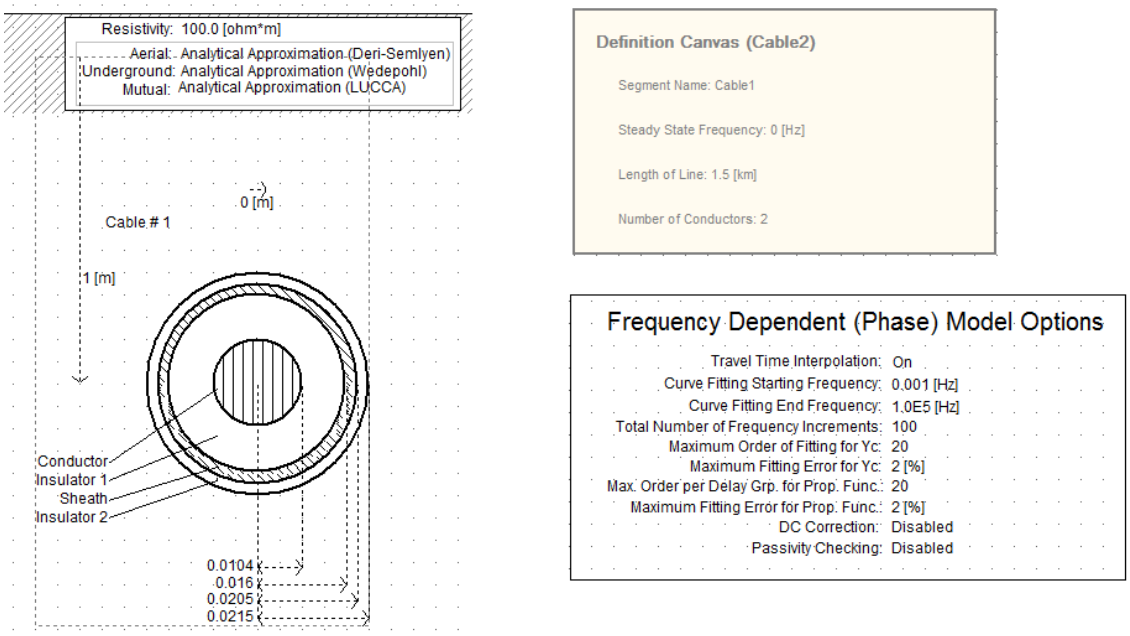

Figure 44: PSCAD Cable Test Parameters

4) The length of the cable segments will be varied to represent cables of different lengths.
5) The cable is divided into two segments. By varying the length of each segment, the location of water-tree can be adjusted.
6) The resistance value of the lump model will remain fixed at 15.51e9. The capacitance value will be varied to simulate water-trees of different severities.

3.2.3 Test Case Results

The shape of the high-frequency pulse is shown below in Figure 45:

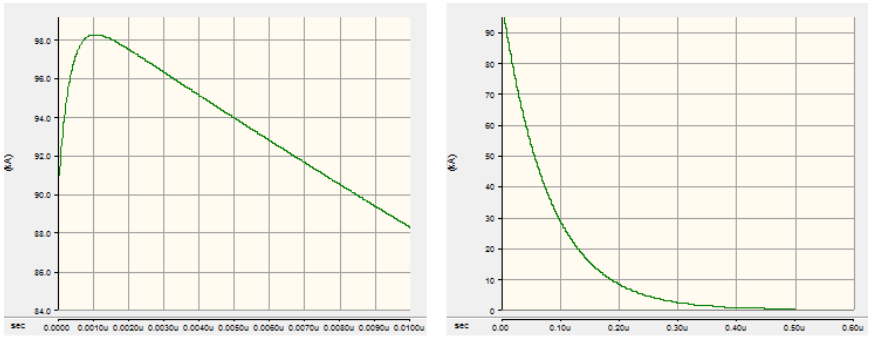

Figure 45: High Frequency Input Pulse: Initial Moment (Left) and Overall (Right)

3.2.3.1 Water-Tree Pulse Response Cases

The first test case result is from a three-system comparison case as shown below in Figure 46:

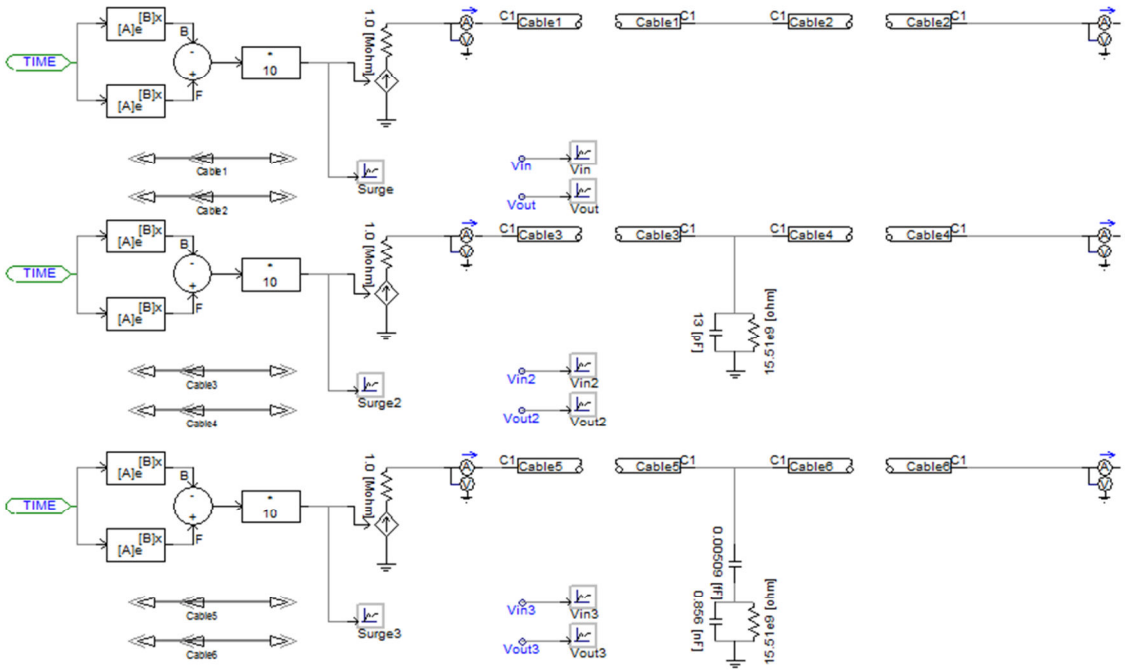

Figure 46: Three-System Comparison Case

The three systems are, from top to bottom: healthy system without water-tree, high corrosion depth water-tree and low corrosion depth water-tree.

The result from the full cycle is shown below in Figure 47:

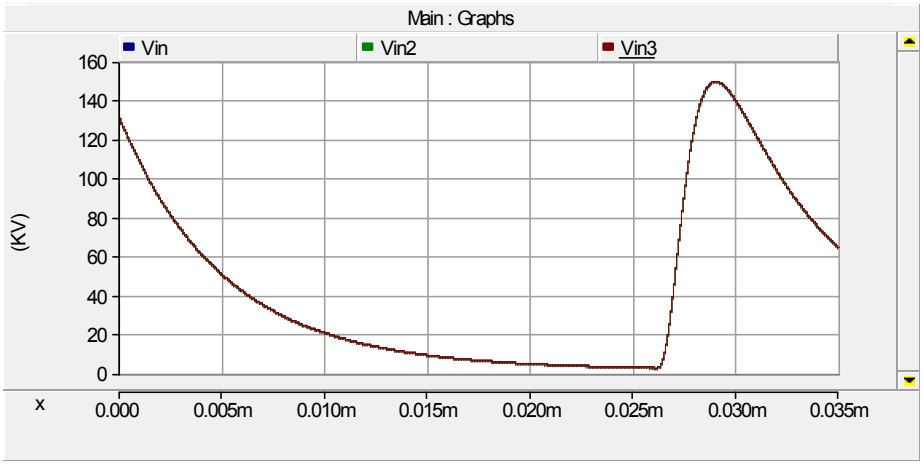

Figure 47: Overall Pulse Response from HFPD Method

The particular test is an offline system test with a 2km cable for 60Hz system. The lump model water–tree capacitance is 13pF. The test pulse is 60kHz and the water-tree is placed 1.5km from the input terminal. The two large pulse responses correspond to the initial pulse and reflected pulse from the other cable terminal.

A zoomed in version on the pulse response is shown below in Figure 47:

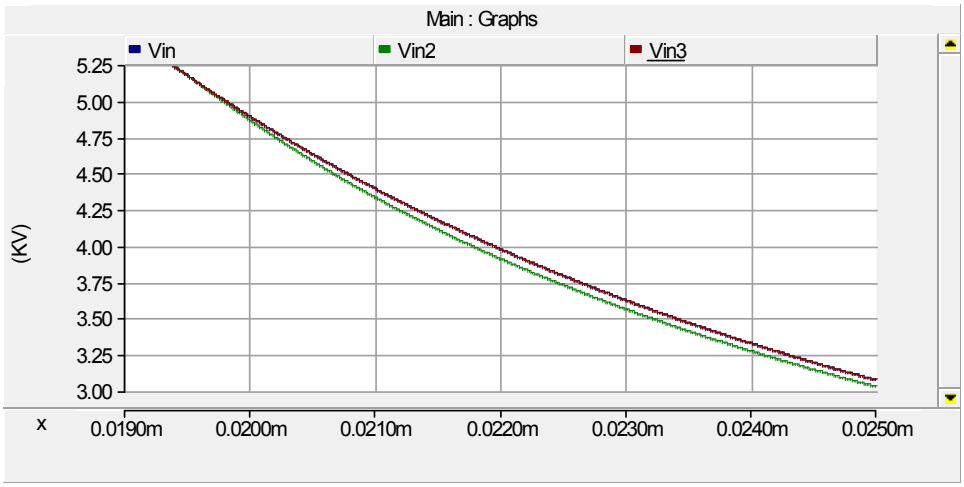

Figure 48: Pulse Response from Water-Tree

Depending the test pulse frequency, there are three potential patterns for the pulse response as shown below in Figure 48:

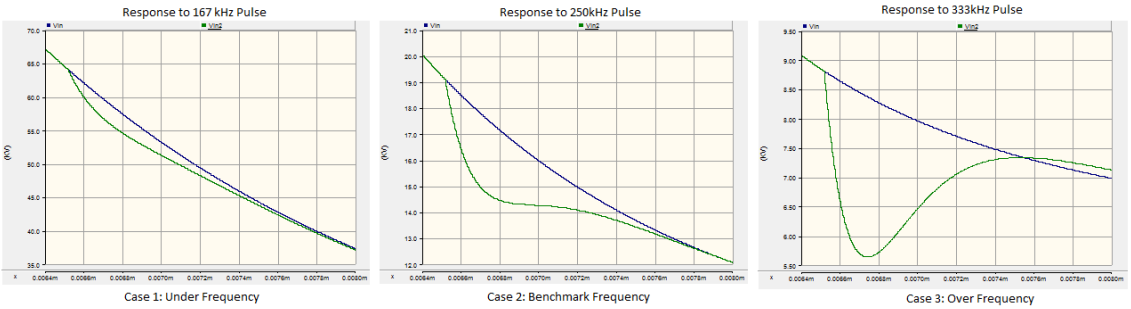

Figure 49: Pattern Identification Possibilities

The three cases are under-frequency, benchmark-frequency and over-frequency. For under-frequency response, the applied frequency is too low. Thus, it cannot effectively reduce the water-tree capacitance; therefore, the pulse response pattern from water-tree afflicted system is essentially the same as the healthy system. The minor deviation is difficult to identify since there is no healthy system response comparison in actual field.

Benchmark-Frequency represents a unique “plateau” pattern as shown below in Figure 50:

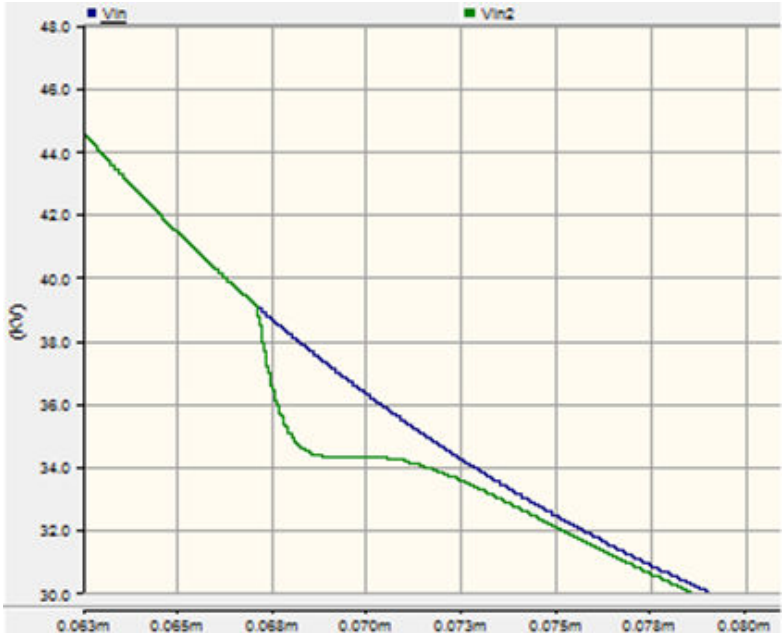

Figure 50: Benchmark Frequency Pattern

For water-tree of certain capacitance, there is a small range of frequencies that generate the flat plateau pattern. In section 3.1, the possibility of building a frequency component profile for high-impedance faults is discussed. Using the same principle, for water-tree of certain capacitance (corrosion depth), there will be a corresponding benchmark-frequency range that serves as its HFPD response signature.

The over frequency case refers to the situation where the applied frequency is too high. In this case, the pulse response from water-tree afflicted system is significantly different from the healthy system. For example, when the applied pulse frequency is increased to 6MHz for the 13pF, 2km cable system, the water-tree pulse response is shown below in Figure 51:

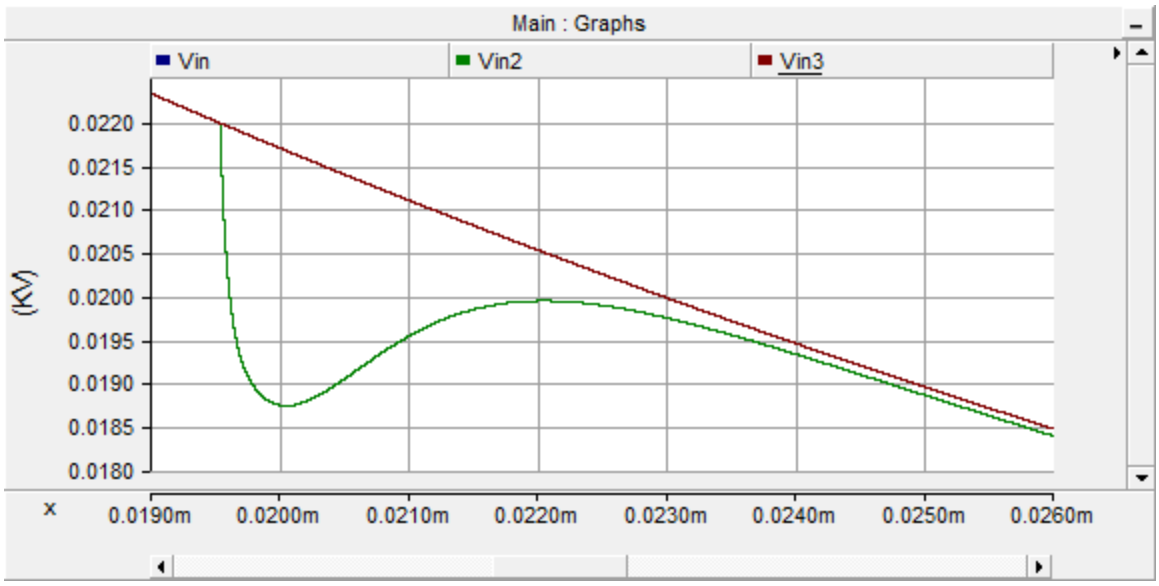

Figure 51: Over Frequency Water-Tree Pulse Response from 6MHz Pulse

Although the over frequency case is useful for locating the water-tree, it lacks distinct, quantifiable features; therefore, it is not useful for estimating the water-tree severity.

The process of determining the benchmark frequency range is referred as benchmark-frequency identification. The three potential cases are summarized below in Table 1:

Table 1: Water-Tree Pulse Responses from HFPD Method

Case	Name	Description
One	Under-Frequency Response	The shape of the water tree afflicted system's response is similar to the healthy system.
Two	Benchmark Frequency Response	Certain part of the water tree afflicted system's response will have a flat plateau.
Three	Over-Frequency Response	The shape of the response from the water tree afflicted system is drastically different from the healthy system.

3.2.3.2 Pulse Response Pattern Identification

In essence, benchmark-frequency identification is a pattern identification technique, which searches for signature patterns in water-tree pulse response. These patterns are the results of variations in important cable test parameters.

The benchmark frequency is created by the superposition of the sending pulse and reflection pulse from water-tree as shown below in Figure 52:

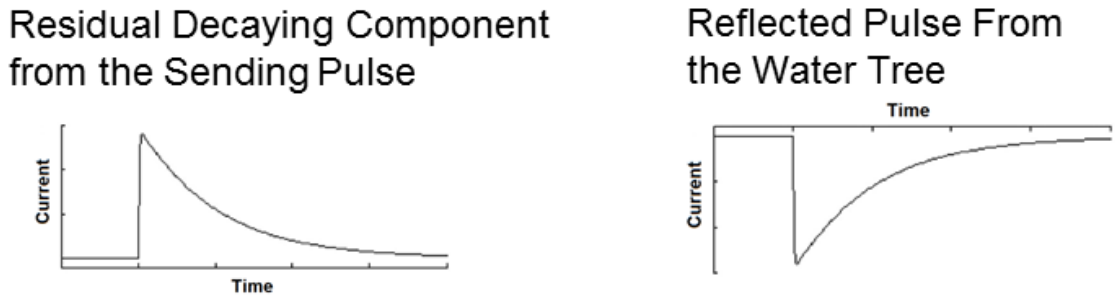

Figure 52: Establishment of the Benchmark Frequency

The variation in the input pulse frequency affects the magnitude of the residual pulse. Since frequency variation also change the water-tree impedance and by extension, the reflection coefficient of the water-tree discontinuity, it affects the magnitude of the reflect pulse as well. Experiments show that for the same water-tree capacitance, location and cable length, varying the frequency will produce a gradually shifting pulse response pattern corresponding to the shifts in frequency.

Other parameter variations also induce pattern shifts in water-tree pulse response. For example, a test case is shown below in Figure 53:

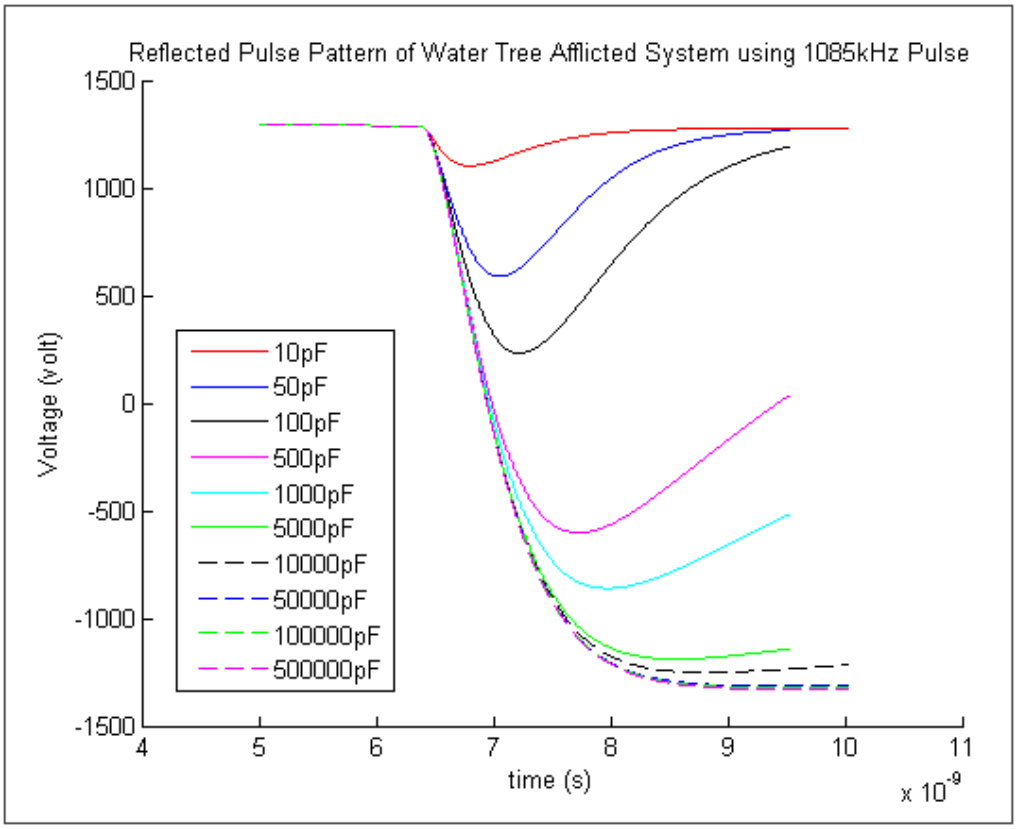

Figure 53: Water-Tree Response Trend Test Case for 1 Meter Cable under 1085kHz Pulse

The test case uses 1085kHz input pulse on one meter cable. The water-tree capacitance is varied for comparison purpose. The test case also shows gradual shifts in the water-tree pulse response pattern corresponding to parameter variation.

The benchmark frequencies are unique points in these pattern shifts. For a certain water-tree capacitance and cable length (water-tree location), there is only be one benchmark frequency range at maximum. In some situations, no benchmark frequency range can be established. The specifically relationship is shown below in Table 2. The table uses the three primary variables for the HFPD test cases: cable length, fault capacitance and the corresponding benchmark frequency.

Table 2: Benchmark Frequency under Different Test Case Parameters

		Water Tree Fault Capacitance (pF)						
		10	50	100	500	1000	5000	10000
Cable Length (m)	1	0	0	0	0	0	0	0
	2	0	0	0	0	0	0	0
	5	20000	0	0	0	0	0	0
	7	17358	0	0	0	0	0	0
	10	15000	0	0	0	0	0	0
	20	9680	3672	0	0	0	0	0
	50	5000	2900	1920	0	0	0	0
	70	3800	2437	1736	0	0	0	0
	100	2900	1920	1500	0	0	0	0
	200	1678	1200	950	384	0	0	0
	500	718	540	480	340	0	0	0
	700	570	500	456	310	245	0	0
	1000	384	300	250	150	98	0	0
	4000	227	160	98	55	40	0	0
	10000	134	117	92	33	25	10	0

The zero entries in the table refer to the combinations of cable parameters where benchmark frequency does not exist.

3.2.3.3 Benchmark Frequency Trends

Certain trends exist for benchmark frequencies. These trends represent the relationship between various HFPD test characteristics and the resultant pulse response. Figure 54 shows the relationship benchmark frequency and distance of water-tree from the input terminal:

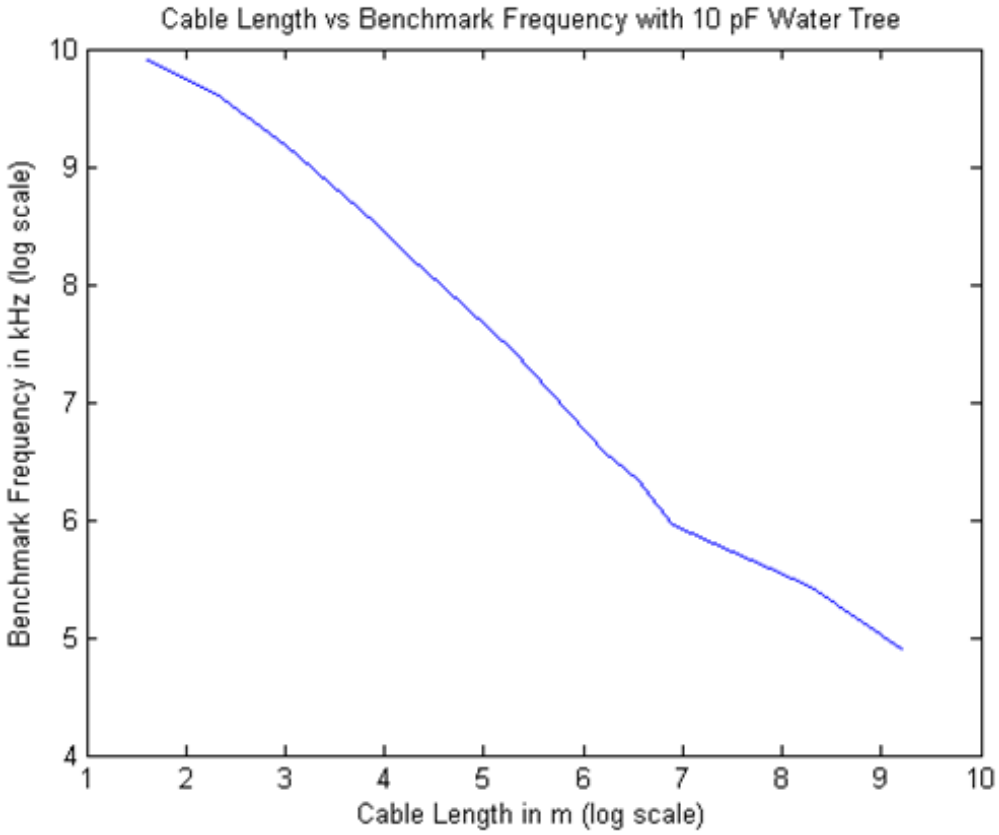

Figure 54: Water-Tree Distance vs Benchmark Frequency

The water-tree distance is represented by the cable length. Variations in cable length move water-tree into different locations. For a certain fault capacitance, the benchmark frequency (log scale) is linearly proportional to water-tree distance (log scale) with a slope of approximately -0.5.

A trend also exists between the relationship of water-tree capacitance and benchmark frequency. The trend is shown below in Figure 55:

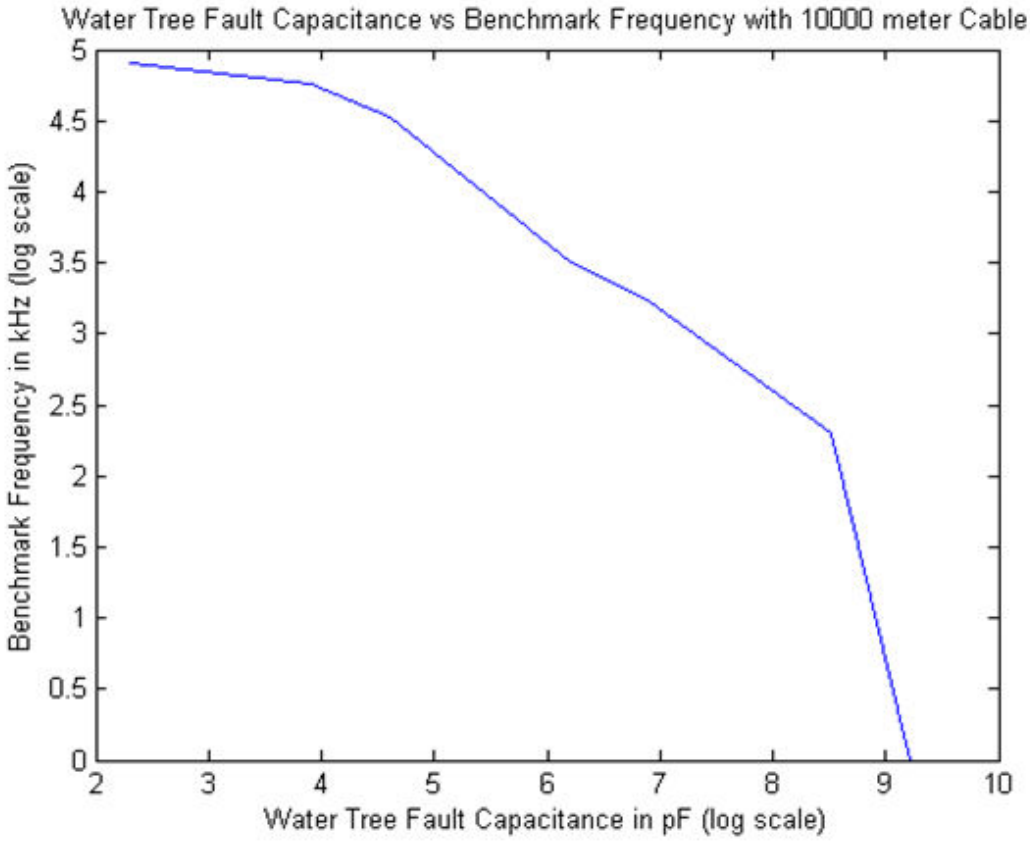

Figure 55: Water-Tree Capacitance vs Benchmark Frequency

The test case is done for 10km cables and the water-tree is located 5km from the input terminal. The x-axis can be viewed as a gradually developing water-tree and the y-axis is the corresponding benchmark frequency at different development stage. Under log scale, the benchmark frequency is approximately inversely proportional to the water-tree capacitance. It is also shifted along both x-axis and y-axis.

Figure 56 shows a three dimensional view of the relationship between water-tree distance, water-tree capacitance and the benchmark frequency. All parameters are under log scale.

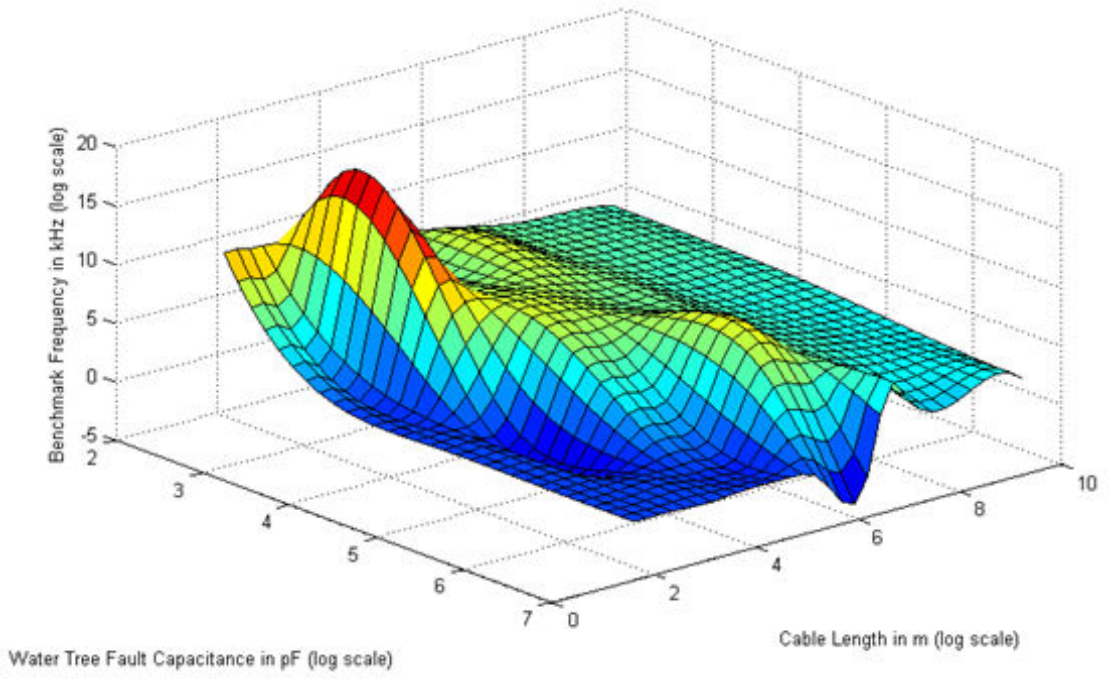

Figure 56: Water-Tree Distance vs Water-Tree Capacitance vs Benchmark Frequency

The following trends are observed for the benchmark frequency:

1. For the same water-tree distance, larger water-tree capacitance results in lower benchmark frequency.

2. For the same water-tree capacitance, farther water-tree distance results in lower benchmark frequency.

3. For very far or very close water-tree, no benchmark frequency can be established.

4. For very large or very small water-tree capacitance, no benchmark frequency can be established.

The benchmark frequency trends are summarized below in Figure 57:

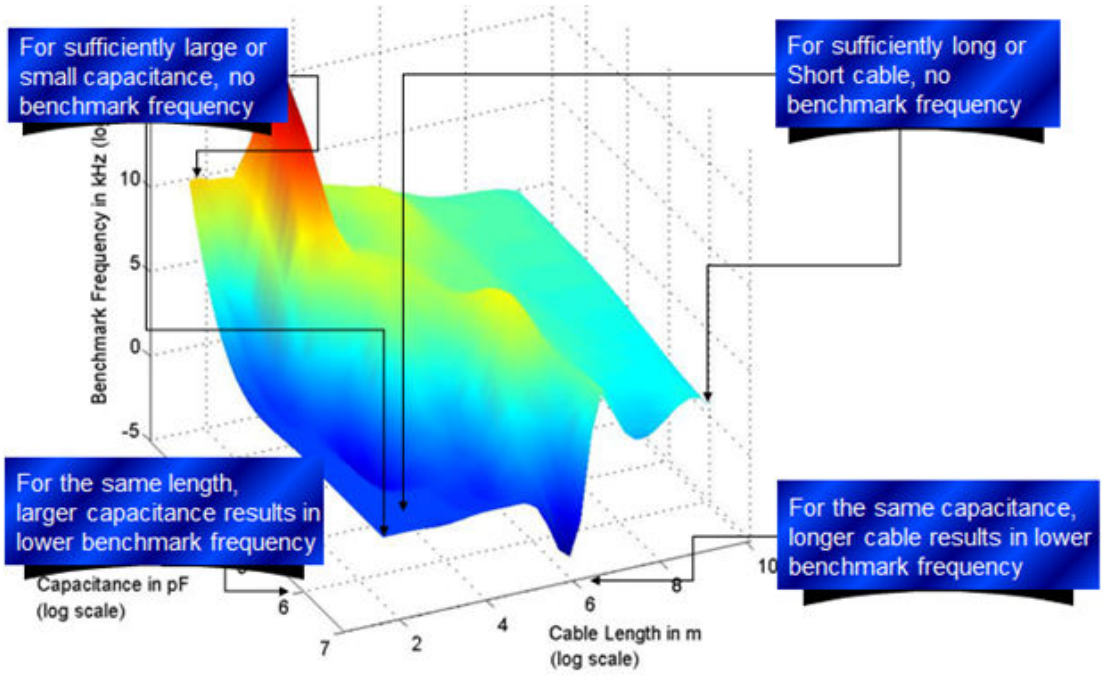

Figure 57: Benchmark Frequency Trend

3.3 Chapter Conclusion

The high-frequency pulse detection method allows remote detection of water-tree location and estimation of its severity. The method, however, does contain some weaknesses. For example, it is shown that HFPD method cannot establish a benchmark frequency for very large capacitances or very short water-tree distances.

It is necessary to remember that the HFPD method is not the sole method for water-tree detection. Different methods exist for practical reasons and different techniques can supplement each other. For example, although the effectiveness of HFPD method diminishes after water-tree capacitance exceeds certain limits, the effectiveness of many traditional detection techniques such as travelling-wave methods will increases. Thus, HFPD method complements the traditional methods.

The high-frequency pulse detection method and benchmark-frequency identification technique specialize in early-stage water-tree detection for long-distance cables. It has the best performance on water-trees with small capacitance and in long cables. Thus, it is well suited for preventative maintenance on long-distance cables.

Chapter 4

Early-Warning of Water-Tree Presence using Deviation Comparison

4.1 Motivation for the Early-Warning System

In the previous chapter, a method is developed to locate water-tree in long distance cables. The benchmark identification method is designed to supplement the HFPD method and it allows estimation of water-tree severity.

There is, however, a significant conundrum associated with practical implementation of the HFPD method. The key element for HFPD method is a pulse with sufficiently high frequency and amplitude. The high frequency is responsible for reducing water-tree impedance to a manageable level and the high amplitude adds greater visibility to the output.

Although commercially available pulse generators are capable of producing the required high-frequency pulse, it is still an expensive piece of equipment. Thus, a utility will only purchase a few of the devices and the availability for high-frequency pulse generators is expected to be limited; therefore, the HFPD test can only be realistically performed on priority targets.

In addition, the magnitude of the generated pulse is very large. As the result, offline test is the preferred choice for HFDP method. Unfortunately, since long-distance cables are often critical connections in the grid, taking these cables offline will result in significant interruption to the grid service. Consequently, it is necessary to limit both the number and duration of the HFPD tests.

Performing HFPD test is also stressful to the cable insulation and cable tests causing damage to the insulation is well documented. Since the method is developed to provide information for preventative maintenance, its ultimate subjective is prolonging the service life of the cable. If the test itself damages the cable insulation, then it is counterproductive.

As the result, although HFPD method is capable of obtaining accurate information on early-stage water-tree, it should only be performed on selective targets; therefore, there is the need for a new process, which can identify potential candidates for the HFPD method.

4.2 Methodology

4.2.1 Method Requirements

The early-warning system is designed as a supplement to the HFPD method. Its goals are monitoring the overall condition of the cable connections and assisting the utilities on locating potential targets for the HFPD test. With the goals in mind, the system must meet the following requirements:

1) The system must be relatively inexpensive: Specialized instrument implies increased operational expense and increased expense leads to less system coverage. The goal of the early-warning system is to monitor and evaluate the conditions of all the long distance cables in service; therefore, the coverage must extend to all the cable connections in the service system. To reduce the corresponding expense, no specialized equipment should be used.

2) The system must be able to monitor the cables over prolong period: Water-Tree is a slow developing phenomenon. The initial appearance and final breakdown can be

separated by years or even decades. In order to develop an economically feasible preventative maintenance schedule, the cables monitoring process must be long term. Although the system coverage does not have to be continuous, it is beneficial for the system to cover as much time as possible. With greater time coverage, more data can be accumulated and the probability estimation is more reliable.

3) The system must be able to monitor the cables without interrupting normal operation: Many long distance cables are critical grid connections and they cannot be taken offline for extended period of time. Thus, long-term monitoring of the cable system must be done in online conditions.

4) The system must not place significant stress on the grid stability and safety: Since the early-warning system is a long-term process added to the standard system, it will naturally have an impact on the grid stability and safety. As the result, it is necessary to minimize any disturbances.

It should be noted that the early-warning system would not directly determine the characteristics of water-tree. Rather, the purpose of the system is to estimate the probability of water-tree presence on certain cable segments. For example, in HFPD method, a reflected pulse pattern from a none-terminal part of the cable will indicate a discontinuity and if the pulse response matches certain patterns, then it is a clear indicator of water-tree presence. The HFPD method presents clear information on water-tree characteristic such as location and capacitance.

In the early-warning system, there will not be a clear indication of cable discontinuities. The observational result will be pattern anomalies in the operational waveforms. These anomalies represent probability of water-tree appearance on the cable

segment. Iterations of the results produce the accumulated probability estimation. If the estimation reaches a certain threshold, then the cable segment becomes a candidate for the more specialized HFPD test.

4.2.2 Naturally Occurring High-Frequency Phenomena in the System

In chapter three, the crux of water-tree detection is discussed. The HFPD method is designed to overcome the very high impedance of early-stage water-tree. As the supplement to HFPD method, the early-warning system must deal with the same issue. Both the mathematical model from chapter two and empirical measurement indicated that steady state water-tree impedance can be as high as 1GΩ for a standard 60Hz system. As the result, observing water-tree response under steady-state conditions is very difficult; therefore, high frequency remains the most practical and cost effective tool to deal with the water-tree impedance. Without a dedicated pulse generator, however, the early-warning system must use alternative sources of high-frequency input.

There are many potential sources of naturally occurring high-frequency events (NOHFE) in the system. For example, offshore windfarms may use wind turbine transformers to raise the transmission voltage. It is observed that when a fault is cleared on the low voltage side of the wind turbine transformer, a recovery voltage can be triggered on the primary-side circuit breaker. The frequency of the recovery voltage can reach as high as 47kHz [99~102]. Windfarms may also experience other types of high-frequency transients, such as loading or breaker switching [103~109].

Another major source of NOHFE in the system is the very high order harmonics. Although harmonic control is a well-established field in power systems, modern day control system tends to focus on the suppressing the 3^{rd}, 5^{th}, 7^{th}, 11^{th}, 13^{th} order harmonics

[110~118]. These harmonics are typically generated by control system components such as diodes and thyristors. For the purpose of water-tree detection, they are low-order harmonics and irrelevant to the detection process. In comparison, transistor-based control system components, such as IGBT, can generate very high order harmonics. These high order harmonics has been observed to reach 40^{th} order and beyond. They are sometimes referred as supra-harmonics and they range from 2.4kHz to 180kHz (2kHz to 150kHz for European systems) [119~124].

From system simulations, it is determined that the threshold for the early-warning system is approximately 3kHz. Greater frequency and amplitude will increase the clarity of the system response.

The DC system is a unique situation. Water-tree structure is primarily capacitive and its impedance is extremely high under DC frequency. Experiments, however, show that the DC ripples can also produce sizable response from water-tree.

4.2.3 Extrapolation-Comparison Method

Although the frequency and magnitude of NOHFE is insufficient for HFPD method, they are sufficiently high that water-tree afflicted system begins to exhibit small differences from a healthy system. In chapter three, it is shown that when the water-tree is subjected to high-frequency events, there are three potential responses as shown below in Figure 58:

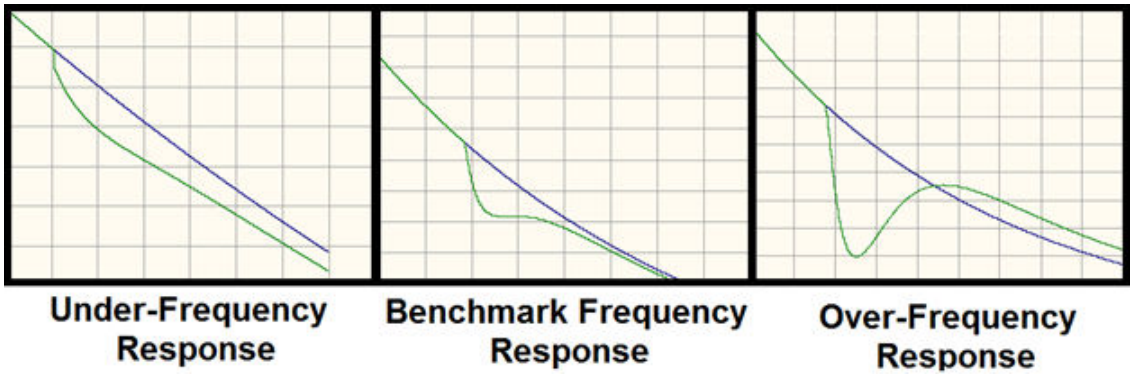

Figure 58: Water-Tree Response to High-Frequency Events

Although the benchmark frequency case is ideal for water-tree detection and estimation, the frequency and magnitude of NOHFE is generally too low. As the result, vast majority of the water-tree response experienced by the early-warning system belong to the under-frequency response case.

In under-frequency response case, the response shape from a water-tree afflicted system closely resembles it counterpart from a healthy system. Although the response waveform does exhibit minor deviations, they are very difficult to identify in practice. For example, Figure 59 shows the water-tree response from a high-frequency pulse:

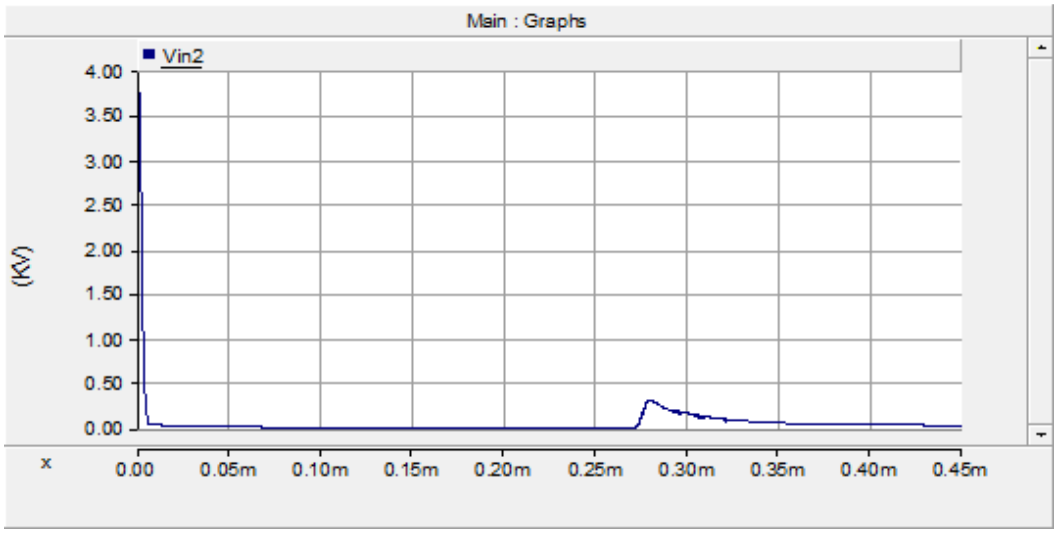

Figure 59: Overall View of Water-Tree Response from a High-Frequency Pulse

The pulse at t = 0.00 second and t = 0.28 millisecond are the input pulse and the pulse reflection from the cable terminal. The response portion correspond to the water-tree is not visible in the figure. The zoomed-in version is shown below in Figure 60:

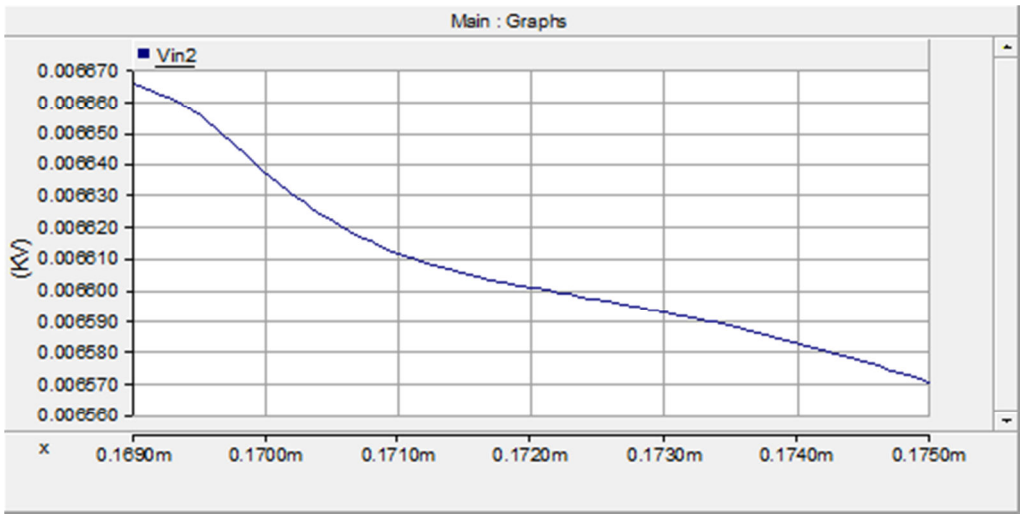

Figure 60: Specific View of Water-Tree Response from a High-Frequency Pulse

Essentially, the water-tree response is a 0.02V drop in the waveform over three microseconds. In combination with noise and other attenuation effects, it is difficult to identify the response through direct observation; therefore, there is a need to develop an identification method. The method must not only capture the differences caused by water-tree presence, it also needs to be able to recognize the source of these differences.

The extrapolation-comparison method consists of two parts: recognizing anomalies in the system through data extrapolation and identifying the potential cause of the anomalies through deviation comparison.

4.2.3.1 Extrapolation

A sample waveform from normal operation is shown below in Figure 61:

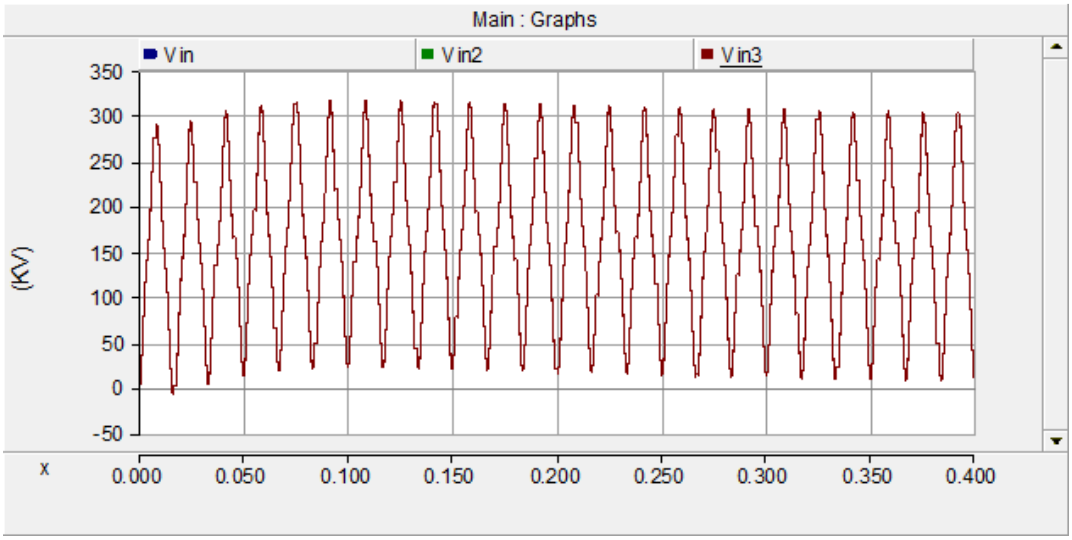

Figure 61: Normal Operation Waveform

The figure above contains the fundamental, third, fifth and seventh order harmonics. Since these frequency components are well below the 3kHz threshold, when viewed from the time scale of the water-tree detection process, the system will resemble Figure 62 below:

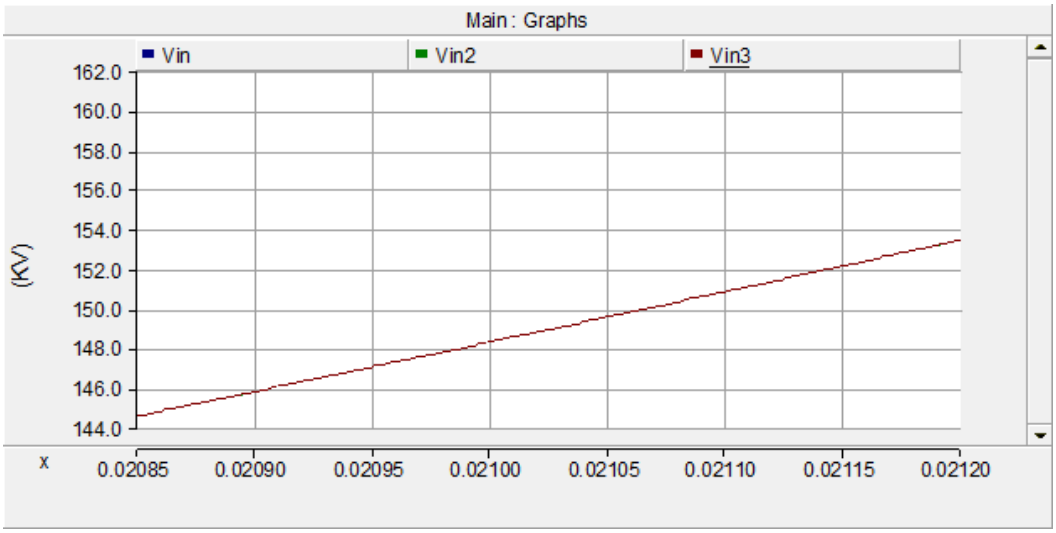

Figure 62: Normal System Operation in the Time Scale of Water-Tree Detection

Without the presence of water-tree, the healthy system waveform should be a straight line when viewed from the time-scale of water-tree detection. The presence of water-tree, on the other hand, will cause disturbances observable and only observable in this time scale.

The simplest extrapolation scheme is straight-line extrapolation using two previous data points as illustrated below in Figure 63:

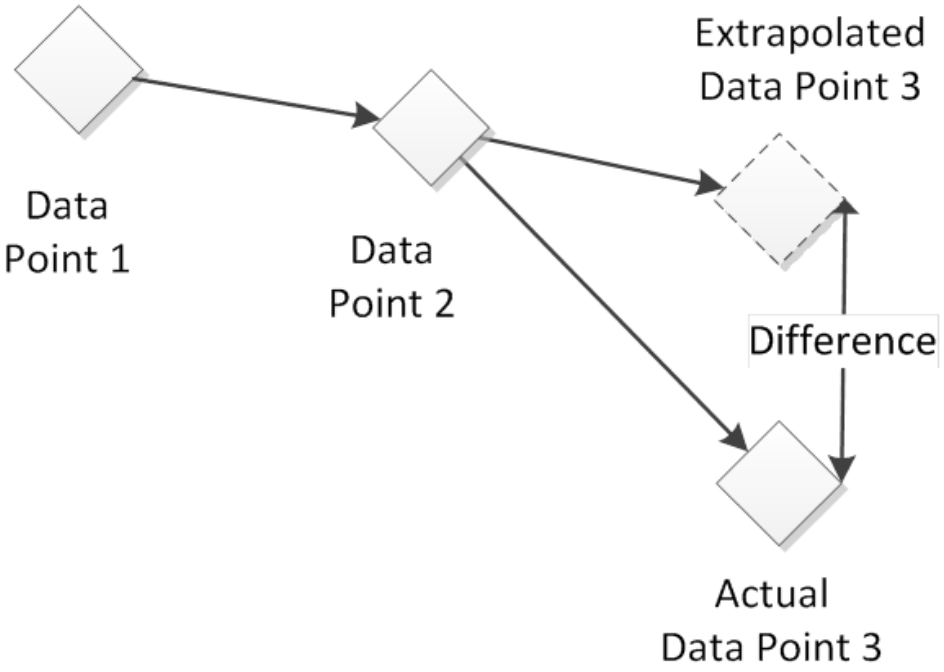

Figure 63: Straight Line Extrapolation Using Two Data Points

In two data-point straight-line extrapolation (2DSL) scheme, two data points are used to extrapolate the third data point. The extrapolated data point is then compared with the actual third data point and the difference is recorded. The difference is referred as data deviation from the expected norm, or deviation for short.

Depending on the specific situation, the extrapolation scheme can be modified and expanded. For example, a straight-line extrapolation can use n data points with time stamp t and voltage v. The extrapolated value can be obtained by:

$$v_m = \frac{\sum_1^n (t_i - \bar{t})(v_i - \bar{v})}{\sum_1^n (t_i - \bar{t})^2} t_m + (\bar{v} - \frac{\bar{t} \sum_1^n (t_i - \bar{t})(v_i - \bar{v})}{\sum_1^n (t_i - \bar{t})^2}) \quad \text{.....(25)}$$

If the waveform is expected to contain known high-frequency background components or the time-scale is large, then it is also possible to use non-straight line extrapolation schemes.

For the simple 2DSL scheme, the deviation can be solved in the steps below:

$$D(t) = E(t) - M(t) \quad \text{.....} \quad (26)$$

Where:

D(t) is the deviation value.

M(t) is the measured value obtained from the system voltage record.

E(t) is the estimation value from previously measurement points.

The healthy system is approximately a straight-line over the observation time interval. E(t) can be represented by the equation below:

$$E(t) = 2 * M(t - \Delta t) - M(t - 2\Delta t) \quad \text{.....} \quad (27)$$

Where Δt is the sampling time step.

Now to determine the water-tree response parameter, the water-tree junction is shown below in Figure 64:

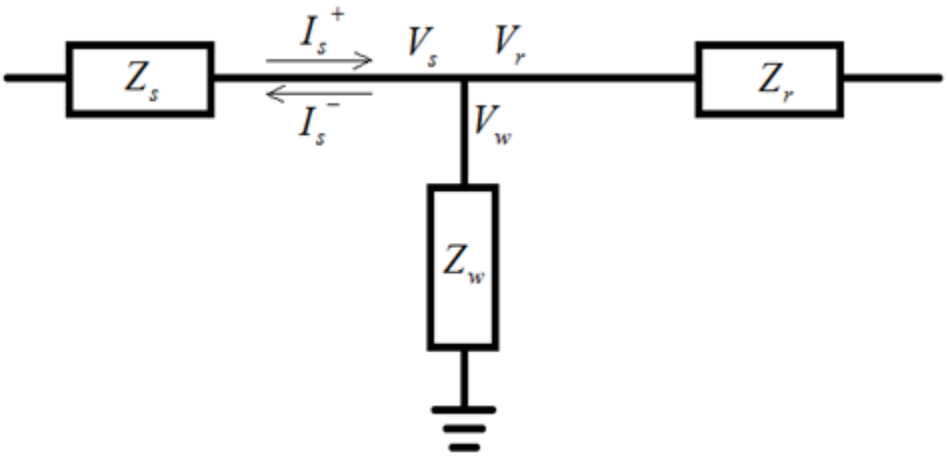

Figure 64: Water-Tree Junction

The water-tree response pattern is the super-imposed form of the residual input pattern and water-tree reflection pattern. The junction can be modelled after a cable bifurcation and the reflection coefficient is shown in the equation below:

$$\Gamma = \frac{I_s^-}{I_s^+} = \frac{Z_s - \frac{Z_r Z_w}{Z_r + Z_w}}{Z_s + \frac{Z_r Z_w}{Z_r + Z_w}} \quad \text{..... (28)}$$

Where:

Z_s is the characteristic impedance for the first half of the cable.

Z_r is the characteristic impedance for the second half of the cable.

Z_w is the characteristic impedance for the water-tree.

Z_s and Z_r are equal under normal conditions.

Thus, the measured pulse will be represented by:

$$M(t) = C(t) + P(t) + (-1) * \Gamma * P(t - 2\Delta\tau) \quad \text{..... (29)}$$

Where:

C(t) is the base operation waveform, including low-order harmonics.

P(t) is the NOHFE.

$\Delta\tau$ is the NOHFE travel time from the measurement point to the water-tree location.

Since C(t) is a straight-line over the observation interval:

$$D(t) = [2P(t-\Delta t) + P(t-2\Delta t) + P(t)] - \Gamma[2P(t-\Delta t-2\Delta\tau) + P(t-2\Delta t-2\Delta\tau) + P(t-2\Delta\tau)] \quad \ldots\ldots\ldots\ldots\ldots\ldots\ldots\ldots (30)$$

Since P(t) is observable, the deviation D(t) can be used to determine if there is a reflection coefficient caused by water-tree.

A simplified deviation equation is shown below:

$$D_{n+2} = V_{n+2} - [(V_{n+1} - V_n) * \alpha + V_{n+1}] \quad \ldots\ldots\ldots\ldots\ldots\ldots\ldots\ldots\ldots\ldots\ldots\ldots\ldots\ldots\ldots\ldots\ldots\ldots\ldots\ldots (31)$$

Where:

α is a compensation parameter

D_n is the deviation at time step n

V_n is the actual voltage read at time step n

The compensation parameter can be changed according to the extrapolation scheme. For the simplest 2DSL scheme, the value is one.

4.2.3.2 Comparison

The previous portion of the method will determine the deviation values of the response waveform. These values are not meaningful by themselves. The deviation values need to be compared with the other deviation values from certain time-steps back as shown below in Table 3:

Table 3: Deviation Comparison Table

Deviation Ratio	/Dx-1	/Dx-2	/Dx-3	/Dx-4	/Dx-5	.....
.....	.....	.....	.....	.....	.....	.....
Dn-1	Dn-1/Dn-2	Dn-1/Dn-3	Dn-1/Dn-4	Dn-1/Dn-5	Dn-1/Dn-6	.....
Dn	Dn/Dn-1	Dn/Dn-2	Dn/Dn-3	Dn/Dn-4	Dn/Dn-5	.....
Dn+1	Dn+1/Dn	Dn+1/Dn-1	Dn+1/Dn-2	Dn+1/Dn-3	Dn+1/Dn-4	.....
Dn+2	Dn+2/Dn+1	Dn+2/Dn	Dn+2/Dn-1	Dn+2/Dn-2	Dn+2/Dn-3	.....
Dn+3	Dn+3/Dn+2	Dn+3/Dn+1	Dn+3/Dn	Dn+3/Dn-1	Dn+3/Dn-2	.....
Dn+4	Dn+4/Dn+3	Dn+4/Dn+2	Dn+4/Dn+1	Dn+4/Dn	Dn+4/Dn-1	.....
Dn+5	Dn+5/Dn+4	Dn+5/Dn+3	Dn+5/Dn+2	Dn+5/Dn+1	Dn+5/Dn	.....
.....	.....	.....	.....	.....	.....	.....

The left vertical column represents the deviation value at certain time-step. The top horizontal row represents the time-step interval between the current deviation value and the comparison value. The row items will be referred as time-step interval. They represent the time difference between the two deviation values. The data entries are the ratios between the current deviation value and the deviation value from certain time-step interval in the past.

The key idea is that water-tree is a fixed, slow developing phenomenon. Thus, it represents a fixed distance for disturbance to appear. Since the short-term travelling speed of the waveform remains the same, fixed time-step interval means fixed distance. In essence, fixed-distance phenomenon like water-tree will produce fixed distance response.

4.3 Implementation

In HFPD method, multiple frequencies must be tried before the benchmark frequency can be established. Similarly, the early-warning system requires multiple input iterations to make reliable estimation. The system flow chart is presented below in Figure 65:

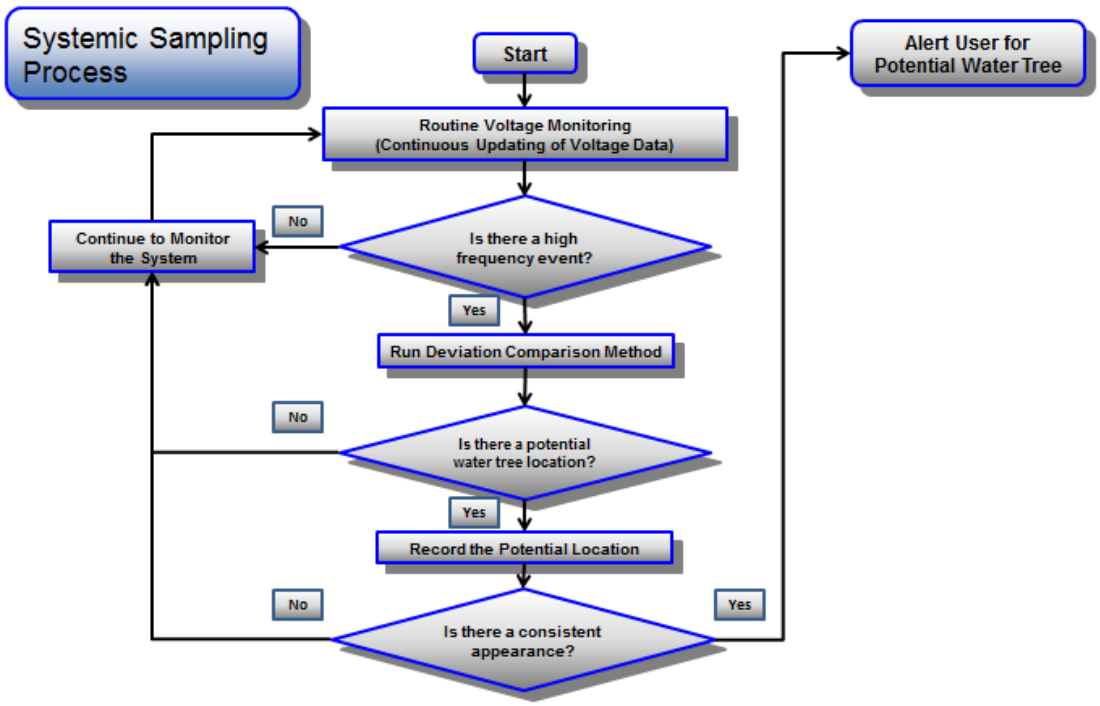

Figure 65: Flow Chart for Early-Warning System

The system will provide long-term and continuous coverage of the cables. In ideal conditions, the operator will continuously record all voltage data at the cable terminal and extract deviation values from these data. The deviation values will then be analyzed through the deviation comparison table.

It should be noted that the length of time-step interval (row items) presented in Table 3 does not have to exceed certain limits. As long as the time-step interval allows the waveform to travel across the entire cable segment length and back, it will be sufficient for deviation comparison purpose.

If computation power is limited, then the extrapolation-comparison algorithm can also be selectively triggered. The flow chart in Figure 65 above shows the process. When NOHFE is detected in the system, the data around NOHFE will be collected and analyzed through the deviation comparison method. If the analysis indicates potential presence of

water-tree at certain locations, then the locations will be recorded. When another NOHFE occurs, the process will be repeated. If there is a consistent indication of water-tree presence at a fixed location, then the operator may choose to apply HFPD method and determine the exact status of the cable.

4.4 Observational Results

4.4.1 System Response for Naturally Occurring High-Frequency Event

A test system is developed to illustrate the effect of naturally occurring high-frequency events on water-tree detection. The system is charged by a lightning pulse. Unlike the test cases for HFPD method, however, the frequency will significantly lower. The lightning pulse serves as an approximation to NOHFE in the system. The system parameter is the same as chapter three simulations.

Four cables systems are tested using the same lightning pulse:

1) Healthy System without Water-Tree
2) System with a Single Water-Tree
3) System with a Single Water-Tree with High Pass Filter at Input
4) System with both Water-Tree and Low Impedance Fault

The water-tree capacitance is set at 10pF and its resistance is set at 1551MΩ. These values are taken from the mathematical model in chapter two. They represent a water-tree, which has corroded through 80% of the insulation layer.

The low impedance fault has a fault resistance of 300Ω. The test system is shown below in Figure 66:

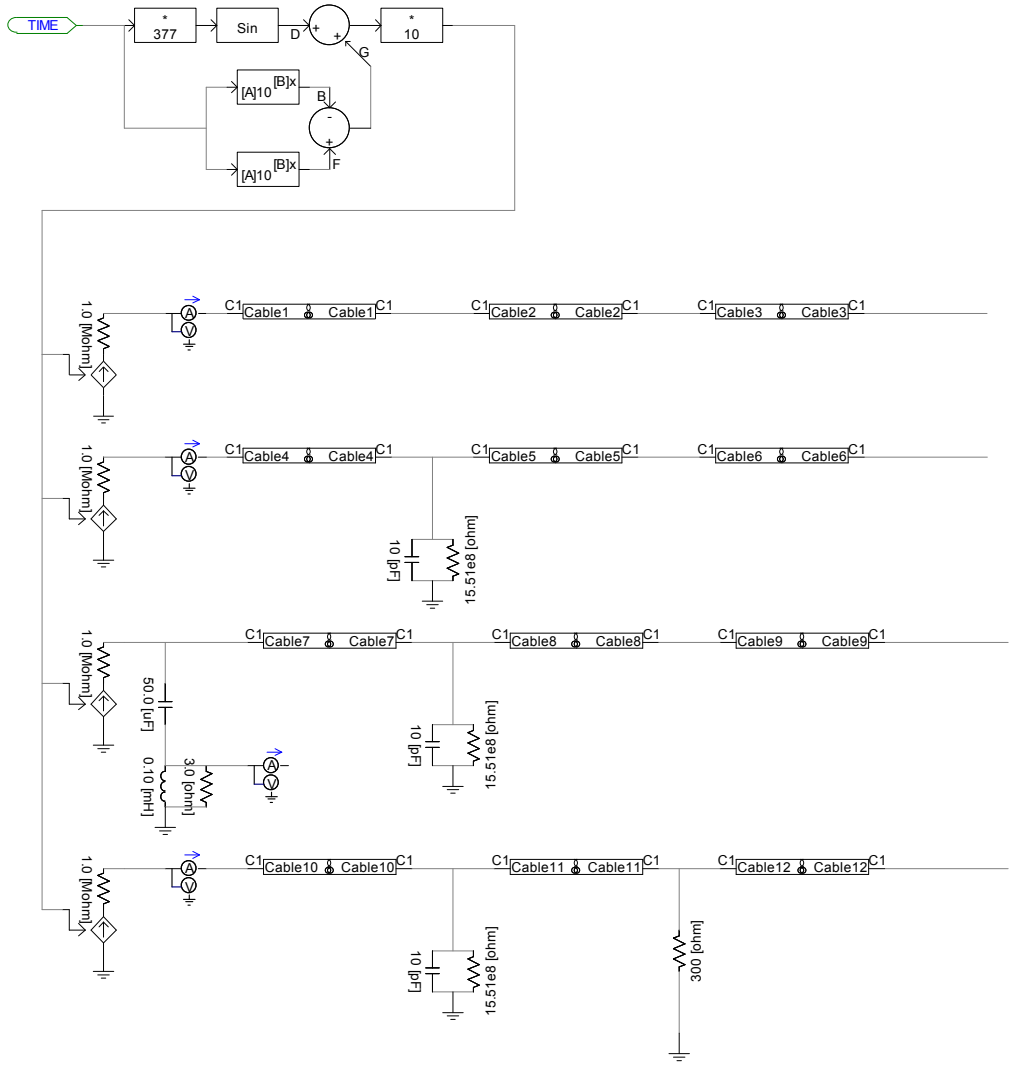

Figure 66: Testing System for Early-Warning System Detection

The system response to an amplified 3kHz pulse is shown below in Figure 67:

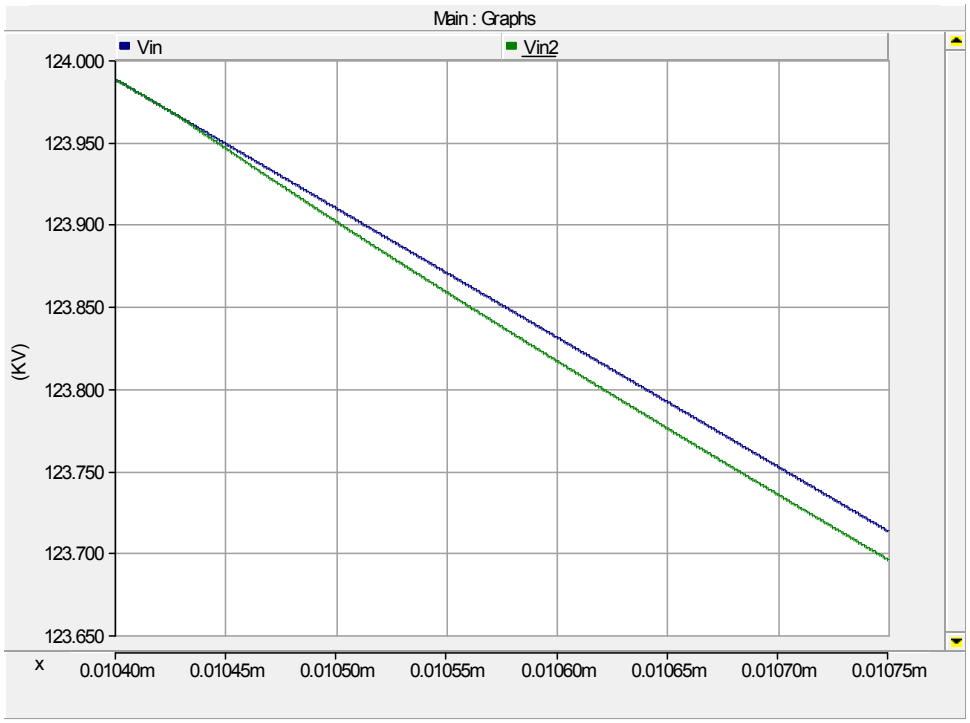

Figure 67: System Response to 3 kHz Lightning Pulse

These are the typically deviations experienced by the early-warning system. Since the lightning pulse is an amplified pulse for easier viewing, the absolute scale of the difference is bigger than normal. The ratio between the healthy system reading Vin and the water-tree afflicted system reading Vin2 is the same as a response using unamplified pulse. Specifically, the 3kHz amplified pulse generated a 0.018% deviation in the water-tree afflicted system.

The deviation cause by the low-impedance fault is significantly bigger. The low-impedance fault response from the same 3kHz pulse is shown below in Figure 68:

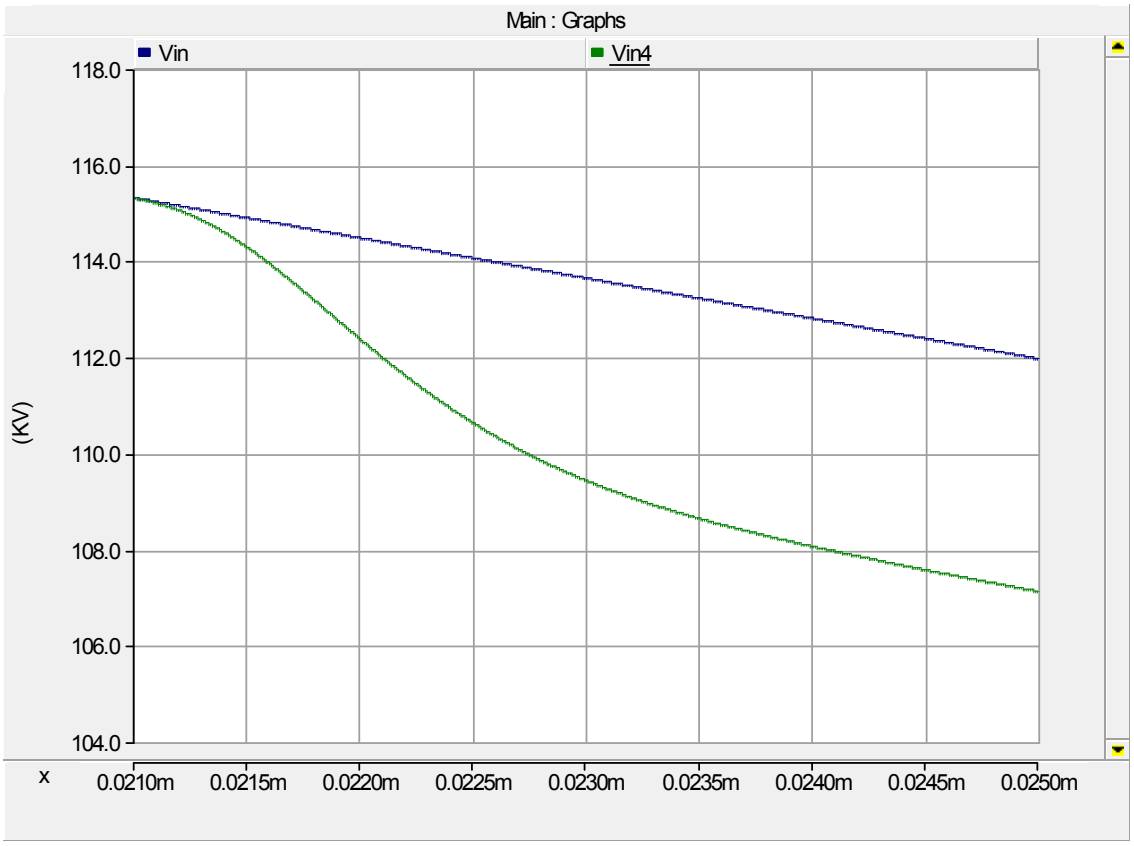

Figure 68: Low-Impedance Fault Response to 3kHz Pulse

The percentage deviation from the low-impedance fault is 4.23%. It is more than 200 times larger comparing to its counterpart from the water-tree.

The deviation between healthy and water-tree afflicted system is linearly proportional to magnitude of the applied pulse. When the fundamental component is removed, the ratio between the deviation and the remaining voltage waveform is constant at the same NOHFE frequency. This ratio will be referred as the percentage deviation.

Depends the fault type, the corresponding percentage deviations have specific ranges. For example, the percentage deviation value of low-impedance faults is significantly different from the percentage deviation caused by water-tree. This allows

the extrapolation-comparison method to categorize its results and attribute the deviations to different causes.

From the test case, two key issues can be observed concerning the feasibility of the early-warning system: instrument accuracy requirement and instrument measurement error.

Instrument accuracy is an issue common to the entire water-tree detection process. It is a key issue in the motivation of HFPD method and the cost of high-accuracy is the factor that motivated the development of the early-warning system. The water-tree response to NOHFE demonstrated that the difference between a healthy system and a water-tree afflicted system is very small; therefore, the feasibility of the early-warning system depends on its ability to identify differences at this scale while upholding its method requirements. Fortunately, there exist methods that can boost measurement accuracy through mathematical analysis techniques. For example, digital synchronous sampling has been known to detect harmonic distortions up to 95^{th} order. The method can measure uncertainties as low as 0.0001% [125]. Thus, the accuracy is sufficient to identify the percentage deviations in the early-warning system.

The second issue is measurement error. Measurements from real world instruments will contain random errors. Their effect is particularly significant for high sensitivity measurements in the early-warning system, but since the percentage deviation remain constant for the same fault parameter and frequency, multiple iterations from different NOHFE can eliminate large amount of these errors. It should be noted that since the frequencies of NOHFEs are random, operators should strive for a large sample size and by extension, better clarity and reliability.

4.4.2 Effect of Filtering on the Result

The third cable segment in the test system is an alternative approach on data acquisition. Instead of mathematically removing the fundamental component in data analysis, a high-pass filter is directly applied to the system. The main benefit for such an approach is reducing measurement magnitude. Since the early-warning system is an online process, cable terminal waveforms are obtained directly from the system. As the result, measurements often require step-downs from voltage/current transformers. It is possible for valuable data to be lost in the step-down process. In comparison, the filtered data will have lower magnitude from the start; therefore, it is possible to use delicate, but more accurate instrument for the measurement. The test case result is shown below in Figure 69:

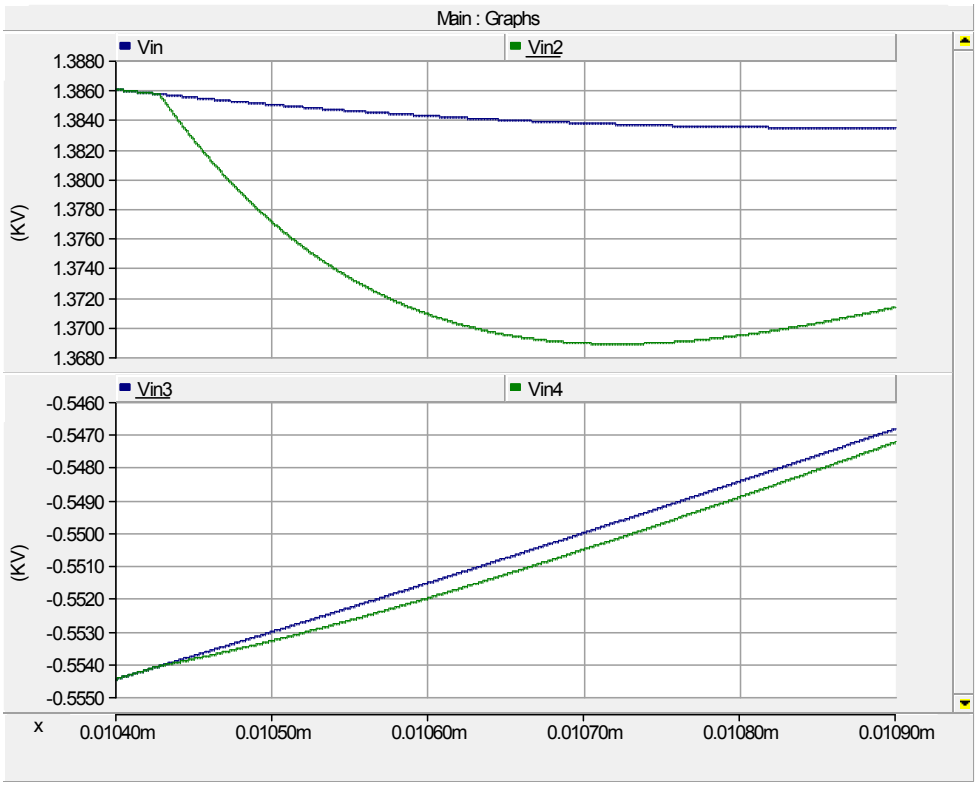

Figure 69: Filtered Results from the Test Case

The graph on top shows the systems without filtering. The graph on the bottom shows the filtered response. The filter is a 2.2kHz first order RLC high pass filter. The lightning pulse frequency is increased to 250kHz for easier viewing. Each graph contains two systems: healthy and water-tree afflicted system.

The filtered response has lower magnitude and it is easier to measure. Unfortunately, the test result also shows two disadvantages:

1. The percentage difference becomes larger after filtering.
2. The pulse response shape is not preserved by the filter.

In essence, filtering the response is a trade-off between measurement accuracy and analysis reliability. The filtered results have better accuracy in raw data, but the analysis process itself becomes less reliable in the process.

In actual application, the source of the NOHFE also affects the result. For example, high frequency transients offer larger pulse magnitude and the results are easier to observe. They are, however, rarer than high-order harmonics. This results in smaller sample pool and potential vulnerability to random measurement error.

High-order harmonics, on the hand, are more common comparing to high frequency transients. They will provide a larger sample pool. Their magnitude, however, is significantly lower. Higher instrument sensitivity is required to measure the resultant deviation.

4.4.3 Deviation Comparison Results

The deviation comparison table provides direct views on the potential location of water-tree. Since the data entries requires deviation value in the past, a table starting at

time=zero will resemble a lower triangular matrix. In contrast, if the monitoring process is constant, then the table will be fully filled.

Part of a sample deviation-comparison table is shown below in Table 4:

Table 4: Sample Deviation-Comparison Table

	1	2	3	4	5	6	7	8	9	10	11	12
1	1.0000e-07	0	0	0	0	0	0	0	0	0	0	0
2	2.0000e-07	0	0	0	0	0	0	0	0	0	0	0
3	3.0000e-07	-1.8519	0	0	0	0	0	0	0	0	0	0
4	4.0000e-07	-1.5649	0.8450	0	0	0	0	0	0	0	0	0
5	5.0000e-07	-1.3192	0.8430	0.7124	0	0	0	0	0	0	0	0
6	6.0000e-07	-1.1091	0.8407	0.7088	0.5989	0	0	0	0	0	0	0
7	7.0000e-07	-0.9296	0.8381	0.7046	0.5940	0.5020	0	0	0	0	0	0
8	8.0000e-07	-0.7763	0.8351	0.6999	0.5884	0.4961	0.4192	0	0	0	0	0
9	9.0000e-07	-0.6455	0.8316	0.6944	0.5820	0.4893	0.4125	0.3486	0	0	0	0
10	1.0000e-06	-0.5341	0.8274	0.6880	0.5746	0.4816	0.4049	0.3413	0.2884	0	0	0
11	1.1000e-06	-0.4393	0.8225	0.6805	0.5659	0.4726	0.3961	0.3330	0.2807	0.2372	0	0
12	1.2000e-06	-0.3587	0.8166	0.6717	0.5557	0.4621	0.3859	0.3234	0.2719	0.2292	0.1937	0
13	1.3000e-06	-0.2904	0.8095	0.6610	0.5437	0.4498	0.3741	0.3124	0.2618	0.2201	0.1856	0.1568
14	1.4000e-06	-0.2325	0.8006	0.6481	0.5292	0.4353	0.3602	0.2995	0.2501	0.2096	0.1762	0.1486
15	1.5000e-06	-0.1836	0.7895	0.6321	0.5117	0.4179	0.3437	0.2844	0.2365	0.1975	0.1655	0.1391
16	1.6000e-06	-0.1423	0.7752	0.6121	0.4901	0.3967	0.3239	0.2664	0.2205	0.1833	0.1531	0.1283
17	1.7000e-06	-0.1076	0.7562	0.5862	0.4628	0.3706	0.3000	0.2450	0.2015	0.1667	0.1386	0.1158
18	1.8000e-06	-0.0785	0.7297	0.5518	0.4277	0.3377	0.2704	0.2189	0.1787	0.1470	0.1216	0.1011
19	1.9000e-06	-0.0542	0.6905	0.5038	0.3810	0.2953	0.2332	0.1867	0.1511	0.1234	0.1015	0.0840
20	2.0000e-06	-0.0340	0.6271	0.4330	0.3159	0.2389	0.1852	0.1462	0.1171	0.0948	0.0774	0.0636
21	2.1000e-06	-0.0173	0.5076	0.3183	0.2198	0.1604	0.1213	0.0940	0.0742	0.0594	0.0481	0.0393
22	2.2000e-06	-0.0035	0.2017	0.1024	0.0642	0.0443	0.0323	0.0245	0.0190	0.0150	0.0120	0.0097
23	2.3000e-06	0.0078	-2.2345	-0.4507	-0.2288	-0.1435	-0.0991	-0.0723	-0.0547	-0.0424	-0.0335	-0.0268
24	2.4000e-06	0.0169	2.1729	-4.8552	-0.9793	-0.4971	-0.3117	-0.2152	-0.1571	-0.1188	-0.0921	-0.0727
25	2.5000e-06	0.0242	1.4327	3.1131	-6.9561	-1.4031	-0.7123	-0.4466	-0.3084	-0.2250	-0.1702	-0.1319
26	2.6000e-06	0.0300	1.2388	1.7749	3.8567	-8.6176	-1.7382	-0.8824	-0.5533	-0.3820	-0.2788	-0.2108
27	2.7000e-06	0.0345	1.1498	1.4244	2.0408	4.4343	-9.9083	-1.9986	-1.0145	-0.6362	-0.4393	-0.3205
28	2.8000e-06	0.0379	1.0988	1.2634	1.5651	2.2424	4.8724	-10.8873	-2.1960	-1.1148	-0.6990	-0.4827
29	2.9000e-06	0.0404	1.0659	1.1712	1.3466	1.6683	2.3901	5.1935	-11.6047	-2.3408	-1.1882	-0.7451
30	3.0000e-06	0.0421	1.0430	1.1117	1.2216	1.4045	1.7400	2.4929	5.4168	-12.1036	-2.4414	-1.2393
31	3.1000e-06	0.0432	1.0262	1.0703	1.1408	1.2535	1.4413	1.7855	2.5582	5.5586	-12.4205	-2.5053

The table is not meaningful by itself. Further analysis must be performed to transform the table into a more presentable form. The zeroes in the table represent data entries that are not available, discarding these entries and take the standard deviation of the remaining data in the column will generate a plot between standard deviation of the deviation values and the time-step interval.

The output will resemble Figure 70 below and they will be referred as standard deviation charts:

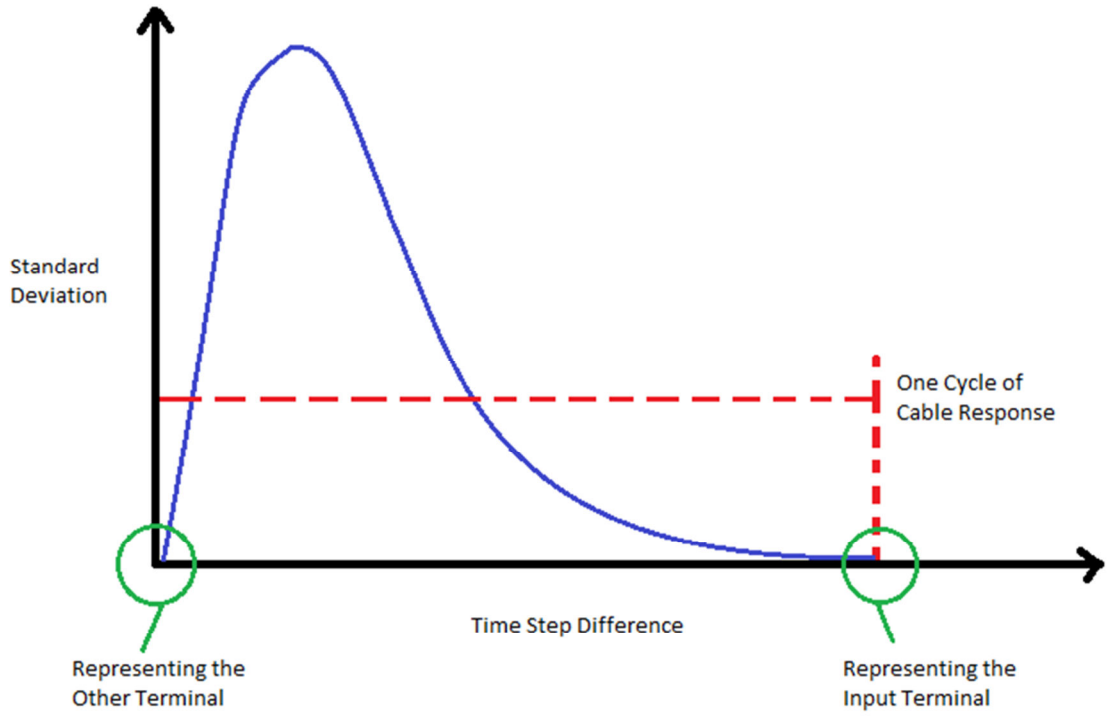

Figure 70: Time-Step Difference vs Standard Deviation

It is important to remember that the input cable terminal is represented by the right most part of a cycle. Specifically, at the rightmost terminal, deviation comparison is made from deviation readings that are exactly one cycle apart. Without factoring in other types of attenuation, the ratio remains the same and the standard deviation is much lower. The large spike on the leftmost portion is created by two factors:

1. The deviation comparison matrix is lower triangular. Thus, the standard deviation on the left side is naturally higher.
2. The left most side compares the deviation from adjacent values. When tracing the deviation value closer in the past, the comparison ratio will become

smaller. This is because the denominator effectively becomes larger due to the decay pattern of the source NOHFE.

For water-tree afflicted systems, the water-tree behaves similar to a cable termination and generates the same effect; therefore, when viewing the standard deviation chart of a water-tree afflicted cable segment, the water-tree location will appear in corresponding positions.

The standard deviation chart of a healthy cable system is shown below in Figure 71:

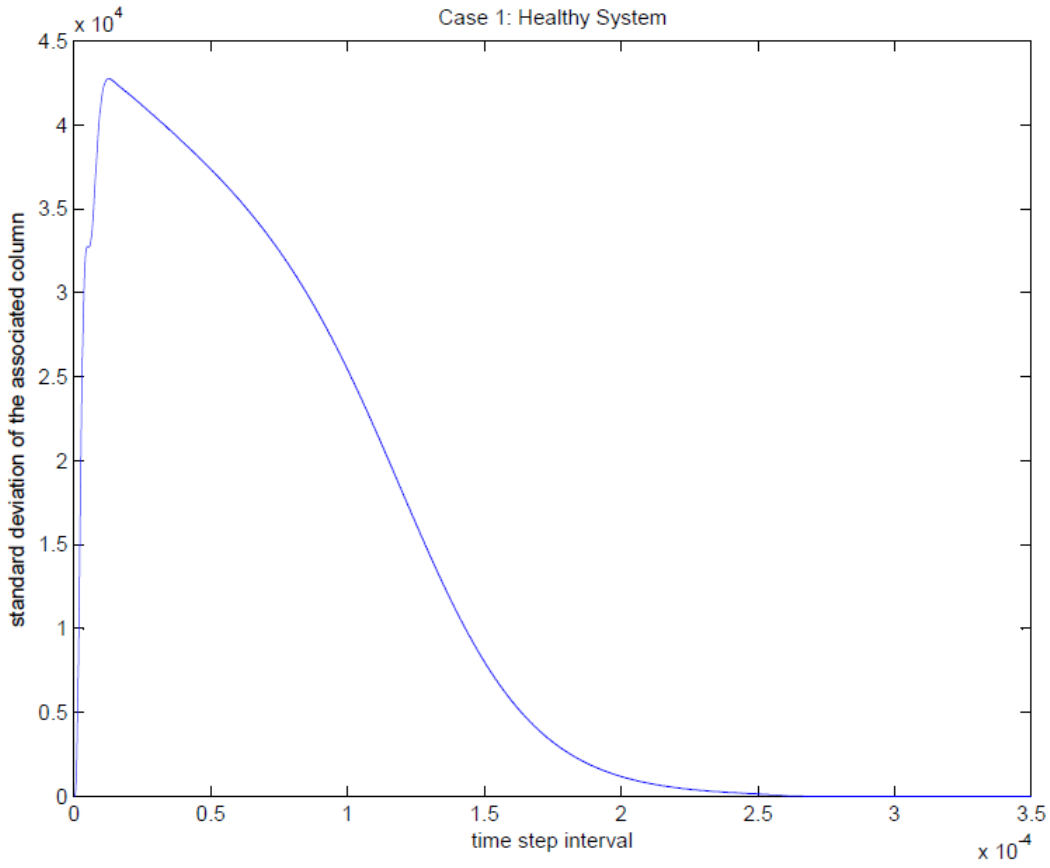

Figure 71: Time-Step Difference vs Standard Deviation for Healthy System

The cable is a 20km long. The applied frequency is 155kHz and the test is done offline. The figure covers a single cycle. More specifically, the maximum range of time-

step interval allowed the pulse to travel from the input terminal to the other end of the cable and then back to the input terminal. The spike near time-step interval=zero is created by the other terminal of the cable. Since there is no water-tree present, the rest of the graph is smooth and continuous.

For the same system, a water-tree is added. The water-tree is placed 10km away from the input terminal, or exactly in the middle of the cable. The comparison graph is shown below in Figure 72:

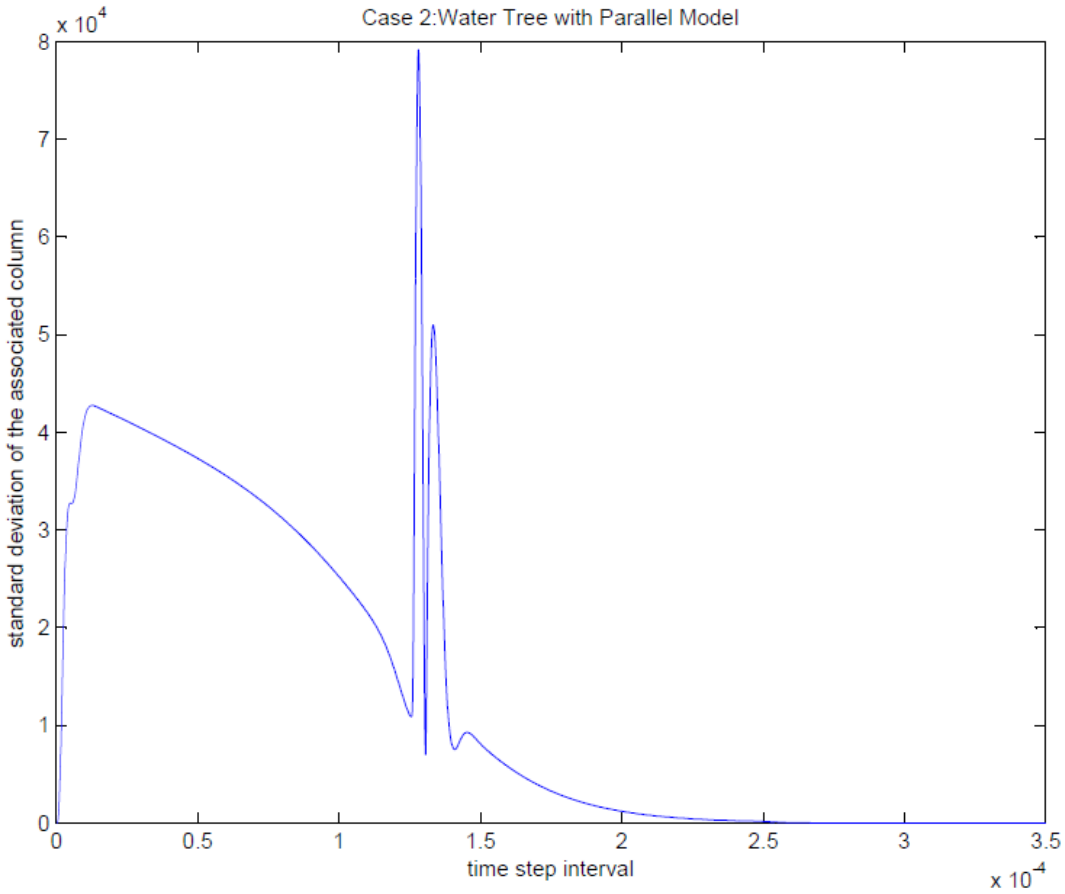

Figure 72: Time-Step Difference vs Standard Deviation with Water-Tree in the Middle

There is a large spike in the standard deviation chart. The locations correspond to the location of water-tree (counting from the rightmost end of the cycle).

The same system is done over four cycles, the healthy system is shown in Figure 73 and water-tree afflicted system is shown in Figure 74:

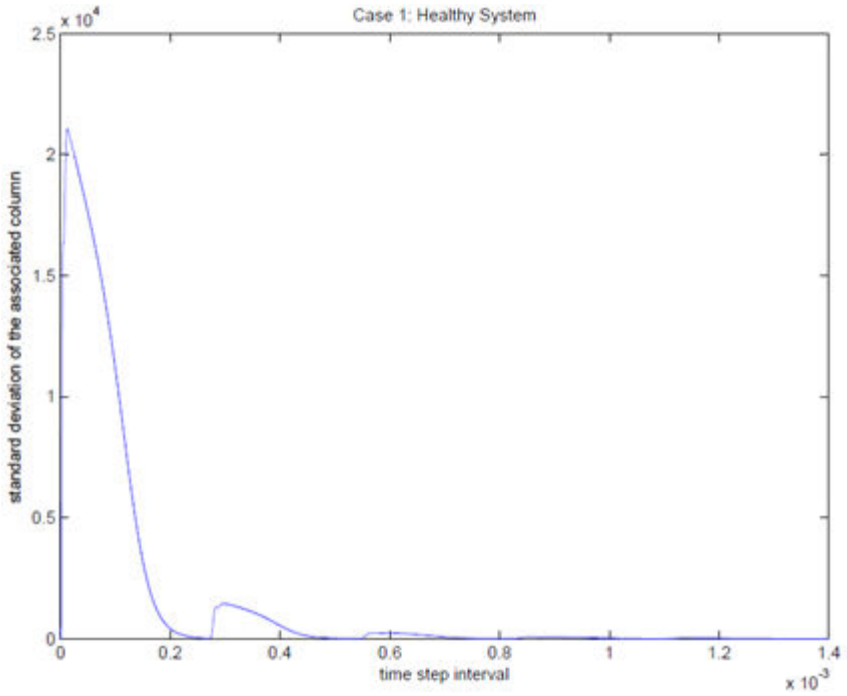

Figure 73: Healthy System Over Four Cycles

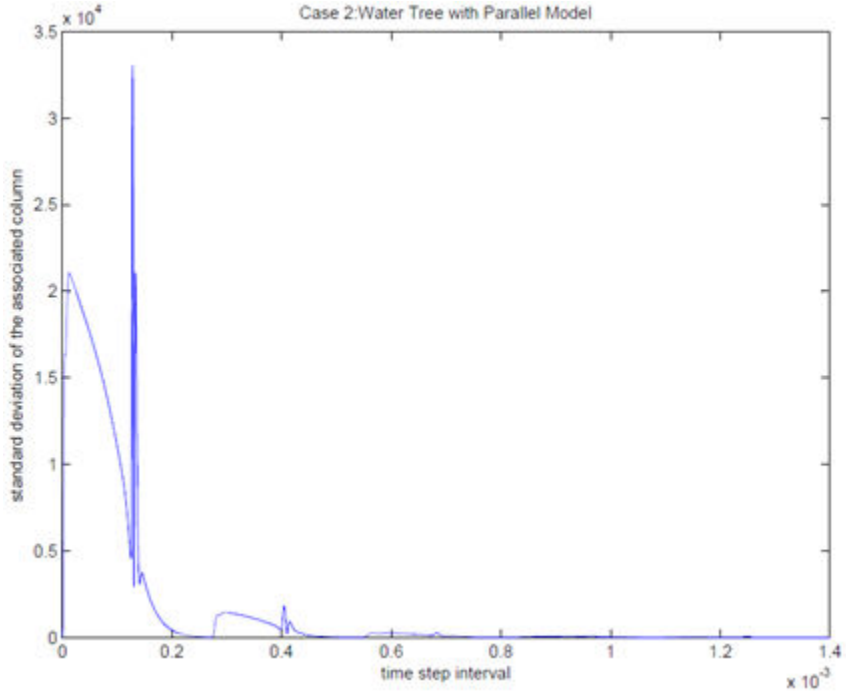

Figure 74: Water-Tree Afflicted System over Four Cycles

The cycles after the first have similar patterns, but their magnitude is significantly smaller; therefore, the time-step interval range only needs to extend over the first cycle.

The water-tree is now moved to 5km from the input terminal. The resultant deviation comparison table is shown below in Figure 75:

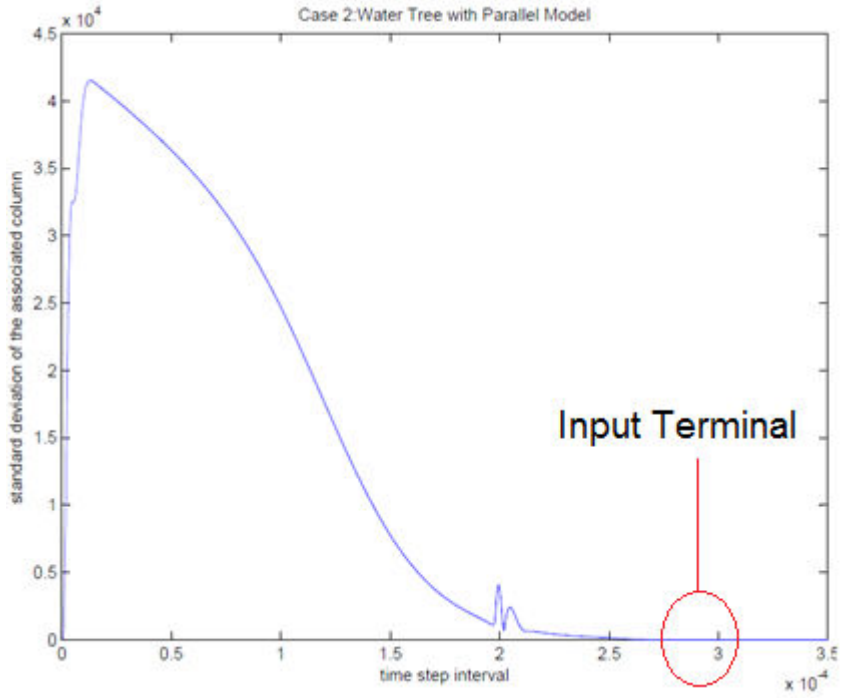

Figure 75: Water-Tree at 5km from the Input Terminal (15km from the Other Terminal)

The standard deviation chart shows a spike at the corresponding water-tree location. Since the spike is closer to the rightmost end of the cycle, its magnitude is smaller, but it is still clearly visible.

For the same system setup, the standard deviation graphs of multiple water-trees are condensed together into a single figure. It is shown below in Figure 76:

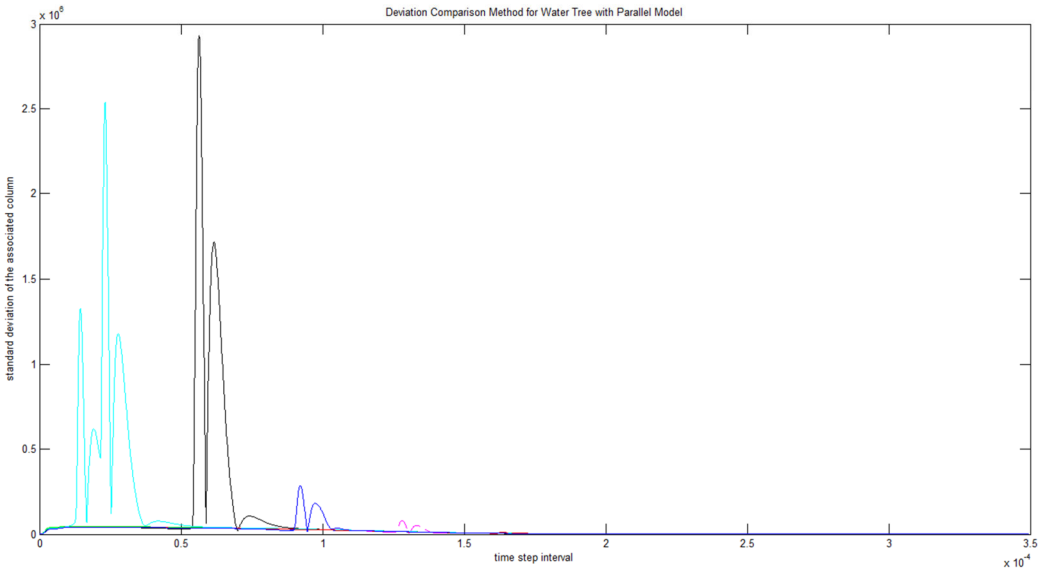

Figure 76: Standard Deviation Graphs of Multiple Water-Trees

A zoomed in view is shown between in Figure 77:

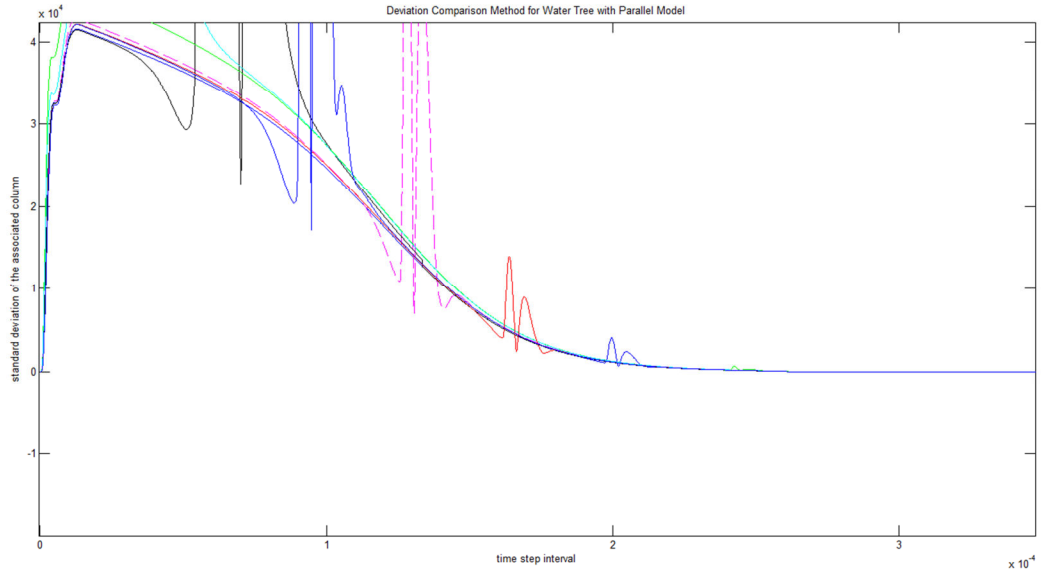

Figure 77: Standard Deviation Graphs for Multiple Water-Trees (Zoomed in)

The water-tree capacitance and resistance parameters remain the same. The water-trees are place at the following distance from the input terminal: 2km, 5km, 7.5km, 10km, 12.5km, 15km and 18km. The difference in spike size is purely caused by the lower triangular nature of the deviation-comparison table.

For the same system, the test is now done online. The water-tree is located 10km from the input terminal. The responses from both offline and online tests are compared below in Figure 78:

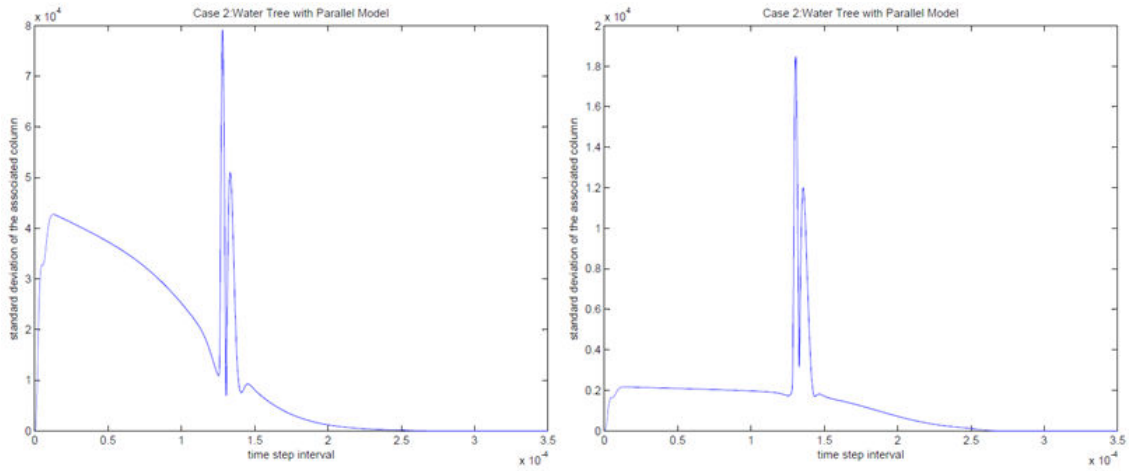

Figure 78: Comparison between Offline (Left) and Online (Right) Test

Both online and offline tests show similar spikes at the water-tree location. The absolute magnitude of the standard deviation value is lower for online test; therefore, offline test is still the better test condition. Although the point is irrelevant for the early-warning system, since it must be online, the extrapolation-comparison method can be used to analyze results from HFPD method as well.

From the observation, it can be seen that the early-warning system still requires frequencies past certain thresholds. For example, if the water-tree capacitance is approximately 13pF, then the threshold is between 20kHz to 60kHz.

If the voltage data is not continuous monitored, the resultant deviation comparison table will be lower triangular. This can create issues for detecting water-trees close to the cable terminals. For lower triangular table cases, the standard deviation of water-tree near input terminal will have very low in magnitude. If the water-tree is near the other terminal, then it may be masked by the cable terminal reflection.

4.4.4 Impact of Harmonics on Deviation-Comparison Chart

Real world power system operations are complex and a number of factors may interfere with the early-warning system and the deviation-comparison chart output. For example, the presence of harmonics is both a source of NOHFE that may aid the detection method and a source of potential interference that may disrupt the result under other circumstances.

Figure 79 below shows the deviation-comparison chart output in the presence of four harmonics typically observed with six pulse converters:

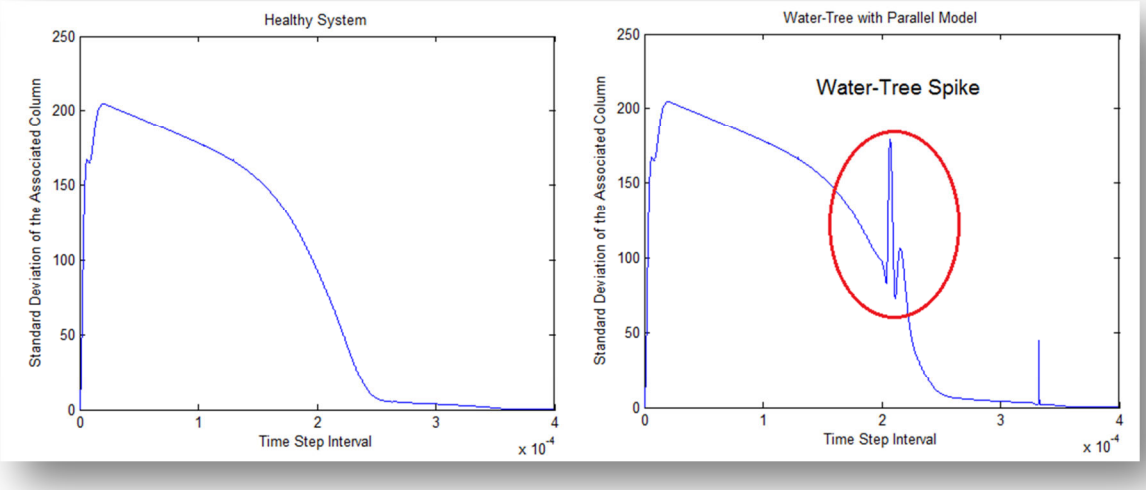

Figure 79: Deviation-Comparison in the Presence of 5th, 7th, 11th and 13th Order Harmonics

The magnitudes of the injected harmonics are listed in percentage of the fundamental components: 5^{th}: 0.02%; 7^{th}: 0.03%; 11^{th}: 0.05% and 13^{th}: 0.08%.

If the magnitude of the harmonics increases, then they may start to interfere with the measurement. For example, a healthy system output with larger harmonics injected is shown below in Figure 80:

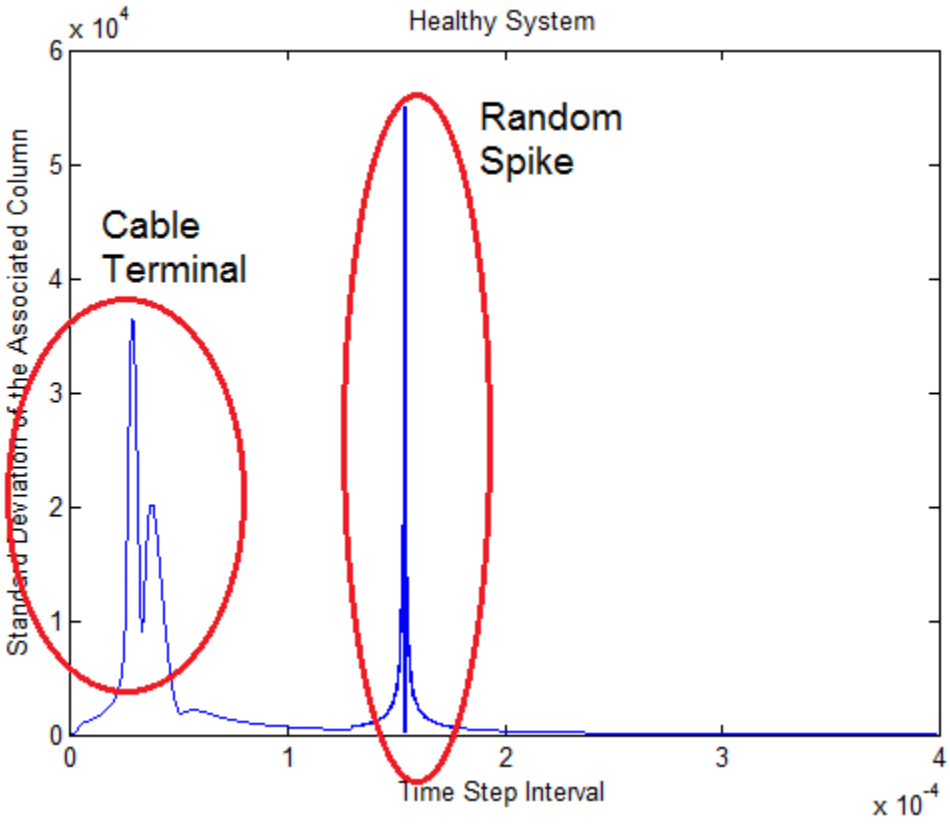

Figure 80: Healthy System Deviation-Comparison Output with Large Harmonic Injection

The very high spike is a mathematical creation and does not reflect any actual cable discontinuity. The magnitudes of the injected harmonics are 5^{th}: 0.3%; 7^{th}: 0.4%; 11^{th}: 0.5% and 13^{th}: 0.8%. They are ten times larger than the harmonics in the previous figure. Since the random spike is very high magnitude, some of the latter comparisons will use log scale for the y-axis.

Figure 81 below shows the comparison between healthy and water-tree afflicted system under large harmonics injection:

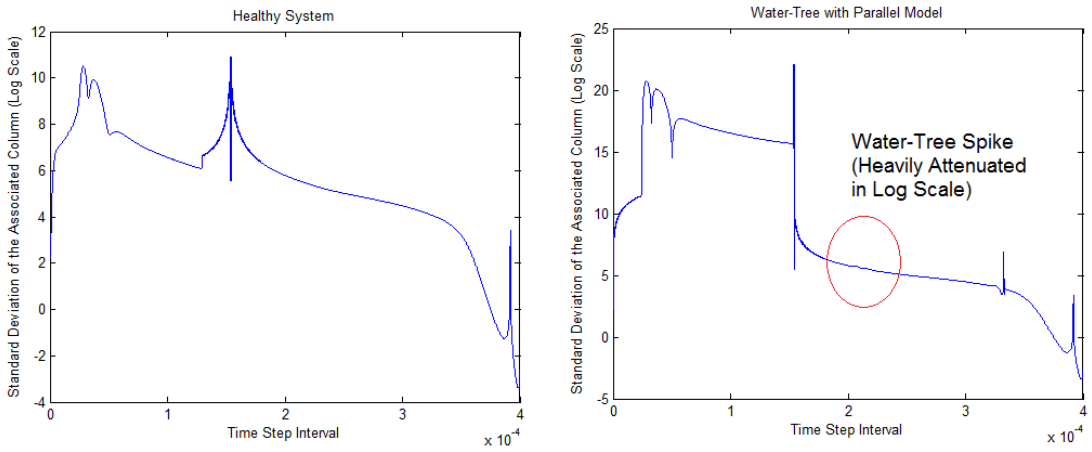

Figure 81: System Comparison with Large Harmonics

The water-tree spike did not disappear, but its magnitude is significantly smaller than the random spike. Figure 82 shows the zoomed-in view of the water-tree afflicted system output in normal scale:

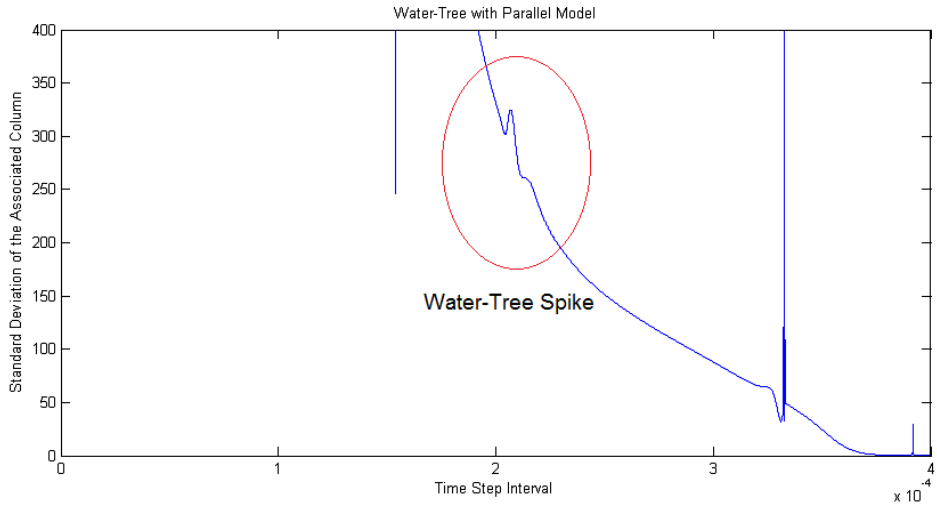

Figure 82: Zoomed-In View of Water-Tree Afflicted System Output

Figure 83 below shows the comparison, but with 11th and 13th order harmonics removed:

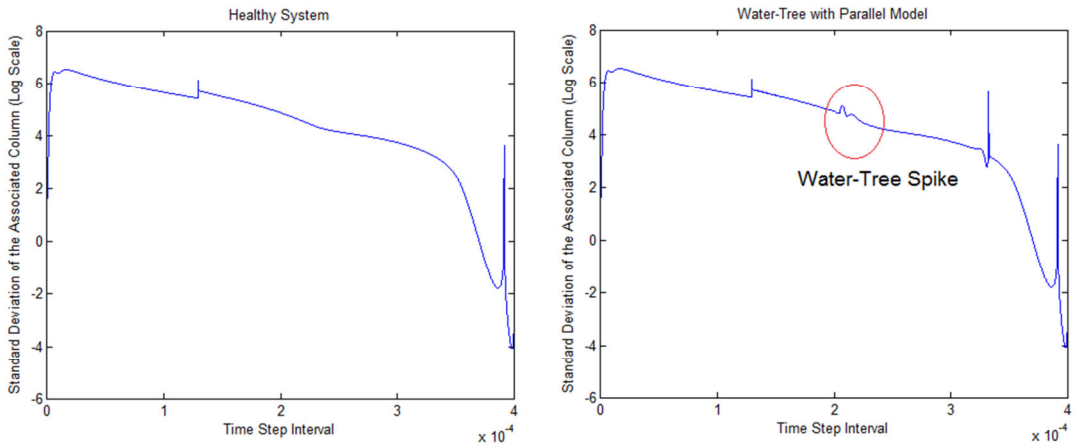

Figure 83: System Comparison with only 5th and 7th Harmonics

Figure 84 below shows the comparison, but with 5th and 7th order harmonics removed:

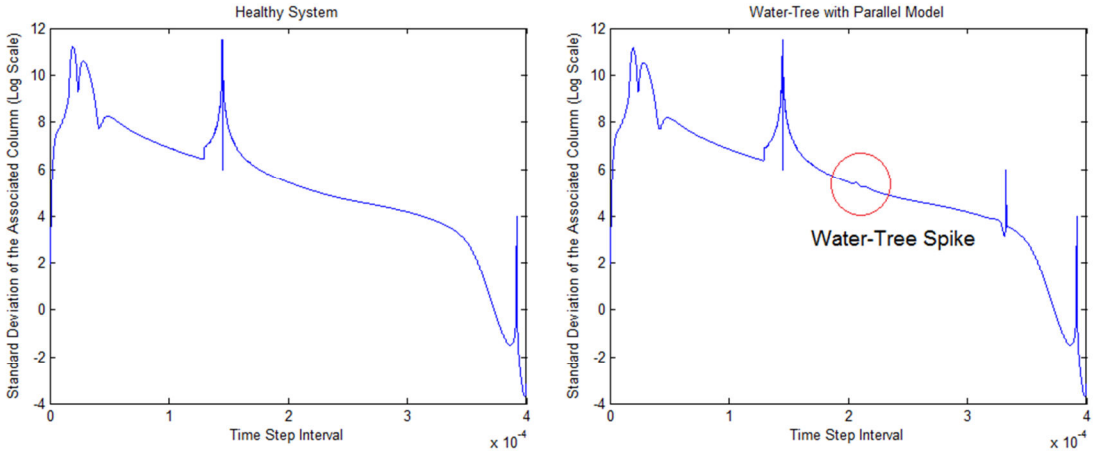

Figure 84: System Comparison with only 11th and 13th Harmonics

Different orders of harmonics will leave different impacts on the deviation comparison chart. To illustrate an extreme example, a 43rd order harmonic is injected to the system at 0.3% of the fundamental. The output is shown below in Figure 85:

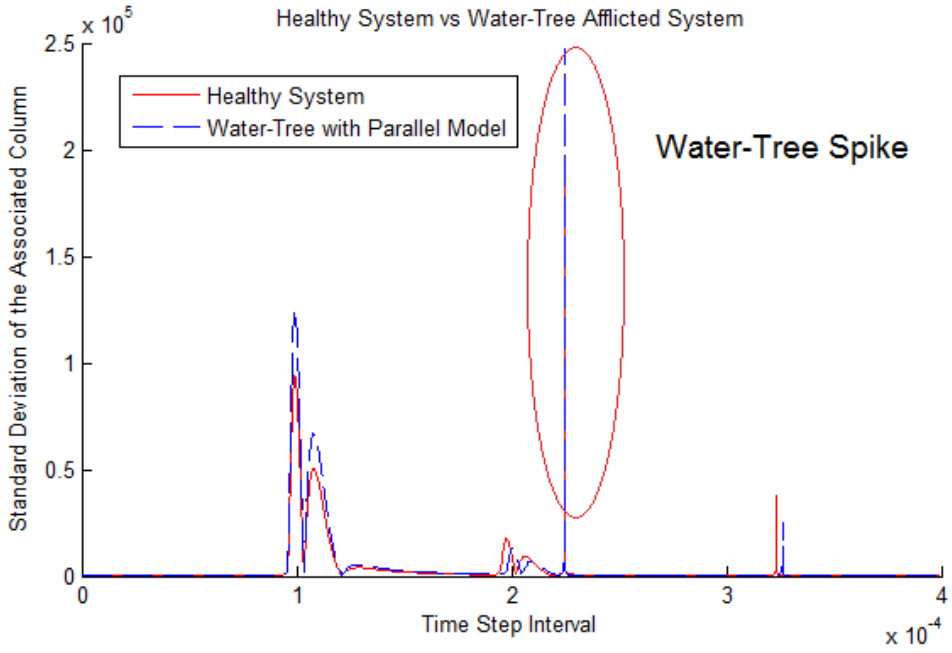

Figure 85: System Response with 43rd Order Harmonic

At the frequency of 43rd order harmonic, the time-step size of the input data starts to because an issue. The random spikes generated by the harmonic begin to interfere with the estimation process for water-tree presence. As the result, in order to actually take advantage of the very high-order harmonics, the time-step must be very small.

The locations of the random spikes change for different harmonic frequencies. In comparison, the water-tree spike remains at the same location throughout the process. As the result, water-trees and other fixed location discontinuities can be identified by their fixed position in the deviation-comparison output chart. Their position will remain fixed through iterations of extrapolation-comparison method regardless of frequency-compositions.

It can be observed that very high-order harmonic does respond to the presence of water-tree. Due to the random spikes, however, it is preferable to use naturally occurring

high-frequency transients instead. If very high-order harmonics are used, additional comparisons must be made across multiple iterations to ensure the accuracy of the result.

4.4.5 Impact of Noise on Deviation-Comparison Chart

In any process involving precise measurement, an important issue is the presence of noise in the system. There are many potential sources of noise:

Thermal noise is generated by random thermal movement of charge carriers such as electrons.

Shot noise is produced by the delay of electrons when crossing a physical barrier. This results in random fluctuation of the current level.

Flicker noise is a random noise associated with frequency spectrum.

Burst noise consists of sudden voltage step-changes associated with semiconductor components.

Many more types of noises exist and any delicate measurement process must consider their presence. Collectively, they can be represented by white noises in cables.

Fortunately, transmission system cables are less affected by the presence of white noise comparing to the control system circuits. The main reason is that transmission systems typically carry much higher power than control circuits; therefore, the signal to noise ratio (SNR) of the transmission system is much larger.

The SNR is the ratio between the power of the signal and the power of the noise. Using the low harmonic scenario from section 4.4.4, Gaussian white noise is added to the system output to simulate the effect of noise.

Figure 86, 87, 88 and 89 shows extrapolation-comparison output at various noise levels:

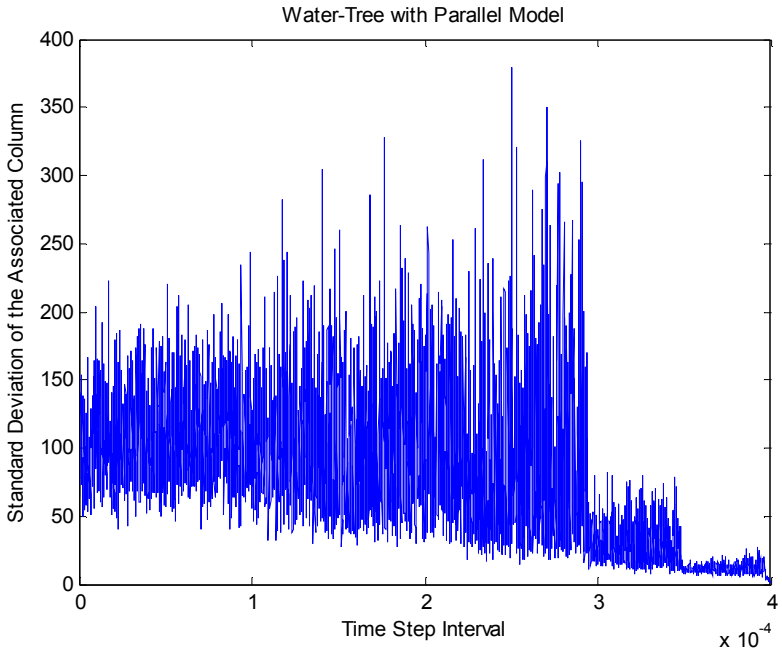

Figure 86: Water-Tree Afflicted System with SNR of 30

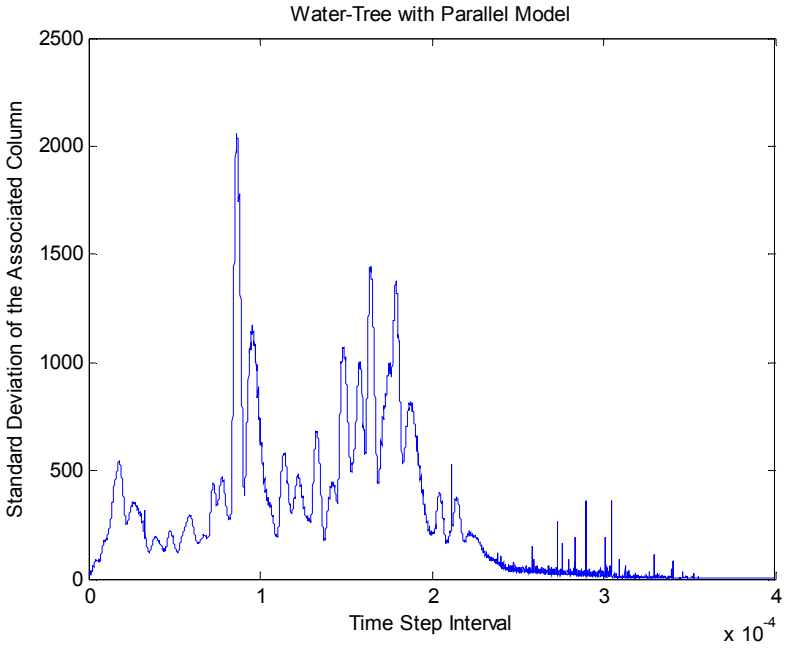

Figure 87: Water-Tree Afflicted System with SNR of 150

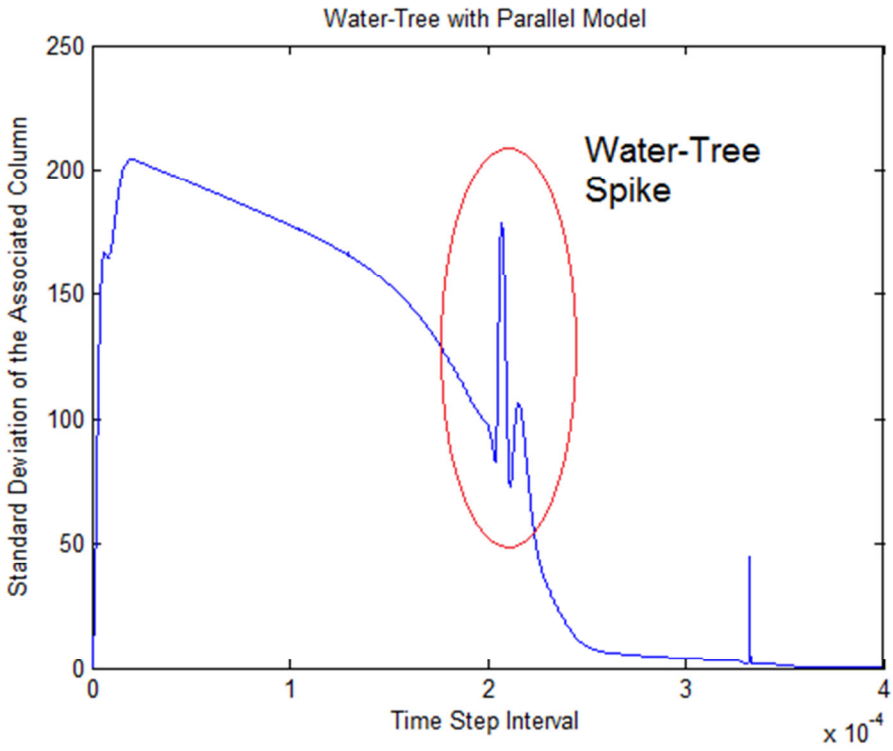

Figure 88: Water-Tree Afflicted System with SNR of 300

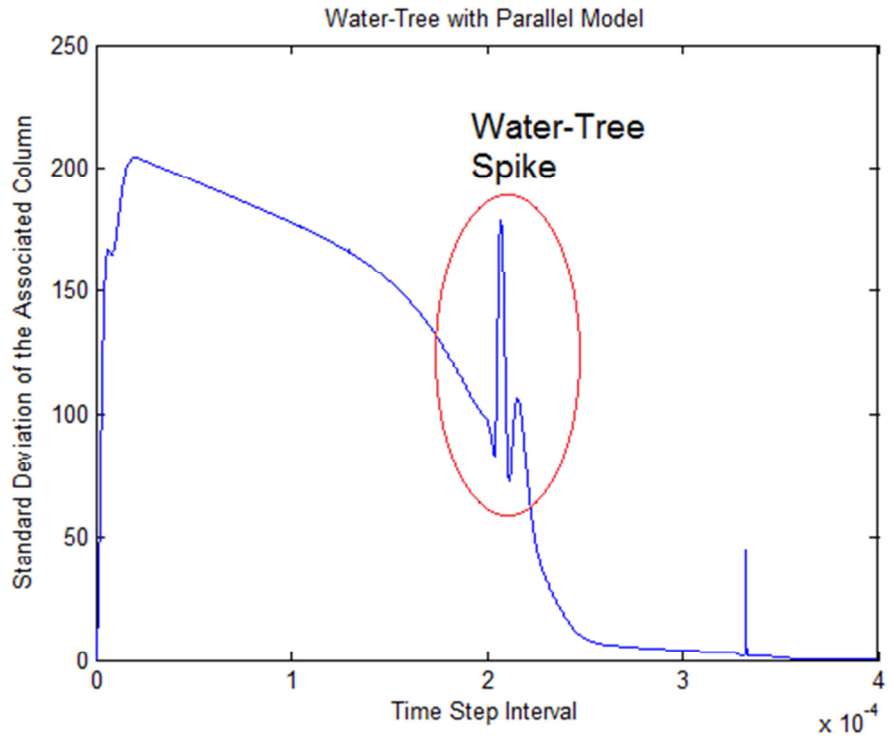

Figure 89: Water-Tree Afflicted System with SNR of 1000

It is necessary to remember that the SNR of transmission cables, particularly ultra-high voltage transmission cables associated with offshore windfarms, are much higher than control or low voltage circuits. For example, an offshore windfarm is delivering 90MW to the grid through three phase ultra-high voltage AC system. Three cables are used per phase. Thus, the power per cable is 90MW/3 phase/3 cable= 10MW. At SNR =300, the noise power is 10MW/300 = 33.3kW. Thus, the white noise must reach up to 33.3kW to have a SNR of 300.

As the result, white noise generally does not affect the extrapolation-comparison process. In addition, the water-tree spikes will remain in fixed locations regardless of noise level; therefore, comparing the result over multiple iterations of the extrapolation-comparison process will further eliminate any effect from random noise.

4.5 Chapter Conclusion

The early-warning system is a supplementary method to the high-frequency pulse detection method. It utilizes naturally occurring high-frequency events in the system to estimate if water-trees are present on the cable.

The system is an online process and does not require specialized instrument such as high-frequency pulse generator. It may also be fitted with filters to improve measurement accuracy, but at the cost of reliability. Ideally, the early-warning system will collect and analyze data continuously.

The feasibility of the method is supported by mathematically enhance detection algorithm. The estimation accuracy can be improved through iterations of NOHFE response. Although the magnitude of water-tree spikes can change, they will remain in

fixed locations regardless of system frequency composition. Results from multiple iterations of the extrapolation-comparison method can be used to determine if such these fixed-location events are present on the cable.

The standard deviation chart provides clear visual identifications of water-tree location. It should be noted, however, the presence of water-tree spike could be masked if there are high-magnitude low-frequency disturbances in the system. Essentially, the method requires the magnitude of the NOHFE to reach certain thresholds with respect to the system waveform.

The extrapolation-comparison method of the early-warning system can also be used to monitor other type of faults. It is especially effective on high-impedance faults.

Chapter 5

Computational Margin Accumulation in Water-Tree Analysis

Preventative maintenance plans are critical components in ensuring the long-term wellbeing of the power infrastructure. Effective formulation of the plans requires detailed information from the system. In chapter four, an early-warning system is developed to estimate the probability of water-tree presence in the cables. By applying the early-warning system, the power utilities can constantly monitor the status of cable connections and if necessary, utilize HFPD method to determine the exact condition of the cable insulation. In this chapter, some of the critical assessment details will be discussed.

5.1 Accurate Water-tree Estimation using Terminal Voltage Data

5.1.1 Motivation

The HFPD method is not limited to locating the water-tree. It allows the operator to determine the exact capacitance of the water-tree.

Remote determination of the water-tree capacitance provides an important advantage. The capacitance of water-tree is closely associated with the depth of water-tree corrosion through insulation layer. By determining the corrosion progression and its advancement rate, it becomes possible to predict and project the potential fail-date of the cable. The fail-date is uniquely important for water-tree fault due to its development rate.

In today's power industry, resource constraints are very realistic issues in treating and preventing system failure. When developing preventative maintenance procedures and schedules, these factors must be taken into consideration. For example, if the

expected fail-date of a cable segment is five years in the future, then immediate resources can be relocated to high priority issues.

Alternatively, ascertaining the corrosion progress may allow alternative solutions. Figure 90 below shows two cables with different level of corrosion:

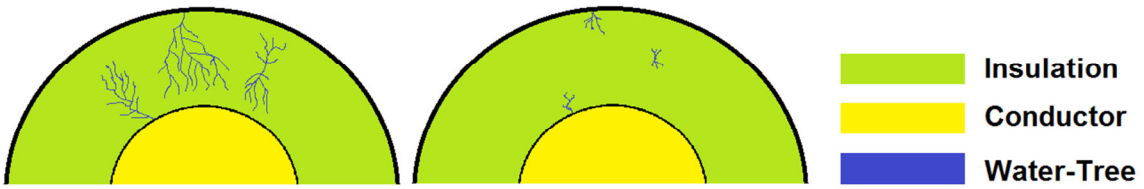

Figure 90: High Corrosion Progression (Left) Vs Low Corrosion Progression (Right)

For high corrosion progression cables, the water-tree has already breached significant part of the insulation. In this case, the cable must be "patched" to prevent further degradation. The patching process involves physically accessing the water-tree site. The micro-fracture is then filled with adhesive/polymer fillings. The root of the tree is also patched and physically reinforced. In extreme cases where water-tree corrosion is too severe, the cable segment must be completely replaced. Such procedures, however, require large amount of investment in labor, time and fund. Depending on the location, the operation itself may cause further problems; therefore, these procedures should not be performed unless they are necessary.

On the other hand, if the water-tree is a low corrosion progression tree, then alternative treatment method can be used. In chapter two, the water-tree formation process is discussed. The tree-growth is primarily motivated by the presence of water and electric field. Although it is difficult to remove water without physically accessing the site, the electric field strength can be reduced by load balancing. In worst-case scenario where water-tree growth cannot be halted, accurate determination of expected fail-dates

allows repair work to be flexibly scheduled in advance. In many cases, the flexible schedule itself will greatly reduce the expenditure.

These plans are contingent on the ability to determine the exact progress of water-tree corrosion in the cable insulation. Thus, accurate water-tree capacitance estimation using terminal voltage data is a very valuable ability.

5.1.2 Capacitance Estimation Process

It is possible to estimate the capacitance value of the water-tree using the previously established water-tree model and HFPD method. The water-tree can be estimated using the following parameters:

- Cable Parameter: Cable Characteristic Impedance
- Pulse Parameters: Modeling Parameters of the High-Frequency Pulse, The Frequency
- Pulse Reflection Parameters: Pulse Time, Pulse Reflection Time

The test system is shown below in Figure 91:

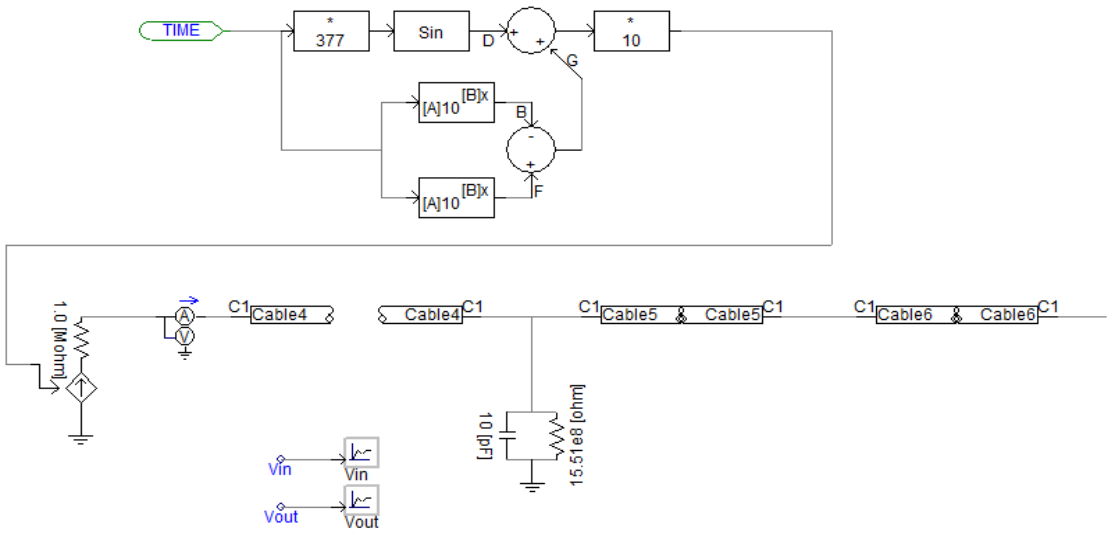

Figure 91: Pulse Reflection Experiment Setup

The test utilizes the radio frequency pulse (between 20kHz to 10MHz in extreme cases) to determine the capacitance of water-tree.

From the HFPD method, it is determined that potential pulse responses will fall under three categories: Under-Frequency, Benchmark-Frequency and Over-Frequency. The early-warning system is based on under-frequency response cases. Estimating the water-tree capacitance, on the other hand, requires the benchmark-frequency cases. It has been determined that the benchmark-frequency is part of a range of frequencies associated with the particular water-tree capacitance and it is unique. Thus, the benchmark-frequencies can be used to calculate the capacitance associated with the particular water-tree.

Mathematically, the pulse waveform (in form of the lightning pulse) can be represented by:

$$f(t) = a(e^{-bt} - e^{-ct}) \quad \text{.....(32)}$$

Where

a, b and c are pulse parameters

t is the time of central plateau point

The benchmark frequency phenomenon is created by the super-position of decaying sending pulse and its reflection from the water-tree branch. At the plateau, the nth derivative of the super-position equation becomes zero. The n parameter is determined by the "flatness" of the plateau pattern. In practice, the benchmark-frequency represents a range of frequencies that allows a plateau like pattern to appear. The situations are illustrated below in Figure 92, Figure 93 and Figure 94:

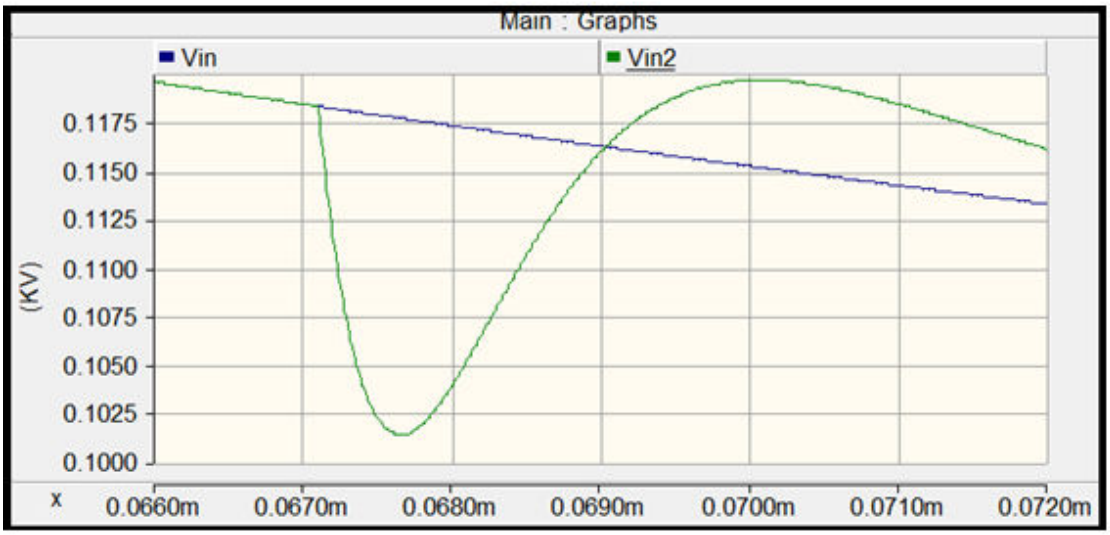

Figure 92: Non-Plateau Pattern

In this figure, the super-positioned waveforms do not form a plateau pattern. This means at n=1, the values of the waveforms are non-zero.

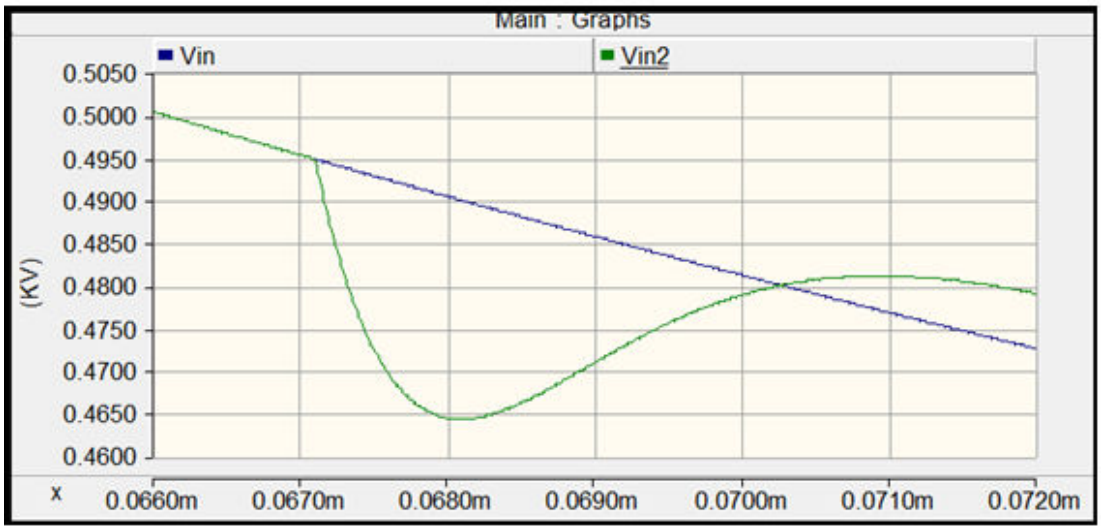

Figure 93: Plateau Pattern (N=1)

In this figure, the super-positioned waveforms show the beginning of the benchmark-frequency range. Specifically, at the start of the range, at n=1, the value is zero, but at n=2 or greater, the values are non-zero.

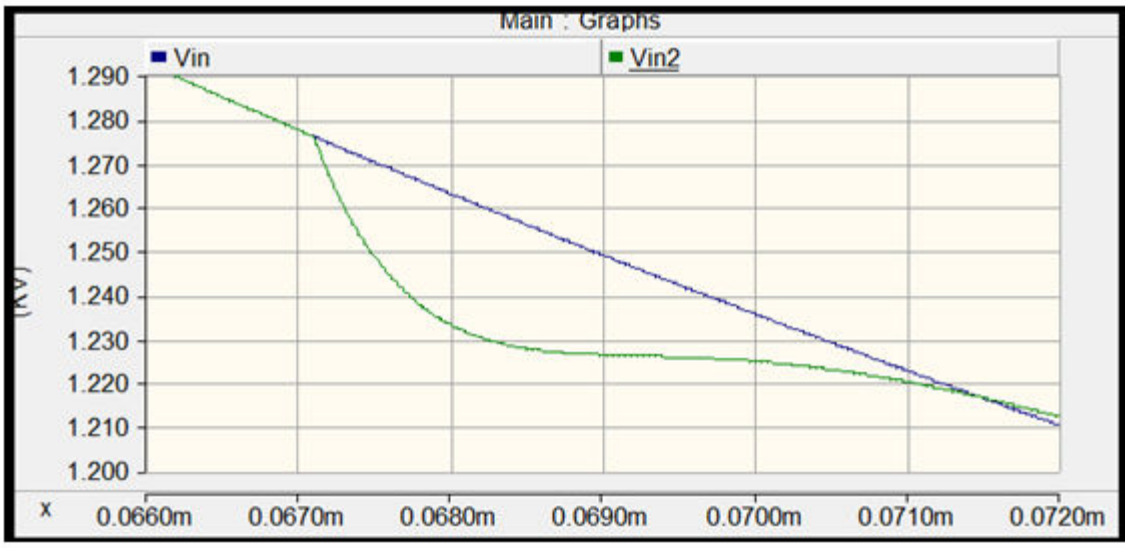

Figure 94: Plateau Pattern #2 (N>2)

This figure shows a frequency is in the middle of the benchmark-frequency range. At these frequencies, the n>= 2 derivatives of the super-positioned waveform are zero. The maximum value of n depends on the specific water-tree.

From the equation below, the super-imposed waveform is:

$$f(t) = a\left(e^{-b(t-\tau)} - e^{-c(t-\tau)}\right) + \Gamma a(e^{-bt} - e^{-ct}) \quad \text{.....(33)}$$

Where

τ is the time before the reflection pulse reaches the terminal

Γ is the reflection coefficient from the water-tree

$$f(t) = ae^{-b(t-\tau)} - ae^{-c(t-\tau)} + \Gamma ae^{-bt} - \Gamma ae^{-ct} \quad \text{.....(34)}$$

$$f'(t) = -abe^{-b(t-\tau)} + ace^{-c(t-\tau)} - \Gamma abe^{-bt} + \Gamma ace^{-ct} \quad \text{.....(35)}$$

$$f^{n}(t) = (-1)^{n}a[b^{n}e^{-b(t-\tau)} - c^{n}e^{-c(t-\tau)} + \Gamma b^{n}e^{-bt} - \Gamma c^{n}e^{-ct}] \quad \text{.....(36)}$$

Let $f^{n}(t) = 0$, then:

$$0 = (-1)^{n}a[b^{n}e^{-b(t-\tau)} - c^{n}e^{-c(t-\tau)} + \Gamma b^{n}e^{-bt} - \Gamma c^{n}e^{-ct}] \quad \text{.....(37)}$$

$$0 = b^n e^{-b(t-\tau)} - c^n e^{-c(t-\tau)} + \Gamma b^n e^{-bt} - \Gamma c^n e^{-ct} \quad \text{.....(38)}$$

Solving for Γ yield:

$$\Gamma = -\frac{b^n e^{-b(t-\tau)} - c^n e^{-c(t-\tau)}}{b^n e^{-bt} - c^n e^{-ct}} \quad \text{.....(39)}$$

The reflection junction model is shown in Figure 64 in chapter four. The reflection coefficient is:

$$\Gamma = \frac{Z_0}{Z_0 + 2Z_w} \quad \text{.....(40)}$$

Where:

Z_0 is the characteristic impedance of the cable

Z_w is the per-unit length capacitance of the water-tree

$$Z_w = \frac{Z_0 - Z_0\Gamma}{2\Gamma} = \frac{1}{\frac{1}{\frac{1}{j\omega C}} + \frac{1}{R}} \quad \text{.....(41)}$$

Since R is extremely large for developing water-tree

$$Z_w \sim \frac{1}{j\omega C} \quad \text{.....(42)}$$

$$C = \frac{1}{j\omega Z_w} = \frac{2\Gamma}{j\omega Z_0(1-\Gamma)} = \frac{-2\frac{b^n e^{-b(t-\tau)} - c^n e^{-c(t-\tau)}}{b^n e^{-bt} - c^n e^{-ct}}}{j\omega Z_0\left(1 + \frac{b^n e^{-b(t-\tau)} - c^n e^{-c(t-\tau)}}{b^n e^{-bt} - c^n e^{-ct}}\right)} \quad \text{.....(43)}$$

It is equivalent to:

$$C = \frac{1}{j\omega Z_w} = \frac{2\Gamma}{j\omega Z_0(1-\Gamma)} = \frac{2\frac{b^n e^{-b(t-\tau)} - c^n e^{-c(t-\tau)}}{b^n e^{-bt} - c^n e^{-ct}}}{j\omega Z_0\left(\frac{b^n e^{-b(t-\tau)} - c^n e^{-c(t-\tau)}}{b^n e^{-bt} - c^n e^{-ct}} + 1\right)} \quad \text{.....(43)}$$

Resolving the equation yields:

$$C = j\frac{2b^n e^{-bt} e^{b\tau} - 2c^n e^{-ct} e^{c\tau}}{2\pi f Z_0 (b^n e^{-bt} e^{b\tau} - c^n e^{-ct} e^{c\tau} + b^n e^{-bt} - c^n e^{-ct})} \quad \text{.....(43)}$$

The result of the equation includes both real and imaginary parts. Since the resistive component is not used in the initial calculation, an imaginary part is left. Thus, the real part represents the capacitance value.

The capacitance value is:

$$C = real(j\frac{2b^n e^{-bt} e^{b\tau} - 2c^n e^{-ct} e^{c\tau}}{2\pi f Z_0 (b^n e^{-bt} e^{b\tau} - c^n e^{-ct} e^{c\tau} + b^n e^{-bt} - c^n e^{-ct})}) \quad \text{.....(44)}$$

Where

Z_c is the cable characteristic impedance

f is the frequency

b and c are pulse parameters

t is the time of central plateau point

τ is the time before the reflection pulse reaches the terminal

n is the derivative number, which yields a flat plateau pattern

Since the benchmark-frequency is a range, the two edge frequencies are positions that represents n=1. The estimated capacitance value represents the range of estimated capacitances.

5.1.3 Test Case Result

For the test case, a 1nF capacitance is used in the water-tree branch. The pulse frequency is varied until a threshold benchmark pattern is established as shown below in Figure 95.

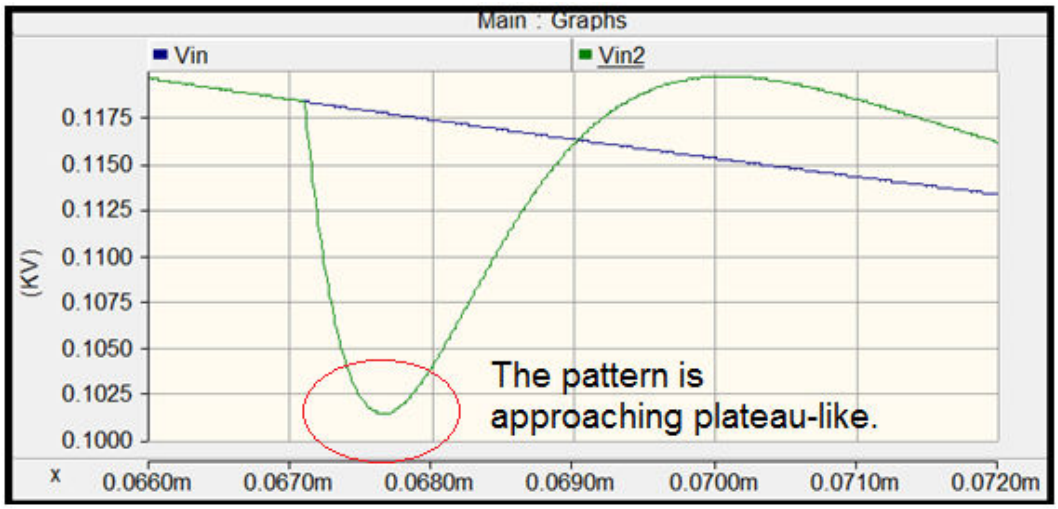

Figure 95: Threshold Benchmark Frequency

At the threshold benchmark-frequency, the frequency is very close to the values that will establish the flat plateau pattern. Mathematically, this means both edge of the benchmark frequency range are close to each other.

At the threshold benchmark-frequency range, the following parameters are determined:

b=1.63e5

c=3e9

f=57.2kHz

t=2.19e-6 (seconds)

τ =6.7075e-5 (seconds)

Using the following additional parameters:

n=1 (at the edge of the benchmark frequency range)

z0=70+j70Ω (cable impedance)

Resultant Calculated capacitance:

Capacitance =**39nF**

Since the capacitance associated with water-tree develops in log-scale, the value is fairly close to the expected value of 1nF.

The test case proves that the mathematical determination algorithm represents a method to estimate water-tree capacitance using HFPD test data. The algorithm only requires terminal readings and does not require the operator to access the water-tree site physically.

5.2 Error Accumulation in Water-tree Detection

In chapter four, the impact of white noise on early-warning system is examined. Other source of error may also influence the accuracy of the water-tree detection process. For example, a potential cause of the inaccuracy is due to measurement errors associated with the parameters in the solution. For example, frequency measurement is measure from the 5% peak value mark at the start and the 5% peak value mark at the end. The actual pulse shape is shown below in Figure 96:

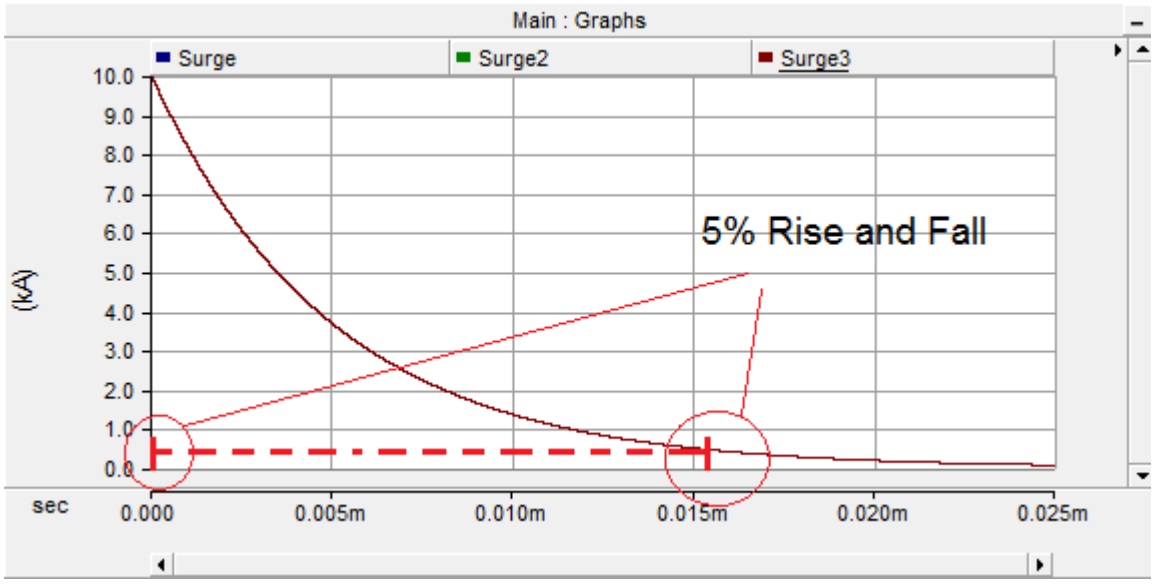

Figure 96: Pulse Frequency Measurement

Depending on the measurement points, the resultant frequency value can change. Consequently, there is certain amount of error associated with the measurement.

The threshold benchmark-frequency also includes certain amount of error. In the test case, the threshold benchmark-frequency is established close to the value that generates the plateau pattern. Due to the cumbersomeness of the lightning pulse model, it may contain certain amount of error. As the result, a slightly higher or lower frequency also resembles the threshold benchmark-frequency. Since the b, c parameters vary exponentially in the model and capacitance calculation, the error margin is greatly amplified in the process.

5.2.1 Water Detection Limitations

There are several limitations associated with the water-tree detection process. They place upper limits on the accuracy of the process. Depending on their specific nature, they may be eliminated using different methods. Alternatively, they can also be critical issues that will only be resolve through future technological development. These limitations can be separated into three categories: material, computational and fundamental.

5.2.1.1 Material Limitation on Water-Tree Detection

The material limitation refers to the natural limitations associated with the physical aspects of the process. For example, the structure of water-tree is highly random and it places a limit on the water-tree modeling process. The small size of water-tree components also means it is difficult to obtain accurate measurements on its characteristic.

Another aspect of material limitation is that the physical characteristic of the material limits applicable detection methodology. For example, VLF and power frequency methods are generally ineffective due to the physical characteristic of the water-tree. For VHF, the withstand strength of insulation must be considered when applying a high magnitude pulse.

The location of the water-tree is also a material limitation. For example, it is very difficult to access long-distance submarine cables. Thus, the water-tree detection process must use terminal readings far from the actual water-tree site. This results in issues such as signal attenuation and impedance masking.

5.2.1.2 Computational Limitation on Water-Tree Detection

Computational limitations tend to appear in analysis algorithm and calculation process. For example, a key computational limitation is the accuracy and sensitivity of terminal voltage readings. With sufficiently advanced voltage sensor, even VLF and OPF methods can detect an early-stage water-tree. This is, of course, impractical in implementation.

The processing power of the computation device is another important limitation. Water-tree has been a long observed phenomenon. The water-tree model and early-warning system proposed in the previous chapters, however, would not be possible without recent advancements in computation technology. For example, the deviation-comparison table uses greater than 10^5x10^5 matrices. The amount of processing power required is only practical in the recent decade.

Analytical algorithm is also part of the computational limitation. In the actual system, signals and parameters extracted by the water-tree detection process can be

contaminated with noise and other random variables. This is especially true for multiple water-tree cases. If the trees are sufficiently close, their pulse response may interfere with each other. In these events, analytic algorithms are required to filter and isolate individual response.

As discussed previously, many frequency-domain techniques form mathematically singularities when dealing with weak signal in long-distance cables. Time-domain techniques, on the other hand, may suffer from error margin amplifications. As the result, the analytical algorithms themselves must be carefully selected. Sometimes, multiple algorithms must work together and supplement each other.

5.2.1.3 Fundamental Limitation on Water-Tree Detection

The fundamental limitation of water-tree detection process is the fact that water-tree is a difficult to observe phenomenon and its characteristic must be determined from secondary data such as terminal voltage and current. In essence, it is a high-sensitivity measurement and requires very high accuracy, but it can only be calculated using secondary data. The secondary data themselves also contain various degree of error. As the result, there is an upper limit on the accuracy of the water-tree capacitance estimation. The limit cannot be overcome without fundamental improvement in secondary data accuracy.

5.2.2 Errors Margins in Water-Tree Capacitance Estimation

5.2.2.1 Error Accumulation

For computation using variables with error margin, an important phenomenon is the propagation and accumulation of errors in the result. Table 5 illustrates the situation:

Table 5: Error Accumulation: Percentage Error vs Number of Variables

	1	2	3	4	5	6
0.03	0.03	0.06	0.09	0.13	0.16	0.19
0.06	0.06	0.12	0.19	0.26	0.34	0.42
0.09	0.09	0.19	0.30	0.41	0.54	0.68
0.12	0.12	0.25	0.40	0.57	0.76	0.97
0.15	0.15	0.32	0.52	0.75	1.01	1.31
0.18	0.18	0.39	0.64	0.94	1.29	1.70
0.21	0.21	0.46	0.77	1.14	1.59	2.14
0.24	0.24	0.54	0.91	1.36	1.93	2.64

The vertical axis represents percentage accuracy in each variable. The horizontal axis represents the number of variables in the calculation. For example, a four variable calculation with 9% error in each variable will result in 41% error in the end-result.

The table demonstrates the propagation of error from variable to the calculation result. The table is the error accumulation in simple multiplicative equations. For equations with exponential variables, such as the water-tree capacitance solution, the error accumulation is even more severe.

5.2.2.2 Material Limitation Induced Error Margins

Material limitation can create several sources of error margins in the water-tree detection process. They are ellipsoid axial ratio, water-tree branch distribution and tree branch dimension.

The ellipsoid axial ratio is part of the assumptions in the water-tree model. Since water-tree branch spread and distribution is controlled by the zero crossing of the service voltage, it is reasonable to assume that the water-tree afflict area is bounded in an ellipsoid area with a certain axial ratio. In practical, the relationship between the axial ratio and the service voltage is not one-on-one. Instead, the ratio can also be influenced

by minor parameters such as material crystallinity, voltage harmonic composition, transients and various other factors. The effects from these factors are relatively small comparing to the zero crossing of the service voltage and the waveform magnitude, but combined, they generate a noticeable error margin in the capacitance calculation.

Similar to the ellipsoidal area axial ratio, the water-tree branch distribution is also subjected to certain amount of random error. Material crystallinity, cause of water-tree origin and its uniformness can influence the tree branch distribution. Variation in these factors can cause error margins, which manifest in form of axial ratio estimation errors.

Finally, the tree branch dimensions are also affected by the physical characteristic of the cable insulation layer. For detection methods, the influence of tree branch dimension mainly appears in the boundary of the ellipsoidal area. For thin branches that are spread out, a significant portion of the tree branch tips are sufficiently small that their dielectric permittivity is essential indistinguishable from healthy insulation. In this case, the estimated ellipsoidal bounded area, by extension the corrosion progress will be smaller than the actual condition. The reverse is also true, physical fracture of the insulation layer due to manufacturing defect may result in higher capacitance and the detection method may overestimate the water-tree corrosion progression.

5.2.2.3 Computational Limitation Induced Error Margins

The computational limitation may also cause error margins in the analysis. These sources of errors include error in frequency estimation, error in benchmark-frequency estimation, error in time measurement and error in pulse modeling.

Figure 96 has shown potential error margin in frequency estimation. In practice, the relationship between the water-tree impedance and the high-frequency pulse is much

more complex than the simple capacitor/high-frequency wave relationship. Water-tree is modelled as a capacitor with multiple dielectrics. It is, however, a simplification of the actual interactions between the tree branch electrical field and the insulation material at microscope level. Although the high-frequency characteristic of water-tree resembles the capacitor, it also includes non-linear components.

Similarly, estimation of benchmark-frequency range may contain error margin. There are two approaches in determining the benchmark-frequency: Single-Frequency Approach and Two-Frequency Approach.

In single-frequency approach, the test pulse frequency is adjusted until the observed waveform begins to show the plateau pattern. This threshold frequency is then used to calculate the water-tree capacitance. In this approach, the threshold hold frequency represents a point where the two boundaries of the benchmark-frequency range is roughly equal. As the result, the capacitance estimation is a single value instead of a range of potential values.

The second approach is the two-frequency approach. In this approach, the pulse frequency is adjusted until a large flat plateau pattern appears. The two boundaries frequencies are used to estimate the potential water-tree capacitance. In this approach, the estimation result will be a range instead of a single value.

The boundaries frequencies are generally more accurate than the threshold frequency in the single-frequency approach. In either case, certain amount of error margin is expected.

Time measurement is a critical component in the water-tree capacitance estimation. Similar to frequency measurement, the time stamp of the waveform pattern is

subjected to certain amount of error. Assuming the measurement devices themselves are accurate, the process of defining the start and finish of the pattern may still create error. For example, field practice tends to choose 5% rise and 5% fall mark as the measurement point for high frequency pulse. This definition is somewhat an arbitrary decision based on past-experiences and ease of measurement. This is especially true for slow decaying pulses where 5% and 3% fall points may have a large time difference.

Finally, the pulse model itself may have error associated with it. There are many commercially available high-frequency pulse generators. Their principle of pulse generation varies. It is also unreasonable to assume that the generated pulses will strictly follow a simple, easy to understand mathematical model. Due to the sensitive nature of the water-tree detection process, any deviation between the mathematical model and the actual, physical pulse form may generate error in the final-result.

Table 6 below shows the types of error margins expected in the water-tree capacitance estimation process using a lightning pulse model:

Table 6: Source of Error in Water-Tree Capacitance Estimation

Parameter	Description	Source of Error	Type of Measurement
n	Derivative Iterration	Measuring the exact location of the center plateau point	Voltage
Z	Cable Characteristic Impedance	Equipment Measurement	Equipment
b	Pulse Model Parameter	Determined by the Pulse Shape	Voltage
c	Pulse Model Parameter	Determined by the Pulse Shape	Voltage
t	Time of Plateau Point	Measuring the exact location of the center plateau point	Voltage
τ	Time before Reflection Pulse Reaches Terminal	Determined by the Pulse Shape	Voltage

The errors can be separated into two categories: voltage measurement induced errors and equipment sensitive related error. The voltage measurement errors are

associated with computational limitations and the equipment sensitivity related errors fall under material limitations of the water-tree detection process.

5.2.3 Potential Method for Improvement on Fundamental Limitation

The fundamental limitation is more difficult to overcome comparing to the other two limitations. Once improvement occurs at the fundamental level, however, the entire processes benefit from it.

There are certain methods to deal with the fundamental limitation of the detection process. For example, numerical averaging is one of the common methods used to reduce random errors. In numerical averaging, the estimation results are compiled into a probability distribution. Additional iterations expand the distribution pool.

Alternatively, better instrument precision greatly improves the accuracy of the final-result. Under the same technological level, higher precision instrument generally means higher cost and the cost increases exponentially as the sensitive approaches the technological limitation. Technological advancement naturally reduces the cost for the same accuracy level. Alternatively, it may allow better instrument accuracy for the same cost.

In practice, technological advancement is an incremental effort and it can be heavily influenced by research focuses; therefore, it is beneficial to establish a cost-effective focus direction. In order to find the most efficient direction for improving water-tree capacitance estimation, it is necessary to understand the dominant factor influencing the estimation accuracy.

The numerical resolution of the water-tree capacitance using a lightning pulse model is listed below:

$$C = real(j\frac{2b^n e^{-bt}e^{b\tau} - 2c^n e^{-ct}e^{c\tau}}{2\pi f Z_0(b^n e^{-bt}e^{b\tau} - c^n e^{-ct}e^{c\tau} + b^n e^{-bt} - c^n e^{-ct})} \quad \text{.....(45)}$$

The equation is effectively created by the lightning pulse medal equation:

$$f(t) = a(e^{-bt} - e^{-ct}) \quad \text{.....(46)}$$

Since the amplitude does not appear in the final solution. The main parameters in the lightning pulse model are measurement parameters (t and voltage value $f(t)$) and modeling parameters (b and c).

Observing the effect of errors in measurement parameters:

$$V + \Delta V = e^{-b(t+\Delta t)} - e^{-c(t+\Delta t)} \quad \text{.....(47)}$$

$$\ln(V + \Delta V) = \ln(e^{-b(t+\Delta t)} - e^{-c(t+\Delta t)}) \quad \text{.....(48)}$$

$$\ln(V) + \ln\left(1 + \frac{\Delta V}{V}\right) = \ln\left(1 - e^{(b-c)(t+\Delta t)}\right) - b(t + \Delta t) \quad \text{.....(49)}$$

The error in voltage measurement is a flat shift depending on the percentage voltage-measure error. For voltage measure error of 5%:

$$lnV + 0.0488 = \ln(1 - e^{(b-c)(t+\Delta t)}) - b(t + \Delta t) \quad \text{.....(50)}$$

Let $\ln\left(1 - e^{(b-c)(t+\Delta t)}\right) = m$ and $1 - e^{(b-c)(t+\Delta t)} = n$

$$S_m = \frac{S_n}{1 - e^{(b-c)(t+\Delta t)}} \quad \text{.....(51)}$$

Where S represents the standard deviation of the probability distribution

$$S_n = e^{(b-c)(t+\Delta t)} S_{(b-c)(t+\Delta t)} = e^{(b-c)(t+\Delta t)} |b - c| S_{\Delta t} \quad \text{.....(52)}$$

To resolve the standard deviation distribution:

$$S_m = \frac{S_n}{1 - e^{(b-c)(t+\Delta t)}} \quad \text{.....(53)}$$

Since b is greater than c, for $e^{(b-c)(t+\Delta t)} \ll 1$,

$$S_m = e^{(b-c)(t+\Delta t)} |b - c| S_{\Delta t} \quad \text{.....(54)}$$

Rearrange equation (50):

$$b = \frac{\ln(1-e^{(b-c)(t+\Delta t)})-(lnV+0.0488)}{(t+\Delta t)} = \frac{m-(lnV+0.0488)}{(t+\Delta t)} \quad \text{.....(55)}$$

As the result, the basic spread of b is entirely dependent on the standard deviation of time measurement.

Using the same principle, it can be determined that the standard deviation of the probability distribution of the time is the dominant factor in the water-tree capacitance estimation process.

Evaluation the capacitance solution equation:

$$C = real(j\frac{2b^n e^{-bt}e^{b\tau}-2c^n e^{-ct}e^{c\tau}}{2\pi f Z_0(b^n e^{-bt}e^{b\tau}-c^n e^{-ct}e^{c\tau}+b^n e^{-bt}-c^n e^{-ct})} \quad \text{.....(56)}$$

Resolving the standard deviation of the top part of the equation:

$$L_1 = 2b^n e^{-bt}e^{b\tau} \quad \text{.....(57)}$$

$$L_2 = 2c^n e^{-ct}e^{c\tau} \quad \text{.....(58)}$$

$$S_{b^n} = nb^n\frac{S_b}{b} = \sqrt{2}nb^{n-1}S_{\Delta t} \quad \text{.....(59)}$$

$$S_{e^{-bt}} = e^{-bt}S_{-bt} = e^{-bt}bt\sqrt{\left(\frac{S_b}{b}\right)^2+\left(\frac{S_{\Delta t}}{t}\right)^2} \quad \text{.....(60)}$$

$$S_{e^{b\tau}} = e^{b\tau}S_{b\tau} = e^{b\tau}b\tau\sqrt{\left(\frac{S_b}{b}\right)^2+\left(\frac{S_{\Delta \tau}}{\tau}\right)^2} \quad \text{.....(61)}$$

$$S_{L_1}$$

$$= b^n e^{-bt}e^{b\tau}\sqrt{2n^2b^{2n-2}{S_{\Delta t}}^2 + e^{-2bt}b^2t^2\left[\left(\frac{S_b}{b}\right)^2+\left(\frac{S_{\Delta t}}{t}\right)^2\right] + e^{2b\tau}b^2\tau^2\left[\left(\frac{S_b}{b}\right)^2+\left(\frac{S_{\Delta \tau}}{t}\right)^2\right]}$$

.....(62)

$$\because S_b = \sqrt{2}S_{\Delta t} = \sqrt{2}S_{\Delta \tau} = S_c \quad \text{.....(63)}$$

$$S_{L_1} \cong b^n e^{-bt}e^{b\tau}\sqrt{2n^2b^{2n-2}+e^{-2bt}b^2+e^{2b\tau}b^2} * S_{\Delta t} \quad \text{.....(64)}$$

$$\because e^{-2bt}b^2 + e^{2b\tau}b^2 \; is \; small$$

$$\therefore S_{L_1} \cong \sqrt{2}nb^{2n-1}e^{-bt}e^{b\tau} * S_{\Delta t} \quad \text{.....(65)}$$

$$\therefore S_{L_2} \cong \sqrt{2}nc^{2n-1}e^{-ct}e^{c\tau} * S_{\Delta t} \quad \text{.....(66)}$$

$$S_{top} = \sqrt{{S_{L_1}}^2 + {S_{L_2}}^2} = \sqrt{2}n\sqrt{(b^{2n-1}e^{-bt}e^{b\tau})^2 + (c^{2n-1}e^{-ct}e^{c\tau})^2} * S_{\Delta t} \quad \text{.....(67)}$$

Resolving the standard deviation of the bottom part of the equation:

$$L_3 = b^n e^{-bt} \quad \text{.....(68)}$$

$$L_4 = c^n e^{-ct} \quad \text{.....(69)}$$

Using the same process and elimination:

$$S_{L_3} \cong \sqrt{2}nb^{2n-1}e^{-bt} * S_{\Delta t} \quad \text{.....(70)}$$

$$S_{L_4} \cong \sqrt{2}nc^{2n-1}e^{-bt} * S_{\Delta t} \quad \text{.....(71)}$$

$$S_{bottom} = \sqrt{2}n\sqrt{(b^{2n-1}e^{-bt})^2(e^{b\tau}+1)^2 + (c^{2n-1}e^{-ct})^2(e^{c\tau}+1)^2} * S_{\Delta t} \quad \text{.....(72)}$$

$$S_{total} = \left|\frac{2b^n e^{-bt}e^{b\tau} - 2c^n e^{-ct}e^{c\tau}}{b^n e^{-bt}e^{b\tau} - c^n e^{-ct}e^{c\tau} + b^n e^{-bt} - c^n e^{-ct}}\right| \sqrt{\left(\frac{S_{top}}{top}\right)^2 + \left(\frac{S_{bottom}}{bottom}\right)^2} \quad \text{.....(73)}$$

Standard Deviation of the Resolution

$$S_{total} =$$

$$\sqrt{2}n \left|\frac{2b^n e^{-bt}e^{b\tau} - 2c^n e^{-ct}e^{c\tau}}{b^n e^{-bt}e^{b\tau} - c^n e^{-ct}e^{c\tau} + b^n e^{-bt} - c^n e^{-ct}}\right| *$$

$$\sqrt{\frac{\left(b^{2n-1}e^{-bt}e^{b\tau}\right)^2 + (c^{2n-1}e^{-ct}e^{c\tau})^2}{(2b^n e^{-bt}e^{b\tau} - 2c^n e^{-ct}e^{c\tau})^2} + \frac{(b^{2n-1}e^{-bt})^2\left(e^{b\tau}+1\right)^2 + (c^{2n-1}e^{-ct})^2(e^{c\tau}+1)^2}{(b^n e^{-bt}e^{b\tau} - c^n e^{-ct}e^{c\tau} + b^n e^{-bt} - c^n e^{-ct})^2}} *$$

$$S_{time} \quad \text{.....(74)}$$

From the standard deviation calculation, it can be determined that the standard deviation of both parameter measurement and capacitance estimation is directly proportional to the accuracy of the time measurement.

5.3 Chapter Conclusion

Estimation of water-tree capacitance is a necessary step on designing effective preventative maintenance process. Successful determination of water-tree status allows utilities to efficiently organize their resource and avoid unnecessary service-interruptions. At the same time, it is necessary to remember that the estimation process is subjected to material, computational and fundamental limitations. The central theme of water-tree detection research is reduction of measurement error while working under resource constraints.

In the short-term, more advanced mathematical technique and computation algorithm is the key for immediate improvement, but at the end of the day, improvement in measurement tools accuracy, especially in dominant parameters such time measurement, will provide the fundamental improvement to the reliability of the water-tree detection and estimation process.

Chapter 6

Conclusion

The Water-Tree Modelling and Detection for Underground Cables study focuses on mathematical modelling of the water-tree, detection of its location and estimation of its capacitance in long-distance transmission cables. It is an effort to understand the physical implications of water-tree structure, its interaction with the grid and developing methods to combat water-tree related power failures.

The research is primarily motived by power infrastructure aging around the world. In particular, cable transmission systems around the world are rapidly approaching the end of a development cycle. The end of this cycle naturally heralds gradual degradation of power transmission system, in both reliability and quality. Due to economic constraints, however, replacement and renewal efforts have become stagnant in many parts of the world; therefore, the utilities are forced to operate the cable systems beyond their original design life. Consequently, prolonging the lifespan of the current system becomes a top priority.

Among the successful attempts to revitalize the existing system, preventative maintenance plans have proven to be cost-effective. Successful plans prevent system degradation to reach critical stage and improve the performance of older equipment. In order to develop preventative maintenance plans, the operators must have detailed information on the cable system status and parameters, especially potential issues that may negatively affect the system in the future. In essence, the operator can only prevent a problem if they are aware of it in the first place.

Assessing the system status and parameters is not an easy task. Older system often implies more issue, both in quantity and complexity. Among the issues associated with older cable system, the water-tree phenomenon is especially important. They are slow developing, but difficult to detect prior to critical breakdown. In addition, many difficult to detect water-trees reside in critical connections such as long-distance transmission cables. The length of the cable not only hinders the detection process, but also amplifies the potential impact. Their failures often result in significant economic loss, both in the repair cost and service interruption.

Prevention of water-tree is a difficult endeavor. Water-tree characteristic, its development process and system interaction are less understood subjects. Without these understandings, it is difficult to develop preventative maintenance plans suitable for water-tree prevention. As the result, research is needed to understand the water-tree structure, its interactions with the cable system and developing the corresponding detection methods.

Thus, the first step in understanding water-tree modelling and detection in underground cables is building a mathematical model for the particular phenomenon. Water-trees are complex structures with complicated electromagnetic interactions with the insulation. Fortunately, many of its physical characteristics follow certain trends and their boundary conditions can be estimated using system operating parameters. Although water-tree electromagnetic interactions are difficult to quantify, recent advancements in analytical technique and computation technology can breakdown the complex topic into manageable parts. By applying finite element analysis to the water-tree, its capacitance is

estimated. The results are confirmed by empirical measurement results and electromagnetic simulations.

The mathematical model is able to highlight key characteristics in the developing water-tree. It is a primarily capacitive phenomenon with Giga-ohm range impedance. The next logical step is developing techniques for locating water-trees in the system. Due to the impedance, traditional detection methods are ineffective on early-stage water-trees, especially if they are located in long-distance cables. With the help of the mathematical model, however, it becomes possible to overcome the high impedance. Since mathematically model shows that the water-tree is a capacitive structure, very high frequency input will effectively reduce the detection difficulty. The resultant high frequency pulse detection method utilizes MHz range input to neutralize the water-tree impedance. The result is a method that can successfully detect the location of an early-stage water-tree. In addition, the pulse response patterns can be used to estimate the corrosion progress of water-tree.

After developing the detection method for water-tree, it becomes necessary to consider its implementation. The transfer from laboratory theory to actual implementation must always be tempered with practical constraints. Although the high-frequency pulse detection method allows accurate detection of water-tree, it is also a specialized test requiring specific and most importantly, expensive equipment. The cost of instrument is a very real concern for the utility. In addition, the potential risk in test stress and economic cost in service interrupt also become factors to be considered. Due to these constraints, the high-frequency pulse detection method should be selective and only performed when necessary. As the result, a supplementary system is developed to

identify potential targets for the high-frequency test. The early-warning system is designed to assess cable status using naturally occurring high-frequency events in the system. Its extrapolation-comparison method allows the operators to identify cable waveform anomalies without specialized equipment. These anomalies are analyzed through standard deviation charts and potential sites of water-tree are indicated. By using the early-warning system, operators can assess the probability of water-tree presence on the cable segment. If the cable is likely to be afflicted with water-tree, it becomes a candidate for the high-frequency pulse detection method.

The research now contains implementable detections methods that assess the probability of water-tree presence in the cable system. The potential candidates are tested using an accurate detection method that allows accurate determination of water-tree location. Supported by the mathematical model, it becomes possible to estimate the capacitance of water-tree through mathematical analysis and the cable high-frequency pulse response. The analysis results allow the operators to determine water-tree corrosion progress and prepare the appropriate response. In addition, it also becomes possible to evaluate measurement parameters that affect the accuracy of water-tree detection and estimation process. Mathematical analysis revealed that time-step measurement is the dominant factor on water-tree detection accuracy. Future technology advancement in this regard will allow fundamental improve to the overall water-tree detection and estimation process.

In addition to provide a reasonable method for water-tree detection and estimation, the water-tree develop in power system research also offer other benefits:

The mathematical modelling process can be expanded and extended to other types of structures in the cable insulation.

The high-frequency pulse detection method can be retooled for other types of faults in long-distance cables.

The early-warning system can monitor the appearance of many types of cable faults and degradations.

The error margin analysis in water-tree detection process can show cost-effective direction for future technological development.

In the future, it will be beneficial to explore methods of improving measurement accuracy. For example, digital synchronous sampling has been known to increase the accuracy of very high-order harmonics. Due to error margin accumulation and propagation, potential improvements in base parameter measurements will provide large benefits to the water-tree detection process.

APPENDICES

APPENDIX A Sample Finite Element Analysis Code for Water-Tree Model

The overall structure of the finite element analysis algorithm is shown below in Figure 97:

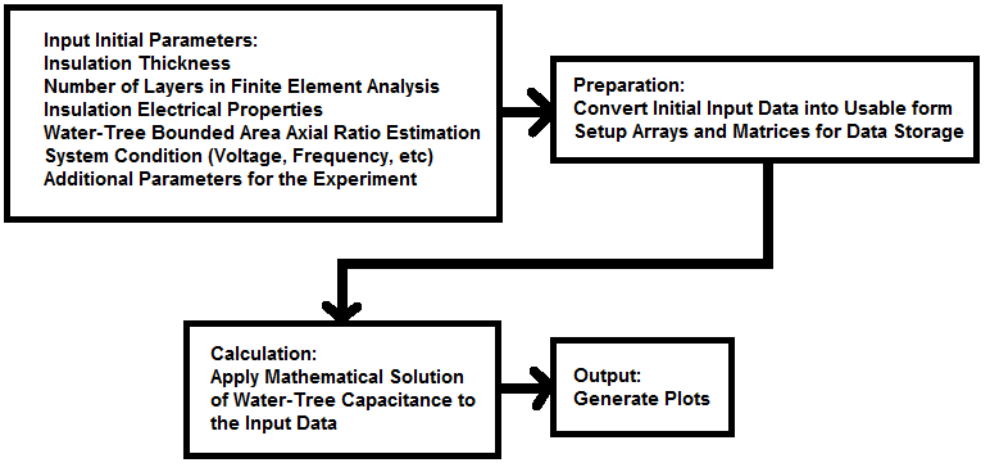

Figure 97: Finite Element Analysis Algorithm Flow Chart

The codes below are sample finite element analysis algorithm for Chapter 2.

```
%water tree capacitance of a ellipsoid area using
%linearly change permittivityt

clear all

hold on



%user input data
e0=8.854187817e-12;       %permittivity of vacuum
e2=2.3*e0;                   %relative permittivity of the insulation
e1_relative=88;
e1=e1_relative*e0;                %relative permittivity of at the base of the
tree
f=60;                     %frequency in Hz
rho_base=10e-2;           %conductivity at the base of the tree
rho_tip=10e-16;           %conductivity at the tip of the tree
%end user input data



%data preparation
radius_cable=(4.547e-2)/2;       %radius of the cable
radius_conductor=(2.474e-2)/2;   %radius of the conductor
```

```
w=2*pi*f;
healthy_percent=0.05; %starting percentage depth of insulation layer that is
                      %healthy data range is from 0 to 1 (0% to 100%)
upper=0.95;           %upper limit on health calculation
health_layer=10000;   %the number of different health depth to check
health_step=(upper-healthy_percent)/health_layer;
                      %each increment between health depth
trim=0.05;            %how much of the ellipsoid ends are trimmed off
length_layer=10000;   %the number of finite element layers for each case
%end input data preparation



%data storage matrice and arrays
L_stored=zeros(1,health_layer);
dimension=zeros(3,health_layer);
C_series=zeros(1,health_layer);
C_series_complement=zeros(1,health_layer);
C_parallel=zeros(1,health_layer);
R_parallel=zeros(1,health_layer);
C_total=zeros(1,health_layer);
C_total2=zeros(1,health_layer);
R_total=zeros(1,health_layer);
corrosion=zeros(1,health_layer);
r_collection=zeros(1,health_layer);
%end data storage matrice and arrays




%loop data
t=healthy_percent;
counter=1;
%end loop data



%start capacitance calculation
while t <= upper

L=(radius_cable-radius_conductor)*(1-t)/2;
                      %dimensional term for ellipsoid shape calculation
a0=L;                 %vertical axis radius of the ellipsoid shape
b0=0.2*L;             %horizontal axis radius of the ellipsoid shape
c0=0.2*L;             %depth axis radius the ellipsoid shape
z0=radius_cable-2*L; %healthy depth
radius_healthy=z0;
L_stored(1,counter)=L;
dimension(1,counter)=a0;
dimension(2,counter)=b0;
dimension(3,counter)=c0;

C_series(1,counter)=(2*pi*e2)/log(radius_healthy/radius_conductor);
C_series_complement(1,counter)=(2*pi*e2)/log(radius_cable/radius_healthy);
%series capacitance calculation
length_step=2*L/length_layer;
r=radius_healthy;
accumulate=0;
counter_2=1;
    while r <= radius_cable
```

```
        A=(b0/a0)^2-1;
        B=-(2*z0+2*L*(b0^2)/(a0^2));
        C=r^2-z0^2;
        y3_1=(-B-sqrt(B^2-4*A*C))/(2*A);
        y3_2=(-B+sqrt(B^2-4*A*C))/(2*A);
        if y3_1>y3_2
            y3=y3_1;
        else
            y3=y3_2;
        end
        x0=abs(sqrt(r^2-(y3+z0)^2));
        alpha=atan(x0/(y3+z0));
       if alpha < 10e-8;
            etotal=0;
       else
            etotal=2*r*(e1-e2)*sin(alpha)/(2*L)+2*alpha*(e2-z0*(e1-e2)/(2*L));
       end
       accumulate=accumulate+log((r+length_step)/r)/(e2*(1-
2*alpha/(2*pi))+etotal/(2*pi));
 %       y3_collection(counter,counter_2)=y3;
 %       x0_collection(counter,counter_2)=x0;
 %       alpha_collection(counter,counter_2)=alpha;
       counter_2=counter_2+1;
       r=r+length_step;
    end
r_collection(1,counter)=r;
%start paralll resistance calculation
L=(radius_cable-radius_conductor)*(1-t)*(1+2*trim)/2;
                    %dimensional term for ellipsoid shape calculation
a0=L;               %vertical axis radius of the ellipsoid shape
b0=0.2*L;           %horizontal axis radius of the ellipsoid shape
c0=0.2*L;           %depth axis of radius the ellipsoid shape
z=a0/1.2;            %half of the vertical height after the trim
L_stored(1,counter)=L;
dimension(1,counter)=z;
dimension(2,counter)=b0;
dimension(3,counter)=c0;
length_step=2*z/length_layer;
r=0;
accumulate_2=0;
    while r <= 2*z
        y=z-r;
        x2=(1-(y/a0)^2)*(b0^2);
        rho=(rho_base-rho_tip)*r/2/z+rho_tip;
        accumulate_2=accumulate_2+length_step/(rho*pi*x2);
        r=r+length_step;
    end
corrosion(1,counter)=(1-t)*100;
R_parallel(1,counter)=accumulate_2;
%end paralll resistance calculation



corrosion(1,counter)=(1-t)*100;
C_parallel(1,counter)=2*pi/accumulate;
E=1/(w*C_series(1,counter))+w*(R_parallel(1,counter)^2)*C_parallel(1,counter)/(
1+w*(R_parallel(1,counter)^2)*(C_parallel(1,counter)^2));
D=R_parallel(1,counter)/(1+w*(R_parallel(1,counter)^2)*(C_parallel(1,counter)^2
));
C_total(1,counter)=1/(w*E);
C_total2(1,counter)=1/(1/C_parallel(1,counter)+1/C_series(1,counter));
R_total(1,counter)=D;
```

```
counter=counter+1;
t=t+health_step;
end
%end capacitance calculation




%start plot output
plot(corrosion,C_series,'r')
xlabel('Water Tree Percent Growth Across Insulation')
ylabel('Capacitance (F/m)')
legend('C_h_e_a_l_t_h_y')
figure
hold on
plot(corrosion,C_series_complement,'r')
plot(corrosion,C_parallel,'--b')
xlabel('Water Tree Percent Growth Across Insulation')
ylabel('Capacitance (F/m)')
title(['Relative Permittivity at the Base of the Tree is
',num2str(e1_relative)])
legend('C_c_o_m_p_r_o_m_i_s_e_d complement','C_c_o_m_p_r_o_m_i_s_e_d')
hold off
figure
hold on
plot(corrosion,C_total,'b')
legend('C total with Resistor')
xlabel('Water Tree Percent Growth Across Insulation')
ylabel('Capacitance (F/m)')
figure
hold on
plot(corrosion,C_total2,'b')
legend('C_t_o_t_a_l')
xlabel('Water Tree Percent Growth Across Insulation')
ylabel('Capacitance (F/m)')
figure
plot(corrosion,R_total,'m')
legend('R total')
xlabel('Water Tree Percent Growth Across Insulation')
ylabel('Resistance (ohm/m)')
%end plot output
```

APPENDIX B Cable Parameters for Benchmark Frequency Identification

The figures below shows basic PSCAD configuration used in benchmark frequency identification.

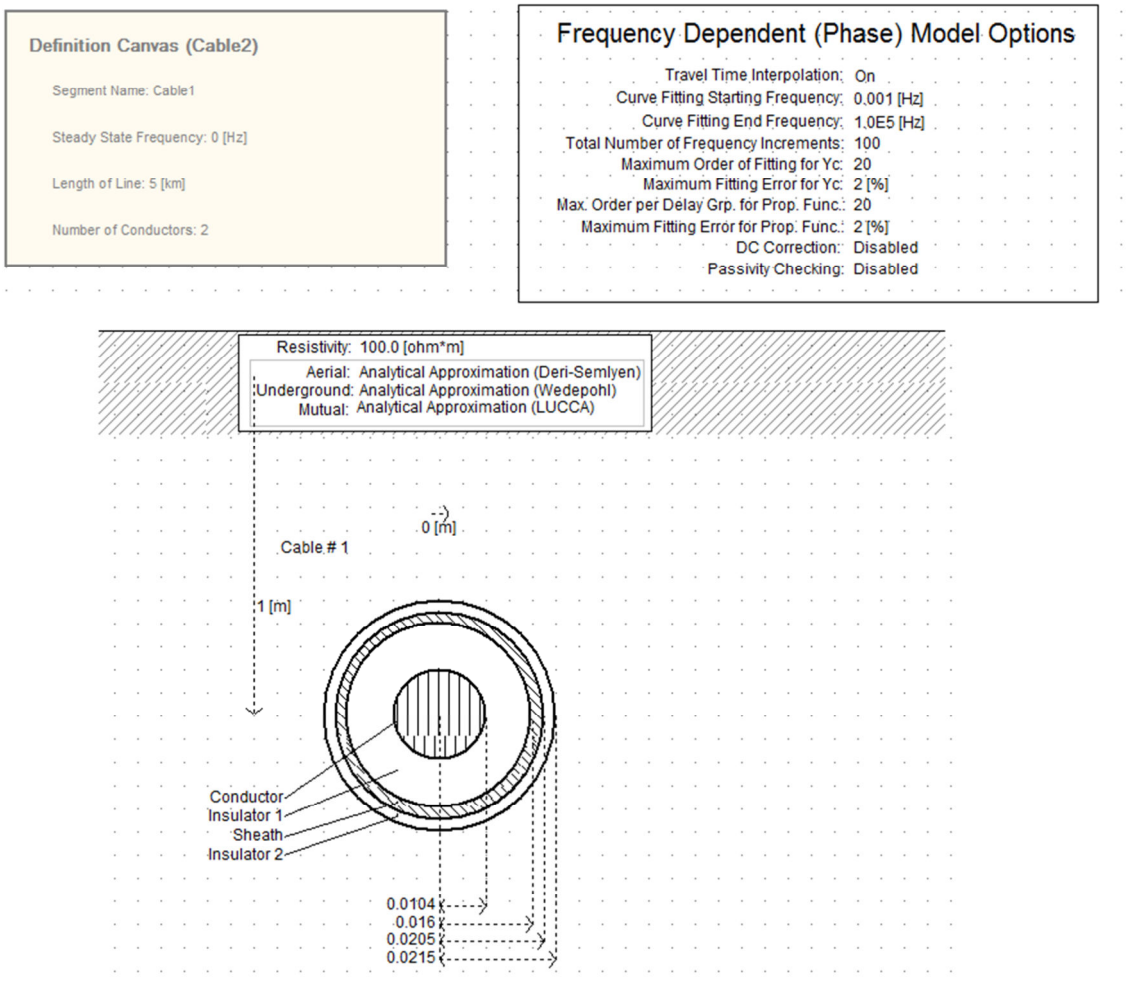

Figure 98: Cable Dimensions

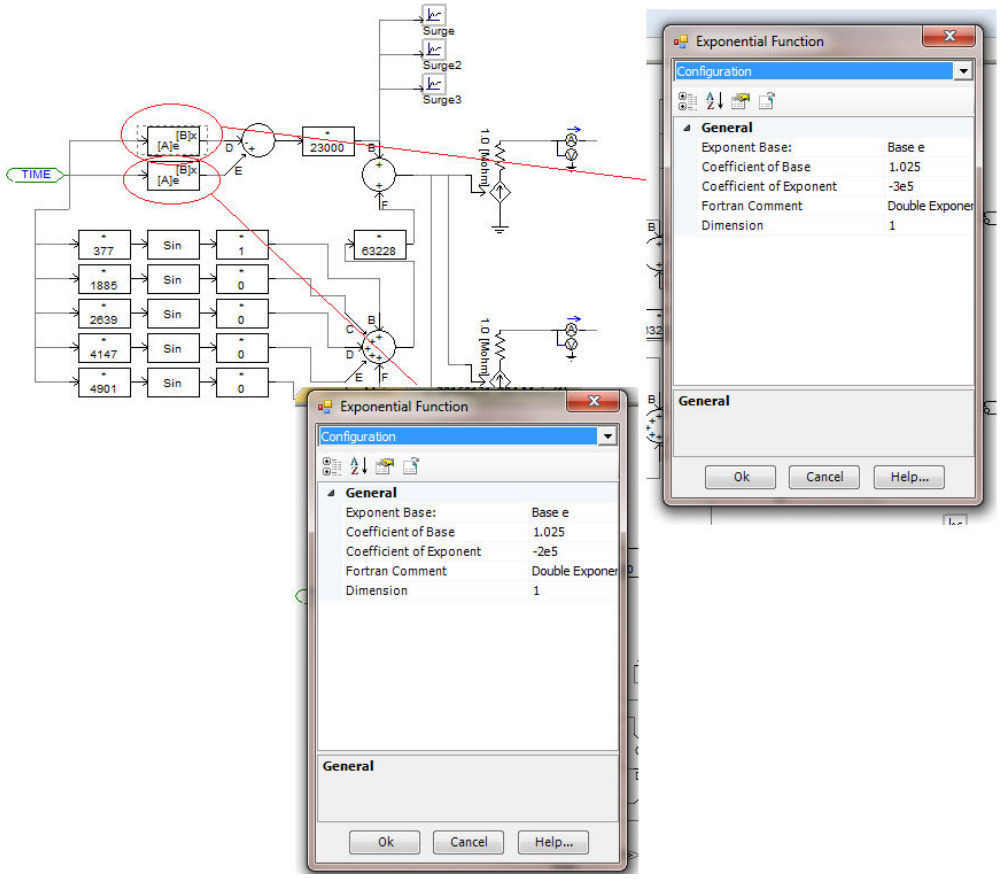

Figure 99: Lightning Pulse Generation

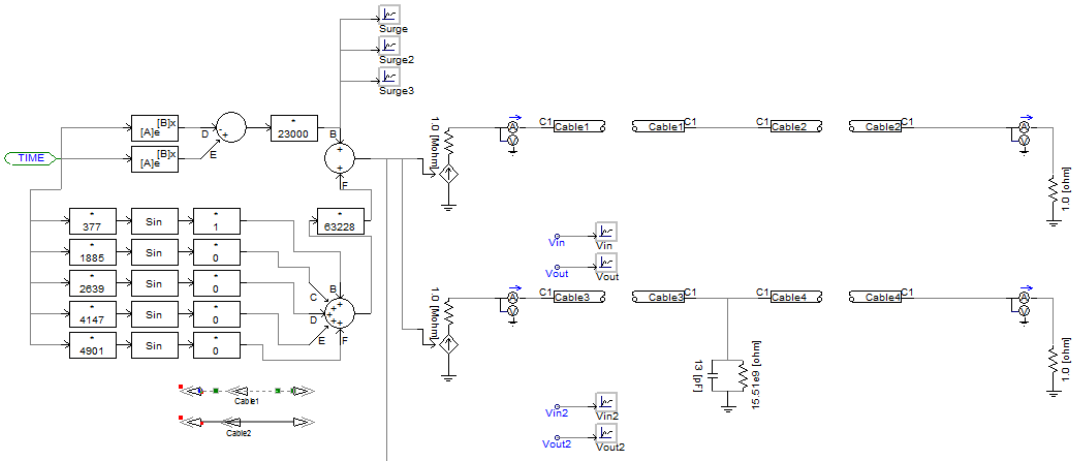

Figure 100: Overall System with Harmonics Injected

APPENDIX C Deviation Comparison Chart Code for Two Point Extrapolation Scheme with Gaussian Noise

The overall structure of the Deviation-Comparison Chart Output for the Early Warning System is shown below in Figure 101:

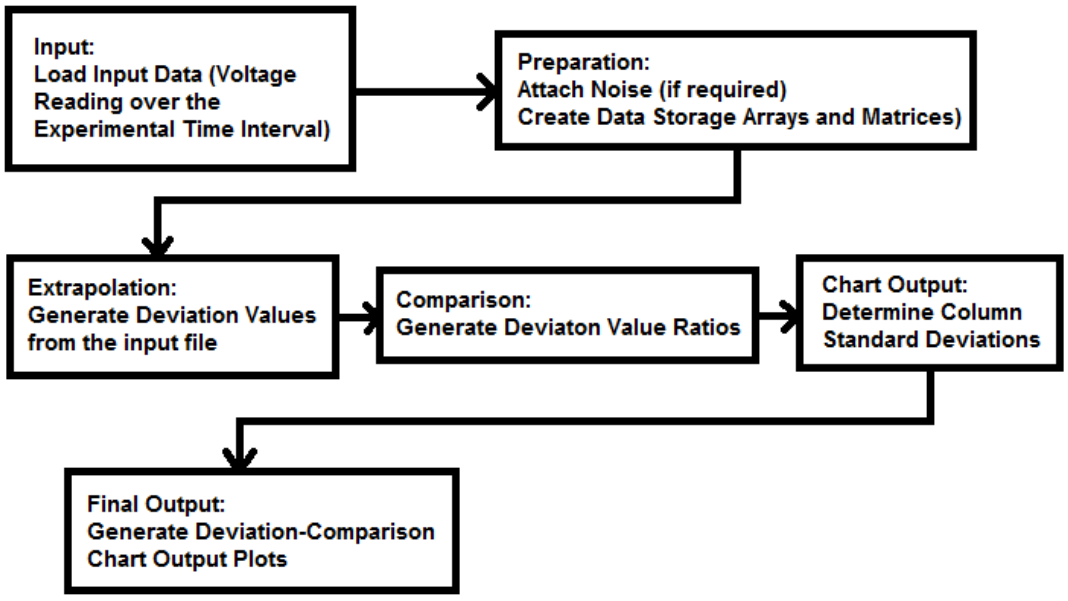

Figure 101: Deviation-Comparison Chart Output Algorithm Flow Chart

The codes below are sample deviation-comparison chart generation for Chapter 4.

```
clear all

%the program require minimum FIVE sets of data to yield any meaningful
%analysis, the plot function require at least five sets of data to run

%this is a test file made to work with offline impulse reaction test output
with four
%columns of output data.
%The first column is the time
%The second column represents healthy system with no water tree.
%The third column represents system afflicted with water tree using parallel
only fault capacitance.
%The fourth column represents system afflicted with water tree using series-
parallel fault impedance.


load simfile.txt                    %importing voltage profile into program
voltage_profile_0 = simfile;          %voltage profile array without noise
%voltage_profile_0 = voltage_profile_1*100;  %amplifying original waveform
```

```
%case study
voltage_profile=awgn(voltage_profile_0,200,'measured');          %voltage
profile array with noise,
                                                                 %scalar value
refers to the SNR, higher SNR result in lower noise
t_interval=voltage_profile_0(2,1)-voltage_profile_0(1,1);            %time step
s=size(voltage_profile);        %dimension of the voltage profile array
length=s(1,1);                  %length of the array
raw_analysis_matrix1=zeros(length, length+2); %creating empty analysis matrix
for deviation ratio
raw_analysis_matrix2=zeros(length, length+2);
raw_analysis_matrix3=zeros(length, length+2);
std_dev_deviation1=zeros(1,length+2); %creating empty array for the column
standard deviation observation
std_dev_deviation2=zeros(1,length+2);
std_dev_deviation3=zeros(1,length+2);
alpha=1;                        %weighting modification parameter alpha,
default=1;



%Calculation: Generate Deviation value and Deviation Ratio
index_1=1;      %row index
while index_1 <=length

        raw_analysis_matrix1(index_1,1)=voltage_profile_0(index_1,1); %time
axis
        raw_analysis_matrix2(index_1,1)=voltage_profile_0(index_1,1);
        raw_analysis_matrix3(index_1,1)=voltage_profile_0(index_1,1);
                                                    %on the first column
        if index_1 >= 3                               %populating raw deviation
value
            raw_analysis_matrix1(index_1,2)=voltage_profile(index_1,2)-
(1+alpha)*voltage_profile(index_1-1,2)+alpha*voltage_profile(index_1-2,2);
            raw_analysis_matrix2(index_1,2)=voltage_profile(index_1,3)-
(1+alpha)*voltage_profile(index_1-1,3)+alpha*voltage_profile(index_1-2,3);
            raw_analysis_matrix3(index_1,2)=voltage_profile(index_1,4)-
(1+alpha)*voltage_profile(index_1-1,4)+alpha*voltage_profile(index_1-2,4);
        else
            raw_analysis_matrix1(index_1,2)=0;
            raw_analysis_matrix2(index_1,2)=0;
            raw_analysis_matrix3(index_1,2)=0;
        end
        index_2_1=1;          %column index
        index_2_2=1;          %column index
        index_2_3=1;          %column index
        while index_2_1 <= length
            if index_1-index_2_1 <= 0     %preventing program from accessing
times that are not available
                raw_analysis_matrix1(index_1,index_2_1+2)= 0;
                index_2_1=index_2_1+1;
            elseif raw_analysis_matrix1(index_1-index_2_1,2)== 0;   %preventing
program from accessing raw deviations that are not available
                raw_analysis_matrix1(index_1,index_2_1+2)=0;
                index_2_1=index_2_1+1;
            else

raw_analysis_matrix1(index_1,index_2_1+2)=raw_analysis_matrix1(index_1,2)/raw_a
nalysis_matrix1(index_1-index_2_1,2);  %calculating deviation ratio
                index_2_1=index_2_1+1;
            end
        end
```

```
        while index_2_2 <= length
            if index_1-index_2_2 <= 0     %preventing program from accessing
times that are not available
                raw_analysis_matrix2(index_1,index_2_2+2)= 0;
                index_2_2=index_2_2+1;
            elseif raw_analysis_matrix2(index_1-index_2_2,2)== 0;   %preventing
program from accessing raw deviations that are not available
                raw_analysis_matrix2(index_1,index_2_2+2)=0;
                index_2_2=index_2_2+1;
            else

raw_analysis_matrix2(index_1,index_2_2+2)=raw_analysis_matrix2(index_1,2)/raw_a
nalysis_matrix2(index_1-index_2_2,2);  %calculating deviation ratio
                index_2_2=index_2_2+1;
            end
        end
        while index_2_3 <= length
            if index_1-index_2_3 <= 0     %preventing program from accessing
times that are not available
                raw_analysis_matrix3(index_1,index_2_3+2)= 0;
                index_2_3=index_2_3+1;
            elseif raw_analysis_matrix3(index_1-index_2_3,2)== 0;   %preventing
program from accessing raw deviations that are not available
                raw_analysis_matrix3(index_1,index_2_3+2)=0;
                index_2_3=index_2_3+1;
            else

raw_analysis_matrix3(index_1,index_2_3+2)=raw_analysis_matrix3(index_1,2)/raw_a
nalysis_matrix3(index_1-index_2_3,2);  %calculating deviation ratio
                index_2_3=index_2_3+1;
            end
        end

        index_1=index_1+1;
end



%Chart Output: Generate the Column Deviation Value
index_3_1=2;    %column index for populating column standard deviation
observation
index_3_2=2;
index_3_3=2;

while index_3_1<=length+2
    index_4_1=1;    %index for eliminating empty blocks for each column
    temp=zeros(length-index_3_1,1);
    while index_4_1+index_3_1<=length
        temp(index_4_1,1)= raw_analysis_matrix1(index_3_1+index_4_1,index_3_1);
        index_4_1=index_4_1+1;
    end
    std_dev_deviation1(1,index_3_1)=std(temp);
    index_3_1=index_3_1+1;
end
while index_3_2<=length+2
    index_4_2=1;    %index for eliminating empty blocks for each column
    temp=zeros(length-index_3_2,1);
    while index_4_2+index_3_2<=length
        temp(index_4_2,1)= raw_analysis_matrix2(index_3_2+index_4_2,index_3_2);
        index_4_2=index_4_2+1;
    end
    std_dev_deviation2(1,index_3_2)=std(temp);
```

```
    index_3_2=index_3_2+1;
end
while index_3_3<=length+2
    index_4_3=1;    %index for eliminating empty blocks for each column
    temp=zeros(length-index_3_3,1);
    while index_4_3+index_3_3<=length
        temp(index_4_3,1)= raw_analysis_matrix3(index_3_3+index_4_3,index_3_3);
        index_4_3=index_4_3+1;
    end
    std_dev_deviation3(1,index_3_3)=std(temp);
    index_3_3=index_3_3+1;
end

%data matrix display (Warning, do not display for large data sets)
%raw_analysis_matrix1
%std_dev_deviation1

%raw_analysis_matrix2
%std_dev_deviation2

%raw_analysis_matrix3
%std_dev_deviation3


index_5_1=1;   %index used to generate plotting array
time_m=1; %multiplier used to populate x1
x1=zeros(length+2-4-2,1);
y1=zeros(length+2-4-2,1);
y1log=zeros(length+2-4-2,1);
while index_5_1<=length+2-4-2;
    x1(index_5_1,1)=time_m*t_interval;
    y1(index_5_1,1)=std_dev_deviation1(1,index_5_1+2);
    y1log(index_5_1,1)=log(std_dev_deviation1(1,index_5_1+2));
    index_5_1=index_5_1+1;
    time_m=time_m+1;
end



%Final Output: Generating Deviation-Comparison Chart Output
%x1
%y1
figure % opens new figure window
plot(x1,y1)
title('Healthy System')
xlabel('Time Step Interval') % x-axis label
ylabel('Standard Deviation of the Associated Column') % y-axis label

figure % opens new figure window
plot(x1,y1log)
title('Healthy System')
xlabel('Time Step Interval') % x-axis label
ylabel('Standard Deviation of the Associated Column (Log Scale)') % y-axis
label


index_5_2=1;   %index used to generate plotting array
time_m=1; %multiplier used to populate x1
x2=zeros(length+2-4-2,1);
y2=zeros(length+2-4-2,1);
y2log=zeros(length+2-4-2,1);
while index_5_2<=length+2-4-2;
```

```
    x2(index_5_2,1)=time_m*t_interval;      %multiple of time step
    y2(index_5_2,1)=std_dev_deviation2(1,index_5_2+2);
    y2log(index_5_2,1)=log(std_dev_deviation2(1,index_5_2+2));
    index_5_2=index_5_2+1;
    time_m=time_m+1;
end
%x2
%y2
figure % opens new figure window
plot(x2,y2)
title('Water-Tree with Parallel Model')
xlabel('Time Step Interval') % x-axis label
ylabel('Standard Deviation of the Associated Column') % y-axis label

figure % opens new figure window
plot(x2,y2log)
title('Water-Tree with Parallel Model')
xlabel('Time Step Interval') % x-axis label
ylabel('Standard Deviation of the Associated Column (Log Scale)') % y-axis
label



index_5_3=1;   %index used to generate plotting array
time_m=1; %multiplier used to populate x1
x3=zeros(length+2-4-2,1);
y3=zeros(length+2-4-2,1);
y3log=zeros(length+2-4-2,1);
while index_5_3<=length+2-4-2;
    x3(index_5_3,1)=time_m*t_interval;
    y3(index_5_3,1)=std_dev_deviation3(1,index_5_3+2);
    y3log(index_5_3,1)=log(std_dev_deviation3(1,index_5_3+2));
    index_5_3=index_5_3+1;
    time_m=time_m+1;
end
%x3
%y3
figure % opens new figure window
plot(x3,y3)
title('Water-Tree with Series-Parallel Model')
xlabel('Time Step Interval') % x-axis label
ylabel('Standard Deviation of the Associated Column') % y-axis label

figure % opens new figure window
plot(x3,y3log)
title('Water-Tree with Series-Parallel Model')
xlabel('Time Step Interval') % x-axis label
ylabel('Standard Deviation of the Associated Column (Log Scale)') % y-axis
label
```

REFERENCE

[1] C. Barnes, Power Cables, Their Design and Installation, vol. XIV. London,UK: Chapman and Hall, 1953.

[2] H. Orton, "History of underground power cables," in IEEE Electrical Insulation Magazine, vol. 29, no. 4, pp. 52-57, July-August 2013.

[3] K. Suzuki, S. Saito and S. Yoshida, "Power Cable Insulation," in IEEE Transactions on Electrical Insulation, vol. EI-21, no. 6, pp. 945-952, Dec. 1986.

[4] F. Precopio, "The invention of chemically crosslinked polyethylene," IEEE Electr. Insul. Mag., vol. 15, no. 1, pp. 23–25, 1999.

[5] T. Uematsu, "Historical review of water-trees in XLPE cables," Furukawa Rev., no. 10, pp. 31–48, 1992.

[6] J. L. Johnson, "Our Infrastructure is Aging and Maintenance Costs are Rising -- Extending the Life Expectancy of Transmission Lines Through the Use of Data, Inspection and Planning," *ESMO 2006 - 2006 IEEE 11th International Conference on Transmission & Distribution Construction, Operation and Live-Line Maintenance*, Albuquerque, NM, 2006, pp. .

[7] Zuyi Li and Jiachun Guo, "Wisdom about age [aging electricity infrastructure]," in IEEE Power and Energy Magazine, vol. 4, no. 3, pp. 44-51, May-June 2006.

[8] R. E. Brown and H. L. Willis, "The economics of aging infrastructure," in IEEE Power and Energy Magazine, vol. 4, no. 3, pp. 36-43, May-June 2006.

[9] N. Singh, "Condition assessment of cables and transformers in an aging infrastructure (and aging talent base)," 2011 Electrical Insulation Conference (EIC)., Annapolis, MD, 2011, pp. 1-9.

[10] J. D. Bouford, J. M. Teixeira and C. A. Warren, "The Natural Replacement Process Versus the Aging Infrastructure of Distribution Poles," in *IEEE Transactions on Power Delivery*, vol. 23, no. 3, pp. 1522-1526, July 2008.

[11] S. Chakravorti, "Key Issues Pertaining to Aging, Maintenance and Reliability of Electricity Infrastructure," *2006 IEEE International Power and Energy Conference*, Putra Jaya, 2006, pp. 1-6.

[12] H. Ge and S. Asgarpoor, "Reliability and Maintainability Improvement of Substations With Aging Infrastructure," in *IEEE Transactions on Power Delivery*, vol. 27, no. 4, pp. 1868-1876, Oct. 2012.

[13] A.C. Ashcraft, "Treeing Update Part III: Water Trees". Kabelitems 152, Union

Carbide Corporations. Based on “Water Treeing in Polymer Dielectrics”, Presented at World Electrotechnical Congress in Moscow, June, 1977

[14] A. J. Thomas and T. K. Saha, "A new dielectric response model for water-tree degraded XLPE insulation - part a: model development with small sample verification," in IEEE Transactions on Dielectrics and Electrical Insulation, vol. 15, no. 4, pp. 1131-1143, August 2008.

[15] J. P. Crine, S. Pelissou and J. L. Parpal, "Influence of insulation morphology, impurities and oxidation on some electric properties of cables," in IEEE Transactions on Electrical Insulation, vol. 26, no. 1, pp. 140-145, Feb 1991.

[16] S. Pelissou and H. J. Wintle, "Water content of XLPE cable insulation," Conference Record of the 1992 IEEE International Symposium on Electrical Insulation, Baltimore, MD, 1992, pp. 165-168.

[17] H. M. Li, R. A. Fouracre and B. H. Crichton, "Transient current measurement for the detection of water-tree growth in polymeric power cables," in IEEE Transactions on Dielectrics and Electrical Insulation, vol. 2, no. 5, pp. 866-874, Oct 1995.

[18] A. T. Bulinski, S. S. Bamji, R. J. Densley and C. Au, "Effect of temperature on the growth of vented water-trees in laboratory molded polyethylene specimens," Conference on Electrical Insulation & Dielectric Phenomena — Annual Report 1987, Gaithersburg, MD, USA, 1987, pp. 440-447.

[19] T. Maeda, D. Kaneko, Y. Ohki, T. Konishi, Y. Nakamichi and M. Okashita, "Effect of the applied voltage frequency on the water-tree shape in polyethylene," Proceedings of the 2004 IEEE International Conference on Solid Dielectrics, 2004. ICSD 2004., 2004, pp. 276-279 Vol.1.

[20] B. V. Wong, Yuan Tian and T. Neier, "Practical experience using VLF Tan Delta and Partial-discharge measurement in medium voltage cable," 2016 International Conference on Condition Monitoring and Diagnosis (CMD), Xi'an, China, 2016, pp. 106-109.

[21] C. K. Chakrabarty, A. R. Avinash and A. G. A. Basri, "Development of high frequency Tan Delta measurement method for 132kV transmission underground cables," 2014 IEEE 2nd International Symposium on Telecommunication Technologies (ISTT), Langkawi, 2014, pp. 436-441.

[22] A. B. Ghani, C. K. Chakrabarty, W. J. K. Raymond and G. C. Hock, "Tan delta measurement of paper insulated laminates using capacitance method from 300kHz to 50MHz," 2013 IEEE International Conference on Solid Dielectrics (ICSD), Bologna, 2013, pp. 996-1000.

[23]A. Ponniran and M. S. Kamarudin, "Study on the performance of underground XLPE cables in service based on tan delta and capacitance measurements," 2008 IEEE 2nd International Power and Energy Conference, Johor Bahru, 2008, pp. 39-43.

[24] B. N. Rao and K. Mallikarjunappa, "Assessment of water logged cables by very low frequency tan delta testing technique," 2012 IEEE 10th International Conference on the Properties and Applications of Dielectric Materials, Bangalore, 2012, pp. 1-4.

[25] T. Neier, A. Gerstner and M. Jenny, "Identification of jointsaffected by water ingress in complex hybrid MV cable networks: 2 Field examples of combined VLF withstand testing, with Tan Delta (TD) and Partial-discharge(PD) diagnostics," 2012 IEEE International Conference on Condition Monitoring and Diagnosis, Bali, 2012, pp. 1018-1022.

[26] D. Fynes-Clinton and C. Nyamupangedengu, "Partial-discharge characterization of cross-linked polyethylene medium voltage power cable termination defects at very low frequency (0.1 Hz) and power frequency test voltages," in IEEE Electrical Insulation Magazine, vol. 32, no. 4, pp. 15-23, July-August 2016.

[27] A. R. Mor, P. H. F. Morshuis, P. Llovera, V. Fuster and A. Quijano, "Localization techniques of partial-discharges at cable ends in off-line single-sided partial-discharge cable measurements," in IEEE Transactions on Dielectrics and Electrical Insulation, vol. 23, no. 1, pp. 428-434, February 2016.

[28] A. R. Mor, P. H. F. Morshuis and J. J. Smit, "Charge estimation methods in partial-discharge cable tests," 2015 IEEE Electrical Insulation Conference (EIC), Seattle, WA, 2015, pp. 463-466.

[29] G. C. Montanari, "Partial-discharge detection in medium voltage and high voltage cables: maximum distance for detection, length of cable, and some answers," in IEEE Electrical Insulation Magazine, vol. 32, no. 5, pp. 41-46, September-October 2016.

[30] H. A. Illias, M. A. Tunio, A. H. A. Bakar, H. Mokhlis and G. Chen, "Partial-discharge phenomena within an artificial void in cable insulation geometry: experimental validation and simulation," in IEEE Transactions on Dielectrics and Electrical Insulation, vol. 23, no. 1, pp. 451-459, February 2016.

[31] P. J. Phillips, "Identification & Location of Microscopic Inorganic Impurities in Cable Insulation," in IEEE Transactions on Electrical Insulation, vol. EI-13, no. 6, pp. 451-453, Dec. 1978.

[32] S. Pelissou and S. St. -Antoine, "Influence of cable processing on the insulation impurity content," Conference Record of the 1998 IEEE International Symposium on Electrical Insulation (Cat. No.98CH36239), Arlington, VA, 1998, pp. 97-100 vol.1.

[33] A. Garton, J. H. Groeger and J. L. Henry, "Ionic impurities in crosslinked polyethylene cable insulation," in IEEE Transactions on Electrical Insulation, vol. 25, no. 2, pp. 427-434, Apr 1990.

[34] J. L. Parpal, J. P. Crine, A. Houdayer and P. Hinrichsen, "Study of semiconductor impurity diffusion in XLPE cable insulation under electrical aging," 1993 Third International Conference on Power Cables and Accessories 10kV - 500kV, London, 1993, pp. 153-156.

[35] S. Tantipattarakul, A. Vaughan and T. Andritsch, "On the effects of molecular composition, morphology and ageing on the electrical properties of polyethylene," 2016 IEEE Conference on Electrical Insulation and Dielectric Phenomena (CEIDP), Toronto, ON, 2016, pp. 889-892.

[36] J. P. Crine, "Influence of insulation morphology, impurities and oxidation on cables electric properties," Proceedings., Second International Conference on Properties and Applications of Dielectric Materials, Beijing, 1988, pp. 451-454 vol.2.

[37] P. Rohl and B. Andreß, "Investigation on the processes of oxidation and oxidation inhibition of polyethylene," Conference on Electrical Insulation & Dielectric Phenomena - Annual Report 1985, Amherst, NY, USA, 1985, pp. 290-295.doi: 10.1109/CEIDP.1985.7728283

[38] T. Bao and J. Tanaka, "The diffusion of ions in polyethylene," [1991] Proceedings of the 3rd International Conference on Properties and Applications of Dielectric Materials, Tokyo, 1991, pp. 236-239 vol.1.

[39] A. Garton, S. S. Bamji, A. Bulinski and J. Densley, "Oxidation and water-treeing in XLPE cable insulation," Conference on Electrical Insulation & Dielectric Phenomena - Annual Report 1986, Claymont, DE, 1986, pp. 404-410.

[40] A. Garton, S. Bamji, A. Bulinski and J. Densley, "Oxidation and Water-tree Formation in Service-Aged XLPE Cable Insulation," in IEEE Transactions on Electrical Insulation, vol. EI-22, no. 4, pp. 405-412, Aug. 1987.

[41] W. G. Linzey, N. H. Turner, A. M. Bruning and B. S. Bernstein, "Correlation of the thermal history and level of oxidation with field failure in a primary distribution cable study," Conference Record of the 1998 IEEE International Symposium on Electrical Insulation (Cat. No.98CH36239), Arlington, VA, USA, 1998, pp. 105-108 vol.1.

[42] A. T. Bulinski, S. S. Bamji, R. J. Densley, J. P. Crine, B. Noirhomme and B. S. Bernstein, "Influence of oxidation on water-tree initiation and growth in XLPE cables," Proceedings of the 3rd International Conference on Conduction and Breakdown in Solid Dielectrics, Trondheim, 1989, pp. 422-426.

[43] S. Bamji, A. Bulinski, J. Densley, A. Garton and N. Shimizu, "Properties of water treed and non-treed XLPE cable insulation," Conference on Electrical Insulation & Dielectric Phenomena - Annual Report 1984, Claymont, DE, USA, 1984, pp. 141-147.

[44] S. Haridoss, J. P. Crine, A. Bulinski, J. Densley and S. Bamji, "Oxidation in water-trees grown in field-aged cables," 1988. Annual Report., Conference on Electrical Insulation and Dielectric Phenomena, Ottawa, Ont., 1988, pp. 86-93.

[45] Shuaishuai Liu, L. S. Fifield and N. Bowler, "Towards aging mechanisms of cross-linked polyethylene (XLPE) cable insulation materials in nuclear power plants," 2016 IEEE Conference on Electrical Insulation and Dielectric Phenomena (CEIDP), Toronto, ON, 2016, pp. 935-938.

[46] E. F. Stennis and F. H. Krueger, “Water-treeing in polyethylene cables”, IEEE Trans. Electr. Insul., Vol. 25, pp. 989-1028, 1990.

[47] S. Arcone, S. Grant and G. Boitnott, "Broadband TDR permittivity spectra of lossy soils at medium to high water contents: Separation of electrode polarization from Maxwell-Wagner relaxation by modeling," Proceedings of the 15th International Conference on Ground Penetrating Radar, Brussels, 2014, pp. 186-191.

[48] R. Patsch, M. Ortolf and J. Tanaka, "Hydration of ions-how does it influence water-treeing," Proceedings of 5th International Conference on Properties and Applications of Dielectric Materials, Seoul, 1997, pp. 410-413 vol.1.

[49] Steennis, E.F.; Kreuger, F. H., "Water-treeing in polyethylene cables," Electrical Insulation, IEEE Transactions on, vol.25, no.5, pp.989,1028, Oct.

[50] H. Suzuki, Y. Ohki, Y. Nakamichi and K. Ajiki, "Water-tree characteristics in low-density polyethylene under power-frequency voltages with high-frequency components," Proceedings of Conference on Electrical Insulation and Dielectric Phenomena - CEIDP '96, Millbrae, CA, 1996, pp. 742-745 vol.2.

[51] Y. Ohki, H. Ishikawa, G. Morita, T. Konishi, Y. Nakamichi and M. Tanimoto, "Role of the voltage zero-crossing in the growth of water-trees - Effect of superposition method of a high-frequency voltage and a low-frequency voltage -," 2008 International Conference on Condition Monitoring and Diagnosis, Beijing, 2008, pp. 328-331.

[52] S. Mukai, H. Suzuki, Y. Ohki, Y. Nakamichi, K. Ajiki and Y. Li, "Role of voltage zero-crossing in propagation of water trees," IEEE 1997 Annual Report Conference on Electrical Insulation and Dielectric Phenomena, Minneapolis, MN, 1997, pp. 300-303 vol.1.

[53] T. Maeda, D. Kaneko, Y. Ohki, T. Konishi, Y. Nakamichi and M. Okashita, "Effect of the applied voltage frequency on the water-tree shape in polyethylene," Proceedings of

the 2004 IEEE International Conference on Solid Dielectrics, 2004. ICSD 2004., 2004, pp. 276-279 Vol.1.

[54] D. Kaneko et al., "Role of number of consecutive voltage zero-crossings in propagation of water-trees in polyethylene," in IEEE Transactions on Dielectrics and Electrical Insulation, vol. 11, no. 4, pp. 708-714, Aug. 2004.

[55] D. Kaneko et al., "Role of the number of consecutive voltage zero-crossings on the water-tree growth in polyethylene," Proceedings of the 7th International Conference on Properties and Applications of Dielectric Materials (Cat. No.03CH37417), 2003, pp. 932-935 vol.3.

[56] Maeda, T.; Kaneko, D.; Ohki, Y.; Konishi, T.; Nakamichi, Y.; Okashita, M., "Effect of the applied voltage frequency on the water-tree shape in polyethylene," Solid Dielectrics, 2004. ICSD 2004. Proceedings of the 2004 IEEE International Conference on, vol.1, no., pp.276,279 Vol.1, 5-9 July 2004,

[57] T. Uematsu, Z. Iwata, S. Irie and O. Fujii, "Bow-tie-tree in EPR cables are accelerated water-treeing test," in *IEEE Transactions on Power Delivery*, vol. 7, no. 4, pp. 1667-1676, Oct 1992.

[58] M. Morita, M. Hanai, H. Shimanuki and F. Aida, "Effect of Bow-Tie tree on PE and XLPE insulation," Conference on Electrical Insulation & Dielectric Phenomena - Annual Report 1975, Gaithersburg, MD, USA, 1975, pp. 335-343.doi: 10.1109/CEIDP.1975.7736668

[59] B. M. Aucoin and B. D. Russell, "Distribution High Impedance Fault Detection Utilizing High Frequency Current Components," in IEEE Power Engineering Review, vol. PER-2, no. 6, pp. 46-47, June 1982.

[60] M. Aucoin and B. D. Russell, "Detection of Distribution High Impedance Faults Using Burst Noise Signals Near 60 Hz," in IEEE Power Engineering Review, vol. PER-7, no. 4, pp. 40-41, April 1987.

[61] M. Aucoin, "Status of High Impedance Fault Detection," in IEEE Power Engineering Review, vol. PER-5, no. 3, pp. 39-40, March 1985.

[62] B. M. Aucoin and B. D. Russell, "Distribution High Impedance Fault Detection Utilizing High Frequency Current Components," in IEEE Power Engineering Review, vol. PER-2, no. 6, pp. 46-47, June 1982.

[63] M. Aucoin and B. D. Russell, "Detection of Distribution High Impedance Faults Using Burst Noise Signals near 60 HZ," in IEEE Transactions on Power Delivery, vol. 2, no. 2, pp. 342-348, April 1987.

[64] M. Aucoin, "Status of High Impedance Fault Detection," in IEEE Transactions on Power Apparatus and Systems, vol. PAS-104, no. 3, pp. 637-644, March 1985.

[65] G. Mugala, R. Eriksson and P. Pettersson, "High Frequency Characteristics of Water-Tree Degraded XLPE Insulation in Power Cables," in IEEE Transactions on Dielectrics and Electrical Insulation, vol. 14, no. 5, pp. 1271-1277, October 2007.

[66] P. Tharning, Water-tree dielectric spectroscopy, Licentiate thesis, RoyalInstitute of Technology (KTH), Stockholm, Sweden, 1997.

[67] B. Holmgren, Dielectric response, breakdown strength and water-tree content of medium voltage XLPE cables, Licentiate thesis, RoyalInstitute of Technology (KTH), Stockholm, Sweden, 1997.

[68] P. Werelius, Development and application of high voltage dielectricspectroscopy for diagnosis of medium voltage XLPE cables, Ph.D. thesis, Royal Institute of Technology (KTH), Stockholm, Sweden, 2001.

[69] R. Papazyan, Techniques for localization of insulation degradationalong medium-voltage power cables, PhD thesis, Royal Institute of Technology (KTH), Stockholm, Sweden, 2005.

[70] G. Mugala, High frequency characteristics of medium voltage XLPE power cables, PhD thesis, Royal Institute of Technology (KTH), Stockholm, Sweden, 2005.

[71] R. Papazyan and R. Eriksson, "High frequency characterisation of water-treed XLPE cables," Proceedings of the 7th International Conference on Properties and Applications of Dielectric Materials (Cat. No.03CH37417), 2003, pp. 187-190 vol.1.

[72] R. Papazyan, R. Eriksson, "Calibration for Time Domain Propagation Constant Measurements on Power Cables," In Conf. on *Precision Electromagnetic Measurements CPEM02*, pp.232-233, 2002

[73] R. Papazyan and R. Eriksson, "Calibration for time domain propagation constant measurements on power cables," in IEEE Transactions on Instrumentation and Measurement, vol. 52, no. 2, pp. 415-418, April 2003.

[74] R. Papazyan, P. Pettersson. H. Edin, R. Eriksson. U.Gafvert, "'Extraction of the high frequency power cable characteristics from S-parameter measurements." IEEE *Trans. Dielecr. and Elect. Insulation*, submitted Jan. 2003.

[75] T. Suzuki, K. E. Walrath. M. Zahn and 1. R. Melcher. "Dielectric study at microwave frequencies of water-treed crosslinked polyethylene," IEEE Trans. Elect. Insulation. vol. 27. pp. 1083-1088, Dec. 1992.

[76] M.J. Given, M. Judd. S.J. MacGregor, J. Mackerste and R.A Fouracre. "Broad band dielectric spectroscope as a diagnostic technique for water-tree growth in cables," in *1999 CEIDP Ann. Rep*., pp. 118-121.

[77] R. Neimanis, R. Eriksson and R. Papazyan, "Diagnosis of moisture in oil/paper distribution Cables - Part II: Water penetration in cable insulation - experiment and modeling," in IEEE Transactions on Power Delivery, vol. 19, no. 1, pp. 15-20, Jan. 2004

[78] Y. H. M. Thayoob, Y. S. Visvanathan, S. K. Ahmed and A. B. A. Ghani, "Analysis and characterization of water-tree condition in XLPE cables from dielectric spectroscopy measurement in frequency domain," 2015 IEEE International Conference on Signal and Image Processing Applications (ICSIPA), Kuala Lumpur, 2015, pp. 526-531.

[79] Werelius, P., Tharning, P., & Erikson, R., "Dielectric Spectroscopy for Diagnosis of Water-tree Deterioration in XLPE Cables," IEEE Transactions on Dielectrics and Electrical Insulation. Vol. 8, No 1, pp.27-42, 2001.

[80] Programma Electric Ab. 2002. User's Manual for Insulation Diagnostic System IDA 200.

[81] Bolarin Oyegoke, Petri Hyvonen, Martti Aro & Ning Gao, "Application of Dielectric Response Measurement on Power Cable Systems," IEEE Transactions on Electrics and Electrical Insulation. Vol. 10, No 5, pp. 862-873, October 2003.

[82] P. S. Ghosh. 2007. TNB Distribution Division Maintenance Manual: Underground Cable System.

[83] H. Li et al., "Singularity point detection of high frequency signal for fault location," 2015 5th International Conference on Electric Utility Deregulation and Restructuring and Power Technologies (DRPT), Changsha, 2015, pp. 1004-1009.

[84] M. Vitins, "A Correlation Method for Transmission Line Protection," in IEEE Transactions on Power Apparatus and Systems, vol. PAS-97, no. 5, pp. 1607-1617, Sept. 1978.

[85] Y.G.Paithankar, M.T.Sant. "A New Algorithm for Relaying and Fault Location Based on Autocorrelation," Electric Power System Research, vol.8, no.2, pp.179-185, 1985

[86] S. Rajendra and P. G. McLaren, "Travelling-Wave Techniques Applied to the Protection of Teed Circuits: Principle of Travelling-Wave Techniques," in IEEE Power Engineering Review, vol. PER-5, no. 12, pp. 50-51, Dec. 1985.

[87] E. H. Shehab-Eldin and P. G. McLaren, "Travelling wave distance protection-problem areas and solutions," in IEEE Transactions on Power Delivery, vol. 3, no. 3, pp. 894-902, Jul 1988.

[88] C. Christopoulos, D. W. P. Thomas and A. Wright, "Signal processing and discriminating techniques incorporated in a protective scheme based on travelling waves (power lines)," in IEE Proceedings C - Generation, Transmission and Distribution, vol. 136, no. 5, pp. 279-288, Sept. 1989.

[89] Liang Jie, S. Elangovan and J. B. X. Devotta, "Adaptive travelling wave protection algorithm using two correlation functions," in IEEE Transactions on Power Delivery, vol. 14, no. 1, pp. 126-131, Jan 1999.

[90] D. Spoor and Jian Guo Zhu, "Improved single-ended traveling-wave fault-location algorithm based on experience with conventional substation transducers," in IEEE Transactions on Power Delivery, vol. 21, no. 3, pp. 1714-1720, July 2006.

[91] A. Elhaffar and M. Lehtonen, "Signal Processing Applications to Current Traveling Wave Fault Locators for EHV Transmission Networks," 2007 IEEE International Conference on Signal Processing and Communications, Dubai, 2007, pp. 616-619.

[92] M. Silva, M. Oleskovicz and D. V. Coury, "A fault locator for transmission lines using traveling waves and wavelet transform theory," 2004 Eighth IEE International Conference on Developments in Power System Protection, 2004, pp. 212-215 Vol.1.

[93] "Global Wind Report 2014 - Annual Market Update". report. GWEC. 22 April 2016. Retrieved 23 May 2016

[94] "Wind Energy Report 2013". Report. Global Wind Energy Council. February 2014. Retrieved 13 February 2014.

[95] "Wind Energy Report 2012". Report. Global Wind Energy Council. February 2013. Retrieved 14 February 2013.

[96] "Wind Energy Report 2011". Report. Global Wind Energy Council. February 2012. Retrieved 7 February 2012.

[97] G. L. Toole, M. Fair, A. Berscheid and R. Bent, "Electric power transmission network design for wind generation in the Western United States: Algorithms, methodology, and analysis," IEEE PES T&D 2010, New Orleans, LA, USA, 2010, pp. 1-8.

[98] J. E. Schmidt, "A statistical analysis of wind power in the Eastern Interconnect of the United States," IEEE PES General Meeting, Minneapolis, MN, 2010, pp. 1-8.

[99] Badrzadeh, B.; Hogdahl, M.; Isabegovic, E., "Transients in Wind Power Plants—Part I: Modeling Methodology and Validation," *Industry Applications, IEEE Transactions on* , vol.48, no.2, pp.794,807, March-April 2012

[100] D. Smugala, W. Piasecki, M. Ostrogorska, M. Florkowski, M. Fulczyk and O. Granhaug, "Wind Turbine Transformers Protection Method Against High-Frequency Transients," in IEEE Transactions on Power Delivery, vol. 30, no. 2, pp. 853-860, April 2015.

[101] Y. L. Xin, W. H. Tang, L. Luan, G. Y. Chen and H. Wu, "Overvoltage protection on high-frequency switching transients in large offshore wind farms," 2016 IEEE Power and Energy Society General Meeting (PESGM), Boston, MA, 2016, pp. 1-5.

[102] P. Elhaminia and M. Vakilian, "Frequency response features of a multi-objective wind turbine transformer design," 2016 24th Iranian Conference on Electrical Engineering (ICEE), Shiraz, 2016, pp. 643-648.

[103] H. Ye, Yao Liu, Z. Qi, T. An and X. Zhou, "A low-order AC-frequency and DC-voltage response model of HVDC grid connected with wind farms," 2016 IEEE PES Asia-Pacific Power and Energy Engineering Conference (APPEEC), Xi'an, 2016, pp. 681-686.

[104] X. Yang, F. Chun-en, L. Wei, Z. Bi-de, R. Xiao and L. Yan, "Modeling of high frequency transients of vacuum circuit breaker switching transformers in offshore wind parks," 2016 27th International Symposium on Discharges and Electrical Insulation in Vacuum (ISDEIV), Suzhou, 2016, pp. 1-4.

[105] K. Clark, N. W. Miller, M. Shao, S. Pajic and R. D'Aquila, "Transient Stability and Frequency Response of the Us Western Interconnection Under Conditions of High Wind and Solar Generation," 2015 Seventh Annual IEEE Green Technologies Conference, New Orleans, LA, 2015, pp. 13-20.

[106] F. S. Villar, M. Reza, K. Srivastava and L. C. P. da Silva, "High frequency transients propagation and the multiple reflections effect in collection grids for offshore wind parks," 2011 IEEE Power and Energy Society General Meeting, San Diego, CA, 2011, pp. 1-7.

[107] L. Meegahapola and D. Flynn, "Impact on transient and frequency stability for a power system at very high wind penetration," IEEE PES General Meeting, Minneapolis, MN, 2010, pp. 1-8.

[108] Y. Shibuya and S. Fujita, "High frequency model and transient response of transformer windings," IEEE/PES Transmission and Distribution Conference and Exhibition, 2002, pp. 1839-1844 vol.3.

[109] Chang Ying, J. Duan, Sun Lei, He Yu and S. Cui, "Applicability analysis of differential protection for dispersed wind generation in distribution network," 2016 IEEE PES Asia-Pacific Power and Energy Engineering Conference (APPEEC), Xi'an, 2016, pp. 2148-2152.

[110] A. Reis and J. C. Oliveira, "Physical Concepts Related to Harmonics Produced by Wind Turbines Operation," in IEEE Latin America Transactions, vol. 14, no. 4, pp. 1792-1799, April 2016.

[111] U. Vargas and A. Ramirez, "Extended Harmonic Domain Model of a Wind Turbine Generator for Harmonic Transient Analysis," in IEEE Transactions on Power Delivery, vol. 31, no. 3, pp. 1360-1368, June 2016.

[112] S. H. Qazi, M. W. B. Mustafa, S. Soomro and R. M. Larik, "Comparison of reference signal extraction methods for active power filter to mitigate load harmonics from wind turbine generator," 2015 IEEE Conference on Energy Conversion (CENCON), Johor Bahru, 2015, pp. 463-468.

[113] P. Xiong and D. Sun, "Backstepping-Based DPC Strategy of a Wind Turbine-Driven DFIG Under Normal and Harmonic Grid Voltage," in IEEE Transactions on Power Electronics, vol. 31, no. 6, pp. 4216-4225, June 2016.

[114] U. Vargas and A. Ramirez, "Harmonic domain model of a wind turbine generator for steady-state analysis," 2015 North American Power Symposium (NAPS), Charlotte, NC, 2015, pp. 1-6.

[115] A. Reis, L. P. Moura and J. C. de Oliveira, "Mitigation of harmonic current produced by wind turbine throughout converter switching control," 2016 17th International Conference on Harmonics and Quality of Power (ICHQP), Belo Horizonte, 2016, pp. 255-260.

[116] K. Van Reusel and S. Bronckers, "Summation rule for wind turbines' harmonics challenged by measurements," 2016 17th International Conference on Harmonics and Quality of Power (ICHQP), Belo Horizonte, 2016, pp. 362-366.

[117] A. Shafiu, A. Hernandez, F. Schettler, J. Finn and E. Jørgensen, "Harmonic studies for offshore windfarms," 9th IET International Conference on AC and DC Power Transmission (ACDC 2010), London, 2010, pp. 1-6.d

[118] K. Yang, M. H. J. Bollen and E. O. A. Larsson, "Aggregation and Amplification of Wind-Turbine Harmonic Emission in a Wind Park," in IEEE Transactions on Power Delivery, vol. 30, no. 2, pp. 791-799, April 2015.

[119] Bollen, M.; Olofsson, M.; Larsson, A.; Ronnberg, S.; Lundmark, M., "Standards for supraharmonics (2 to 150 kHz)," Electromagnetic Compatibility Magazine, IEEE , vol.3, no.1, pp.114,119, 1st Quarter 2014

[120] J. Meyer, S. Mueller, S. Ungethuem, X. Xiao, A. Collin and S. Djokic, "Harmonic and supraharmonic emission of on-board electric vehicle chargers," 2016 IEEE PES Transmission & Distribution Conference and Exposition-Latin America (PES T&D-LA), Morelia, 2016, pp. 1-7.

[121] I. Angulo, A. Arrinda, I. Fernández, N. Uribe-Pérez, I. Arechalde and L. Hernández, "A review on measurement techniques for non-intentional emissions above 2 kHz," 2016 IEEE International Energy Conference (ENERGYCON), Leuven, 2016, pp. 1-5.

[122] A. Moreno-Munoz, A. Gil-de-Castro, E. Romero-Cavadal, S. Rönnberg and M. Bollen, "Supraharmonics (2 to 150 kHz) and multi-level converters," 2015 IEEE 5th International Conference on Power Engineering, Energy and Electrical Drives (POWERENG), Riga, 2015, pp. 37-41.

[123] J. Behkesh Noshahr, "Emission phenomenon of supra-harmonics caused by switching of full-power frequency converter of wind turbines generator (PMSG) in smart grid," 2016 IEEE 16th International Conference on Environment and Electrical Engineering (EEEIC), Florence, 2016, pp. 1-6.

[124] D. Agudelo-Martínez, M. Limas, A. Pavas and J. Bacca, "Supraharmonic bands detection for low voltage devices," 2016 17th International Conference on Harmonics and Quality of Power (ICHQP), Belo Horizonte, 2016, pp. 1003-1009.

[125] Iuzzolino, R.; Ihlenfeld, W.G.K., "High-Accuracy Methods and Measurement Procedures for Power Quality Parameters Using the Digital Synchronous Sampling Technique," Instrumentation and Measurement, IEEE Transactions on , vol.56, no.2, pp.426,430, April 2007